64^Cu-bis(thiosemicarbazone) Complexes for Delineating Myocardial Hypoxia

Handley, Maxwell

Awarding institution:
King's College London

^{64}Cu-bis(thiosemicarbazone) Complexes for Delineating Myocardial Hypoxia

A thesis submitted by

Maxwell G Handley

In fulfilment of the requirements for the degree of

Doctor of Philosophy

University of London

2012

Division of Imaging Sciences and Medical Engineering, King's College, London.

Abstract

Coronary artery disease and coronary microvascular disease, as well as acute myocardial infarction and adverse remodelling are often characterised by tissue hypoxia. They benefit from the earliest possible diagnosis and treatment. Positron Emission Tomography (PET) is a highly sensitive technique capable of non-invasively imaging the biochemistry of the body, with the capacity to track biochemical changes over time. In this project, we aim to characterise a series of novel PET imaging agents able to identify and characterise hypoxic myocardium with a view to optimising the treatment of a range of cardiovascular diseases.

Bisthiosemicarbazone (BTSC) ligands readily chelate positron emitting copper isotopes, and have been demonstrated to selectively accumulate in hypoxic tissue *in vitro*, *in vivo*, and in isolated perfused hearts. While the lead compound Cu-ATSM has been widely investigated, a library of related Cu-BTSC complexes exist which may have better pharmacokinetics and selectivity for application in cardiology.

We employed isolated ventricular myocytes and isolated perfused hearts to screen a number of ^{64}Cu-labelled BTSC complexes, to assess their hypoxia selectivity and accumulation in cardiac tissue. For this purpose we developed a novel incubation chamber for maintaining isolated cardiomyocytes under hypoxic conditions. We also developed a novel gamma radiation detector array comprising three Na/ I γ-detectors, for monitoring the flow of radioactivity through isolated perfused hearts in real-time.

We have demonstrated the hypoxia selective accumulation of ^{64}Cu-ATSM in adult rat ventricular myocytes (ARVM) incubated under hypoxic conditions. Using isolated perfused hearts we demonstrated that all ^{64}Cu-BTSC readily accumulate within cardiac tissue in an oxygen-dependent manner. We also identified a relationship between the structure of Cu-BTSCs and their tissue retention, with lower molecular weight complexes providing the greatest hypoxic to oxygenated tissue contrast. In doing this we have identified two complexes, Cu-ATS and Cu-CTS, which could potentially supersede Cu-ATSM as the agent of choice for imaging the hypoxic myocardium.

Declaration

I Maxwell Handley confirm that no part of this thesis has been submitted in support of any other application for a degree or qualification of King's College, or any other university or institute of learning. I confirm that this work is my own. Where information has been derived from other sources it has been indicated in this thesis.

Acknowledgements

I would like to thank my supervisor Dr Richard Southworth for giving me the opportunity to study towards a PhD, and for his help and guidance throughout my project, and whilst I was writing this thesis. I am especially appreciative of his approachability and enthusiasm, but mainly his patience and trust. I look forward to more conversations (and some friendly pints) with you, Supervising Man.

I owe a special mention and a thousand thanks to Prof. Phil Blower for his support, guidance, mentoring and inspiration, from my B.Sc to Ph.D.

I would also like to thank my second supervisor Prof. Eike Nagel, Dr Thomas Eykyn, Dr Gregory Mullen, and Prof. Michael Shattock for their help and advice.

I owe special thanks (and numerous pints) to Mr David (DT) Thakor for all of the great work that he does within the department, and also to Miss (soon to be Dr) Fiona Shaughnessy for sharing the good, the bad, and the ugly (mainly Heineken induced) times.

Thank you to Dr Kazumi Chia for demonstrating calm during the storm that was my first and second years, and for ‘sharing’ the cost of certain pieces of equipment.

I would like to thank Dr Rowena Paul for supplying us with bis(thiosemicarbazone) ligands and ^{64}Cu, and Dr Karen Shaw for all the lovely ^{64}Cu that she made, and NMR spectroscopy that she did. Karen you saved my backside.

I would also like to thank all of the students, post-docs and staff who worked in Imaging Sciences during my time there, particularly my desk buddy Mr Levente Meszaros, Miss Erika Mariotti, Miss Putthiporn Charoenphun, Dr Rodolfo (Rudy) Medina, Dr Maggie Cooper, and my lucky charm Dr Kavitha Sunassee.

I should certainly mention my good friend Mr David List for putting a very cheap roof over my head, and for putting up with my moaning and groaning.

Thank you to my parents and family for all of the love and support that they have always given me.

I would like to dedicate this thesis to my exceptionally brilliant and wonderful girlfriend Dr Michela Mazzon for her unwavering, multi-modal support and guidance, but mainly for her love and companionship.

Table of Contents

List of Figures

Chapter 1

Chapter 2

Chapter 3

Chapter 4

Chapter 5

List of Tables

Chapter 1

Chapter 2

Chapter 3

Chapter 4

Chapter 5

List of Abbreviations

2/ 3-D: Two/ Three Dimensional

Acetyl CoA: Acetyl Coenzyme A

Acps: Actual counts per second

ADP: Adenosine diphosphate

ARVM: Adult rat ventricular myocyte/s

ATP: Adenosine triphosphate

ATS: 2,3-butanedione bis(thiosemicarbazone)

ATSE: Diacetyl bis(N^4-ethlythiosemicarbazone)

ATSM: Diacetyl bis(N^4-methlythiosemicarbazone)

BAPN: Bis(amine-phenol)-nitroimidazole

BAT-NI: 2,10-dimercapto-2,10-dimethyl-4-,8-diaza-6-[4-(2-nitroimidazolyl)butyl]-undecane

BCA: Bicinchoninic acid

BTSC: bis(thiosemicarbazone)

CAD: Coronary artery disease

CAS: Coronary artery spasm

CHO cells: Chinese hamster ovary cells

CIRC: Circumflex coronary artery

CK: Creatine kinase

CMD: Coronary microvascular disease

Cpm: Counts per minute

Cps: Counts per second

CSH: Coverslip Hypoxia

CT: Computed tomography

CTS: 2,3-pentanedione bis(thiosemicarbazone)

CTSM: 2,3-pentanedione bis(N^4-methylthiosemicarbazone)

DG: Deoxyglucose

DMSO: Dimethyl sulfoxide

DTS: 3,4-hexanedione bis(thiosemicarbazone)

DTSM: 3,4-hexanedione bis(N^4-methylthiosemicarbazone)

ECG: Electrocardiograph

ETC: Electron transport chain

FA: Fatty Acid/s

FAD: flavin adenine dinucleotide

$FADH_2$: Reduced flavin adenine dinucleotide

FCS: Fetal calf serum

FMISO: Fluoromisonidazole

GDP: Guanine nucleotide diphosphate

GTP: Guanine nucleotide triphosphate

hESC: Human embryonic stem cells

iBKG: Initial background counts per second

IVM: (Iodovinyl)misonidazole

ITLC: Instant thin layer chromatography

(m)KHB: (Modified) Krebs- Henseleit Buffer

M199: Medium 199

LAD: Left anterior descending coronary artery

LM: Left main coronary artery

LVDP: Left ventricular developed pressure

LVEDP: Left ventricular end diastolic pressure

MRI: Magnetic resonance imaging

MTT: 1-(4,5-Dimethylthiazol-2-yl)-3,5-diphenylformazan

Na_2-EDTA: Di-sodium ethylenediaminetetraacetic acid

NAD+: Nicotinamide adenine dinucleotide

NADH: Reduced nicotinamide adenine dinucleotide

PBS: Phosphate buffered saline

Pcps: Peak counts per second

PDA: Posterior descending coronary artery

P_i: Inorganic phosphate

PnAO-1-(2-nitroimidazole): Propyleneamine oxime-1-(2-nitroimidazole) (BMS181321)

PTSE: Pyruvaldehyde bis(N^4-ethylthiosemicarbazone)

PTSM: Pyruvaldehyde bis(N^4-methylthiosemicarbazone)

RCA: Right coronary artery

Radio- HPLC: Radio- High Performance Liquid Chromatography

Rcps: Residual counts per second

ROS: Reactive oxygen species

RP170: 1-(2-hydroxy-1-[hydroxyl-methyl]ethoxy)methyl-2-nitroimidazole

Trypan Blue: Tetrasodium 3,3'-[(3,3'-dimethyl[1,1'-biphenyl]-4,4'-diyl)bis(azo)]bis[5-amino-4-hydroxynaphthalene-2,7-disulphonate])

TγDS: Triple Na/I gamma detector system

TR: Percentage tissue retention

TRF: Tissue retention factor

TCA cycle: Tricarboxylic acid cycle

Chapter 1.

Introduction

1.1 Ischaemic Heart Disease

According to World Health Organisation statistics ischaemic heart disease is the leading cause of mortality in the Western world, and for the foreseeable future its incidence is expected to continue to rise (figure 1.1) [1]. There is therefore a need to continually improve the means by which ischaemic heart disease is diagnosed and treated. The development of hypoxia avid radiotracers, and the application of positron emission tomography (PET) and single photon emission computed tomography (SPECT), present a means by which hypoxic but viable myocardial tissue could potentially be delineated non-invasively. While unlikely to be useful for imaging acute myocardial ischaemia where faster, cheaper, and more widely available approaches are more appropriate, PET and SPECT demonstrate unique promise in imaging the subtle degrees of hypoxia associated with chronic cardiac dysfunction, such as myocardial hibernation, hypertrophy, microvascular disease, and the progression of the myocardium into heart failure.

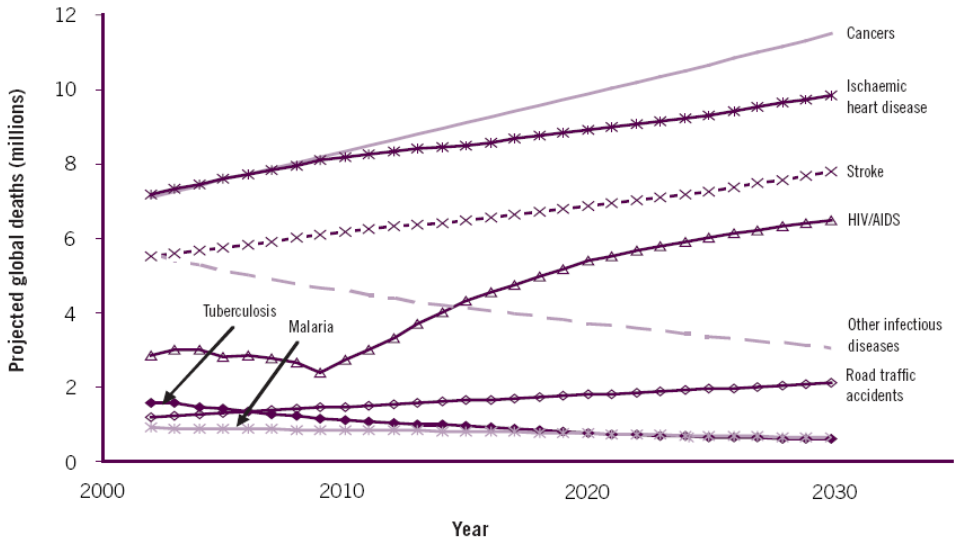

Figure 1.1 Projected worldwide causes of mortality 2002- 2030. Reproduced from [1].

1.2 Hypoxia/ Ischemia: Definitions and Considerations

A constant supply of oxygen is required for normal cellular metabolism. Hypoxia manifests in a number of disease states such as; coronary artery disease, acute myocardial infarction [2-3], stroke [4], certain types of cancer [5], rheumatoid arthritis [6] and diabetic vasculopathies [7]. Hypoxia may also be present in diseases where oxygen tensions are likely to be reduced due to poor respiratory function, e.g. cystic fibrosis and chronic bronchitis, sleep apnoea [8], epilepsy [9-10], as well as in benign proliferative diseases like psoriasis.

Hypoxia is defined as a disparity between oxygen availability and the amount required by a biological system to function optimally, and may be subdivided into two categories; supply hypoxia and demand hypoxia. Supply hypoxia is a condition that is caused by an inadequate supply of oxygen. Demand hypoxia on the other hand arises when cellular energy consumption increases, for example during exercise, without a concomitant increase in oxygen delivery.

Ischaemia, like hypoxia, is also defined as a disparity between supply and demand, but refers specifically to blood. Ischaemia is therefore a more complex situation than hypoxia in that blood not only transports oxygen, nutrients and signalling molecules, but also removes metabolic waste produces (e.g. lactate). The accumulation of waste metabolites due to low blood flow can have a detrimental effect on cellular function, and may compromise cellular integrity and viability. While hypoxia is therefore an intrinsic element of ischaemia, the latter is a more complex multifaceted condition.

1.3 The Pathogenesis of Cardiac Ischaemia/ Hypoxia

1.3.1 Ischaemic Cardiomyopathies

Cardiac ischaemia is caused by diseases which occur as the result of structural and functional changes to the coronary vasculature and cardiac tissue. It is therefore pertinent to provide a brief introduction of the ischaemic cardiomyopathies, in order to demonstrate how and why hypoxia avid agents could be used to diagnose, and assess the progression and treatment of these diseases.

1.3.2 Coronary Artery Disease

Coronary artery disease (CAD) is caused by the formation and growth of atherosclerotic plaques within the walls and lumen of the coronary arteries [11]. This is a chronic process, and it may take many years for the pathophysiological consequences of CAD to manifest into clinical symptoms [12]. Progressive narrowing of the coronary arteries compromises the supply of blood to the affected region of the heart, initially causing demand ischaemia. The supply of blood is inversely correlated to the severity of the occlusion, and while sufficient nutrients may be delivered to the affected region when the sufferer is at rest, as the demand for energy substrates and oxygen increases, such as during exercise (or in severe cases by simply walking or even standing), perfusion may fail to meet the requirements of the contracting myocardium. The repercussion of this is the manifestation of angina pectoris (chest pain) [11]. CAD is associated with stable angina, whereby the symptoms usually abate within a few minutes of resting. While angina may be discomforting and painful to the sufferer, it is not necessarily life threatening. However other complications that may coincide or arise as result of CAD are

considerably more serious, and may be life threatening. Coronary artery spasm (CAS) may occur in the presence or absence of stenosis, and can alone be a cause of cardiac ischaemia [13]. However when CAS occurs in conjunction with CAD, it is more likely to lead to complete occlusion of the effected artery/s, which will then starve the myocardium of blood, and lead to myocardial infarction (heart attack).

1.3.3 Atherosclerotic Plaque Rupture

The progressive development of atherosclerotic plaques, also pose a serious risk to cardiac viability in the acute setting. The rupturing of an atherosclerotic plaque releases a thrombus into the coronary vasculature. As the coronary arteries branch into the prearterioles and arterioles, and become narrower, the thrombus can become lodged. This may severely restrict, or even completely impede blood flow to myocardium distal to the occlusion. In experimental animals with a coronary perfusion rate that is 10% of normal flow, cardiomyocytes begin to die after about 20 min [14-15]. In sufferers this acute event may cause severe unabated pain in the left arm and chest (unstable angina). As a result of restricted or inhibited perfusion a wave of cell death (infarction) begins to spreads from the subendocardial zone, which requires the most energy, outwards towards the epicardium [14]. If treatment is not administered in order to breakdown or remove the thrombus and restore blood flow, the most severely ischaemic regions of the myocardium will become unsalvageable within 60 minutes.

1.3.4 Cardiac Hibernation

In ~40 % of patients with chronic cardiac ischaemia down-regulation of myocardial contractility has been observed, as a means of limiting the possibility of myocardial infarction, in a response commonly referred to as "myocardial hibernation" [16-17]. Diagnosis of myocardial hibernation is particularly important because it has been shown that upon the restoration of blood flow, these areas recover and contraction improves [18-19], meaning that once identified this group of patients have an excellent prognosis. While the mechanisms underlying this phenomenon remain poorly understood despite having been described almost 30 years ago [20], the two most prominent theories suggest the existence of either "perfusion contraction matching" [21] or "repetitive stunning" [22], or possibly a combination of the two.

Perfusion contraction matching has been described as a state of chronic hypoperfusion with reduced function in the absence of significant necrosis [23]. One may therefore expect these regions to be chronically hypoxic but viable. In the absence of a sufficient supply of oxygen, contractility is down-regulated in the affected region in order to preserve myocardial viability [18-19]. If this is the prevalent mechanism by which myocardium hibernates, then a hypoxia-specific imaging agent would potentially have some utility in its diagnosis.

Myocardial stunning is the delayed recovery of contractility following a transient ischaemic episode. Calcium overload that results from the reperfusion of ischaemic tissue is thought to cause the production of reactive oxygen species (ROS), which may cause

damage to cellular membranes, and the contractile apparatus of cardiomyocytes. Myocardial stunning is completely reversible but before normal contractility can resume a period of repair is required, during which time there will be a contractile deficit [22, 24]. In this context it may be likely that for much of the time hibernating myocardium is actually relatively well perfused, and therefore normoxic. The current gold standard technique for identifying hibernating myocardium is demonstration of elevated myocardial glucose uptake by ^{18}F-fluorodeoxyglucose (^{18}FDG) PET, coupled with demonstration of either normal or down-regulated flow (usually by perfusion imaging with $^{15}NH_3$) – a "perfusion-metabolism mismatch". If hibernating myocardium is predominantly normoxic and chronically stunned, then the lack of retention of a hypoxia imaging agent where hibernation has already been suggested by ^{18}FDG accumulation, could possibly be used to confirm this mechanism.

1.3.5 Coronary Microvascular Dysfunction

Coronary microvascular dysfunction (CMD) refers specifically to the narrowing of the prearterioles and intramural arterioles, which branch off of the main epicardial coronary arteries. This compromises blood flow to the endocardium, but unlike CAD, CMD affects the entire microvasculature of the heart. CMD may occur in the presence or absence of other cardiomyopathies, and has many causes which include, luminal obstruction, vascular remodelling, hormonal changes in females, and microvascular spasms [25]. The clinical symptoms of CMD are often persistent episodes of angina in the absence of CAD [26]. CMD is also associated with other factors such as smoking, hyperlipidaemia, and diabetes and because of this there is some debate as to whether the

causes of CMD are cardiac or non-cardiac [27]. CMD is more prevalent in females and often occurs in patients with normal coronary angiograms. What is apparent is that after almost 40 years since Arbogast and Bourassa [28], and Kemp [29] described CMD, the mechanisms that cause it remain elusive, and it is still somewhat difficult to diagnose. Hypoxic radiotracers could therefore provide a means of confirming global hypoxia resulting from CMD, and aid in the diagnosis of this condition.

1.3.6 Pathological Cardiac Hypertrophy

Pathological cardiac hypertrophy or adverse remodelling is the enlargement of cardiac myocytes, and therefore the heart muscle, without adequate compensatory angiogenesis. It usually occurs in response to vascular hypertension, valvular disorders, myocardial hibernation, or infarction. This is because the heart has to increase the amount of contractile force that it generates to overcome additional vascular resistance, or to compensate for loss of contractile function elsewhere [30-31]. Pathological hypertrophy is characterised by increased cell size, which results in decreased vascular density, and increased diffusion distance between blood vessels and myocytes**.** This combination of insufficient angiogenesis and increased diffusion distance may then lead to ischaemia or hypoxia. There is also evidence to suggest that hypertrophic cardiac myocytes have a reduced T-tubule network [32]. This in combination with the other effects of hypertrophy would further restrict the diffusion of oxygen to the mitochondria within each myocyte, and may also exacerbate hypoxia at the sub-cellular level.

This brief introduction highlights the complex and interlinked nature of the ischaemic cardiomyopathies, and also demonstrates similarities between the pathological consequences of these diseases. It also provides some insight into why a hypoxia specific imaging agent may be useful in cardiology. In addition hypoxia radiotracers may also be useful for assessing the effectiveness of drug therapy and revascularisation surgery, by confirming the reversal of tissue hypoxia.

1.4 Carbohydrate Metabolism and Cellular Respiration

Aerobic respiration is fundamental to the existence all vertebrates. Some unicellular organisms, for example yeast, function adequately even optimally without oxygen. However an inadequate supply of oxygen to tissues in multicellular organisms is almost invariably linked to a pathological process. Before discussing hypoxia and its relevance to diseases of the heart, normal cellular energy metabolism should be reviewed.

1.4.1 Cardiac Energy Metabolism

The heart is an omnivorous organ capable of metabolising fatty acids, glucose, lactate, and ketone bodies as substrates to feed the electron transport chain, and drive ATP synthesis. In the healthy heart, cardiomyocytes preferentially metabolise fatty acids by β-oxidation, because of their higher energetic yield [33-35]. While the complete oxidation of a molecule of glucose yields 30 molecules of ATP, the complete oxidation of palmitic acid, which has an acyl chain length of sixteen carbon atoms, yields 129 molecules of ATP [36-37].

1.4.2 β-Oxidation of Fatty Acids

Fatty acids are bound to albumin before being transported around the body, and are taken up into by the myocardium in the unbound form, which is mediated by transport proteins in the sarcolemma [38-39]. Inside the cardiomyocyte, fatty acids are activated by the addition of acyl-CoA by the action of acyl-CoA synthetase. To aid its entry in the mitochondria this acyl group is first passed from acyl-CoA to carnitine by carnitine-acyl transferase I, to form acyl-carnitine. Fatty acid transport across the inner mitochondrial membrane is facilitated by the exchange of acyl-carnitine for carnitine, by carnitine-acyl-carnitine translocase. Once inside the matrix, carnitine is cleaved off of the fatty acid chain and replaced again with CoA, by carnitine-acyl transferase II. The acyl-CoA molecule is then metabolised in a sequence of four reactions; oxidation, hydration, further oxidation, and a final thiolysis reaction. These reactions continue until the acyl molecule is fully degraded. Each cycle of reactions yield a molecule of acyl-CoA that has been shorted by two carbon atoms and a molecule of acetyl-CoA (figure 1.2), that passes on to the tricarboxylic acid cycle (TCA). The first oxidation reaction also generates one molecule each of $FADH_2$ and NADH, both of which pass directly on to the electron transport chain [36-37], described later in section 1.4.5.

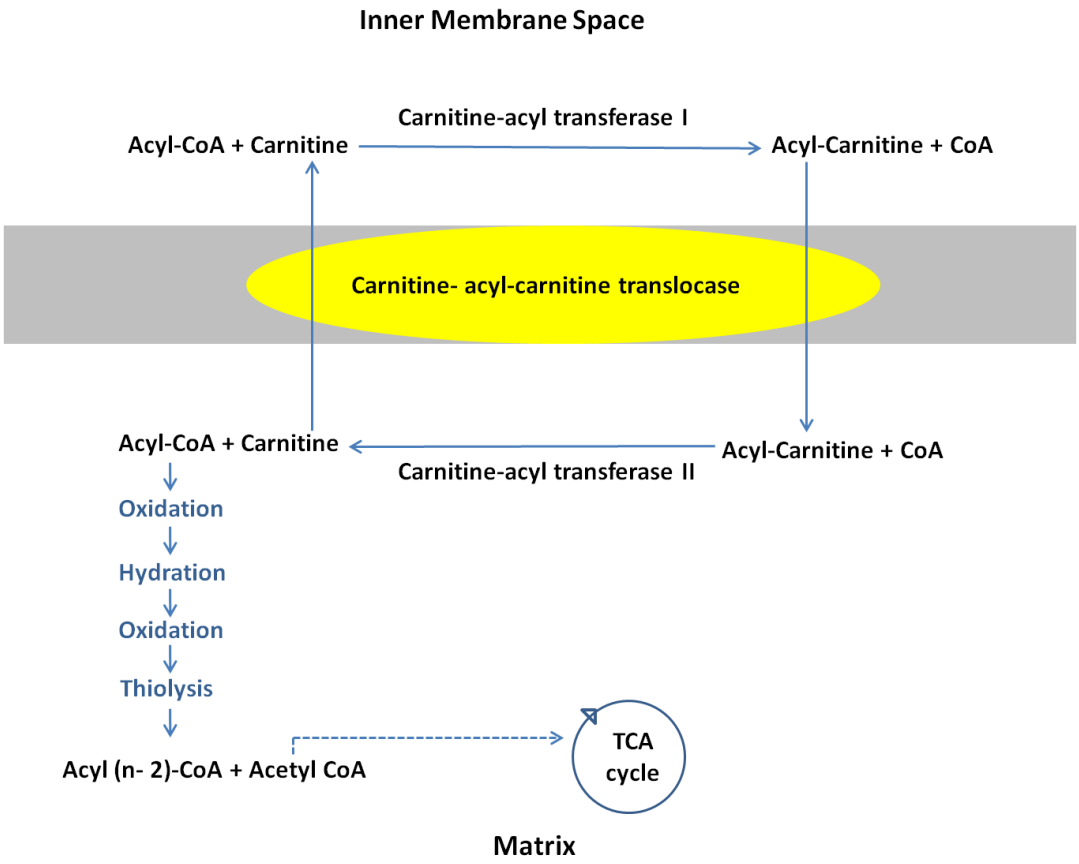

Figure 1.2. β- oxidation of fatty acids. Adapted from [11, 36]

1.4.3 The Glycolytic Pathway

The reactions of the glycolytic pathway (figure 1.3) take place in the cytosol, and may progress in the presence or absence of oxygen. In the presence of oxygen glycolysis leads to the formation of pyruvate, which is further oxidised by the tricarboxylic acid (TCA) cycle. The pathway is capable of providing a substantial amount of ATP, as there is a net production of two molecules of ATP and one molecule of NADH, from the conversion of one molecule of glucose to pyruvate [36-37]. Under anaerobic conditions glycolysis prevails as the major source of ATP synthesis, also producing two molecules of ATP per molecule of glucose, although the NADH that is formed is consumed in the formation of lactate. However, unless the products of glycolysis are metabolised by the tricarboxylic

acid cycle in the mitochondria, glycolysis alone cannot produce enough to ATP to meet the energy requirements of the contracting heart [11].

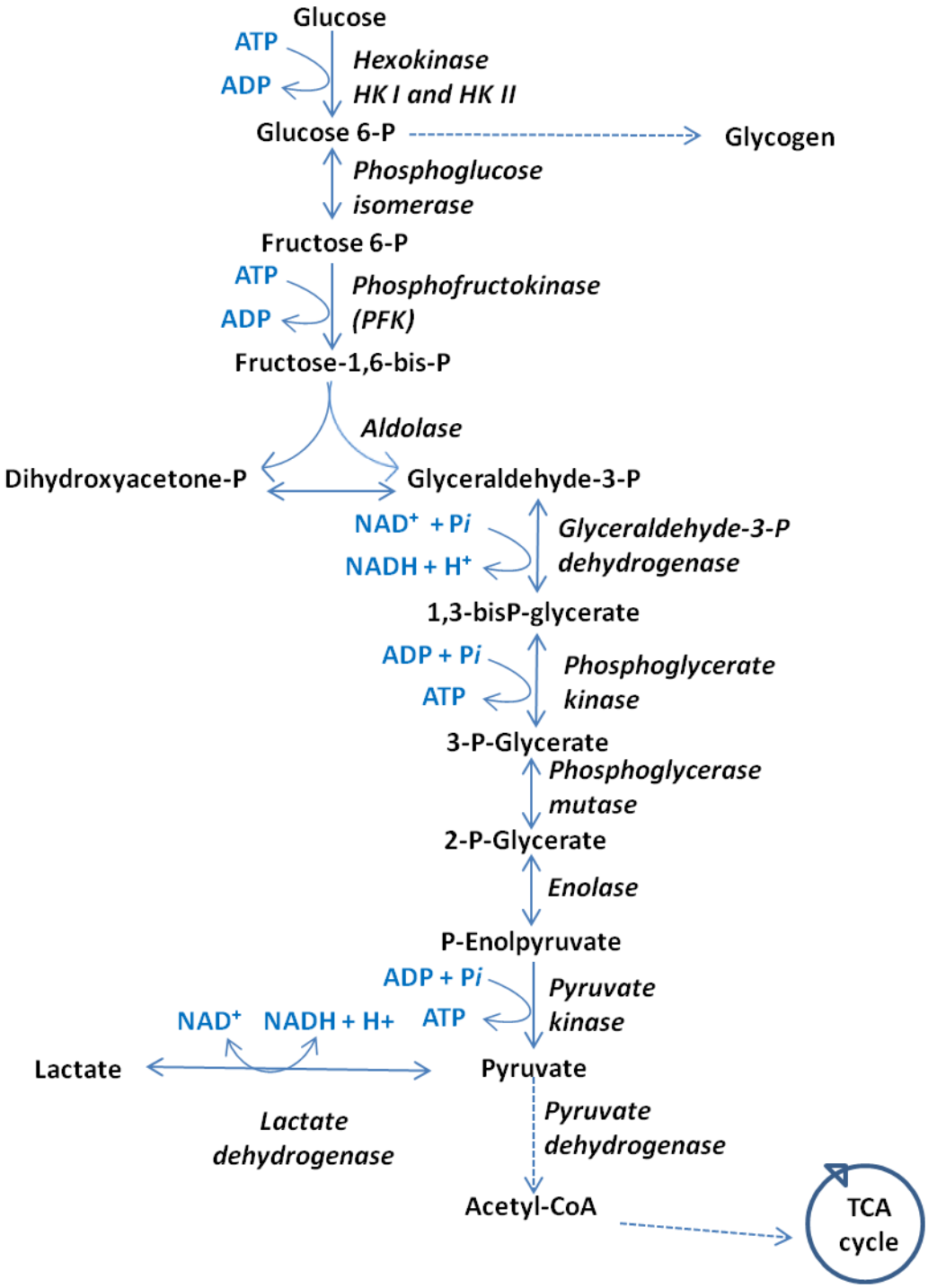

Figure 1.3. The glycolytic pathway. Adapted from [36].

1.4.4 The Tricarboxylic acid cycle

The majority of carbohydrate, fatty acid, and amino acid oxidation takes place in the mitochondrial matrix, via the enzymatic reactions of the tricarboxylic acid (TCA) (Krebs, or citric acid) cycle (figure 1.4) [36-37].

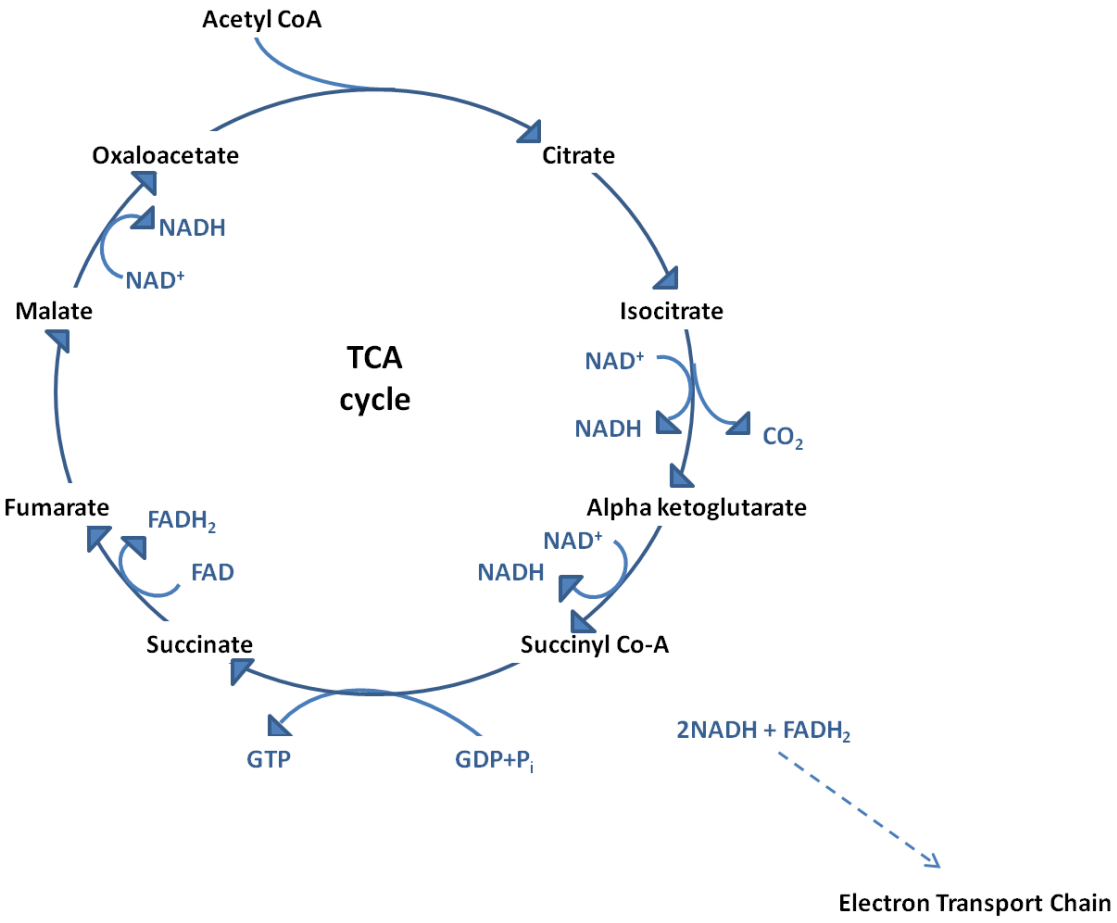

Figure 1.4. The Tricarboxylic acid cycle. Adapted from [36-37]

ATP is not synthesised directly by the enzymes of the TCA cycle, although some of the energy from acetyl-CoA is conserved in the phosphate bond of GTP, which is then passed on to ADP to form ATP by nucleoside diphosphate kinase. More importantly the TCA cycle also reduces three molecules of NAD+ and one molecule of FAD, to form NADH and $FADH_2$ respectively [36-37]. NADH and $FADH_2$ are then oxidised by the electron transport chain to generate a proton gradient which drives ATP synthesis [36-37].

1.4.5 The Electron Transport Chain and Oxidative Phosphorylation

The reduced coenzymes NADH and $FADH_2$ donate electrons to the electron transport chain (ETC) (figure 1.5), which serves to convert the energy of these electrons into the high energy phosphate bonds of ATP, in a gradual and controlled manner. The protein complexes of the ETC contain a series of redox centres with gradually increasing reduction potentials. This allows the passage of electrons up the reduction gradient, whilst simultaneously pumping protons (H^+) from the mitochondrial matrix into the inner mitochondrial membrane space. The proton gradient between the two compartments is then used by ATP synthase to synthesise ATP from ADP and inorganic phosphate (P_i). The process of electron transport is entirely dependent on molecular oxygen, which acts as the terminal electron acceptor. If the supply of oxygen is compromised then the protein complexes of the ETC remain in the reduced form. This inhibits generation of the mitochondrial membrane potential by proton efflux, and therefore also inhibits the activity of ATP synthase [36-37].

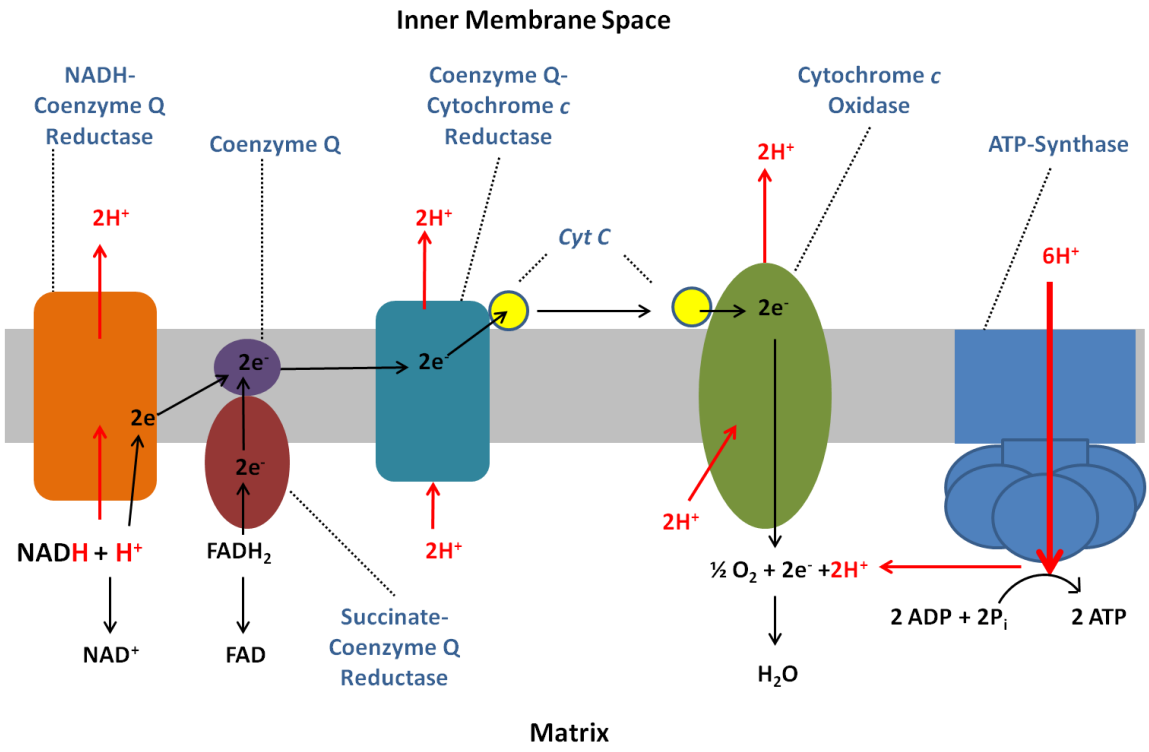

Figure 1.5. The mitochondrial electron transport chain and ATP synthesis. Adapted from [36-37].

The ETC is dependent upon the availability of molecular oxygen. In the absence of sufficient oxygen the ETC shuts down, followed by the TCA cycle, and inhibition of pyruvate dehydrogenase. Pyruvate arising from glycolysis is then converted to lactate by anaerobic glycolysis, as a compensatory (but significantly less effective) mechanism of ATP synthesis.

1.5 The Biochemical Effects of Ischaemia/ Hypoxia

The cellular damage that occurs when cardiac tissue is subjected to ischaemia or hypoxia is largely governed by the severity and duration of that insult. When oxygen is no longer available as the terminal electron acceptor, the ETC, proton efflux, and ATP-synthase

activity are inhibited, and anaerobic glycolysis becomes the major source of ATP synthesis.

As already discussed in section 1.4.3, glycolysis alone cannot produce sufficient ATP to maintain normal contractility, which means that when the supply of oxygen is limited myocytes use ATP faster than it can be re-synthesised. The hydrolysis of ATP to ADP releases protons which decrease the intracellular pH. Although this is somewhat buffered by the efflux of lactate which is coupled to proton efflux, ATP hydrolysis occurs at a faster rate [11]. In prolonged ischaemia or hypoxia, these excess protons and elevated NADH/ NAD+ ratio inhibit phosphofructokinase activity, which down-regulates anaerobic glycolysis [11, 36-37, 40].

Not only is the amount of ATP that is synthesised during ischaemia and hypoxia significantly less than in oxygenated hearts, the activity of ATP synthase is reversed in order to maintain the mitochondrial membrane potential, and a significant amount of ATP is actually consumed in order to pump protons out of the mitochondrial matrix and into the inner membrane space, which further exacerbates cellular acidosis [41].

As myocytes no longer have any means of synthesising ATP, they also lose their capacity to maintain ionic homeostasis through ATP-dependent ion exchangers and pumps [11]. Intracellular acidosis drives the cytosolic influx of sodium (Na^+) through the sarcolemmal Na^+/ H^+-exchanger. The excess Na^+ is transported out of the cell via the reverse mode action of the Na^+/ Ca^{2+}-exchanger. This results in intracellular calcium

overload, because lack of ATP prevents the activity of sarcoplasmic endoplasmic reticulum Ca^{2+} ATPase (SERCA), which in normoxic cells is responsible for calcium reuptake into the sarcoplasmic reticulum [11]. In this situation the mitochondria act as a sink for calcium, which is taken up via the Ca^{2+} uniporter. However, this can lead to mitochondrial calcium overload [42]. It is currently unclear whether calcium overload in itself is capable of causing mitochondrial membrane potential collapse through the generation of reactive oxygen species (ROS) [43], or whether this is caused by opening of mitochondrial permeability transition pores (mPTP), although the later mechanism is usually considered more important during the oxidative burst upon reperfusion [44-45]. Opening of these pores disrupts the proton gradient between the mitochondrial matrix and inner membrane space, which inhibits the normal activity of ATP synthase even further. The open mPTP also allow water and small metabolites in to the mitochondria causing them to swell, which can eventually cause the outer mitochondrial membrane to rupture [45]. Opening of the mPTP also allows leakage of cytochrome c into the cytosol, which both increases free radical production via complex I and IV of the ETC, as well as initiating apoptosis through caspase activation [46].

Increases in cytoplasmic Ca^{2+} concentrations also activate proteases which damage the cytoskeleton, and phospholipases which deplete phospholipids in the cell membrane thereby compromising cell integrity [42]. This cascade of events combine and eventually cause irreversible cellular damage, which lead to necrosis and myocardial infarction. It is therefore of paramount importance to identify ischaemic (or hypoxic) tissue, and intervene as soon as possible.

1.6 The Current State of the Art for Estimating/ Measuring Tissue Oxygenation

There are numerous techniques available that can be used for the assessment of blood perfusion, blood oxygenation, or cellular metabolic status. However as will now be discussed, only hypoxia specific tracers will be able to provide an index of intracellular oxygenation status. Techniques that are used to assess this parameter can be split into four categories: those that measure tissue oxygen tensions directly, those that assess tissue perfusion, those that assess hypoxia indirectly using metabolic processes as parallel biomarkers, and hypoxia avid radiotracers. The majority of these techniques have recently been reviewed by Krohn *et al* [47] and Lapi *et al* [48].

1.6.1 Commonly Employed Invasive Methods

Invasive methods such as coronary angiography [49], temperature and pressure sensors [50], and Doppler flow wires [51] are widely used in the chatherisation lab to assess myocardial perfusion, intracoronary pressure, and coronary flow velocity, respectively. However these techniques can be unreliable especially when repeated analyses are performed, as it is often difficult to accurately re-target the exact same region of tissue [52]. On a practical note with respect to our original definition of hypoxia, these techniques are unable to determine whether the affected tissue is sufficiently oxygenated, or simply poorly perfused.

1.6.2 Oxygen Probes

Oxygen probes are widely used in the clinical setting for measuring tissue and tumour pO_2, but this is an invasive procedure that relies on operator accuracy for repeated measurements. The Oxylab™ and Oxylite™ systems developed by Oxford Optronix (Oxford, UK) employ a fluorescent probe, the accuracy of which increases as the level of tissue oxygenation decrease. The signal from the probe is quenched by O_2 and therefore the signal strength is inversely correlated to O_2 concentration [47, 53-55]. Although this instrument has improved the accuracy of direct pO_2 measurement, it is only able to provide a measure of vascular or interstitial oxygen tensions, rather than intracellular oxygenation status. While it can be used to compare the oxygenation status of normally perfused and stenosed tissue, it is impossible to determine whether or not cellular metabolism has been affected. To our knowledge, oxygen probes of this sort have not previously been evaluated in the myocardium, presumably because it would be a potentially risky invasive procedure, which would be complicated by difficulty of accessing the heart, and compounded by cardiac motion. While it possible to access the coronary vasculature using a coronary catheter, oxygen probes would only provide information on local blood oxygen saturations, with no insight into the oxygenation of the underlying tissues.

1.6.3 Non-Invasive Imaging Modalities

Practically all non-invasive imaging techniques have been applied to the investigation, diagnosis, and prognosis of the ischaemic cardiomyopathies (see table 1.1). However none of the techniques summarised in table 1.1 are able to answer the question “is the heart truly hypoxic”? The majority of these techniques provide a measurement of coronary perfusion, and rely on detecting a contrast between normally perfused and ischaemic tissue. While hypoperfusion may infer that the heart is hypoxic, because of its high work rate, it does not directly address the question of whether it is actually oxygen deficient. Furthermore, perfusion deficit provides no indication of whether or not the affected region is viable or salvageable.

Table 1.1. Summary of cardiac imaging techniques and tracers.

Parameter Assessed	Imaging Modality	Tracers	Selected References
Myocardial perfusion	CT Scan	Iodinated contrast agents	[56]
	MRI	^{1}H Gadolinium enhanced	[57-59]
	Echocardiography	Gas filled micro-bubbles	[60-61]
	SPECT	^{201}Thallium	[62-63]
		^{99m}Tc-Sestamibi	[64-65]
	PET	$^{13}NH_3$	[66-67]
		$H_2{}^{15}O_2$	[68]
		^{18}F-BMS747158-02	[69-72]
		^{60,61,62,63,64}Cu-PTSM	[73-76]
Cellular metabolism	SPECT	^{123}I-15-(*p*-iodophenyl)-3-methyl pentadecanoic acid (BMIPP)	[77]
	PET	^{18}F-Flourodeoxyglucose (^{18}FDG)	[78-79]
		^{18}F-Fluoro-thia-heptadecanoic acid (FTHA)	[80-82]
		^{11}C-octanoate	[83]
		^{11}C-palmitate	[83-85]
		^{11}C-Acetate	[86-88]
Haemoglobin/ myoglobin oxygenation	MRI	Blood/ myoglobin level Dependent MRI	[89-90]/ [91]

Monitoring of cellular metabolism has a distinct advantage over the use of perfusion measurement. An increase in ^{18}F-FDG uptake for example, reflects the switch from beta oxidation of fatty acids to glycolysis during hypoxia [92]. However metabolic radiotracers do not respond solely to cellular oxygenation status. The uptake of these energy substrate radiotracers can also be affected by factors such as diet, and the

presence of other disease states such as diabetes [93-94]. This can confound image interpretation and make it difficult to discern healthy from hypoxic tissue.

Magnetic resonance imaging (MRI) modalities have been developed, that can provide an index of either blood or myoglobin oxygenation status. While oxyhaemoglobin is diamagnetic, deoxyhaemoglobin is paramagnetic [89-90]. This increase in haemoglobin's magnetisation as it becomes deoxygenated causes a more rapid relaxation of the water molecules around it (via T_2* weighted decay), such that MR scans sensitive to T2* show increased signal from oxygenated blood and decreased signal from deoxygenated blood [47, 95-97]. However BOLD MRI does not provide information regarding intracellular pO_2 within the myocardium. A variant of this technique, myoglobin oxygen level dependent (MOLD) MRI, is being developed as a means of specifically assessing the intracellular oxygenation status of cardiac tissue. However, this technique is still in its infancy, and its application is hampered by the significantly weaker signal that deoxymyoglobin has, compared to that of deoxyhaemoglobin [98].

1.6.4 Nuclear Imaging Techniques

The non-invasive imaging techniques single-photon emission computed tomography (SPECT) and positron emission tomography (PET), rely on the use of gamma radiation and positron emitting radionuclides respectively to detect, localise, or monitor biological/ biochemical events. These techniques are usually combined with computed tomography (CT), which is used to orientate PET and SPECT images with anatomical features such as organs and bone.

The rationale for the development of PET and SPECT occurred around the same time, and the techniques have many similarities. The development of SPECT and PET for clinical applications can be divided into three separate phases; the development of the cameras or scanners for imaging, the development of reconstruction algorithms to generate cross sectional and three-dimensional images, and the development of targeted radiotracers which are able to track biological processes or mimic biological molecules. It is this unique attribute that allows the nuclear imaging techniques to be used as diagnostic and prognostic indicators of disease states.

SPECT was first described by Kuhl and Edwards in 1964 [99]. Their crude system consisted of several sodium-iodide scintillation detectors for transaxial tomography. It was not until 1979 that the first whole body scanner, which consisted of multiple Anger cameras, was described by Jaszcak *et al* [100]. SPECT employs gamma (γ) radiation emitting radionuclides (see table 1.2), which are detected by a single collimated camera that rotates around the patient to acquire multiple 2-D images. These are then reconstructed to form a 3-D image.

The first ringed PET tomographs were described by Ter-Pogossian *et al* in 1975 [101]. PET employs positron (β^+) emitting radionuclides. When β^+-particles collide with electrons they annihilate to produce two γ-photons which travel in opposite directions from the point of annihilation. PET scanners work by registering the almost simultaneous coincidence of two β^+-particles, by two separate detectors along a 180^o plane. This is used to build up multiple 2-D images, which are then reconstructed into 3-D images.

PET scanners therefore employ a ring of static detectors, to be able to detect two β^+-particles travelling in opposite directions along the same axis.

Although PET and SPECT are very similar techniques each has advantages and disadvantages. SPECT isotopes are generally obtained from generators or as waste products from the nuclear fuel industry, and are therefore cheaper to obtain. Conversely the majority of PET isotopes are produced using a cyclotron. SPECT is therefore more widely used in the clinical setting. However this is now being overcome by the use of mobile PET imaging units, such as the National Health Service PET/CT Diagnostic Imaging Service in the UK [102]. A disadvantage of SPECT is that the image resolution is usually of lower quality compared to PET, because it detects only single γ-photons. Table 1.2 demonstrates there are more PET isotopes available than there are for SPECT. With regards to the development of new radiotracers this allows for more versatile radiolabelling chemistry. Furthermore non-metallic PET radionuclides, such as ^{11}C, can be incorporated into naturally occurring molecules without the need for bifunctional chelators, which are required to bind metallic radionuclides to biomolecules. This allows the direct measurement and monitoring of biological processes without the biochemistry of the compound being altered by the addition of a chelator group.

Table 1.2. Common SPECT and PET Radionuclides [103].

Radionuclide	Technique Applied	Radioactive Half-life (Time)	Production
^{11}C	PET	20.33 min	Cyclotron
^{13}N	PET	9.97 min	Cyclotron
^{15}O	PET	122 sec	Cyclotron
^{18}F	PET	109.77 min	Cyclotron
^{60}Cu	PET	23.7 min	Cyclotron
^{61}Cu	PET	3.33 h	Cyclotron
^{62}Cu	PET	9.67 min	Cyclotron/ Generator
^{64}Cu	PET	12.70 h	Cyclotron/ Reactor
^{68}Ga	PET	67.71 min	Generator
^{76}Br	PET	16.2 h	Cyclotron
^{82}Rb	PET	1.27 min	Generator
^{99m}Tc	SPECT	6.01 h	Generator
^{111}In	SPECT	2.81 days	Cyclotron
^{123}I	SPECT	13.22 h	Cyclotron
^{124}I	PET	4.17 day	Cyclotron
^{131}I	SPECT (Research)	8.02 days	Cyclotron/ Reactor
^{201}Tl	SPECT	9.33 h	Cyclotron

1.7 Hypoxia Selective Imaging Agents

1.7.1 Potential Application to Cardiac Molecular Imaging

Krohn *et al* stated that 'the best way to measure hypoxia would be with a probe that competes directly with intracellular O_2, one in which the indicator was not trapped when O_2 supply was keeping up with demand, but is retained when the O_2 supply is inadequate to accommodate all of the electrons being produced in the electron- transport chain' [47]. In addition to this Strauss *et al* have stated the potential applications for hypoxic tracers in cardiology as [104]:

- To identify the regions at risk in patients with stable angina
- To evaluate patients admitted as 'rule out' myocardial infarction
- To delineate hibernating myocardium
- To identify transient ischaemia

Nunn *et al* have also suggested that the ideal hypoxia selective tracer should demonstrate high accumulation in hypoxic tissue, but clear rapidly from blood and non-target tissues to give a target to background ratio of 3:1 or greater [105].

In the search for hypoxia-specific imaging tracers two distinct classes of radiolabelled-molecules have been extensively studied, the nitroimidazole derivates and copper bis(thiosemicarbazone) complexes.

1.7.2 2-Nitroimidazoles

Our group has recently published a review article which summaries the data that have so far been published, with respect to the application of ^{18}F-Fluoromisonidazole (^{18}FMISO) and radiocopper-labelled ATSM, as PET imaging agents for myocardial hypoxia [106].

The hypoxia avidity of the 2-nitroimidazoles was discovered by Nakamura in 1955, whilst trying to develop antimicrobial drugs that were effective against microorganisms that proliferate under anaerobic conditions [107]. During the 1970s the 2-nitroimidazoles were also assessed as radiosensitising agents, to enhance the treatment of tumours with hypoxic cores [108-110]. They have subsequently been radiolabelled with a variety isotopes including ^{18}F [111-113], ^{77}Br [114], ^{99m}Tc [115-117], ^{123}I [118] and ^{131}I [119-120], for both PET and SPECT imaging applications.

The nitroimidazoles are thought to enter cells by passive diffusion through the membrane. In normally oxygenated cells they diffuse directly back out of the cell, or undergo bioreduction to form an unstable anion. In oxygenated tissues this unstable anion is rapidly reoxidised back to the neutral form, which is once again able to traverse the cell membrane and leave the cell. In hypoxic tissues reoxidation is less likely to take place and the anion is further reduced to nitroheterocycles, hydroxylamines, or amines (figure 1.6). Each of these species is capable of forming covalent bonds with intracellular macromolecules, which would trap the radionuclide within the cell [121-122]. The identity of the bioreductants is currently unclear, although a number of candidates including cytochrome P450 and xanthine oxidoreductase have been implicated [123].

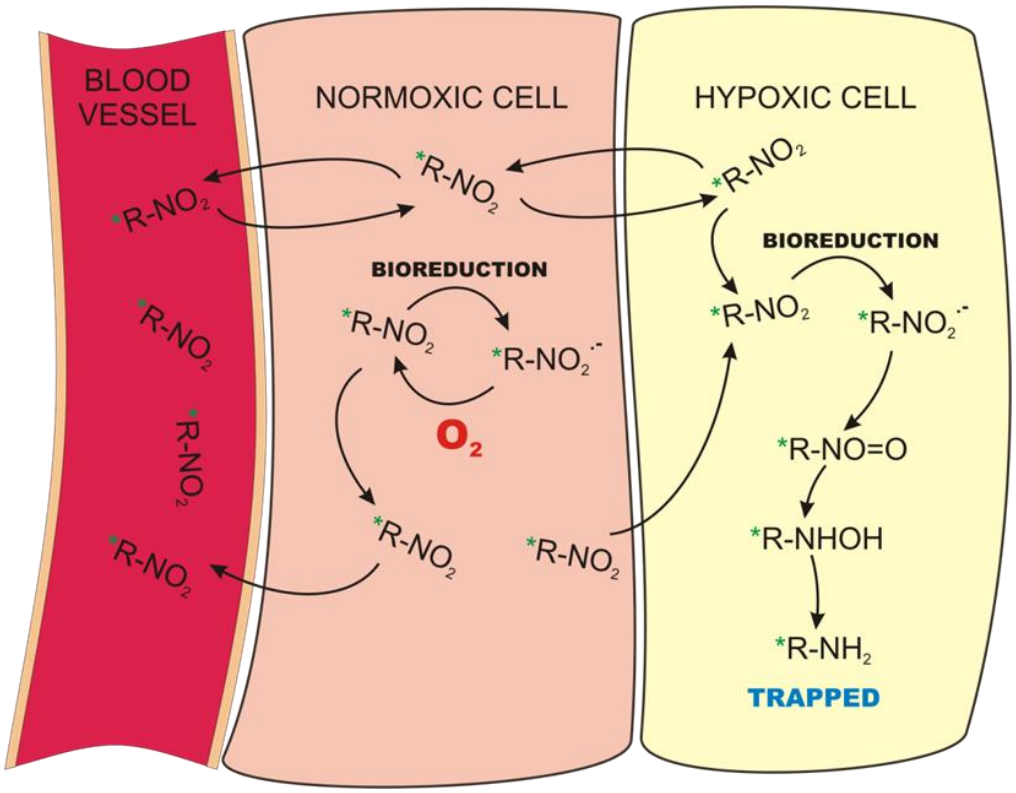

Figure 1.6 Proposed retention mechanism for nitroimidazole based tracers in hypoxic tissue. Reproduced from [106].

1.7.2.1 Fluoromisonidazole (FMISO)

In terms of hypoxia imaging, FMISO (figure 1.7) is perhaps the most extensively studied of the 2-nitroimidazole based compounds. The synthesis of ^{18}F-FMISO was first described by Jerabek *et al* in 1986 [124], to over come the need for an onsite cyclotron Grunbaum *et al* described a method for the synthesis of ^{3}H-FMISO in 1987 [125]. Later that year Mathias *et al* demonstrated increased accumulation of ^{18}FMISO *in vivo* using a stroke model, with ischaemia induced by carotid artery ligation [126].

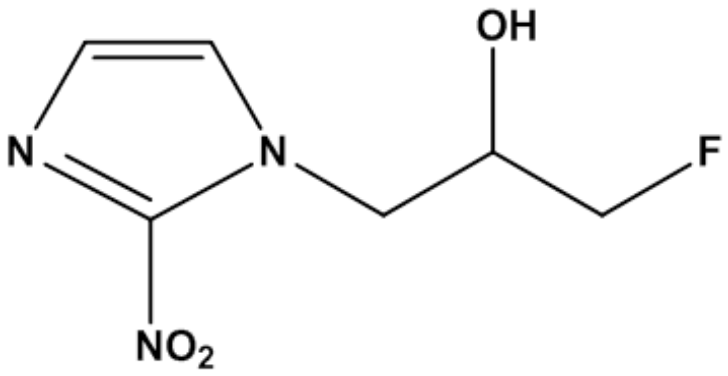

Figure 1.7. Structure of Fluoromisonidazole [126].

The preliminary work by the Mathias group was furthered by Shelton *et al*, who employed Langendorff isolated perfused hearts in combination with Na/ I scintillation detection to characterise this tracer. The constant infusion of ^{18}FMISO under oxygenated conditions resulted in 18 % retention of radioactivity by the heart. However during hypoxia and ischaemia the accumulation of ^{18}FMISO more than doubled, to 41 % and 48 % respectively. Reperfusion with oxygenated buffer or normalising the perfusate flow rate to control values had little effect on the rate of tracer clearance. This lead them to conclude that in all cases, the ^{18}F label became essentially irreversibly bound to hypoxic tissue [127]. This provided support for the feasibility of using ^{18}FMISO as a cardiac imaging agent. However the hypoxic: normoxic tissue contrast was only 2:1, which is lower than the ideal ratio of 3:1 that was suggested by Nunn *et al* [105].

In the same year Martin *et al* also began to investigate FMISO as an agent for cardiac imaging [128], using an open chest canine model of myocardial ischaemia to assess ^{3}H-FMISO uptake *in vivo*. The plasma clearance of ^{3}H-FMISO was biphasic with an initial rapid phase, and a slower secondary phase with a half-life of 275 min. The liver and

kidney demonstrated the highest average retention compared to other organs, but the main route of excretion was via the kidneys. In normally perfused tissue there was no relationship between myocardial blood flow and ^{3}H-FMISO accumulation, but in ischaemic regions an inverse correlation was observed. Furthermore, cardiac tissue sampling demonstrated that a 10– 60 % reduction in flow produced a 1.8- 2.4-fold increase in ^{3}H-FMISO retention, compared to non-ischaemic tissue. This was important because it demonstrated that the tracer was able to accumulate within poorly perfused tissue.

In order to confirm that the accumulation of FMISO was purely due to hypoxia selectivity alone and not dependent upon perfusion, Martin *et al* then went on to employ an isolated cardiac myocyte model. The accumulation of ^{3}H-FMISO in cardiomyocytes incubated under oxygenated conditions, was compared to that in cells maintained under hypoxia (5000ppm O_2) or anoxia. After 1 h they observed 4 and 8-fold increases in tracer retention in the respective groups, compared to controls (room air). ^{3}H-FMISO continued to accumulate for the duration of these experiments, and after 3 h they observed a 15-fold increase in cells incubated under hypoxia, and a 26- fold increase under anoxia [112].

In a continuation of their previous *in vivo* study Shelton *et al* then applied ^{18}FMISO PET, once again using a canine model to determine whether ^{18}F-FMISO was capable of delineating ischaemic but salvageable myocardium [129]. The left anterior descending (LAD) coronary artery of forty six animals were completely occluded for 3, 6, or >24 h. Myocardial perfusion was assessed with $H_2{}^{15}O$, with complete LAD occlusion observed

in twenty four of the animals. Tissue infarction was confirmed using histochemical staining, and the extent on the infarction zone was determined using Lissamine green. Accumulation of ^{18}FMISO was inversely related to the length of the occlusion period and myocardial blood flow. This further demonstrated that ^{18}FMISO preferentially accumulated in hypoxic but viable tissue. However, the group also performed PET imaging on selected animals and found that at least 45 min was required after the tracer was administered, to allow for sufficient blood pool clearance before imaging could take place. This was unfavourable because of the relatively short half-life of ^{18}F. Furthermore PET imaging showed that the contrast between ischaemic and normally perfused tissue was 1.5: 1, much lower that Nunn *et al* suggested.

Despite these unfavourable results Martin *et al* attempted a final *in vivo* PET study with ^{18}FMISO [130]. In this study they observed a contrast of 1.6: 1 for partially occluded tissue, and 1.8: 1 for fully occluded regions compared to normally perfused tissue, but again this was consider too low for clinical applications.

Although all of these studies have demonstrated that ^{18}FMISO selectively accumulates in ischaemic/ hypoxic cardiac tissue, it has not been adopted as a radiotracer for routinely delineating myocardial hypoxia clinically. This is because ^{18}FMISO has poor first pass uptake, leading to suboptimal contrast between ischaemic and normally perfused tissue. Its slow blood pool clearance means the period between injection and imaging is relatively long. This coupled with the relatively short half-life of ^{18}F necessitates having to administer a particularly high dose to the patient, which is also unfavourable. Whilst

^{18}FMISO has not been adopted in the clinic, its synthesis and application served well as a proof of concept for hypoxia tracers. FMISO signified the beginning of the development of hypoxia avid radiotracers for molecular imaging, after which a plethora of novel 2-nitroimdazole and non-nitroimidazole tracers have continued to be developed.

1.7.2.2 BMS181321

Propyleneamine oxime-1-(2-nitroimidazole) (BMS181321) is a ^{99m}Tc-coordinating misonidazole derivative (figure 1.8). It was developed by Bristol-Myers Squibb in an attempt to circumvent the requirement for a cyclotron, and overcome difficulties such as synthesis time, which affect the short half life ^{18}F-containing tracers.

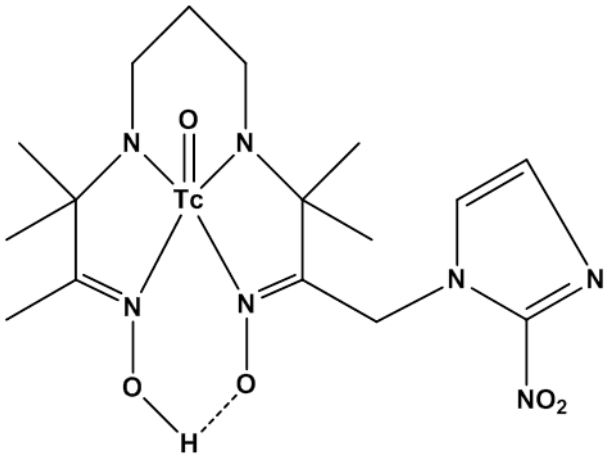

Figure 1.8. Structure of Propyleneamine oxime-1-(2-nitroimidazole) (BMS181321) [131].

Reduction of the complex by nitroreductases had been demonstrated *in vitro* [131], and accumulation of BMS181321 was approximately two-fold higher in hypoxic isolated cardiac myocytes compared to normoxic cells [132]. This was confirmed in isolated heart studies, where an inverse correlation was observed between buffer oxygen saturation and

tracer accumulation [133-134]. Rumsey *et al* demonstrated that it was possible to obtain SPECT images of sufficient contrast after 1 hour, with well resolved images acquired after 2 hours; significantly less time than the 4 hours required for ^{18}FMISO imaging [135]. The faster blood pool clearance of BMS181321 was attributed to its being more lipophilic than FMISO. However this unfortunately also gave rise to considerably higher hepatic retention, which seriously hampered attempts to use BMS181321 for cardiac SPECT imaging [136]. The work with BMS181321 demonstrated that it was possible to significantly alter the structure of 2-nitroimidazoles, whilst still retaining their hypoxia avidity. Furthermore the replacement of the ^{18}F radiolabel with ^{99m}Tc was a practically attractive approach. However the poor pharmacokinetics of BMS181321 halted its advancement to clinical use.

1.7.2.3 (Iodovinyl)misonidazole

^{131}I-(Iodovinyl)misonidazole (IVM) (figure 1.9) was also developed with the aim of avoiding the practical limitations of ^{18}FMISO described above. *In vitro* studies using isolated cardiomyocytes demonstrated that the hypoxic to normoxic retention ratio of IVM was 10: 1 and 22: 1, at 1 and 3 h respectively [120]. This was similar to ^{18}FMISO despite IVM being significantly more lipophilic [137]. *In vivo* studies using open chest dogs then demonstrated that the blood clearance of IVM was biphasic with a half-life of 4.6 h, similar to ^{18}FMISO. In these animals, reduction of myocardial blood flow to 70% of normal or less led to a proportionate increase in IVM deposition within the heart. Induction of additional demand ischemia by pacing or catecholamine stimulation enhanced tracer uptake further still. IVM exhibited the potential to delineate hypoxic

myocardial tissue, however its slow blood clearance and significant liver uptake (three times that of normoxic heart) aborted its further development.

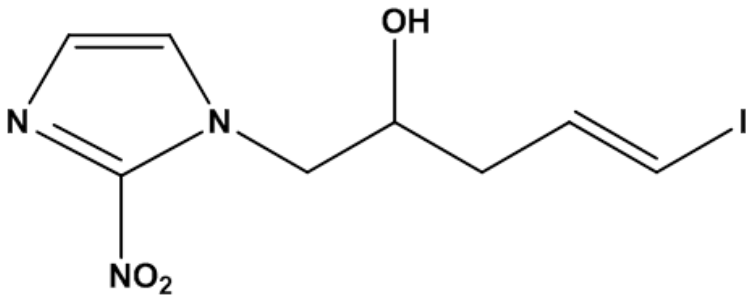

Figure 1.9. Structure of (Iodovinyl)misonidazole [119].

1.7.2.4 Other Nitroimidazole Analogues

A number of other nitroimidazole based tracers have also been investigated, with varying degrees of success. ^{99m}Tc-bis(amine-phenol)-nitroimidazole (^{99m}Tc-BAPN) (figure 1.10) was screened in isolated myocytes, but the complex did not selectively accumulate in anoxic cultures [138].

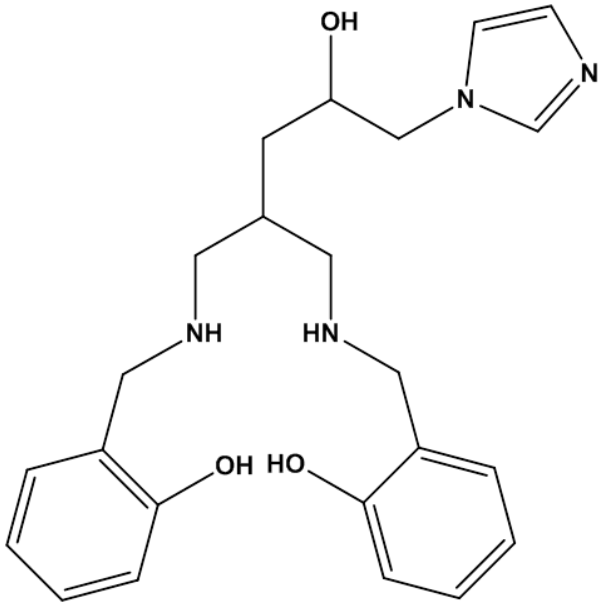

Figure 1.10. Structure of bis(amine-phenol)-nitroimidazole (BAPN) [138].

^{99m}Tc-5-oxa-amine-oxime nitroimidazole (BMS-194769,^{99m}Tc-BRU-59-21) (figure 1.11) an analogue of BMS181321, exhibited hypoxia selectivity *in vitro* in CHO cells [139] and *in vivo* [140-141], with a contrast of 2.4: 1 observed between ischaemic and normally perfused canine myocardium [136]. Unfortunately, a subsequent study showed that tracer accumulation only occurred when administered less than 5 minutes pre-occlusion, but not when administered post-occlusion [141]. This extremely short window of usefulness would limit the clinical application of this tracer to acute ischemic episodes, such as delineating transient ischemia in patients with unstable angina.

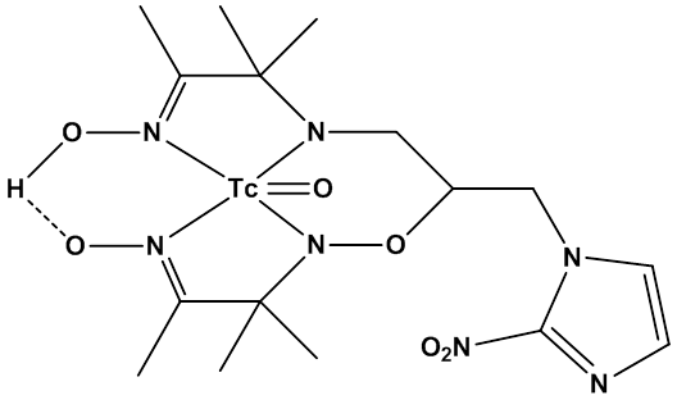

Figure 1.11. Structure of ^{99m}Tc-5-oxa-amine-oxime nitroimidazole (BMS-194769, ^{99m}Tc-BRU-59-21) [139].

Hoffend *et al* synthesised and screened 2,10-dimercapto-2,10-dimethyl-4-,8-diaza-6-[4-(2-nitroimidazolyl)butyl]-undecane (BAT-NI) labelled with $^{99m}TcO^{3+}$ (figure 1.12) [142]. They demonstrated preferential accumulation in ischemic rat myocardium (0.65% ID/ g ischemic, versus 0.2 % ID/ g remote), but hepatic (7.64% ID/g), stomach (1.31 %ID/g) and thyroid (12.7 % ID/g) were significantly higher. This low uptake and low contrast in target tissue led the authors to suggest that this complex is unlikely to have any useful clinical applications.

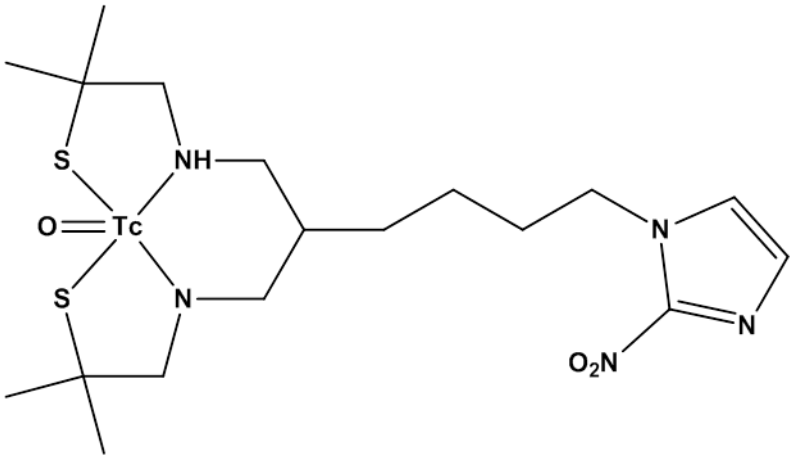

Figure 1.12. Structure of 2,10-dimercapto-2,10-dimethyl-4-,8-diaza-6-[4-(2-nitroimidazolyl)butyl]-undecane (BAT-NI) [142].

1-(2-hydroxy-1-[hydroxyl-methyl]ethoxy)methyl-2-nitroimidazole (RP170) is a hypoxic cell radiosensitiser with an octanol-water partition coefficient of 0.09, significantly lower than that of misonidazole (0.35) [143]. For this reason RP170 has recently been labelled with ^{18}F (figure 1.13) for PET imaging, as it was thought that the lower lipophilicity of this tracer, relative to other nitroimidazole based tracers, may decrease its hepatic retention. In a preliminary clinical trial the main route of excretion was indeed shown to be through the kidneys, with the tracer demonstrating the capacity to delineate hypoxic lung tumours [144]. Liver uptake was initially high (~7 SUV) but decreased by ~50 % over the first 30 min. Accumulation of ^{18}F-FRP170 has subsequently been demonstrated in LAD occluded rat hearts by autoradiography, with increased retention in the left ventricular free wall, concurrent with increased ^{14}C-DG uptake, and decreased accumulation of the perfusion tracer 4-*N*-methyl-^{14}C-iodoantipyrine (IAP), and fatty acid metabolism tracer ^{125}I-BMIPP [113]. Further studies are warranted to characterise and validate the hypoxia selectivity of this tracer, and to assess its possible clinical application in cardiology because of these interesting and promising preliminary data.

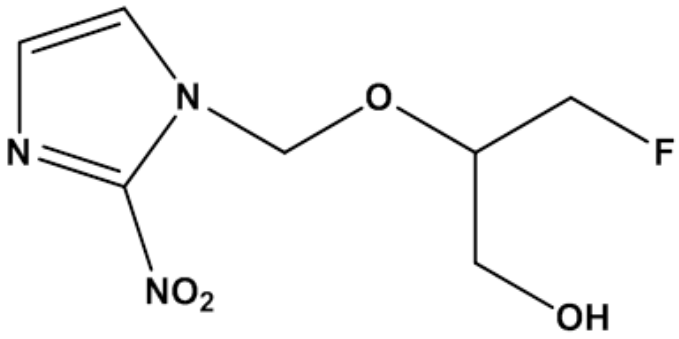

Figure 1.13. Structure of ^{18}F-1-(2-hydroxy-1-[hydroxyl-methyl]ethoxy)methyl-2-nitroimidazole (^{18}FRP170). Adapted from [143].

Other nitroimidazole based radiotracers that have been assessed as candidate hypoxia imaging tracers include; Radio-iodine [145]/ ^{18}F-labelled [146] -iodoazomycin arabinoside (I/FAZA), ^{18}F-FETNIM, ^{18}F-METRO [126] and ^{18}F-EF5 [147]. However at the time of writing these tracers have yet to be characterised in cardiac tissue.

1.7.3 Non- Nitroimidazole Tracers

1.7.3.1 ^{99m}Tc-HL91

4,9-diaza-3,3,10,10-tetramethyldodecan-2,11-dione dioxime (HL91), first reported in 1995, retains the ability to coordinate ^{99m}Tc but lacks a nitroimidazole moiety (figure 1.14) [148]. However despite this ^{99m}Tc-HL91 has demonstrated hypoxia selectivity.

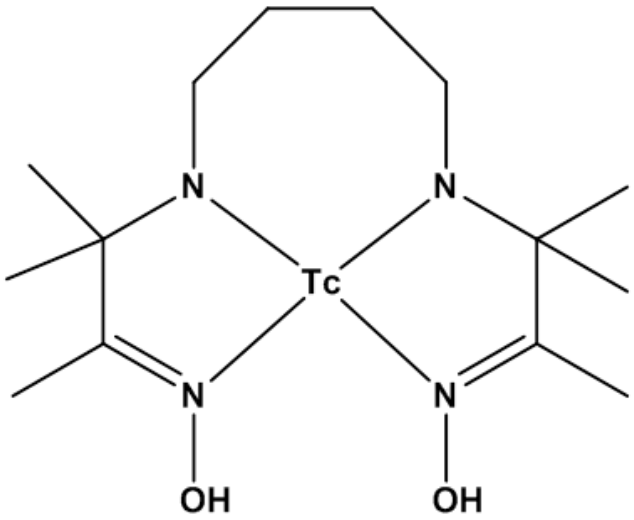

Figure 1.14. Structure of Tc-4,9-diaza-3,3,10,10-tetramethyldodecan-2,11-dione dioxime (HL91) (Tc-HL91) Adapted from [148].

The exact trapping mechanism for this tracer has yet to be established, and its evaluation has produced somewhat contradictory results. In isolated hearts, Okada *et al* demonstrated 7-fold and 1.4-fold increases in ^{99m}Tc-HL91 retention during low-flow

ischaemia (1/6th normal flow), and constant flow hypoxia (95% N_2/ 5% CO_2) respectively [149]. They also demonstrated low uptake in aerobic myocardium irreversibly injured by cyanide, implying that ischemia and/or low oxygen are responsible for tracer uptake rather than non-specific tissue injury [150]. Imahashi *et al* subsequently demonstrated ^{99m}Tc-HL91 uptake to be inversely proportional to perfusion buffer oxygen content with an almost 4-fold greater tracer retention at 0% O_2 [151].

The results of an initial *in vivo* imaging study by Okada *et al* were positive, with ^{99m}Tc-HL91 delineating regional myocardial ischemia in dogs within 15 minutes of tracer injection [152] (significantly faster than had been achieved with ^{18}FMISO and BMS181321). Fukuchi *et al* then compared ^{99m}Tc-HL91 uptake to that of the metabolic tracer ^{14}C-2-deoxyglucose (DG), using an ischaemia reperfusion model [153]. By performing autoradiography on myocardial tissue sections, they found that ^{99m}Tc-HL91 was unable to delineate the infarct zone, while ^{14}C-2-DG could. However they did observe a 4-fold increase in ^{99m}Tc-HL91 retention in the non-infarcted tissue that surrounded the infarct zone, which was considered to be at risk. This suggests that ^{99m}Tc-HL91 may have some application in identifying ischaemically compromised but viable cardiac tissue, but not infarcted tissue.

Subsequent *in vivo* evaluations of ^{99m}Tc-HL91 have been less promising. In LAD occluded pigs, greater than 95% stenosis resulted in significant hypokinesia and perfusion deficit, as demonstrated by ^{201}Tl scintigraphy. However there was no significant uptake of ^{99m}Tc-HL91 in the hearts of these animals [154]. While this study

did not confirm tissue hypoxia by any parallel means, the inability of ^{99m}Tc-HL91 to identify ischaemic tissue cast some doubt over its potential usefulness for clinical imaging. However despite this Yang *et al* conducted the first in patient trail of ^{99m}Tc-HL91 in 2008 [155]. Thirty three acute myocardial infarction patients received ^{99m}Tc-HL91, followed 3 h later by an injection of ^{201}Tl. Dual tracer SPECT was then performed. ^{99m}Tc-HL91 distribution was seen to be perfusion-dependent and also ischemia-sensitive. However significant background uptake was observed in normally perfused cardiac tissue and hepatic tissue, which meant that distinction between normal, ischemic/viable, or necrotic tissue could only be made with the aid of the additional information provided by the perfusion images.

In a recent study that was conducted by Liu *et al* using SPECT/ CT [156], the myocardial distribution of ^{99m}Tc-HL91 was compared to that of ^{99m}Tc-MIBI. This second patient study included forty one individuals suffering from coronary artery disease. Thirty five patients underwent ^{99m}Tc-MIBI perfusion imaging for 1.5 - 2 h followed four hours later by 3 h of ^{99m}Tc-HL91 SPECT. The remaining patients were not administered with ^{99m}Tc-MIBI, so that accumulation of ^{99m}Tc-HL91 could be quantified. The patients then underwent revascularisation surgery, which was followed up 3- 18 months later by ^{99m}Tc-MIBI perfusion imaging. When the quantitative method was employed an ischaemic to normal tissue ratio of 1.7: 1 was observed at 1 h post injection, increasing to 2.6: 1 at 3 and 4 h. Follow up ^{99m}Tc-MIBI scans demonstrated perfusion recovery in sixty six segments. In this study the authors did not report the direct effects of revascularisation therapy on the prognosis of the patients. They only discuss their data in

terms of the number of imaging segments with improved perfusion. Nevertheless this group have employed a protocol of combined ^{99m}Tc-MIBI and ^{99m}Tc-HL91 SPECT imaging to delineate ischaemic yet viable myocardium, with a desirable contrast between normal and ischaemic tissue. They then used this data to guide revascularisation surgery, which succeeded in improving cardiac perfusion. With respect to imaging the hypoxic or ischaemic myocardium, this work possibly represents the most successful *in vivo* pilot study of any hypoxia specific radiotracer to date.

1.7.4 Cu-Bis(thiosemicarbazone) Complexes

The carcinostatic and carcinolytic properties of bis(thiosemicarbazones) (BTSC) were first described by French and Freedlander in 1958 [157-158]. A number of publications then demonstrated increased antineoplastic activity of copper(II)-labelled bis(thiosemicarbazones) (Cu-BTSC) [159-161]. BTSC are neutral, lipophilic, square planar molecules, with an N_2S_2 coordination sphere through which they are able to form stable complexes with copper (figure 1.15).

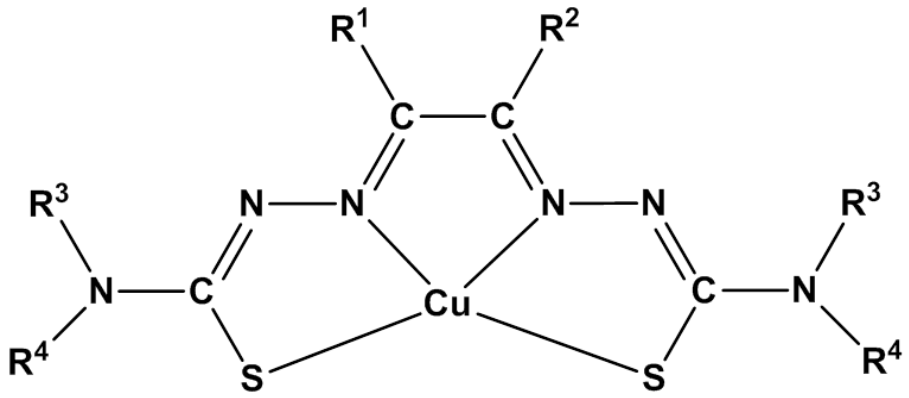

Figure 1.15. General structure of a Cu-bis(thiosemicarbazone) complex [162-163].

It is thought that as Cu-BTSC complexes are relative lipophilic, they are able to passively traverse the cell membrane into the cytoplasm, where the copper(II) moiety undergoes a one electron bioreduction [164-165] to form the anion Cu(I)-BTSC$^-$ [166-167], which is trapped within the cell due to its negative charge. Once reduced, the complex then either slowly dissociates or the copper moiety is removed by binding to intracellular macromolecules, through interactions with intracellular thiol groups [168-169] or complex I of the electron transport chain [165] (figure 1.16). This led to the proposal that it may be possible to use BTSCs labelled with radio-copper for *in vivo* imaging.

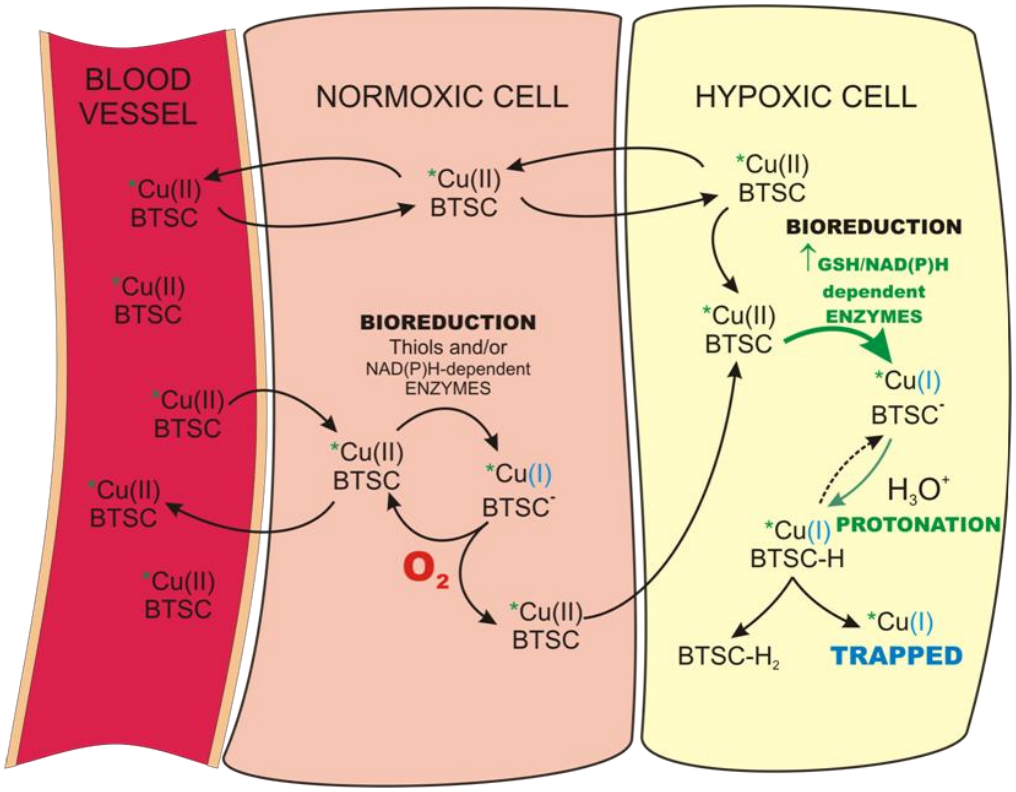

Figure 1.16. Proposed retention mechanism for Cu-BTSC complexes. Figure reproduced from [106].

Cu-pyruvaldehyde-bis-(N^4-methylthiosemicarbazone) (Cu-PTSM) (figure 1.17) was the first Cu-BTSC complex to be assessed as a PET imaging agent. Green *et al* reported that the complex was well retained in heart and brain tissue [73, 170]. Shelton *et al* then used Cu-PTSM for monitoring myocardial and renal blood flow [75-76]. Following this a study of seventeen ^{67}Cu-labelled BTSCs, conducted by John and Green, demonstrated that it was possible to alter the physiochemical properties of these complexes by altering the alkylation pattern at the R^1- R^4 groups [171]. They suggested that this could potentially improve the *in vivo* stability and pharmacokinetics of Cu-BTSC complexes, and lead to the development of better radiotracers.

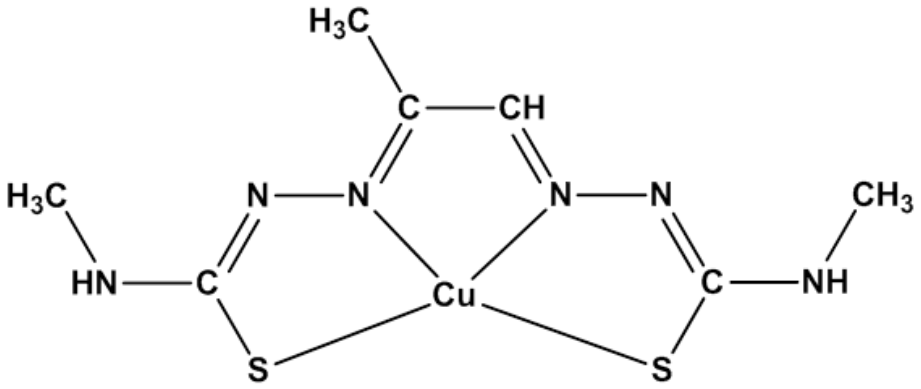

Figure 1.17. Structure of Cu-pyruvaldehyde-bis-(N4-methylthiosemicarbazone) (Cu-PTSM) [162-163].

Blower *et al* then suggested that Cu-BTSC complexes could be used as bifunctional chelators, to radiolabel biomolecules or other tracers with copper isotopes [172]. In an attempt to further decrease the redox potential compared to Cu-PTSM, Fujibayashi *et al* synthesised diacetyl-bis(N^4- methylthiosemicarbazone) (ATSM) (figure 1.18), by further methylation of the di-imine backbone of PTSM.

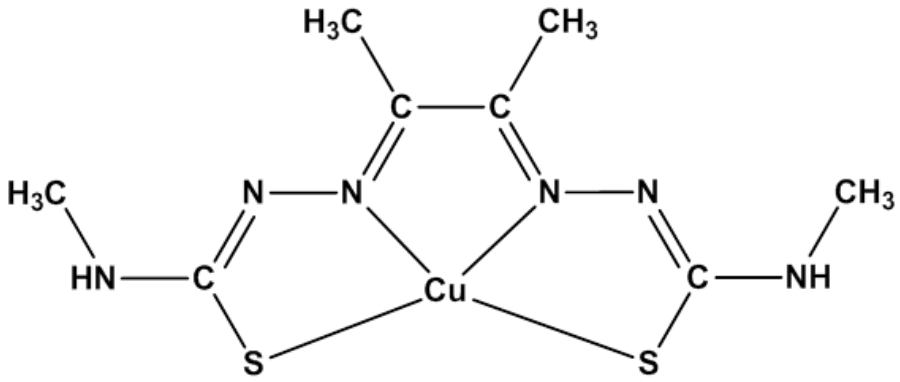

Figure 1.18. Structure of Cu-diacetyl-bis(N4- methylthiosemicarbazone) (Cu-ATSM) [162-163].

The addition of a methyl-group at the R^2 position did indeed lead to a decreased redox potential, from -208mV for Cu-PTSM [173], to -297mV for Cu-diacetyl bis(N4-methylthiosemicarbazone (Cu-ATSM) [174]. Dearling *et al* also observed this shift in redox potential, and reported values of -0.51 V for Cu-PTSM and -0.59 V for Cu-ATSM [167]. The difference in redox potential values obtained by these groups was probably because they used different reference electrodes for their experiments. The shift in redox potential compared to Cu(II)-PTSM, means that copper(II)-ATSM is more resistant to bioreduction, and also infers greater stability on the complex, once it is in the anionic form. In well oxygenated tissue bioreduction of Cu-ATSM does not lead to dissociation of the copper moiety, meaning that in the presence of oxygen it can be reoxidised back to the uncharged form which is then able to diffuse out of the cell, or become reduced once again. In hypoxic tissue however, reoxidation is less likely to take place and the complex dissociates or the copper moiety is removed by reactions with, as yet unidentified, intracellular macromolecules. It is the ability of Cu-ATSM to undergo reoxidation which is thought to imbue it with hypoxia specificity [174].

Copper radionuclides demonstrate a wide array of decay characteristics [172], and because of this radiocopper-ATSM has been intensely investigated in the field of oncology, both *in vitro* and *in vivo* as a diagnostic and prognostic indicator [167, 175-193], and as a therapeutic agent [194-198]. Cu-ATSM has also been assessed as a radiotracer for delineating cerebral ischaemia [199], and more recently as a means of assessing mitochondrial dysfunction and oxidative stress in patients with Parkinson's or Alzheimer's disease [200-201].

While radiocopper-ATSM has been widely investigated for application in oncology, only a limited number of articles have been published investigating its suitability as an agent for imaging cardiac hypoxia [174, 202-204]. Wada *et al* initially reported that at pharmacological concentrations Cu-ATSM exhibited superoxide dismutase-like properties, halving the amount of creatine kinase washing out of hearts, post-ischaemia-reperfusion injury [205]. The focus of this group then moved onto assessing Cu-ATSM as molecular probe for delineating hypoxic tissue. Fujibayashi *et al* observed 4-fold higher retention of ^{62}Cu-ATSM in isolated hearts that were perfused with hypoxic buffer, or subjected to low flow ischaemia, compared to hearts that were perfused with oxygenated buffer [174]. They demonstrated that tracer clearance from non-target tissue was rapid, and that retention of ^{62}Cu-ATSM was inversely related to the accumulation of the perfusion tracer ^{201}Tl. This provided the first evidence that Cu-ATSM was hypoxia selective, and that retention of this tracer in hypoxic tissue was not related to blood flow.

The accumulation of ^{64}Cu-ATSM in cardiac tissue was then assessed by Fujibayashi *et al* using *ex vivo* imaging [202]. Rats were subjected to acute LAD ligation and injected with ^{64}Cu-ATSM 10 min later. A bolus of ^{11}C-Acetate was administered after a further 9 min to delineate myocardial perfusion. Post-mortem autoradiographic imaging of the hearts from these animals, demonstrated that there was an inverse relationship between ^{11}C-acetate and ^{64}Cu-ATSM accumulation. When blood flow was reduced to 35- 40 % of normally perfused controls the retention of ^{64}Cu-ATSM began to decrease, and when the flow was reduced to 20 % or less no uptake was observed. As there was also no accumulation of ^{11}C-actetate in these areas, the authors suggested that the occlusion may have been too severe, and that blood flow could have been completely inhibited. However, areas surrounding the regions of zero flow demonstrated high uptake of ^{64}Cu-ATSM, suggesting that this tissue was ischaemic but viable.

The translation of Cu-ATSM to cardiac research then very rapidly moved to the clinical setting, due to the fact that the ^{62}Cu-ATSM had already been cleared for use in cancer patients [182]. Seven patients with coronary artery disease were assessed using ^{62}Cu-ATSM and ^{18}FDG PET [204]. Of these, six had prior infarcts but were clinically stable and the seventh had been diagnosed as having unstable angina. PET imaging demonstrated increased glucose metabolism in five patients, but increased ^{62}Cu-ATSM retention was only observed in the patient with unstable angina. The authors suggest that the lack of ^{62}Cu-ATSM uptake in the remaining patients, when ^{18}FDG uptake was observed, could be due to the fact that chronically hypoperfused myocardium was in a state of hibernation, and therefore the tissue may not have been hypoxic. They further

suggested that previous infarcts may have damaged the biological pathways required for ^{62}Cu-ATSM bioreductive trapping. They concluded that Cu-ATSM may not be useful for imaging the chronically ischaemic myocardium, but that it could potentially be used for delineating acute ischaemia. In terms of patient numbers this was a very limited trial, but it was still promising that ^{62}Cu-ATSM uptake was observed in one patient with unstable angina, and that this correlated with the accumulation of ^{18}FDG.

At the time of writing, Lewis *et al* were the last group to apply of Cu-ATSM PET to cardiac hypoxia imaging [203]. In this study systemic hypoxia, acute myocardial ischaemia, and demand ischaemia were initiated *in vivo* in a canine model. During systemic hypoxia, induced by inhalation of 90% N_2/ 10% O_2, the cardiac accumulation of ^{60}Cu-ATSM increased 2-fold. An increase in the average myocardial accumulation of Cu-ATSM was also observed in regions of the myocardium that had been made acutely ischaemic by LAD ligation. Significantly more $^{60, 61}$Cu-ATSM was detected in ischaemic but viable tissue compared to non-ischaemic regions, especially when the size of the infarct was considered by the authors to be relatively small. The third and perhaps most clinically relevant protocol was that which modelled demand ischaemia, initiated by LAD stenosis. This model represents the pathophysiology of ischaemic yet salvageable myocardium. The authors observed a contrast between normally perfused and ischaemic tissue. Moreover, kinetic modelling demonstrated that at just 13 min post-injection, the ratio of retention in ischaemic to normally perfused cardiac tissue was at least a 3:1.

Despite the very promising preliminary results, it has now been 10 years since Cu-ATSM was last investigated as a cardiac hypoxia imaging agent. This is mostly likely because hypoxia imaging *per se* has been perceived to have limited application in cardiology when compared with oncology, where hypoxia tracers show potential as diagnostic, prognostic, and therapeutic agents. However we would argue that hypoxia as a facet of ischaemia remains an important biomarker of cardiac pathology, which warrants further investigation and development. The initial patient study by Takahashi *et al* [204] may not at first appear to have been wholly successful. However it is important to remember that this was a small study, and six of the seven patients were considered clinically stable after myocardial infarction. It is therefore feasible that the infarcted tissue was necrotic, and unable to accumulate the tracer. It is also feasible that even though these patients had been diagnosed with coronary artery disease and demonstrated increased ^{18}FDG uptake, the remaining viable myocardium may not have been hypoperfused at the time of imaging and therefore not pathologically hypoxic. The data that was acquired from the single patient where increased ^{62}Cu-ATSM accumulation was observed, demonstrate the potential for using ^{62}Cu-ATSM PET to image transiently ischaemic viable myocardium. This is supported by the results from the third protocol described Lewis *et al*, where they initiated demand ischaemia by partial ligation of the LAD, and observed a contrast between ischaemic and normoxic tissue of ~3: 1 [203]. Finally, with the insight from the successful recent patient trial with ^{99m}Tc-HL91, we suggest that there is a need for a larger patient trial with Cu-ATSM, using ^{99m}Tc-MIBI as a comparative agent. ^{99m}Tc-MIBI would not only delineate myocardial perfusion, but as it accumulates within mitochondria to it may also be able to provide an index of mitochondrial function. The

mitochondrial electron transport chain has been implicated in the bioreductive trapping of Cu-ATSM [174, 195, 206]. ^{99m}Tc-MIBI could therefore be used to determine whether these bioreductive components are functional. We also suggest that such a trial must include CAD patients that have not suffered a heart attack, as these should present viable but salvageable myocardium.

These very promising results suggest that Cu-ATSM PET most certainly warrants further investigation, both in the research and clinical setting. Moreover Cu-ATSM is just one of a family of Cu-BTSC complexes that have already demonstrated some degree of hypoxia selectivity. However, to date none of the novel complexes that were reported by Dearling *et al* [162-163, 167], Blower *et al* [207] and McQuade *et al* [208], have been characterised in the heart. In fact with the exception of these early studies, the novel Cu-BTSC complexes described by these authors have not been investigated at all. It is logical that with so much attention having been paid to the 2-nitroimidazole based tracers, none of which has demonstrated any significant improvement over FMISO, the Cu-BTSC complexes should also be thoroughly investigated. A library of Cu-BTSC complexes was developed because further methylation of the ligand backbone of the PTSM, led to the development of the hypoxia specific complex Cu-ATSM. However it was noticed early on that Cu-ATSM is only retained in cells exposed to extreme hypoxia [167, 209], therefore a library of other BTSC ligands were synthesised with a range of redox potentials, and lipophilicities with a view to targeting cells subjected to less extreme levels of hypoxia. While the addition of longer alkyl chains at the R^1 and R^2 positions did little to affect the redox potential of the complexes [162], increasing their

molecular weight by varying the alkylation pattern at the R^3 position did alter their lipophilicity relative to Cu-ATSM. This could potentially affect the tissue accumulation of these complexes as well as the rate at which they elute from cells. This in turn would mean that they could potentially demonstrate higher uptake, or more rapid clearance from non-target tissue and blood, compared to Cu-ATSM. Our work will therefore focus on characterising the myocardial accumulation of the most promising Cu-BTSC complexes described by Dearling, Blower, McQuade, and their co-workers.

1.8 Aims of this Project

We have recently summarised what needs to be done to develop and validate the Cu-BTSCs for cardiac imaging application [106]:

- Further screening of the Cu-BTSC library
- Determine the effect of perfusion, oxygen, and acidosis
- Determine the site of intracellular reduction and bioreductants
- Determine the fate of radiocopper released from the complexes

The aim of this thesis was to build upon the structure activity work of Dearling, Lewis, Blower, McQuade *et al*, focusing on whether any of the novel Cu-BTSC complexes are suitable for cardiac imaging, or more specifically better than Cu-ATSM. For this purpose we have employed isolated cardiac myocytes and isolated perfused hearts, to screen and characterise the accumulation of Cu-BTSC complexes in oxygenated and hypoxic cardiac tissue. This necessitated the careful development and construction novel purpose built experimental apparatus, and its testing and calibration. The viability of isolated

myocytes and perfused hearts was also assessed, to confirm that the procedures used in this lab resulted in cells and organs that were fit for experimental purposes, before commencing screening the library of ^{64}Cu-BTSC complexes.

Chapter 2.

Development of an Isolated Ventricular Myocyte Assay for Screening Hypoxia Tracer Selectivity

2.1 Introduction

The first method that we planned to use in order to characterise our library of novel ^{64}Cu-BTSC complexes, was an isolated adult rat ventricular myocyte (ARVM) based screening assay. However before assessing the accumulation of ^{64}Cu-BTSC in ARVM, we first had to validate the adult rat ventricular myocyte (ARVM) isolation procedure. This involved monitoring the cells in culture, in terms of their viability and morphology, which was done in order to determine the optimum time-frame for their use. We then had to design, build, and characterise an incubation chamber that was suitable for maintaining ARVM cultures under oxygenated or hypoxic conditions.

2.1.1 Why use Adult Rat Ventricular Myocytes?

In vitro cultures of primary cardiac ventricular myocytes are been widely applied in cardiovascular research. They have been employed for the morphological, biochemical, biophysical, and molecular investigation of myocardial function at the cellular level [210-215], as well as for assessing the effects of pharmaceuticals and toxins [216]. ARVM based models have the advantage that they are uniform cell populations, free from the influence other cell types, neuronal or hormonal signalling, and can be maintained in a stable and controllable environment. Data from these types or experiments are therefore more likely to be reproducible, compared to those from isolated perfused hearts for example, as multiple conditions or replicates can be run in parallel. Finally, using ARVM based models may be more cost effective than *in vivo* or *ex vivo* methods, which often require one heart per condition or experiment.

Canavaugh first described a method for the isolation of cells from embryonic chick hearts in 1955 [217]. Although these cells were used initially, there was a need to isolate mammalian cardiac cells to more accurately model the human heart. In 1960 Harary and Farley reported the successful isolation of cells from neo-natal rat hearts. The focus then moved on to isolating cardiac myocytes from adult animals, this was first achieved by Kono in 1969 [218]. In the years following Kono's work, cardiac myocytes were successfully isolated from the hearts of numerous mammalian species including; rat [210-211, 218] rabbit [219], guinea pig [220], ferret [221] and more recently mouse [222]. Of all the species from which cardiac myocytes have been successfully isolated, the adult rat heart is perhaps the most widely employed. This is because the rat heart is of a convenient size for experimental purposes, and yields ~2- 5x 10^6 cells/ heart, with between ~70- 98 % intact rod shaped myocytes [211, 223-226]. Other factors which make the rat heart a popular choice include lower upkeep costs compared to larger mammals, and the wealth of experimental data available relating to the characterisation of this system.

A variety of cardiac myocyte preparations are available, these include neonatal, adult, and immortalised cells. There is a certain amount of debate amongst cardiac researchers as to which is the better preparation, but each has its advantages and disadvantages. Cardiac myocytes isolated from embryonic or neonatal hearts, are immature cells that have yet to fully differentiate. For this reason they tend to be used for studying the developing heart. Immature cells lose their characteristic rectangular or rod-shaped morphology once isolated, but they are more robust than adult myocytes and therefore

they endure the isolation process better. The robustness of immature cardiomyocytes compared to the fragility of adult cells, is highlighted by the gap of more than a decade between the first successful isolation of embryonic cardiomyocytes [217], and Kono's first successful isolation of adult cardiomyocytes [218]. Immature cardiomyocytes also undergo a small number of division cycles when initially placed in culture, which may somewhat increase the yield of cells and offset the relatively small size of these hearts. However the main advantage of using immature cells is their ability to spontaneously contract in culture. Their demand for nutrients and metabolites therefore more closely reflects the metabolism of cardiac myocytes *in vivo*.

Adult cardiac myocytes are large, rod-shaped, terminally differentiated cells that have ordered sarcomeres, and form strong interactions with other cardiac cells and the extra-cellular matrix. Adult cardiac myocytes cultured *in vitro* maintain their *in vivo* phenotype for up to two weeks. They are therefore considered by some to be a more accurate model of the mature myocardium. A distinct disadvantage to using adult cardiomyocytes is that healthy cells are essentially quiescent in culture and accordingly their demand for nutrients is not comparable with that of cardiomyocytes *in vivo*. They do however respond to externally applied electrical stimuli. Another disadvantage is that mature cells cannot proliferate, and therefore the number of cells is entirely limited by the efficiency of the isolation procedure.

Recently Claycomb *et al* have derived the immortalised cell line HL-91, from murine AT-1 tumours cells line [227]. In vitro these cells displays an organised sarcomeric

structure and spontaneous contraction, a phenotype that is sustained through serial passages. However this is a relatively new cell line that requires further characterisation, before it can be considered a suitable model for cardiac research. They therefore were not considered suitable for our studies.

The *in vitro* differentiation of human embryonic stem cells (hESC) into cardiomyocytes has been demonstrated by Kehat *et al* [228], and more recently by Zhu *et al* [229]. In the future these cells may prove useful as a model for cardiac research. They could also potentially be implanted into humans to repair damaged cardiac tissue. However at the present time the source of these cells is limited, and therefore it is unlikely that these cells will become a widely used research tool in the foreseeable future. Due to the difficulty in obtaining these cells, and because of the lack of data available for them, we did not consider them for use in our experiments.

Unless the focus of a particular area of research dictates that cells are obtained from a specific region of the heart, adult ventricular myocytes are most widely used for basic cardiac research. As digestion of the ventricles provides a uniform cell population, and yields the greatest number of myocytes, we employed ARVM throughout the cell based radiotracer characterisation experiments in this study.

2.1.2 Considerations of Ventricular Myocyte Isolation and Culture

Cardiac myocytes used in the first phase of this study were obtained from the ventricles of adult male Wistar rats. As discussed previously the isolation and culture of viable,

calcium tolerant ARVM has been refined over many years. It is therefore important to discuss some of the finer points of ARVM isolation, and culture techniques that we have incorporated into our own methodologies.

2.1.2.1 Tissue Disruption Methods

In vivo, mature cardiac myocyte form strong interactions with other cells and the extracellular matrix, which are difficult to disrupt. Early attempts to obtain isolated cardiac myocytes used mechanical means to dissociate cells, but this proved to be too harsh and compromised cell viability. Enzymatic digestion of tissue fragments is another method which is still used to isolate cells from embryonic or neo-natal hearts. This is because the small size of these organs makes them extremely difficult to cannulate for perfusion digestion. The problem with this approach is that the enzyme solution does not penetrate into the core of the tissue, which limits its efficiency. Wherever possible, retrograde perfusion of hearts in the Langendorff mode with a digestion solution is generally accepted to be the most efficient means of obtaining viable cardiac myocytes. A series of oxygenated solutions that contain EGTA and/ or collagenase are then perfused through the heart to breakdown the extracellular matrix. This is followed by mechanical tissue disruption, which usually involves cutting the heart into small pieces (~1mm), and then aspirating these numerous times using a Pasteur pipette to disperse the cells [211, 230-233].

2.1.2.2 Calcium Tolerance and Cell Substratum Attachment

Not only is the meticulous regulation of intracellular Ca^{2+} an integral component of the contraction-relaxation cycle, but Ca^{2+} is also instrumental to the formation of interactions between cells and with the extra-cellular matrix. A calcium free perfusion step is therefore incorporated into the isolation procedure, to reduce the extracellular Ca^{2+} concentration and weaken these interactions. At this point a metal chelator, such as EGTA, is often used to increase the efficiency of this process. However, reintroduction of Ca^{2+} at a physiological concentration may cause calcium overload, which can lead to massive cellular injury including myofibrillar hypercontraction, membrane disruption, and mitochondrial damage. This is accompanied by the release of intracellular enzymes, and changes in myocyte morphology, and can ultimately compromise cell viability. This process, which is known as the 'calcium paradox,' was possibly the most difficult obstacle for the pioneers of adult cardiomyocyte isolation to overcome [211, 234-236]. It is solved by the gradual repletion of Ca^{2+} in a step-wise manner to prevent overload, by allowing time for gap junctions to seal and the sarcolemma to repair.

In order to maintain viable cultures of ARVM for more than a few hours, the cells require a substratum to which they can attach [237]. Without this attachment myocytes enter "anoikis", which is a form of apoptosis that is initiated when normally adherent cells become detached from tissues of organs [238-239]. ARVM cannot form attachments to glass or plastic cultureware, so culture vessels have to be pre-coated with a protein based matrix such as laminin [219, 224].

2.1.3 Ultrastructure of the Cardiac Myocyte

As their name suggests cardiomyocytes (figure 2.1) are only found in the heart. They are shorter in length than skeletal myocytes and do not connect to bone. Cardiomyocytes also have gap junctions between the intercalated discs of individual cells, which allow the exchange of small molecules. Contraction of skeletal muscle is controlled by the somatic nervous system, whereas contraction of cardiac muscle is controlled automatically by the sinoatrial node [11, 240].

Although smaller than skeletal myocytes, cardiomyocytes are still relatively large cells. They contain an extensive network of myofibrils, which are organised into units called sarcomeres. The sarcomere is composed of a Z- disc at each end, to which the proteins CapZ and titin are attached, which respectively anchor actin and myosin to the Z-disc. Contraction occurs when myosin head units interacts with actin filaments, and pull the filaments towards the centre of the sarcomere [11, 240].

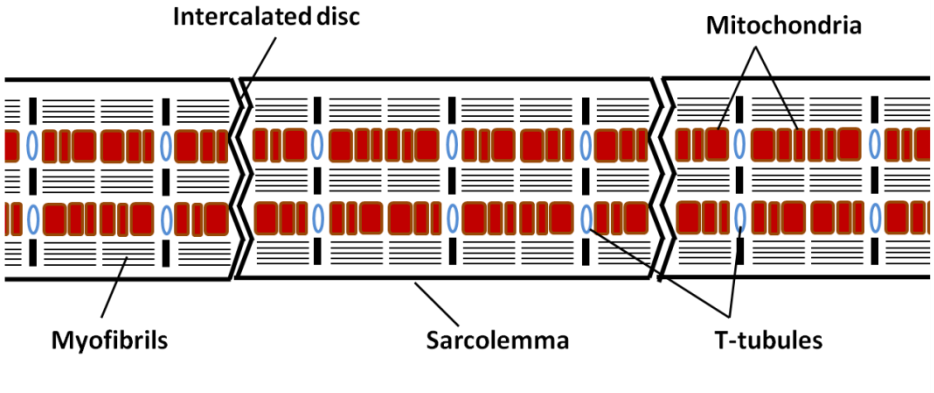

Figure 2.1. Schematic representation of a cardiac myocyte

The sarcolemma of cardiomyocytes is invaginated with a network of transverse (T) tubules. The T-Tubular network allows for more efficient delivery of oxygen, and other nutrients into the cytoplasm. This is achieved by decreasing the diffusion distance between the sarcolemma and cellular organelles. Cardiomyocytes also contain many flattened mitochondria that are located in close proximity to T-tubules, and an extensive sarcoplasmic reticulum that serves as a source and sink for Ca^{2+} [11, 240].

2.1.4 Incubating Cells in a Controlled Environment

2.1.4.1 Criteria for the Ideal Cell Incubation Chamber

The ideal incubation chamber for the studies that we envisage should be low cost and reusable. It should also be airtight, and have a small internal volume to allow for rapid gas exchange. The chamber should also have a gas line, as well as ports for the insertion of a pO_2 sensor, the addition of radiotracers, and for the removal of aliquots of culture medium. Furthermore the system must be temperature controlled so that cell cultures can be maintained at 37 ºC.

2.1.4.2 Why the need for a purpose built incubation chamber?

Incubating mammalian cells under hypoxic/ anoxic conditions is practically very difficult. Apart from the obvious difficulty of attaining and maintaining a steady state of hypoxia/ anoxia, there is the need to maintain an adequate temperature of 37ºC. The cells also have to be provided with sufficient medium and nutrients. While there are a number of commercially available pieces of apparatus that can be used to maintain cells in a hypoxic/ anoxic environment, none of them meet all of the criteria discussed previously.

This has lead several laboratories to develop their own apparatus for incubating cells under hypoxic/ anoxic conditions [162-163, 167, 241-242].

2.1.4.3 Methods and Apparatus for Hypoxic Cell Incubation

We will now discuss the methods/ apparatus that are currently available for maintain cells under hypoxic conditions, to highlight the current state of the art.

2.1.4.3.1 Hypoxic Solutions

One of the most basic methods used to attain a state of hypoxia is to use "hypoxic solutions" or "hypoxia bags", which contain an oxygen scavenger such as sodium dithionite. The problem with these approaches is that air tends to slowly diffuse in to the solution/ bag, and eventually saturate the oxygen scavenger. Oxygen then contaminates the system and causes a rise in pO_2. While these approaches are relatively cost effective, they are neither reliable nor reusable, and they do not have the capacity to regulate temperature. After careful consideration we decided that these methods were not appropriate for our study.

2.1.4.3.2 Hypoxia Chambers

There are a number of commercially available anaerobic/ hypoxia chambers. These are large sealed systems that have inbuilt gloves, to allow the manipulation of samples and equipment within the chamber. However because of their size this type of chamber takes a long time to purge of oxygen. Furthermore they do not have the capacity to maintain cultures at 37ºC. Some commercially available hypoxia chambers, such as the modular

incubation chamber (Billups-Rothenburg Inc.) [243] are designed to fit into standard lab incubators. These are airtight chambers, but the manufacturer reports that the lowest pO_2 that can be achieved is 35mmHg, which is much too high for the purpose of this study. Furthermore the chamber needs to be sealed, purged with the required gas mixture, and then remain unopened for the duration of the experiment. In addition this system does not have a dedicated tracer administration/ sampling port, only a gas inlet and outlet. We would therefore have to add our complexes to the culture medium before the system is sealed and equilibrated with the required gas mixture, to avoid the possibility of radioactivity being blown out as it is injected onto the cells. This would also make it practically difficult to acquire samples of culture medium or cells during an experiment. This approach was therefore also rejected.

2.1.4.3.3 Coverslip/ Thin Film Hypoxia

Coverslip hypoxia (CSH) is a novel *in vitro* method for studying the effect of hypoxia/ ischaemia [244-246]. Cells are grown on culture plates, and then coverslips are gently rested on top of them to create a thin film of medium between the culture vessel and the slip. The slip limits the diffusion of oxygen from the larger volume of medium which surrounds the covered area, whilst also limiting the diffusion of metabolic waste products from beneath the slip. This restricts the delivery of fresh medium and nutrients to cells, which generates a pseudo- ischaemic environment as the only point for nutrient and gas exchange is the small area around the edges of the slip. CSH is a relatively low cost, low-tech approach. Depending upon the size of the cells, the space between the cells and the coverslip is around 9.8μm [245], which means that it is not possible to measure the pO_2

of medium that is beneath the slip using commercially available oxygen sensors. Since this is a relatively new (2004) technique there is very little data available regarding its validation/ optimisation, and therefore it has yet to be widely adopted. It was however an interesting approach that we briefly considered. We performed a preliminary study to assess the accumulation of ^{18}FDG and ^{64}Cu-ATSM into hypoxic cells underneath the coverslip. Unfortunately we found that removal of the coverslip, which was necessary to wash off excess tracer in order to perform autoradiography, dislodged the majority of ARVM that were attached to the vessel. We therefore did not pursue this method any further.

Mineral oil suspended over culture medium to form an air tight film has also been used to maintain hypoxic environments [247-248]. With this approach the volume of medium is only restricted by the volume of the culture vessel. It would therefore in theory be possible to select a vessel that would hold sufficient medium, to allow the pO_2 to be measured using conventional oxygen probes. However we intended to use certified gas mixtures in order to generate oxygenated or hypoxic conditions, and we soon realised that the culture medium would have to be equilibrated before it was added to the ARVM cultures. This is because if the medium was gassed after plating the gas bubbles would agitated the cells and potentially cause them to detach from the culture vessel. This posed another practical problem, if we equilibrated the medium with gas before it was plated, it would be technically difficult to then plate the medium without exposing it to atmospheric oxygen. Furthermore, afterwards there would be no way of maintaining the medium pO_2. We therefore decided that this method was not suitable.

The thin film technique described by Koch [249] also seemed a potentially useful approach, as this method was employed by Martin *et al* for investigating ^{3}H-FMISO accumulation in cardiac myocytes [112]. In this technique cells are cultured on cover-slips which are then placed on a raised platform in the centre of a culture vessel. Enough medium is then added to the vessel so that the coverslip and cells are only slightly submerged by a thin film of medium. However unlike CSH the supply of nutrients and removal waste products is not restricted, because diffusion from or to the larger volume of medium beneath the slide can freely occur. The main advantage of this system is that the thin film allows for rapid gaseous exchange (~6 sec). This means that when cells are exposed to hypoxic condition less time is required to equilibrate the medium before adding the tracer, which decreases the potential damaging effects of incubating cells under this condition. However a disadvantage of this approach is that because the medium film is so thin, it would not possible to use an oxygen probe to measure the pO_2 of the culture medium to confirm that it is hypoxic. For these reasons this method was not employed.

2.1.4.4 Development of a Purpose-built Cell Incubation Chamber

After careful consideration of the commercially available equipment and techniques that have been previously used to study hypoxia in isolated cells, it was decided that none of these approaches fulfilled the criteria that we originally established. It was therefore necessary to develop a purpose built system ourselves. Our first crude prototype chamber was built from plastic kitchenware (figure 2.2). After finalising our design based on what we had learned for this prototype, We commissioned Labglass Ltd

(Cambridge, UK) [250] to manufacture our MKII incubation chamber (figure 2.3 and 2.4).

The prototype chamber system is shown in figure 2.2. The chamber was a plastic sandwich box into which ARVM cultures were placed. The lid of the box was pierced four times to accommodate a gas line inlet, a gas outlet, an injection port, and a pO_2 probe port. To ensure that the culture medium was warmed the incubation chamber was then placed into a water-bath set to 37 ºC, and weighed down do prevent movement. Gas was introduced into the system after first bubbling through a smaller plastic box containing water, which acted as a gas humidification chamber to prevent the culture medium from drying out.

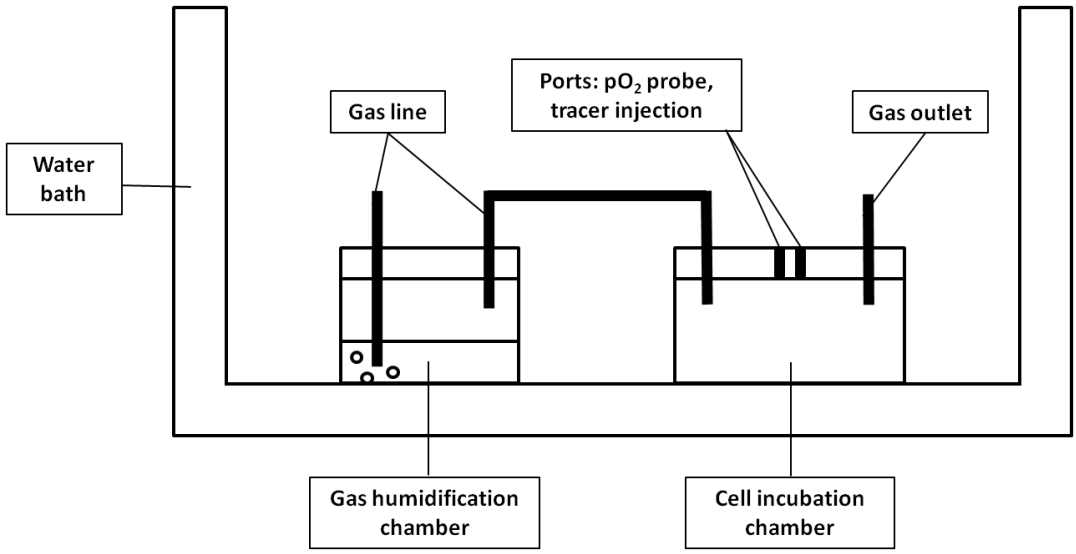

Figure 2.2. Schematic representation of prototype cell incubation chamber system.

A schematic representation of the MKII incubation chamber is shown in figure 2.3. This chamber had an internal diameter of 9.2 cm, and a depth of 6.0 cm. The internal and external walls and base of the chamber were moulded so that there was a hollow space between them, to allow the circulation of thermostatically warmed water via inlet and outlet ports. The top of the system was sealed with a large rubber bung with two pieces of steel tubing (5 mm diameter) inserted through it, to serve as a gas inlet, and outlet. A third plastic tube was inserted through the bung in order to accommodate a pO_2 probe, and also to serve as a sampling/ tracer injection port. A petroleum jelly based lubricant was often applied to the outer rim of the bung, to ease it's insertion into and removal from the chamber. This also helped form an airtight seal between the bung and the chamber, which was maintained by placing two lead weights on top of the bung once it was in position.

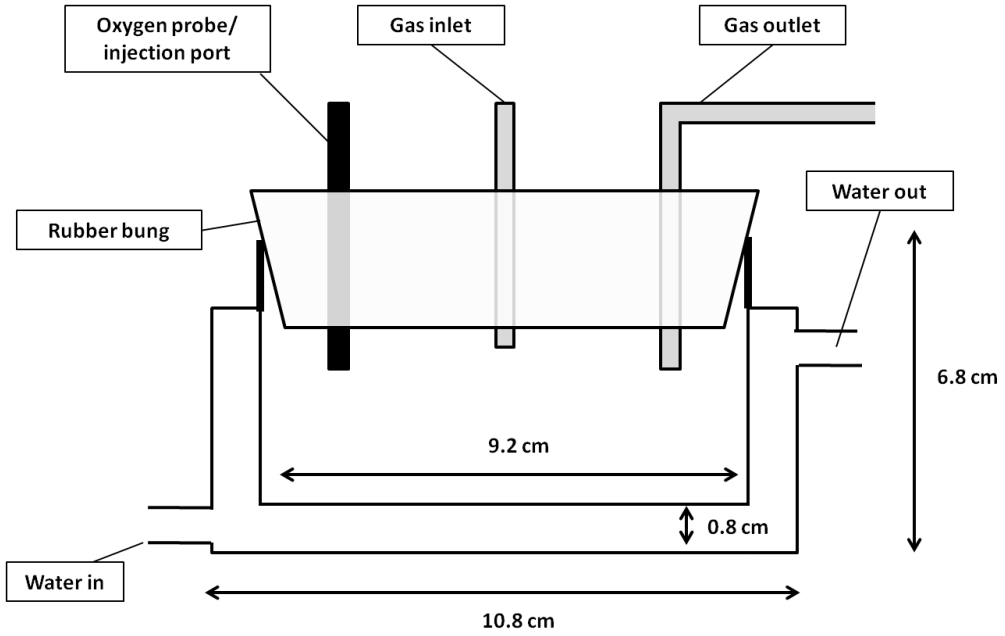

Figure 2.3. Schematic representation of MKII cell incubation chamber.

Figure 2.4 presents the completed MKII incubation chamber system. The chamber was positioned on top of a plate rocker, which was in turn was placed on top of a water heater/ circulator. Behind this equipment (not shown in figure) are two glass humidification chambers that were incorporated into the gas line. Gas flowed into the chamber via a heated gassing line, and out through a separate port. Although the system was always under positive pressure when gas was flowing through it, a tube led from the gas outlet port into a water filled flask to ensure that atmospheric air could not flow into the chamber via this port. A pO_2 probe and the Oxylab™ system are also shown in place.

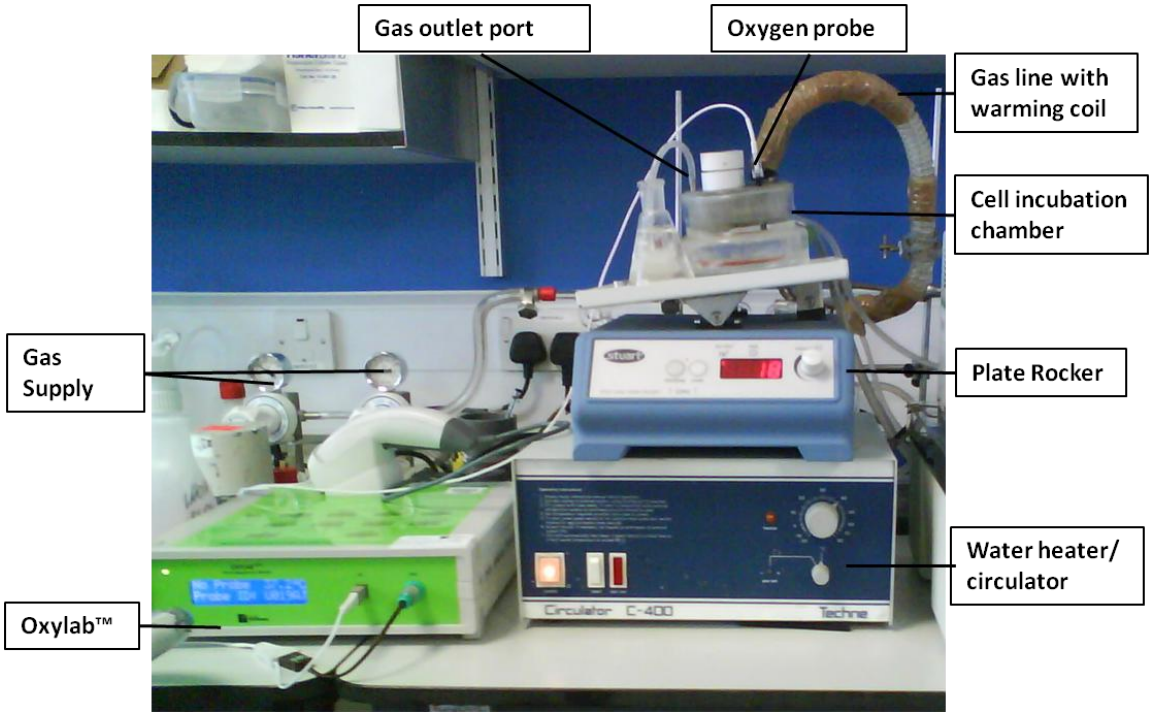

Figure 2.4. MKII cell incubation chamber system.

2.1.5 Aims

The aims of this part of the study were; (i) to assess the ARVM isolation procedure to ensure that cells were viable and to ascertain the optimum time-frame for using ARVM for experiments. (ii) to develop and characterise a cell incubation chamber that was able to maintain ARVM cultures, and fulfil the criteria that we set out in set out section 2.1.4.1. (iii) Determine the linear range of the laboratory gamma well counter in terms of its sensitivity for detecting the radiation emitted by ^{64}Cu.

2.2 Materials and Methods

2.2.1 Chemicals and Reagents

Unless stated otherwise all chemicals were of analytical grade and were purchased from Sigma-Aldrich (Poole, Dorset, UK).

2.2.2 Gas mixtures

All gas mixtures were purchased from BOC, UK. Specialist gas mixtures were certified by the manufacturer. Gas mixtures used for this series of experiments were: oxygenated (95 % O_2/ 5 % CO_2), and anoxic (95 % N_2/ 5 % CO_2).

2.2.3 ^{64}Cu production

^{64}Cu was kindly provided by Dr K. Shaw or Dr R. Paul, and was produced at the PET Imaging Centre, St. Thomas' Hospital, London, [251-252]. The concaved tip of a solid gold target was electroplated with enriched (~99%) ^{64}Ni. ^{64}Cu was generated using a CTI RDS 112 cyclotron, accelerating protons to 11MeV. The ^{64}Cu was then dissolved off of the target using 9 M HCl, and transferred to a column packed with AG1-8X anion exchange resin (Bio-Rad, UK) made up in 9 M HCl. ^{64}Cu was eluted from the column by titrating with HCl (9- 0.1 M), and the amount of radioactivity was measured using a dose calibrator (CRC-25R Capintec, USA). Co-impurities were removed in fractions just before the ^{64}Cu eluted from the column. Typically the fractions contained 1 M HCl.

2.2.3.1 Measurement of the Amount of Radioactivity in Radionuclide Stock Solutions

In all experiments where radioactive isotopes were used, a dose calibrator (CRC-25R Capintec, USA) was employed to measure the amount of radioactivity in the stock solutions. These stocks were always in excess of 20 MBq so that they could be accurately measured using the dose calibrator. The specific activity of the solutions was then calculated according to a known volume, and from this smaller aliquots were removed as necessary.

2.2.4 Isolation and Culture of Adult Rat Ventricular Myocytes

Table 2.1. Formulation of modified Tyrode stock solution.

Chemical	Mol. Wt	Concentration (mM)	Amount/ l
Sodium Chloride	58.44	130	7.6g
Potassium Chloride	74.55	5.4	0.4g
Magnesium Chloride 1M solution	95.21	1.4	1.4ml
Sodium Hydrogen Phosphate	142	0.4	0.06g
HEPES	283.3	4.2	1.2g
D-Glucose	180.16	10	1.8g
Taurine	125.1	20	2.5g
Creatine	131.1	10	1.3g

A stock solution of Tyrode's was made up according to Table 2.1, heated to 37 ºC and adjusted to pH 7.4 with 0.5 M NaOH. In order to accurately manipulate the Ca^{2+} concentration at each step of the isolation procedure, the Tyrode's stock solution was

split into 5x 50 ml aliquots and modified by adding or omitting $CaCl_2$, EGTA, or collagenase.

Mature ventricular myocytes were isolated from the hearts of male Wistar rats (220-240 g) (B&K Universal, U.K.) by enzymatic digestion, as described previously [233]. Briefly, rats were anaesthetised with sodium pentobarbitone (100 mg/ kg i.p.). Once the animal was sedated to the point that no reflex actions were observed, heparin (200IU) was injected into the femoral vein. The heart was then rapidly excised, immersed in ice cold Tyrode's stock solution containing 0.75 mM $CaCl_2$. Excess tissue was carefully removed and the heart was cannulated in the Langendorff mode. Hearts were then perfused at 37- 37.4 ºC as follows: (1) with modified Tyrode's solution containing 0.75 mM $CaCl_2$, for 4 min, (2) with nominally calcium-free modified Tyrode's solution containing 0.1 mM EGTA, for 4 min, and (3) with modified Tyrode's solution containing 0.1 mM $CaCl_2$ and 0.75 mg/ ml collagenase (Worthington Biochemical Corp. USA) for 7 min. All solutions were gassed with 100% O_2 and coronary flow rate was maintained at 8 ml/ min. Hearts were then cut down from the cannula, the atria were removed and the ventricles were chopped into ~1 mm pieces in modified Tyrode's solution containing 0.1 mM $CaCl_2$ and 0.75 mg/ ml collagenase. The tissue fragments were then gently gassed with 100% O_2 for ~15 min to facilitate cell dispersion before being allowed to settle iso-gravimetrically. The calcium concentration of modified Tyrode's solution was increased in two steps to 1 mM. Isolated myocytes were then washed with Medium 199 (M199) (Invitrogen, UK) containing penicillin (100IU/ml), streptomycin (100IU/ml), L-carnitine (2mM), creatine (5mM) and Taurine (5mM). Myocytes were then resuspended in 50 ml

M199 ready for plating on 90 mm Petri dishes pre-coated with laminin (15 µg/ ml) (Sigma- Aldrich, UK). Cells were allowed to settle and attach for two hours, after which the culture medium was removed along with dead/ unattached cells, and replenished with 10 ml fresh M199. Culture medium was changed before the start of each experiment, or every 24 h when experiments required that cells be maintained in culture.

2.2.5 Ventricular Myocyte Plating Density Study

Cell attachment is essential for maintaining ARVM in culture. The number of cells that can attach is therefore limited by the surface area of the culture vessel. To maximise the number of cells and to avoid wastage through plating at too high a density, a series of experiments were performed to ascertain the optimum volume for diluting ARVM suspensions prior to them being plated.

Freshly isolated calcium tolerant ARVM from one heart were suspended in 12 ml M199. 2 ml of the suspension was then diluted with various volumes of M199 (Table 2.2).

Table 2.2. Dilution volumes for ARVM plating study

Number of Plates coated	Volume of cell suspension (ml)	Volume of medium (ml)	Final Volume (ml)
1	2	0	2
2	2	2	4
3	2	4	6
4	2	6	8
5	2	8	10
6	2	10	12

In order to allow all of the dilutions to be made using myocytes from the same heart, the experiment was scaled from 6 to 24 well plates.

2.2.6 Quantification of Cell Numbers

In order to quantify the number of ARVM per culture well/ plate, a bright-field microscope fitted with an eyepiece mounted reticule (GX Optical, UK) was employed. In all cell based experiments the number of ARVM attached to culture vessels was estimated by counting the number of cells in a 1 mm grid that was etched onto the reticule. This was repeated multiple times and the cell number was calculated as:

Total cell number = cells counted x (area of plate (mm)/ area counted (mm)) *(Eqn 2.1)*

2.2.7 ARVM Cell Culture Stability Study

In order to monitor the characteristics of ARVM in culture, their cell number and morphology were recorded over seven days. This also served as a means of validating the quality of the ARVM used throughout the study in terms of cell number, and viability which is closely related to cell morphology.

Freshly isolated ARVM were diluted in 50 ml M199, and 2 ml of this suspension were then added to each well of a six well plate. Cell cultures were incubated at 37 ºC with 95 % air/ 5 % CO_2 for one week. Every 24 h the culture medium was replaced with fresh M199, before counting the number of rod-shaped, distorted rod-shaped, and rounded cells in each well.

2.2.8 Trypan Blue Viability Staining

Trypan Blue (Tetrasodium 3,3'-[(3,3'-dimethyl[1,1'-biphenyl]-4,4'-diyl)bis(azo)]bis[5-amino-4-hydroxynaphthalene-2,7-disulphonate]) is a commonly used vital staining method for assessing cell viability. Cells are exposed to Trypan Blue for usually no more than one minute. Trypan Blue cannot traverse the intact cell membrane of viable cells, and the dye therefore positively stains compromised/ dead cells.

Trypan Blue (Sigma, UK) was used to monitor cell viability over seven days. ARVM were cultured on 2x 12-well plates and each day three wells were used to assess cell viability. 10% Trypan blue was added to each well for 30 seconds the medium was then removed, and replaced with 500 µl of fresh M199. The cell numbers were then counted, and viability was calculated as the percentage of unstained (live) vs. stained (dead) cells.

2.2.9 MTT Assay for Assessing ARVM Viability

The 3-(4,5-Dimethyl-2-thiazolyl)-2,5-diphenyl-2H-tetrazolium bromide (MTT) assay was first described by Mossman (1983) [253]. It has previously been used to measure the activity of dehydrogenase enzymes [254], and to assess the metabolic activity and viability of many cell types, including cardiac myocytes [255-257]. We employed the assay to measure the metabolic status of ARVM over seven days, to determine the maximum length of time that ARVM cultures would remain fit for experimental use. The principal of the assay is that MTT, which forms a yellow solution when dissolved in water, is taken up by cells. In viable cells MTT is then reduced by intracellular NADH/ NADPH dependent reductases, to form 1-(4,5-Dimethylthiazol-2-yl)-3,5-

diphenylformazan **(**MTT formazan). MTT formazan is a purple solid that is insoluble in aqueous solutions, which causes it to precipitate and accumulate within cells. The purple solid can be dissolved using an organic or acidic solvent, which then elutes from cells. The solution is then collected, and the optical density measured at between 500 - 600nm. The relative absorbance can then be used to compare the viability of cells over time, as more metabolically active (viable) cells will reduce MTT at a faster rate than compromised or dead cells.

2.2.9.1 Assay Optimization

Before using the MTT assay to monitor cell viability the assay protocol was optimised to determine the most appropriate concentration of MTT and incubation time.

2.2.9.1.1 MTT Formazan Titration Curve

A titration curve was produced to convert the optical density of solutions containing MTT formazan to concentration.

A stock solution was prepared by dissolving 2mg/ ml MTT formazan in dimethyl sulfoxide (DMSO). From this stock solution a 1 in 2 dilution series was made from 0.5-$3x10^{-5}$ mg/ ml. 100 µl of each solution was added in triplicate to a 96 well plate and the optical absorbance at 570nm (Abs_{570nm}), was read on a multiwell plate reader (SpectraMax Plus, Molecular Devices, UK). The results were plotted as Abs_{570nm} vs. concentration. In all cell based experiments least squares regression was used to relate

the amount of MTT formazan produced per well. These data were then normalised, and expressed as the amount of MTT formazan (pg)/ cell.

2.2.9.1.2 MTT Assay Timescale Optimisation

To determine the optimum time for incubating ARVM with MTT cells were exposed to the compound for between 1- 5 h.

A stock solution was prepared by dissolving MTT (1mg/ ml) in PBS. MTT solution (20% v/v) was then added to ARVM cultures. At various times from 1-5 h the medium was removed and the cultures were washed once with PBS to remove excess medium. 120 µl of DMSO was then added to each well to dissolve the MTT formazan precipitate. The cells were incubated for a further 20 min to allow MTT to diffuse from the cells. After this the DMSO-MTT solution was removed and centrifuged at 2000g for 2 min, to pellet any contaminating cells. 100 µl of the supernatant was then removed from each well and the Abs_{570nm} was recorded.

2.2.9.1.3 Optimisation of MTT Concentration

ARVM were then incubated with various concentrations of MTT, to determine the optimum concentration to use in our experiments,

MTT was dissolved in H_2O to give a range of solutions from 0.25- 4 mg/ml. An aliquot of each was added to ARVM cultures (24 h after plating) at 20 % MTT solution per volume of medium, and the cultures were incubated for 2 h. Each well was then washed

once with PBS, before 120 µl of DMSO was added. The cells were incubated for a further 20 min to allow MTT to diffuse from the cells. After this the DMSO-MTT solution was removed and centrifuged at 2000g for 2 min. 100 µl of the supernatant was then removed from each well, and the Abs_{570nm} measured.

2.2.10 ARVM Viability Assessed by MTT Assay

To determine the optimum time for using ARVM cultures, cell viability was assessed over seven days using the fully optimised MTT assay protocol that we established above.

Freshly isolated ARVM were cultured on 12 well plates as above. To start the assay 20 % (v/v) MTT in PBS (1mg/ ml) was added to three wells. The cells were then incubated at 37ºC 95 % air/ 5% CO_2 for 1 h. After this period the culture medium was removed, and the cells were washed once with PBS. 200 µl DMSO was then added to each well to dissolve MTT formazan precipitate. After 20 min the DMSO-MTT formazan solution was removed and centrifuged at 2000g for 2 min to remove cells. 150 µl of the DMSO-MTT formazan solution was then removed, and the amount of MTT formazan in the solution was determined as described above. The assay was repeated every 24 h for 7 days.

2.2.11 Rapid Attachment versus Suspension ARVM Culture

In order to maintain viable ARVM cultures for more than a few hours, cardiac myocytes must be allowed to attach to the surface of their culture vessel. However this limits the

number of cells that can be maintained in that vessel. This is problematic because if there are not enough cells in the vessel, the amount of radiotracer that is extracted from the medium by cells may not be sufficient for quantifying by gamma well counting. In an attempt to maximise the number of cells a feasibility study was conducted, to determine whether it would be possible to use ARVM cultured in suspension. In order to ascertain the time frame over which ARVM remain viable when kept in suspension, a comparison was made between cells which had been plated as normal, and cells which had been maintained in suspension for 1- 5 h.

ARVM were isolated as in section 2.2.4 and diluted with 50 ml M199. They were then divided into two lots. Half of the cells were plated immediately, and the remaining cells were incubated in suspension at 37ºC 95 % air/ 5% CO_2, for between 1- 5 h. Every 60 min triplicate aliquots of cells from the suspension culture were plated, and allowed to attach as normal. After being incubated for 2 h to allow cells to attach the cell numbers were recorded, and the MTT assay was used to assess their viability.

2.2.12 Calibration of Cell Incubation Chamber

2.2.12.1 pO_2 and Temperature Measurement

During the course of each experiment it was necessary to measure both the pO_2 and temperature of the cell culture medium. This was done in order to confirm that the culture conditions were oxygenated or hypoxic/ anoxic. For this purpose an OxyLab pO_2™ system coupled with a combined pO_2-temperature sensor (BF/OT/E) (Oxford Optronix, Oxford, UK) was employed [54]. This system is designed to function under

physiological conditions and has been applied in oncology, stroke research, and organ transplantation. The system uses fibre-optic sensors tipped with a fluorescent dye, which sends a photon signal to the main instrument controller. The fluorophore signal is quenched by molecular oxygen, and therefore the strength of the signal is inversely proportion to the level of oxygen. This means the accuracy of the Oxylab pO_2™ increases as the level of oxygen decreases, unlike traditional oxygen probes such as the Clarke type oxygen sensor, which consume oxygen and therefore lose accuracy at low pO_2. The sensors used by the Oxylab pO_2™ are also much smaller than the Clarke electrode, and therefore more amenable to use in low volumes of liquid. On their website the manufacturer stipulates that OxyLab pO_2™ and the sensors that are used with it accurately measure pO_2 in the range 0- 100 mmHg, as the fluorophore is totally quenched above this level of oxygen. However in a personal communication with a representative of the company, they suggested that the equipment could measure up to 150 mmHg, but the error may be as much as ± 15 %. This unfortunately meant that it was not possible to obtain measurements of pO_2 with this system when using a 95% O_2/ 5% CO_2 gas mixture. However because 95% oxygen is much greater than that of atmospheric O_2 (21%), we assumed that all media and buffers were maximally oxygenated under this condition.

2.2.12.2 Calibration of Incubation Chamber Temperature and pO_2

Before the MKII incubation chamber was used a series of calibration experiments were performed, to determine the time required for the pO_2 to fall below 0.8 mmHg in the medium. In previous studies this threshold has resulted in the most significant

accumulation of ^{64}Cu-ATSM [209]. The time taken for the temperature of the culture medium to reach 37°C was also ascertained.

A Petri dish containing ARVM and 10 ml medium was placed inside the chamber. The chamber was then sealed and gently gassed with 95% N_2/ 5% CO_2 until the pO_2 of the culture medium reached 0.8mmHg. Temperature and pO_2 were recorded using an OxyLab pO_2™ coupled with a combined pO_2/ temperature sensor (Oxford Optronix, Oxford, UK).

2.2.13 Universal Gamma Counter Linearity

Before embarking on a series of experiments to assess the accumulation of ^{64}Cu-ATSM in ARVM, it was necessary to determine the sensitivity and linear range of the universal gamma counter (1282 Compugamma, LKB Wallac, Australia). This equipment was to be used to measure the amount of radioactivity within ARVM cell pellets. By determining the counts per minute (cpm) emitted by a given amount of ^{64}Cu, it would enable us to accurately convert this to the amount of radioactivity associated with the cell pellets from our experiments. Furthermore the data from this study were also used to determine how much radioactivity was required for our cell based experiments. This ensured that the amount of radioactivity within the pellets was detectable, whilst also ensuring that the cpm did not exceed the upper limit of the gamma counter.

2 MBq was removed from a stock solution of $^{64}CuCl_2$ (aq) containing 20 MBq, the volume was adjusted to 200 µl, and a 1 in 2 dilution series was performed with a range

from 9.5 $x10^{-7}$ to 1.0 MBq per vial. The radioactive decay (cpm) was then measured using the universal gamma counter. The results were plotted as KBq vs. cpm, which allowed the conversion of cpm to Bq using least squares regression.

2.3 Results

2.3.1 Determine Optimal ARVM Culture Conditions

2.3.1.1 ARVM Plating Density Study

Results of the ARVM plating density study are shown in figure 2.5. The dilution series produced a bell shaped distribution. The maximum average number of rod-shaped ARVM was observed using a 1 in 4 dilution of cell suspension to M199. This dilution was therefore used for all subsequent experiments in this section.

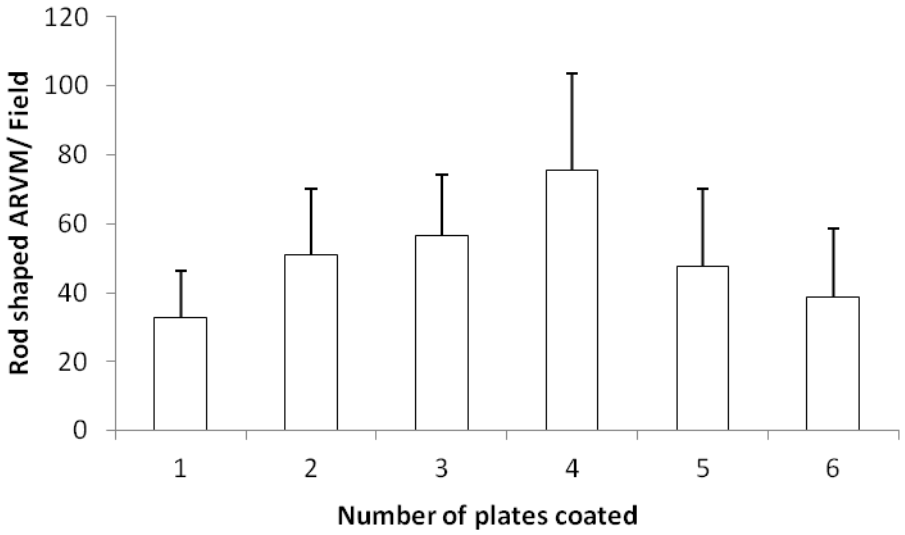

Figure 2.5. Number of rod shaped ARVM per field. A dilution series of ARVM was used to determine the titre, which resulted in attachment of the highest number of rod-shaped ARVM. Data represent mean (n= 3) ± SD.

2.3.1.2 ARVM Cell Number and Morphology over Time

The changes in ARVM cell number and morphology over a seven day period are shown in figure 2.6. On day 0 the average number of ARVM per well was: Rod-shaped (27764 ± 3371), distorted rods (1435 ± 566) and rounded (5840 ± 2594). On day 1 the cell numbers remained similar to day 0, with: rod-shaped (27406 ± 3376), distorted rods (3329 ± 824) and rounded (6098 ± 3049). However by day 2 the number of rod-shaped ARVM had decreased by 23 % (21531 ± 4487) compared to day 0. Up to day 7 the number of rod-shaped cells/ well continued to decrease to 3576 ± 1158. Conversely the number of distorted and rounded cells increased to 7744 ± 1549 and 6736 ± 1549 cell/ well respectively.

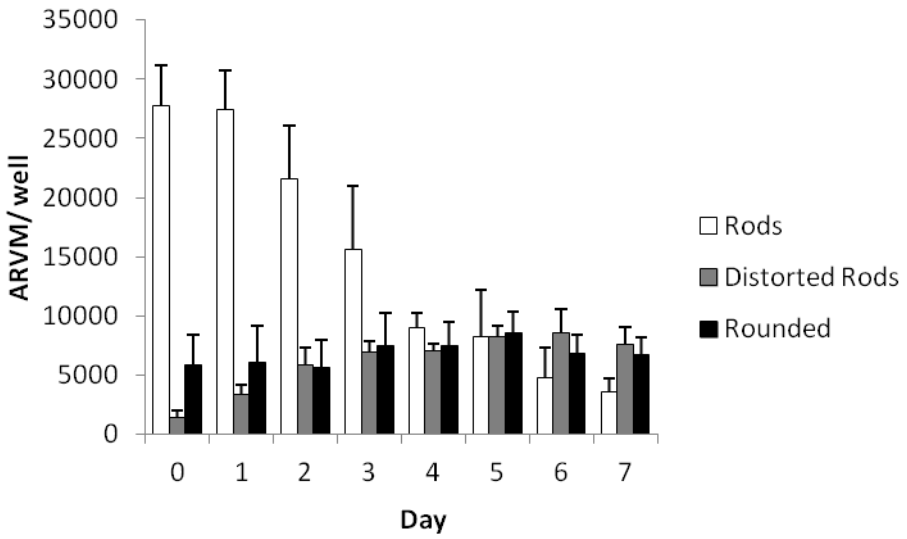

Figure 2.6. Number of ARVM and cell morphology over seven days. Data represent mean (n = 3) ± SD.

On day one rod- shaped ARVM comprised on average 80.0 ± 8.0 % of the total cell population, distorted rods represented 4.1 ± 3.2 %, and rounded cells 16.2 ± 7.2 % (figure 2.7). Throughout the experiment the number of rod shaped ARVM declined steadily, falling to 18.5 ± 11.23 % on day 7. Conversely the number of distorted rods increased to 43.2 ± 13.6 % over the same time. The number of rounded cells remained constant at 16% between days 0- 2, but increased to 25.9 ± 10.9% on day 3 and continued to rise to 38.0 ± 11.3 % of the total cell population by day 7. By day 7 the total number of cells/ well had decreased to 51% of the day 0 counts but the number of rod shaped ARVM had decreased by 77 %.

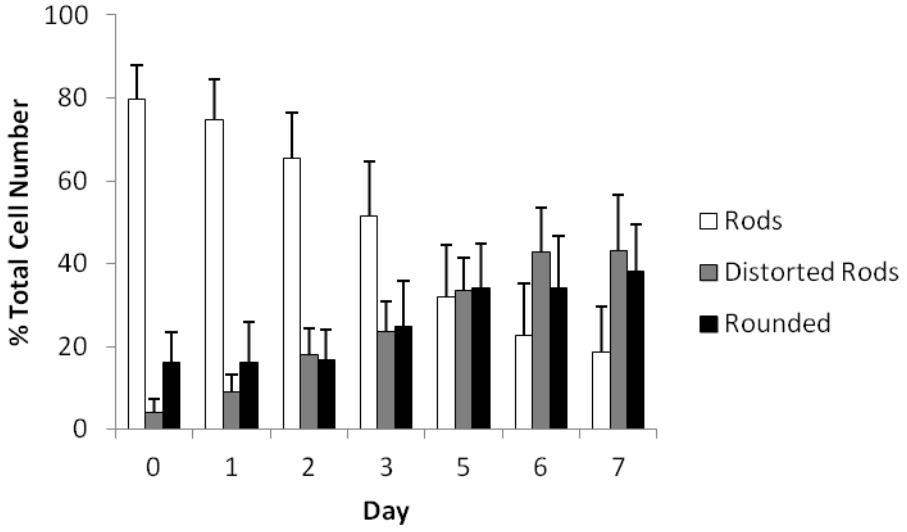

Figure 2.7. Cell morphology over seven days, expressed as a percentage of the total cell population. Data represent mean (n = 3) ± SD.

2.3.1.3 Cardiac Myocyte Images

Images of ARVM cultures were acquired using bright-field microscopy at x10 and x40 objective magnification (figure 2.8). The number of cells can be seen to decrease each day, with their morphology gradually changing from the distinctive rod-shape of cardiac myocytes *in vivo*, to distorted or rounded cells.

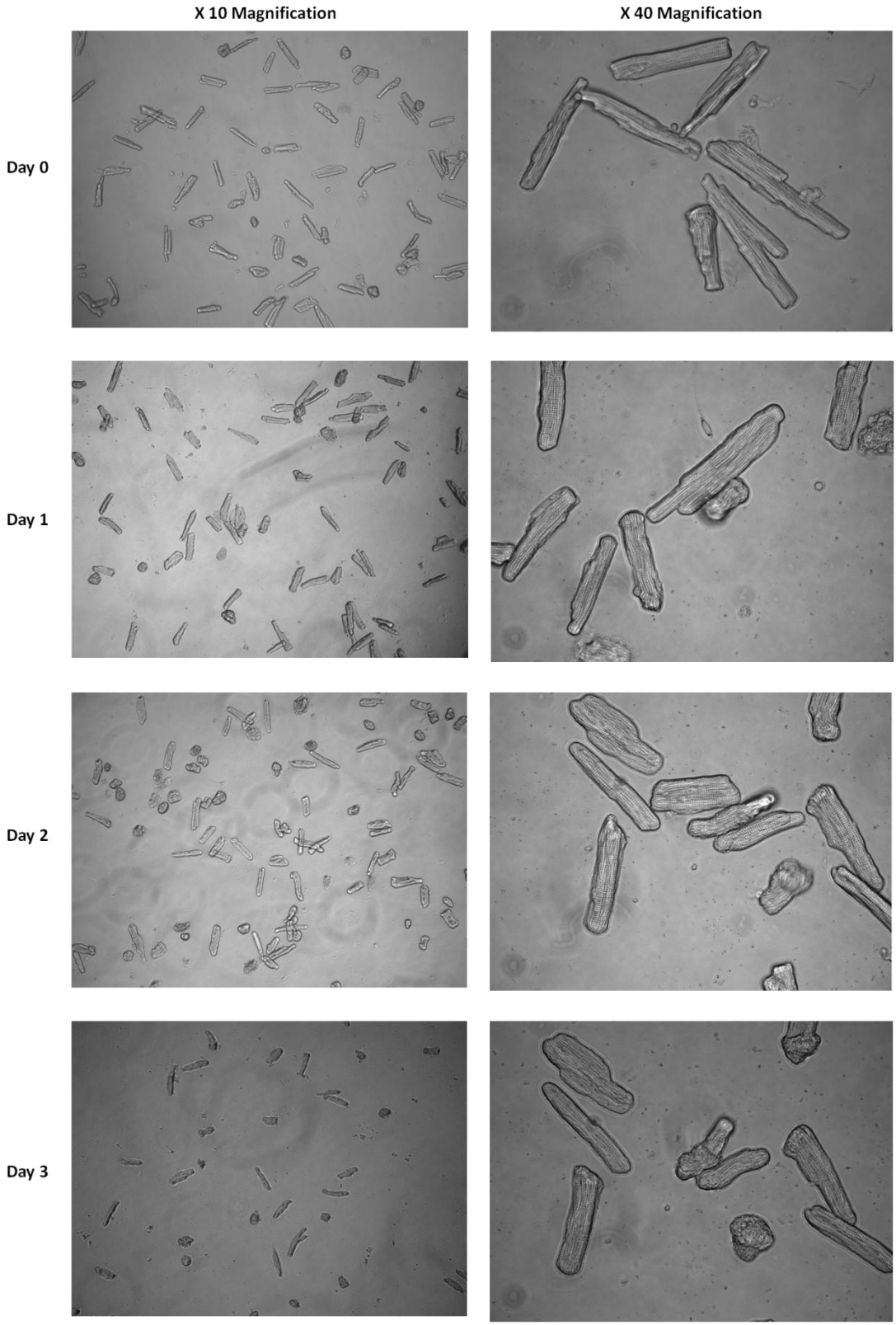

Figure 2.8. Bright-field microscopy images of ARVM, x10 and x40 objective magnification. Images were taken every 24 h for 4 days.

2.3.1.4 ARVM Viability over time Trypan Blue Viability

The percentage of viable cells on day 0 was on average 83.8 ± 6.6 %, which increased steadily to a maximum of 97.0 ± 5.6 % on day 4 before declining to 87.4 ± 18.3 on day 7 (figure 2.9).

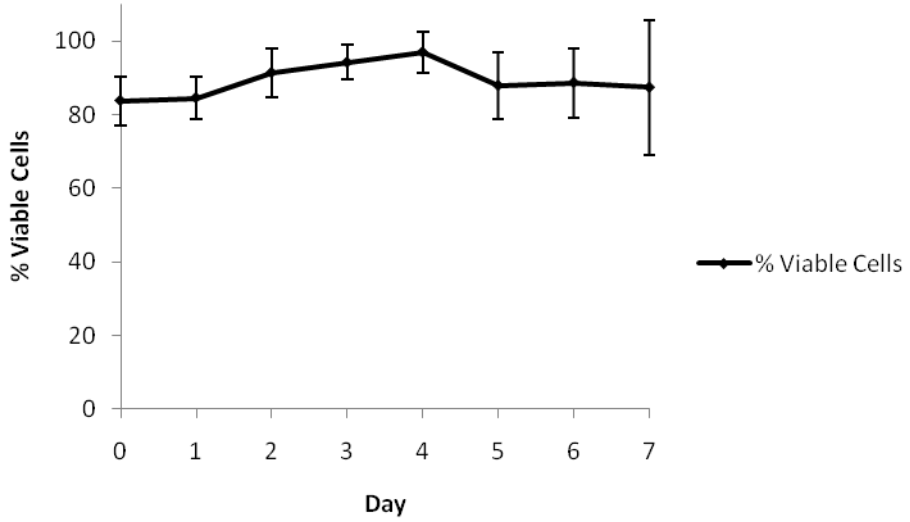

Figure 2.9. Viability of ARVM cultures over seven days, assess by Trypan Blue exclusion. Data represent mean (n = 3) ± SD.

On day 0, 19.2 ± 18.8 % of the rounded cell population were capable of excluding Trypan Blue. This increased to 88.4 ± 20.7 % on day 4, before declining to 70.9 ± 27.1 % on day 7 (figure 2.10).

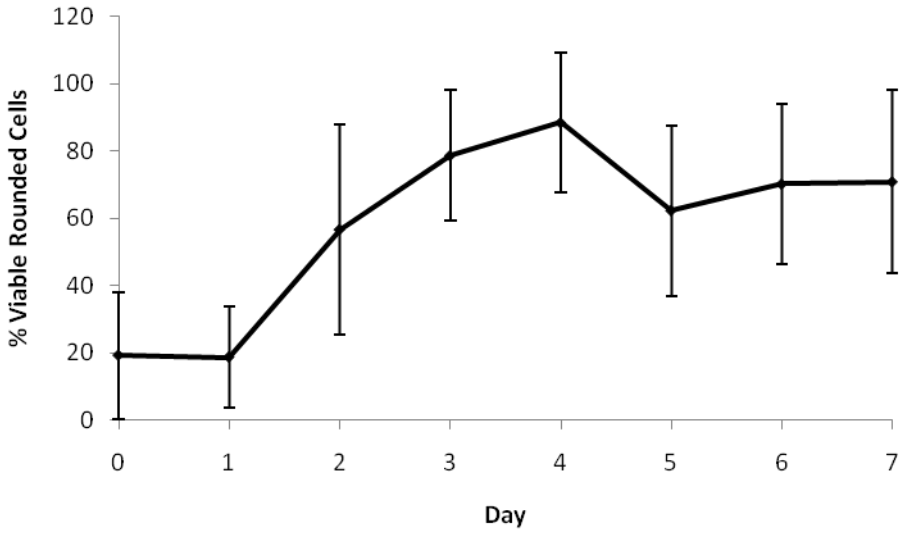

Figure 2.10. Percentage of viable rounded ARVM over seven days. Assessed by Trypan Blue exclusion. Data represent mean (n = 3) ± SD.

2.3.1.5 MTT Assay Optimisation

2.3.1.5.1 MTT Formazan Titration Curve

The concentration titration curves (figure 2.11) demonstrate that the relationship between the concentration of MTT and Abs_{570nm} remained linear between 0.09-3.03 (R^2 = 0.9984). This represented a concentration range of 7.8 x 10^2- 5 x 10^4 ng/ well of MTT formazan.

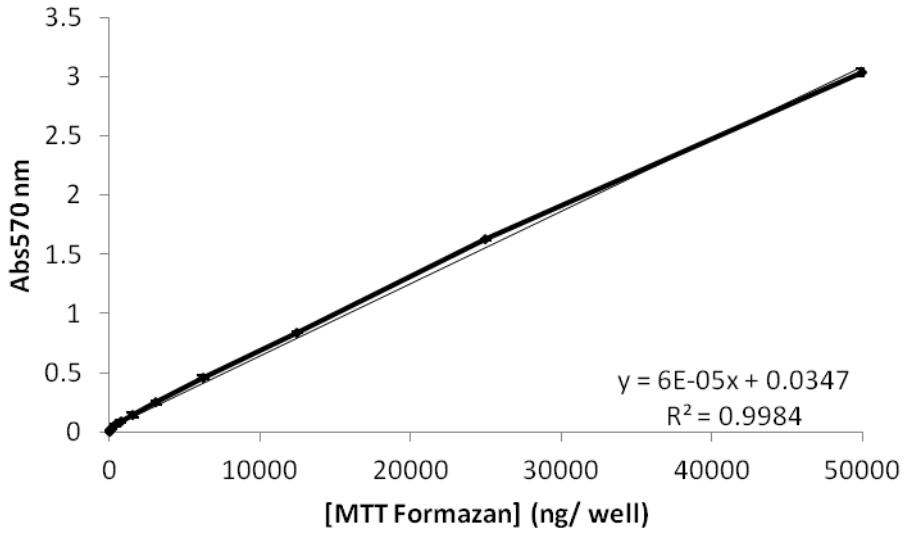

Figure 2.11. MTT formazan titration curve. Relationship between the concentration of MTT formazan (ng/ well) and Abs_{570nm}, 0 – 5.0 x 10^4 ng/ well. Data represent mean (n = 3) ± SD.

2.3.1.5.2 Optimisation of MTT Incubation Time

Experiments to ascertain the optimum time for incubating ARVM with MTT, initially demonstrated that a 3 h incubation period would be optimal (figure 2.12). However during these experiments it was noticed that from 2 h onwards, a proportion of viable rod-shaped ARVM had become detached from the laminin substratum. This was most likely due to the intracellular precipitation of formazan crystals.

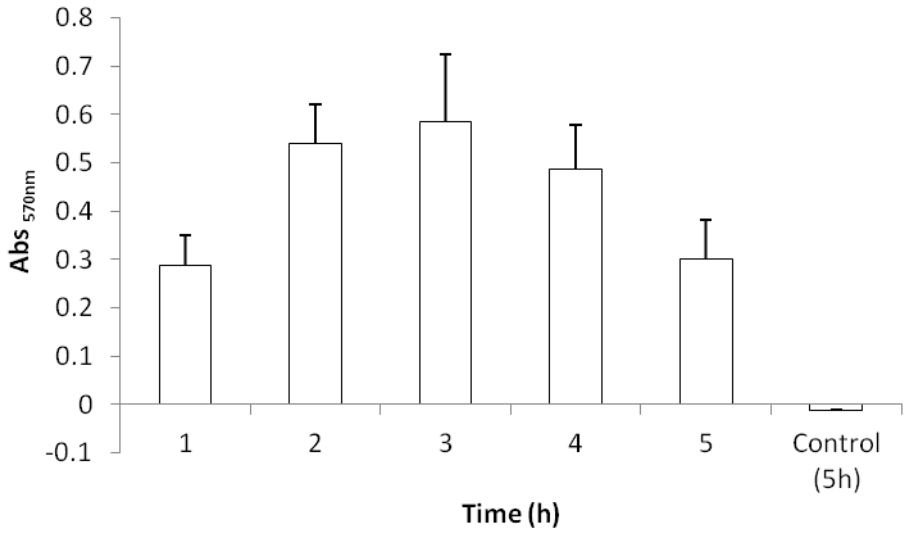

Figure 2.12. Optimisation of MTT incubation time. Abs_{570nm} versus the amount of time that ARVM cultures were exposed to 20 % (v/v) MTT 1 mg/ ml. Data represent mean (n = 3) ± SD.

2.3.1.5.3 Optimisation of MTT Concentration

By screening a range of solutions which contained various concentration of MTT (0.25-4.0 mg/ ml), we determined that a 1 mg/ ml MTT stock provided the highest average Abs_{570nm} after 1 hr (figure 2.13). At concentrations of MTT greater than 1mg/ ml ARVM began to detach from the surface of the culture vessel.

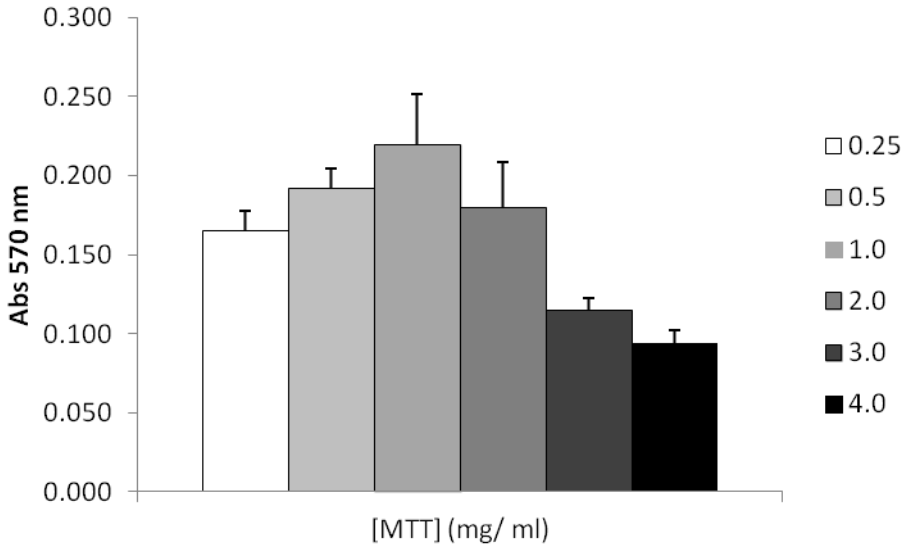

Figure 2.13. Optimisation of MTT concentration, $Abs_{570\ nm}$ versus MTT stock concentration. Data represent mean (n = 3) ± SD.

2.3.1.5.4 Assessment of ARVM Viability over Time Using the MTT Assay

The MTT assay was used to assess the viability of ARVM on each day, over 5 day period (figure 2.14). The results show the capacity of the cells to convert MTT to MTT formazan. The average amount of MTT formazan associated with each cell on day 0 was 299.3 ± 92.2 pg/ cell. By day 1 this decreased to 265.0 ± 51.3 pg/ cell. MTT Formazan production continued to decrease throughout the experiment with an average of only 92.8 ± 33.0 pg/ cell observed on day 4. The experiment was terminated on day 5 because all of the cells detached from the culture vessel. This presumably occurred because the cells were no longer able to tolerate exposure to MTT or the MTT formazan precipitate.

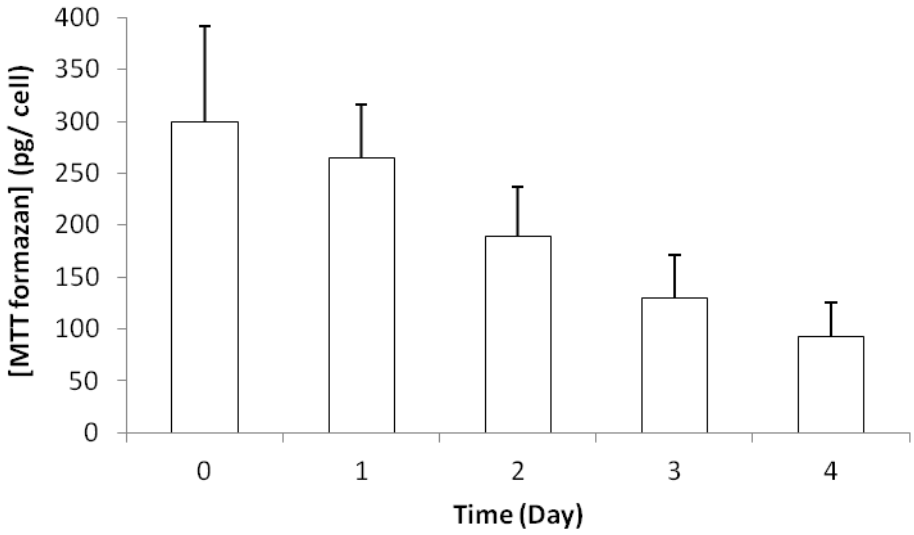

Figure 2.14. MTT Formazan production per ARVM. Optimised MTT assay was performed on separate cell cultures each day for 5 days. Data represent mean (n = 4) ± SD.

2.3.1.6 Static versus Suspension Culture of ARVM

2.3.1.6.1 Comparison of Viability using the MTT Assay

A comparison was made between cells that were cultured as normal, and cells that were maintained in a suspension of M199 for 1- 5 h and then plated. This was done in order to assess the feasibility of performing radiotracer accumulation studies, using ARVM in a suspension of M199. At all time points the ability of cells that were kept in suspension to convert MTT to MTT formazan, was comparable to cells that were plated immediately (figure 2.15).

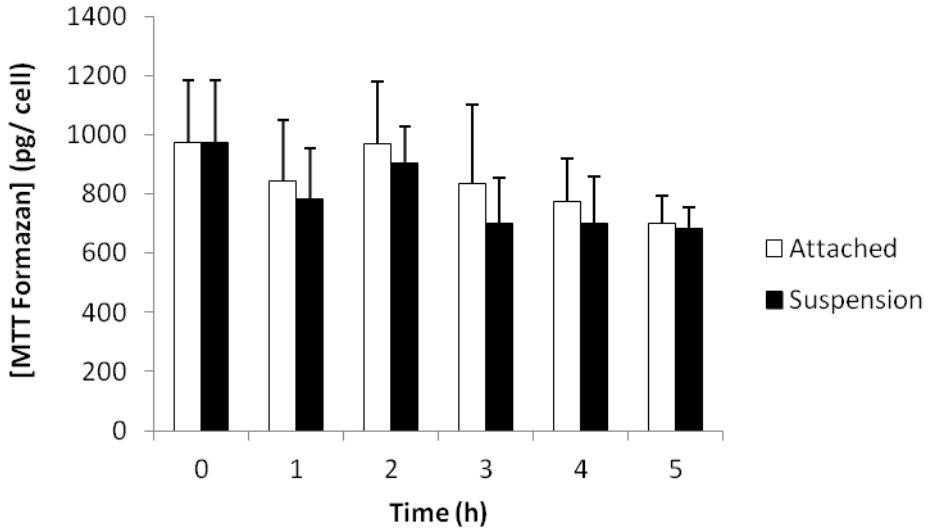

Figure 2.15. MTT Assay Attached versus suspension cells. Comparison between the reduction of MTT to the formazan product by ARVM. Cells were either plated immediately or kept in suspension for between 1-5 h and then plated. Data represent mean (n = 3) ± SD.

2.3.1.6.2 Comparison of Cell Numbers

Over 5 h the number of cells in the control group decreased from an average of 1.08 x 10^4 ± 1.78 x10^3 cells/ well, to 8.67 x 10^3 ± 5.35 x 10^2 cells/ well. However cells that were kept in suspension gradually lost their ability to attach to the laminin substratum. After 1 h in suspension the number of cells that attached was 7.5 x 10^3 ± 1.36 x 10^3 cell/ well, much lower than the control group numbers at 5 h. After 5 h in suspension only 4.0 x 10^3 ± 1.30 x 10^3 cells/well were observed. Throughout these experiments the number of unstained (dead) cells remained reasonably constant for each condition (figure 2.16).

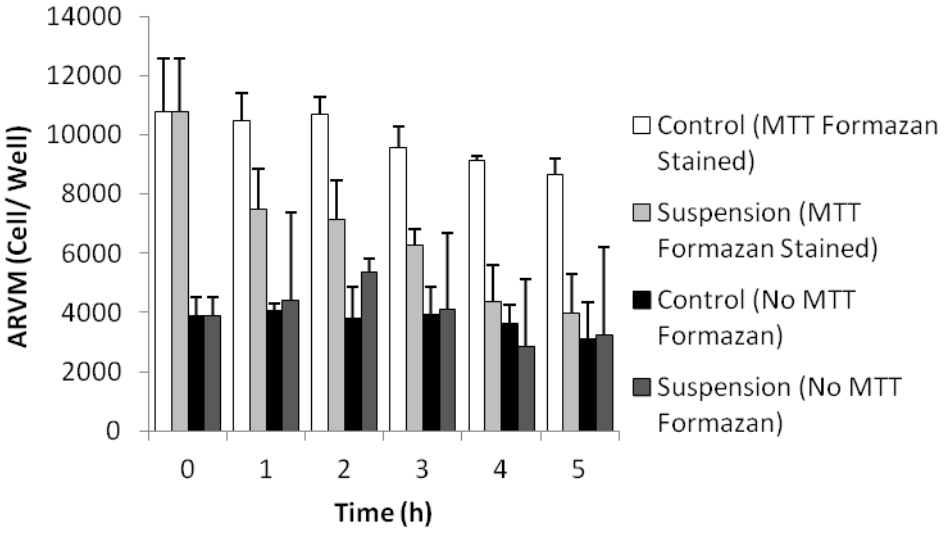

Figure 2.16. Static versus suspension ARVM culture. Number of myocytes attached to culture vessel and ability to reduce MTT. Cells were either plated immediately post-isolation (Control) or kept in suspension for 1-5 h (Suspension). Data represent mean (n = 3) ± SD.

2.3.2 pO2 and Temperature of Medium within the MKII Incubation Chamber

Within 5 min of switching to the hypoxic gas mixture the pO_2 of the culture medium had decreased to 2.23 mmHg. By 15 min it had decreased to 0.91 mmHg, and after 20 min it was 0.67mmHg. This was sufficiently low enough for us to evaluate tracer hypoxia selectivity tracer, at our nominal threshold of 0.8mmHg. The pO_2 continued to decrease to 0.33mmHg by 35 min, and then remained stable until the experiment was stopped at 60 min (figure 2.17).

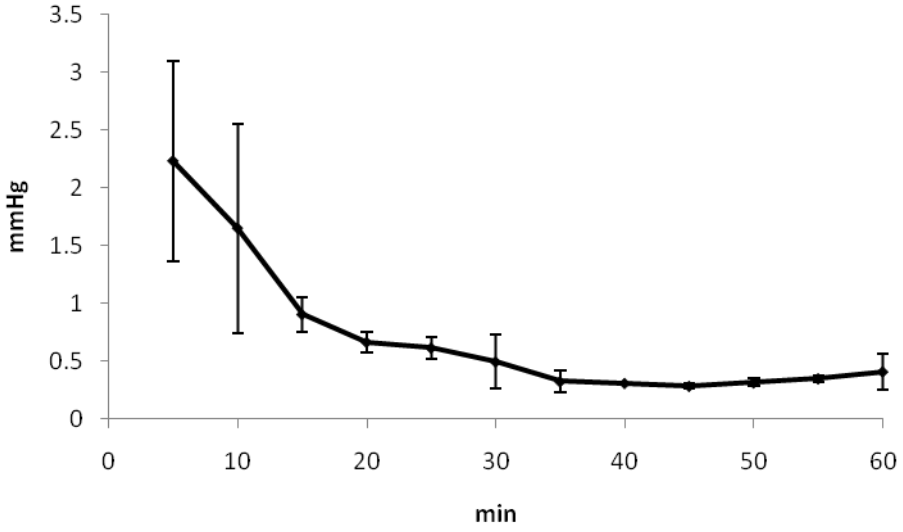

Figure 2.17. MKII incubation chamber pO2 calibration. Medium pO_2 vs. time for a culture of ARVM incubated under hypoxic conditions. Data represent mean (n=3) ± SD.

After moving the cultures from the incubator to the cell incubation chamber, the average temperature of the culture medium was 32.8°C (0 min). By 20 min the temperature had risen to 37.0°C, and from 20- 60 min the temperature of the culture medium remained constant (figure 2.18).

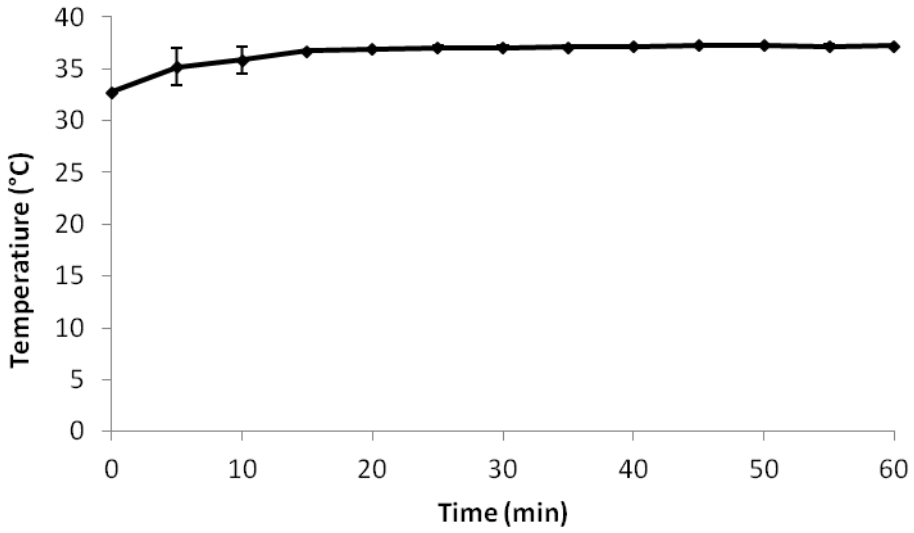

Figure 2.18. MKII incubation chamber temperature calibration. Temperature (ºC) of culture medium versus time (min), for a Petri dish containing ARVM, incubated in the MKII chamber. Data represent mean (n = 2) ± SD.

2.3.3 Linear Range and Dead Time of Universal Gamma Counter

Measurements taken by the universal gamma counter remained linear over the range 135- 5.6 x 10^6 cpm (9.5 x10^{-7}- 1.0 MBq) (R^2= 0.9983) (figure 2.18). Below 135 cpm (15 Bq) linearity decreased slightly (R^2= 0.9928) (figure 2.20), therefore values below 135 cpm were not plotted for least squares regression. In order to convert cpm to Becquerels the range 135- 3.2 x 10^6 cpm (1.5x10^{-5}- 0.5 MBq) was used (figure 2.21).

The dead time is the time taken by the universal gamma counter to register, and if necessary, extrapolate the number of counts in order to determine the cpm. As the amount of radioactivity increased the counting efficiency decreases, because an increasing number of decay events are missed during the time that it takes the gamma counter to calculate the cpm. Samples of greater than 62 KBq had a dead time that exceeded 10% of the total counting time. However, as the results shown in figure 2.20 demonstrate, the universal gamma counter was able to accurately compensate for the detector dead time up to 3.2 $x10^6$ cpm. We therefore decided to use no more than 500 KBq of radioactivity for our cell based experiments.

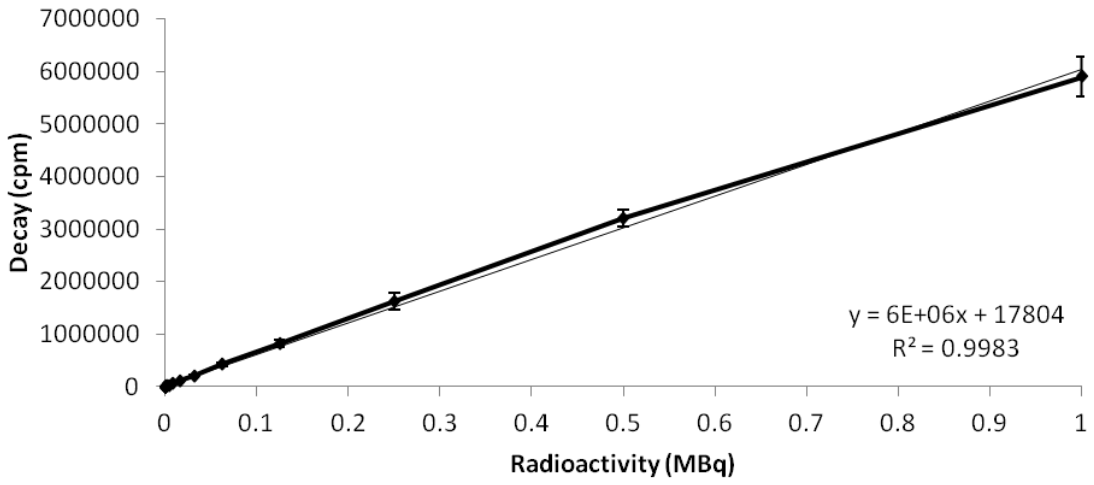

Figure 2.19. Gamma counter linearity curve showing the entire range of activities (9.5 $x10^{-7}$- 1.0 MBq per vial) measured and the associated R^2 value (0.9983). Data represent mean (n = 6) ± SD.

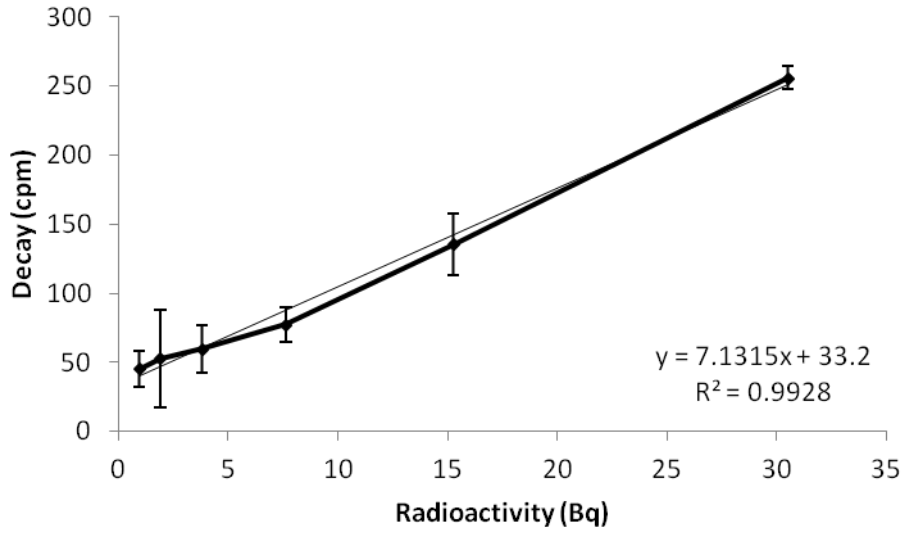

Figure 2.20. Gamma counter linearity curve non-linear range. Range of radioactivity (0.95- 30.5 Bq per vial) below which linearity diminished (R2= 0.9928). Data represent mean (n = 6) ± SD.

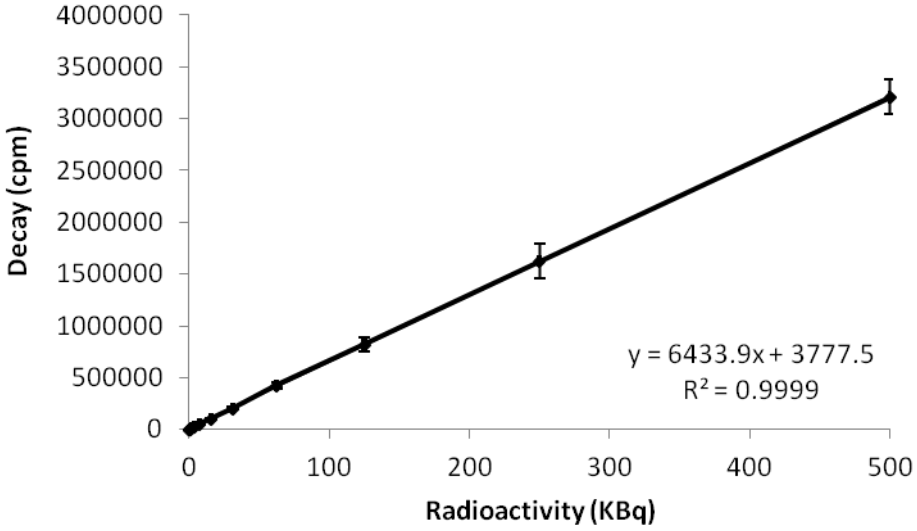

Figure 2.21. Gamma counter linearity curve linear range. Range of radioactivity ($1.5x10^{-5}$- 0.5 MBq per vial) which allowed the most accurate conversion of cpm to KBq (R2=0.9999). Data represent mean (n = 6) ± SD.

2.4 Discussion and Conclusions

2.4.1 ARVM Culture, viability and morphology

The optimum plating density was determined to ensure that cells were not wasted by over-plating. ARVM can be lost if the plating density is too high because the cells will tend to lie on top of each other, but only those that make contact with laminin substratum are able to attach. This exercise also ensured that the maximum practical number of cells was used, to achieve the highest possible range of uptake in the subsequent cell based experiments. We found that a 1 in 4 dilution of the original 12 ml suspension of ARVM gave the highest number of rod-shaped ARVM. When freshly isolated ARVM were plated the cell population comprised of 80 % rod shaped cells, a value that is within the 60- 85% range reported by others [223-224, 231, 237]. We had therefore validated our ARVM isolation protocol.

As discussed previously cell morphology is intrinsically linked to ARVM viability. Monitoring cell morphology serves as a simple yet effective means of qualitatively assessing the efficiency of the isolation procedure, and cell viability [219, 223, 231, 258]. De Young *et al* defined a rod shaped myocyte as a cell that has a length to width ratio of 5 to 1 [223]. Cell morphology was therefore employed as a means of determining the maximum time frame for maintaining ARVM in culture, before they were used for experiments. Morphology was monitored over seven days, and bright-field microscopy was used to acquire images of the cells during this time, to provide a visual reference to accompany data from cell viability assays. These results in section 2.3.1.2, and images in section 2.3.1.3 demonstrate the well documented transition of ARVM in culture from

morphologically distinct viable rod-shaped cardiac myocytes, to distorted rod-shaped cells. These distorted cells then undergo further morphological, ultra-structural, and biochemical changes which include increased membrane permeability, loss of calcium regulation, and hypercontraction of the myofibrils. This causes the cells to round up before they die and detach from the culture vessel [219, 223, 231, 237]. On day 0, 80 % of cells were rod-shaped ARVM, with regular myofibrils striations observable even under the light-microscope. On day 1 the number of cells and their morphology distribution were similar to day 0. Images taken on day 1 show that cells were rounded at the intercalated discs, because they had internalised their gap junctions in order to seal them [259-260]. From day 2 the total number of rod-shaped myocytes began to decline, but the percentage of rounded and distorted ARVM started to increase. This pattern continued for the duration of the study. Our observations were similar to those previously reported by others [219, 231, 261-262].

Trypan Blue exclusion was employed over the course of seven days, to assess ARVM sarcolemmal integrity. However the data obtained using this approach provide a false impression of what actually happened during these experiments, as it appears from these results that cell viability actually increased throughout the course of these experiments. However ARVM do not divide, and therefore their viability cannot increase. As dead cells detached from the cultureware and were removed each time the culture medium was changed, live cells became fractionally enriched although their total number decreased at each measurement time. However these results provided valuable insight into how the viability of ARVM in culture alters over time. At no point during the experiment was the

accumulation of Trypan Blue observed in any distorted/ rod-shaped ARVM, but interestingly the data also show that even rounded cells are capable of excluding Trypan Blue. Thus although the majority of rounded cells may be progressing towards cell death on day 0, it is possible that after 48 h in culture, some rounded cells may also be adapting to cell culture conditions. For this reason we used the total cell number, which included rod-shaped, distorted, and rounded cells, for normalising the data from our cell based radiotracer characterisation experiments. We did this because it was likely that Cu-BTSC complexes would also accumulate within rounded cells if they were still viable, and therefore omitting these cells could potentially distort our experimental results.

The cleavage of MTT to the formazan product provides an index of the integrity of intracellular reductases, which is used to infer of cell viability [253]. In these experiments the assay was employed in conjunction with other methods, to determine the maximum time frame for using ARVM cultures. Although there are a number of studies that have used the MTT assay with cardiac myocytes [255-257], we optimised the assay to determine the most suitable concentration of MTT and exposure time. Through this process we found that a stock concentration of 1mg/ ml MTT, used at a ratio of 1: 5 per volume of culture medium, and an exposure time of 1 h were optimal. We demonstrated that MTT formazan production decreased continuously throughout the experiment, which shows that the cellular and metabolic integrity of ARVM became compromised from the moment the cells were isolated. The assay also highlighted to us the fragility of isolated ARVM, and demonstrated that when maintained in culture the viability of these primary cells quickly diminishes.

Claycomb *et al* demonstrated that for the first twelve hours after being isolated, cultured ARVM preferentially metabolise glucose instead of fatty acids (FA) [263]. They postulated that this was most likely due damage to the mitochondria, which occurred during the isolation process. A period of repair is therefore required before oxidative phosphorylation can be re-established. This is an important consideration for our study, because the mitochondrial electron transport chain is thought to be involved in the reductive trapping of Cu-BTSC complexes. It was therefore thought necessary to allow mitochondrial repair to take place before we used ARVM for experiments. Collation of the data from sections 2.3.1.2 and 2.3.1.5.4 demonstrated that the maximum number of rod shaped ARVM was present on day 0. Day 0 cells also had the greatest ability to reduce MTT. There was however little difference between the number of ARVM, and their morphology and viability on day 1. We therefore concluded from the results of our experiments and the previous observations by Claycomb *et al*, that our radiotracer accumulation studies should be conducted using cells that were cultured over-night, to allow cellular repair to take place. However, in all of our experiments the cells were used within 24 h of being isolated.

We then assessed the viability of ARVM kept in suspension for between 1- 5 h, and compared this to cells that had been plated immediately after being isolated. At all time points the ability of cells kept in suspension to reduce MTT was comparable to the control cells, which suggested that these cells were equally viable. However the number of cells that were capable of attaching to culture vessels decreased over time, to only 46 % of the control cell numbers after 5 h in suspension. While we did not investigate this

any further, we assumed that their inability to attach signified that they were undergoing changes that would ultimately lead to cell death. We therefore concluded that if we chose to use ARVM that had been maintained in suspension, they should be used immediately after being isolated.

2.4.2 Incubation Chamber Calibration

The prototype incubation system was built to assist in the development of the professionally manufactured MKII chamber. We conducted a number of ^{64}Cu-ATSM extraction experiments using the prototype chamber, which allowed us to develop a detailed experimental protocol. Furthermore, we also learned from these experiments that aliquots of culture medium taken in order to monitor radiotracer extraction were often contaminated with cells, and this significantly increased the variance between sample replicates. We therefore included a centrifugation step in future experiments to negate this issue.

The MKII chamber system was a considerably more effective design. This glass chamber was water-jacketed and connected to a temperature controlled water heater/ circulator. This allowed the culture medium to be warmed to 37 °C within 20 min, and maintained at this temperature. The heater/circulator was also connected to a coil of tubing that was wrapped around the gassing line, thereby preventing the formation of condensation in the line. Condensation could potentially spill over into the chamber and contaminate the culture medium. Such contamination could compromise cell viability and also dilute the culture medium, thereby lowering the effective radiotracer dose, factors that would

certainly compromise the accuracy of our experiments. The chamber was placed on a plate rocker in order to facilitate gas exchange between the culture medium and the internal chamber environment. This significantly decreased the time taken for the culture medium pO_2 to reach ≤0.8mmHg, from 100 min for the prototype chamber, to between 15- 20 min. The diameter of the chamber was also reduced to prevent culture vessels from moving. This prevented medium spillage and radioactive contamination of the vessel. The reduced internal volume of the MKII chamber also facilitated gas exchange between culture medium and the environment within the chamber.

2.4.3 Gamma Counter Linearity and Dead Time

The linear range of the gamma counter when measuring the radioactivity of ^{64}Cu was between 135- 3.2 x 10^6 cpm (1.5 x 10^{-5}- 0.5 MBq). During our cell based radiotracer characterisation experiments (discussed in chapter 3), the amount of radioactivity that was measured in the cell pellets was well within this range ($2.1x10^{-4}$- $1.5x10^{-2}$ MBq). In our initial experiments with the prototype system, the accumulation of ^{64}Cu-ATSM was assessed using various amounts of radioactivity. As a result of this we determined that after adding 100 KBq ^{64}Cu-ATSM to the culture medium, the amount of radioactivity that was retained by ARVM was within the linear range of the gamma counter. We therefore used 100 KBq of ^{64}Cu-ATSM for all our cell based experiments.

2.4.4 Conclusions

Having determined the linear range of the gamma counter, ensuring that isolated ARVM were of a suitable standard for our experiments, and after designing, constructing, and characterising the MKII cell incubation chamber, it was then time to apply them to the

investigation of ^{64}Cu-BTSC complexes. In the first instance ^{64}Cu-ATSM accumulation was to be characterised in isolated ARVM to assess the feasibility of developing a high-throughput multiple radiotracer screen.

Chapter 3.

Assessment of ^{64}Cu-ATSM Accumulation in Isolated Ventricular Myocytes

3.1 Introduction

In chapter 2 we demonstrated that we were able to isolate and maintain viable rod-shaped ARVM, for longer than the anticipated time-frame of our experiments. We also demonstrated that the MKII cell incubation system was able to maintain ARVM cultures at a stable temperature, under both oxygenated and hypoxic conditions. We were therefore in a position were would could move on to the next phase of our study, which was to develop a high throughput screen for assessing our library of novel Cu-BTSC complexes in cardiac tissue. As a first step it was necessary to determine whether this isolated cell approach would be suitable for this purpose. Cell-based assays could be advantageous to this end, as they would allow multiple replicates of the same tracer or multiple tracers to be assessed at the same time using cells from the same heart. This approach could be a more efficient means of screening our library of Cu-BTSC complexes, by decreasing inter-preparation variability.

Our first aim was to determine whether we could observe hypoxia-dependent retention of ^{64}CuATSM in ARVM. If we were able to easily observe a contrast using our relatively large scale system, we could then establish to what degree it would be possible to scale down the assay for the purpose of high throughput screening. This is because we had envisaged that such a system would use multiwell culture plates, which would accommodate fewer cells per well.

In cell based radiotracer characterisation experiments there are two approaches for quantifying radiotracer uptake, either i) measuring the extraction of tracer from the

culture medium, or ii) by directly measuring intracellular accumulation. In the case of attached cells the measurement of uptake from culture medium allows for longitudinal studies. However it was necessary to determine if this approach would be sufficiently sensitive, and also whether it would allow us observe a contrast between ^{64}Cu-ATSM retention in hypoxic and normoxic cells. We therefore investigated both methods to determine which was the most appropriate for our experiments.

3.2 Materials and Methods

3.2.1 Gas mixtures

Gas mixtures used for this series of experiments were: oxygenated (21 % O_2/ 5 % CO_2/ 74 % N_2) and (95 % O_2/ 5 % CO_2), and anoxic (95 % N_2/ 5 % CO_2).

3.2.2 Synthesis of ATSM

ATSM was kindly provided by Prof. P Blower and Dr R. Paul (Dept. Imaging Sciences and Medical Engineering, King's College, London). Ligands were synthesised as previously reported [172, 264].

3.2.3 Radiolabelling ATSM with ^{64}Cu

3.2.3.1 Radiolabelling Methodology

ATSM was dissolved in DMSO (1mg/ ml). 10 µl of the ligand solution, and 30 MBq of ^{64}Cu were then added to 1 ml ultrapure water. The solution was gently shaken to mix, stored at room temperature for 20 min, and then filtered through a SEP-PAK® C18 Classic cartridge (Waters, UK). The cartridge was then washed through with 2 ml H_2O to remove excess ^{64}Cu and HCl, before ^{64}Cu-ATSM was eluted using 0.5 ml ethanol. 30µl of ascorbic acid (aq) (10mg/ ml) was then added immediately to restrict radiolysis. The amount of radioactivity in the stock vial was then measured using a radioisotope dose calibrator (CRC-25R Capintec, USA), before the radioactivity was adjusted to 1 MBq/ ml with M199.

3.2.3.2 Assessment of Radiolabelling Efficiency

Ligand labelling efficiency was assessed by radio-ITLC, using Silica Gel 60 F_{254} strips (Merck, Germany) as the stationary (sorbent) phase, and 100 % ethanol as the mobile phase. In this system the relatively lipophilic Cu-BTSC complexes migrate with the solvent, but $^{64}Cu^{2+}$ interacts with the sorbent phase and remains at the origin.

1µl of the labelled solution was pipetted onto an ITLC strip (1 cm x 10 cm), which was then placed in ethanol to a depth of 0.5 cm. The mobile phase was allowed to run to 90 mm before it was removed and allowed to dry. The ITLC strip was then placed onto a Flow Count (B-FC-3600) ITLC plate reader, fitted with a $\beta^{-/+}$ detector (B-FC-3600) (LabLogic, UK). The radiolabelling efficiency was then determined using Laura (v. 4.0.3.75) software (LabLogic, UK). The radiolabelling efficiency was always greater than 97% (Fig.3.1).

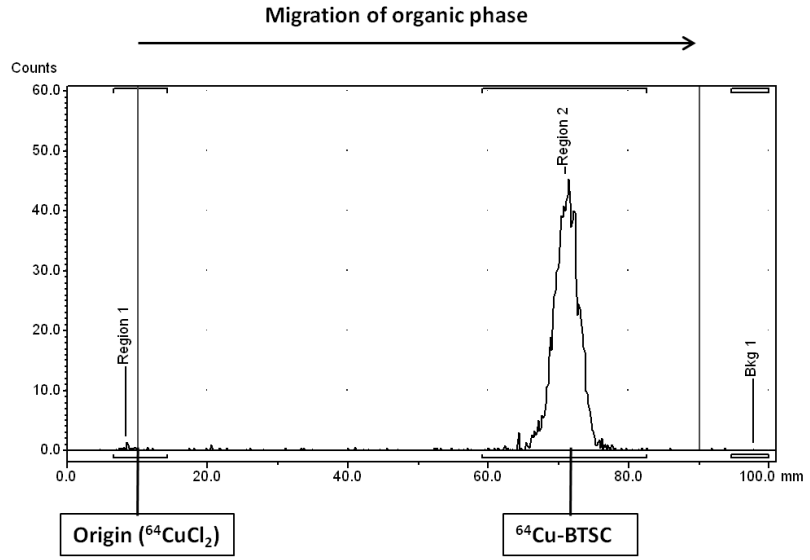

Figure 3.1. Assessment of BTSC ligand radiolabelling efficiency: An example of a typical ITLC trace. $^{64}CuCl_2$ remained at the origin, but ^{64}Cu-BTSC complexes migrate with the organic solvent phase.

3.2.3.3 Assessment of ^{64}Cu-ATSM Stability in Medium 199

In our cell based studies ^{64}Cu-ATSM was diluted to with M199 before being used for experiments. We therefore assessed the stability of ^{64}Cu-ATSM in a solution of M199 to ensure that the complex remained stable throughout the day.

ATSM was first labelled with ^{64}Cu, and the radiolabelling efficiency was determined as described in section 3.3.3.2. This provided the control, 0 h time point. ^{64}Cu-ATSM was then diluted to 5 MBq/ ml with M199. The stock was stored on the bench throughout the day, and refrigerated overnight. At 1, 3, 6, and 24 h, 2- 5 µl of the solution was removed and analysed by radio-ITLC.

3.2.4 ^{64}Cu-ATSM Characterisation Using ARVM

3.2.4.1 Extraction of ^{64}Cu-ATSM from Cell Culture Medium

In order to monitor the uptake of Cu-BTSC complexes over time, the majority of studies to date have used cells that were suspended in culture medium [162-163, 167, 209, 241]. However, the rapid attachment method of ARVM culture that we used made this approach more complicated, because cell samples cannot be aspirated using a pipette or syringe. With our system this would mean that the chamber would have to be opened to retrieve cell samples, which would equilibrate the atmosphere within the chamber with the external atmosphere, and invalidate the experiment. We therefore chose to monitor the accumulation of ^{64}Cu-ATSM indirectly, by measuring the amount of radioactivity that ARVM extracted from the culture medium. Aliquots of medium were taken via the sampling port, which allowed rapid repeated sampling without perturbing the system.

3.2.4.2 The Effect of Hypoxia on the Extraction and Intracellular Accumulation of ^{64}Cu-ATSM in ARVM

ARVM cultures were prepared on 90 mm Petri dishes using the attachment method and incubated overnight. The following day, culture medium was replaced with 15 ml fresh medium and the cell numbers were recorded. The dish of cells was placed inside the MKII chamber, which was then sealed. Depending upon the condition to be examined the system was gently gassed with either an oxygenated (95% O_2/ 5% CO_2), or anoxic (95% N_2/ 5% CO_2) gas mixture for 20 min. Cultures were then agitated on a rotary plate-shaker at 10 RPM to facilitate gas exchange. After 20 min, 100 KBq of ^{64}Cu-ATSM was added to the medium. Between 1- 30 min, triplicate aliquots of 100 µl of culture medium were removed. The aliquots were spun at 2000 g for 2 min, to ensure that they were not contaminated by cells, before 80 µl of supernatant was removed from each aliquot for gamma well counting. At the end of each experiment cells were washed once with 5 ml fresh M199, and the number and morphology of the cells was recorded. ARVM were then gently detached from the plate using a cell scraper, and pelleted by centrifuging at 2000 g for 2 min. The wash step was repeated with 1 ml PBS, which was then aspirated before the radioactivity in the pellet was counted. The counts were then decay corrected, before the amount of radioactivity within the sample was determined using least squares regression. For this purpose the gamma count linearity curve (figure 2.21) was used.

3.2.4.3 The Effect of Time on the Retention of ^{64}Cu-ATSM

ARVM cultures were prepared as described in section 2.2.4, and incubated overnight. The following day the culture medium was replaced with 5 ml fresh medium, and the cell

number was recorded. A dish of cells was placed into the MKII incubation chamber, which was sealed and supplied with either an oxygen rich (95% O_2/5% CO_2) or anoxic (95% N_2/5% CO_2) gas mixture. To assist gas exchange the culture medium was gently agitated by rocking at 18 RPM, and then allowed to equilibrate for 20 min at 37°C. After this period 100 KBq of ^{64}Cu-ATSM was added and the cultures were incubated for a further 30 or 60 min. The cultures were then removed from the chamber, and the culture medium was replaced with 5ml fresh M199, before cells were counted. ARVM were then gently detached from the dish using a scraper, and pelleted (2000 g, 2 min). The wash and pelleting steps were then repeated with 1 ml PBS, which was removed before the radioactivity was measured. The counts were then decay corrected, and the amount of radioactivity associated with the cells pellets was determined by least squares regression, using the gamma count linearity curve (figure 2.21). The data were then expressed as the amount of radioactivity per cell.

3.2.4.4 The Effect of Oxygen Concentration on ^{64}Cu-ATSM Accumulation

The first experiments with the MKII chamber employed extremely low (0 % O_2) and high (95% O_2) and levels of oxygen. In our next series of experiments we included a gas mixture which contained 21 % O_2, alongside the 0 % and 95 % O_2 mixtures. This was done to assess the effects of reducing the concentration of oxygen to a more physiologically relevant level. A similar method to that described in section 3.2.4.3 was used for this series of experiments, however, only a 60 min time point was used.

3.2.4.5 ^{64}Cu-ATSM Accumulation in ARVM Cell Suspensions

One advantage of using cells in suspension is that cell numbers would not be restricted by substrate surface area; in fact the only factor that could limit the number of cells, would be the efficiency of the isolation procedure. Having a greater number of cells should decrease the time taken for tracer accumulation to reach a steady state, and could increase the contrast between normoxic and hypoxic cell uptake, thereby increasing the sensitivity of the method. These results would also be more comparable to those obtained by other groups using cancer cell lines suspended in culture medium [162-163, 167, 209]. Another advantage is that if cells are not plated the costs associated with the day to day maintenance, particularly that of laminin, are reduced. We therefore assessed the feasibility of using this approach.

ARVM were isolated as described in section 2.2.4. The cells were then suspended in 10 ml of M199. ARVM were filtered through a 200 µm mesh to remove undigested tissue and cell aggregates. The suspension was placed directly into an uncoated Petri dish, which was then placed inside the chamber. The cultures were then gently agitated by rocking the chamber at 18 RPM, while the medium was equilibrate with either an oxygen rich (95% O_2/5% CO_2) or anoxic (95% N_2/5% CO_2) gas mixture. After 5 min, when the pO_2 of the culture medium was below 0.8 mmHg, 100 KBq Cu-ATSM was added via the injection port. At 1, 5, 10, 15, 30, 45 and 60 min, 3x 100 µl aliquots were removed and centrifuged at 2000g for 2 min, to obtain a cell pellet and medium fraction. The supernatant was aspirated, and the radioactivity in both the cell pellet and supernatant was counted. Radioactivity in the cells was then expressed as the percentage of the total

counts in the original 100 µl sample. The counts were also converted to radioactivity (KBq) using the gamma counter linearity curve, and expressed as Bq/ mg protein. The total protein content of the cell pellet was determined using a commercial BCA assay (GE Healthcare, UK).

3.2.5 Measurement of Cell Protein Content by BCA Assay

During the cell suspension study it was not possible to accurately determine the number ARVM using a conventional haemocytometer (although attempts were made using number of different chambers, with counting well depths of 100- 250 µm). This was mainly due to the relatively large size of the ARVM, which prevented them from being evenly distributed between the counting chambers of the haemocytometers. We therefore utilised the total protein content of the cell pellets, to relate radiotracer accumulation the size of the cell population. For this purpose we used a commercial bicinchoninic acid (BCA) protein assay (Merck, Germany). The BCA assay is a colourmetric assay that relies on the Biuret reaction, a process whereby Cu^{2+} is reduced to Cu^{+} by peptide bonds. BCA solution is added to the sample to form a complex with Cu^{+}. This process causes the solution to turn from light blue to purple, which is proportional to the amount of protein present in the sample. The optical density of this solution is measured spectrophotometrically at 560nm, and compared to protein standards of known concentration, to determine the actual amount of protein in the sample.

At the end of each ^{64}Cu-ATSM accumulation experiment the cell pellets were frozen and stored at -80 ºC. To prepare samples for the BCA assay, on the day of the experiment the

pellets were slowly thawed on ice. They were then washed twice with 1 ml of PBS (pH 7.4), and centrifuged at 3000g for 5 min. The PBS was removed and cells were lysed by adding 0.5 ml mammalian protein extraction buffer (GE Healthcare, UK), before being quickly frozen at -80ºC, and then immediately thawed at room temperature to facilitate cell lysis. The cell pellet and debris was then resuspended using a pipette, and incubated on ice for 30 min, during which time the samples were regularly vortexed. A protease inhibitor cocktail (Sigma-Aldrich, UK) was also added to the samples at a ratio of 1: 25 (vol/ vol). The samples were then mixed and centrifuged at 20000g for 30 min, after which the supernatant was carefully removed and analysed using the BCA assay. The cell debris and pellet fractions were discarded.

The BCA assay was performed in accordance with the manufacturers recommended procedure. Briefly, a range of protein standards were made from a stock solution of bovine serum albumin (2mg/ ml). 25 µl of each of the protein standards and the cell lysate samples was then added in triplicate to a 96 well plate. 200 µl of BCA solution was then added to each well, and the plates were incubated for 30 min at 37.0 ºC. The plate was then cooled on ice, before the Abs_{562nm} of each well was measured using a multiwell plate reader.

3.2.6 Data and Statistical Analysis

Data analysis was performed using Microsoft Office Excel® 2007. Statistical analyses were performed using GraphPad Prism® (Version 5.04) (GraphPad Software Inc, USA). All values are expressed as the mean ± SD. Data were compared using either unpaired t-

test, or a one way analysis of variance (ANOVA) with the Dunnett's post test where multiple comparisons were made to a control group.

3.3 Results

3.3.1 ATSM Radiolabelling Efficiency and Stability

The radiolabelling efficiency of ATSM at 0 h was always greater than 97 %. The amount of radiolabelled complex in a solution of M199 remained at 97 % of the total radioactivity for up to 6 h. However after 24 h this decreased to 94 % (figure 3.2).

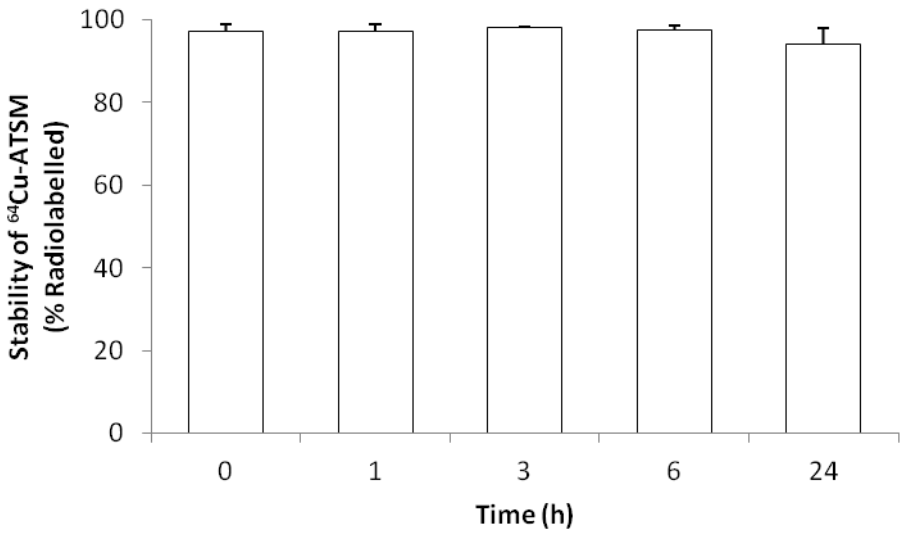

Figure 3.2. Stability of ^{64}Cu-ATSM in a solution of M199 over 24 h, measured using radio-ITLC. Data represent mean (n= 3).

3.3.2 Characterisation of ^{64}Cu-ATSM Using ARVM

3.3.2.1 Extraction of ^{64}Cu-ATSM by ARVM

After 1 min the amount of radioactivity in aliquots of medium exposed to 0% O_2 and 95% O_2 was on average 0.41 KBq/ 100 µl. This decreased over 30 min to 0.31 ± 0.1 and 0.35 ± 0.1 KBq/ 100 µl medium, at 0% O_2 and 95% O_2 respectively (figure 3.3). While tracer extraction tended to be slightly greater in cells under hypoxic conditions from 5 min onwards, at no point did this reach statistical significance.

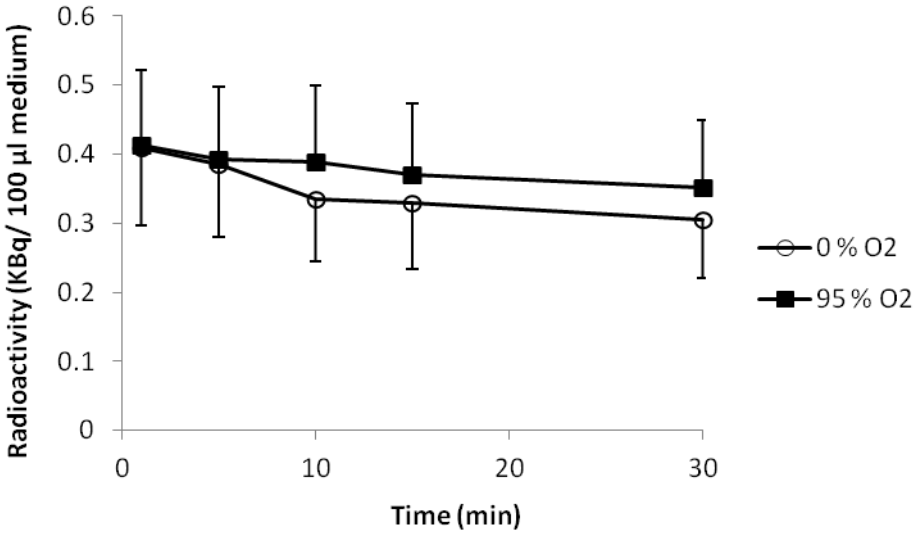

Figure 3.3. Extraction of ^{64}Cu-ATSM from culture medium using the MKII Cell Incubation Chamber. ARVM were incubated with ^{64}Cu-ATSM for 60 min, under oxygenated and hypoxic conditions. Data were compared using an unpaired Student's t- test. Data represent mean (n = 3) ± SD. Radioactivity in samples of medium was not significantly different (p <0.05).

3.3.2.2 ^{64}Cu-ATSM Accumulation in ARVM using the Attachment Culture Method

3.3.2.2.1 Accumulation ^{64}Cu-ATSM in ARVM after 30 min incubation

The amount of radioactivity in each cell pellet was normalised for the total number of cells attached to the Petri dish at the end of each experiment. After 30 min incubation with ^{64}Cu-ATSM the amount of radioactivity that had accumulated was 2.6 ± 0.8 mBq/ cell under hypoxia, and 1.7 ± 0.5 mBq/ cell under oxygenated conditions (figure 3.4). Although tracer accumulation was consistently higher under hypoxia in each paired experiment, the variability in tracer uptake between experiments meant that this did not reach statistical significance.

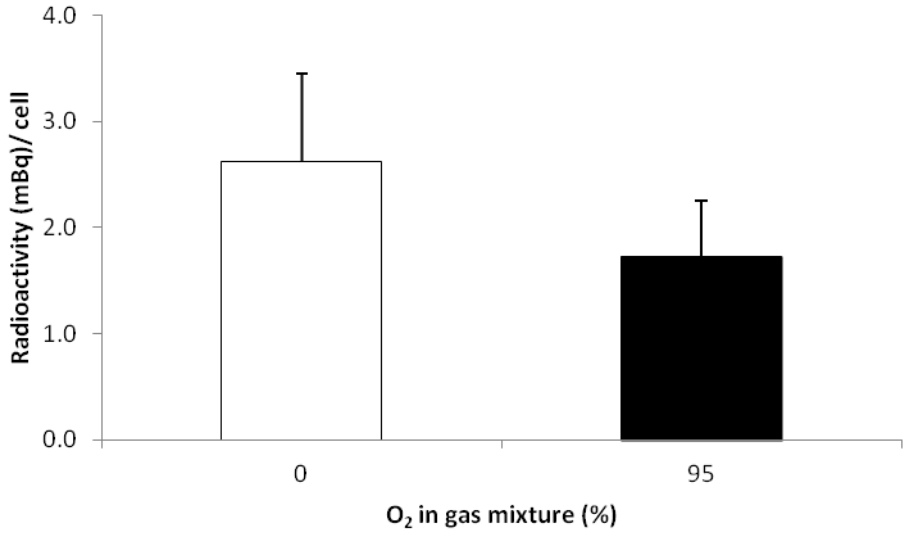

Figure 3.4. Accumulation of ^{64}Cu-ATSM in ARVM exposed to an oxygenated (95% O_2) or deoxygenated (0% O_2) atmosphere. Data were compared using an unpaired Student's t- test. Data represent mean (n = 3) ± SD. Data sets were not significantly different (p <0.05).

3.3.2.2.2 Accumulation ^{64}Cu-ATSM in ARVM after 30 and 60 min incubation

In this study the volume of culture medium used during the experiments was reduced to 5 ml, to increase the concentration of ^{64}Cu-ATSM without having to use more radioactivity. A 1 h time point was also included, to ascertain whether increasing the incubation time would also increase the contrast between normoxic and hypoxic cells. After 30 min hypoxic 20.6 ± 11.1 mBq/ cell was retained, compared to 9.9 ± 3.1 mBq/ cell in normoxic controls. When the incubation period was extended to 60 min the accumulation of radioactivity increased to 33.8 ± 8.4, and 17.1 ± 3.4 mBq/ cell respectively. While the contrast between hypoxic to normoxic cells was 2: 1 after 30 min, it decreased to 1.6: 1 after 60 min. Nonetheless the accumulation of ^{64}Cu-ATSM was always higher in cells that were incubated under hypoxia, but this was only statistically significant ($p<0.05$) after 60 min (figure 3.5). Data were normalised as described in section 3.3.2.2.1, and compared using an unpaired Student's t- test.

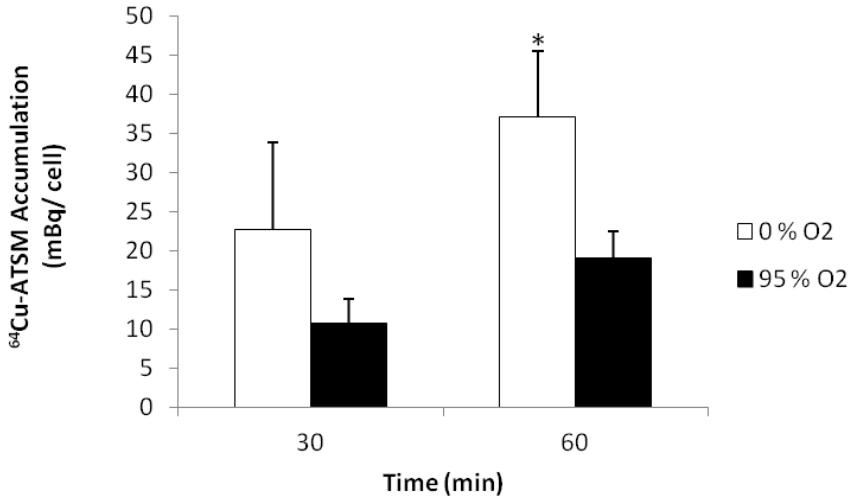

*Figure 3.5. Accumulation of ^{64}Cu-ATSM after 30 or 60 min. ARVM were incubated under deoxygenated (white), or oxygenated (black) conditions. Data were compared using an unpaired Student's t- test. Data represent mean (n=5) ± SD. * = significantly different (p <0.05).*

3.3.2.2.3 The Effect of Oxygen Concentration on the Accumulation of ^{64}Cu-ATSM

A second series experiments were performed to compare ^{64}Cu-ATSM uptake at a mid-range oxygen level (21% O_2). The average amount of radioactivity that was retained by cells was 36.1 ± 3.1 (0 % O_2), 27.3 ± 5.1 (21 % O_2), and 23.9 ± 2.5 mBq/ cell (95 % O_2). Tracer uptake in hypoxic cells was significantly higher ($p<0.05$) than in cells incubated under hypoxic conditions, with contrast between hypoxic to oxygenated cells of 1.3: 1 at 21% O_2, and 1.5:1 at 95% O_2 (figure 3.6). Data were normalised as described in section 3.3.2.2.1, and compared using a one way ANOVA with a Dunnett's post test.

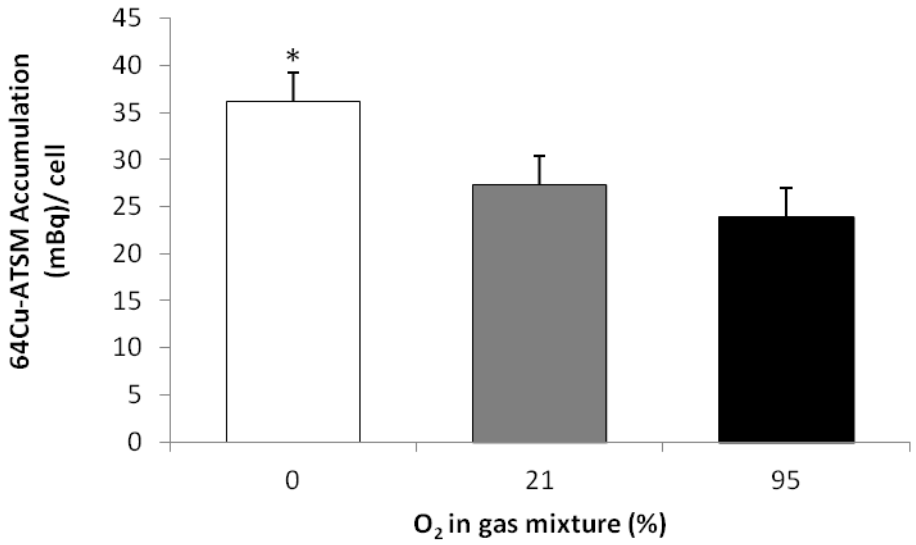

*Figure 3.6. Accumulation of ^{64}Cu-ATSM in ARVM exposed to 0, 21 and 95 % O_2. ARVM were incubated under an atmosphere comprised of 0, 21, and 95 % oxygen for 1 h. Data are expressed as amount of radioactivity (mBq) per cell, and compared using a one way ANOVA with a Dunnett's post test. Data represent the mean (n = 4) ± SD. * = significantly different (p <0.05).*

We then normalised these data for protein content using the data obtained from the BCA assay. When the 0% O_2 samples are compared to those obtained after gassing with 21 and 95% O_2, the ratios of the amount of radioactivity accumulated in each cell were 1.5:1 and 1.4:1. The amount of radioactivity per µg protein was 37.3 ± 8.2 (0 % O_2), 25.2 ± 5.6 (21 % O_2), and 25.9 ± 4.1 Bq/ µg protein. (95 % O_2) (figure 3.7). However, tracer uptake was only significantly different ($p<0.05$) between cells incubated under 0 % and 21 % O_2.

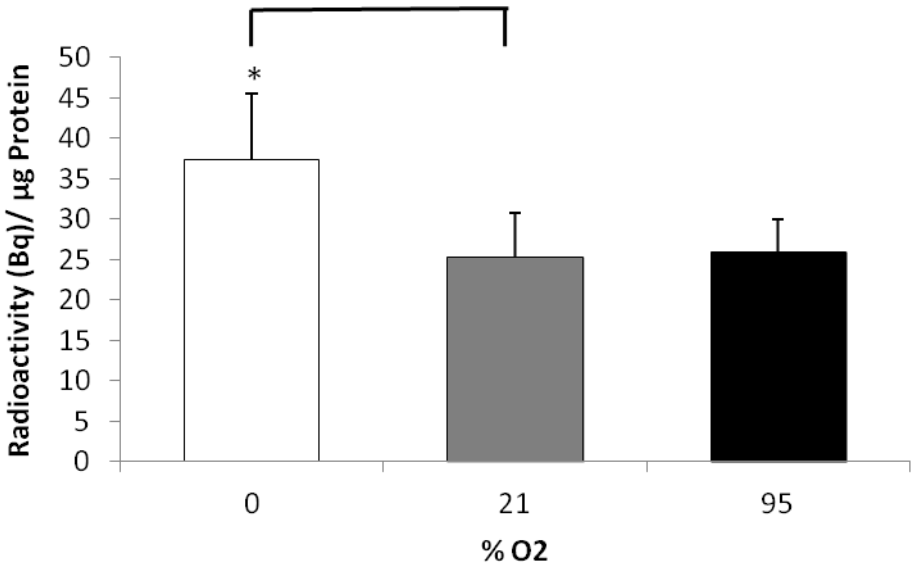

*Figure 3.7. Cellular accumulation of ^{64}Cu-ATSM normalised for total protein content. Data were compared using a one way ANOVA with a Dunnett's post test and represent the mean (n = 4) ± SD. * = significantly different (p<0.05).*

3.3.2.2.4 Morphology of ARVM before and after ^{64}Cu-ATSM accumulation experiments

Figures 3.8 and 3.9 summarise the cells counts for the number of rod-shaped ARVM per 90mm Petri dish, before and after the ^{64}Cu-ATSM accumulation experiments. Before each experiment there were on average between 1.8 x 10^5- 2.2 x 10^5 rod shaped cells/ 90 mm Petri dish, and after 30 or 60 min incubation under both oxygenated and hypoxic conditions the numbers were similar.

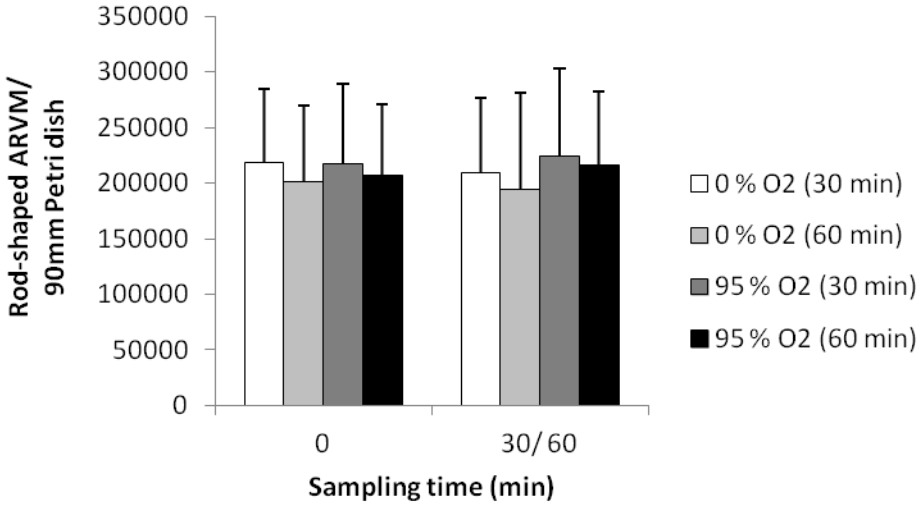

Figure 3.8. Average number of rod-shaped ARVM per 90mm Petri dish after 0, 30 or 60 min incubation. ARVM were incubated under oxygenated or hypoxic conditions for 30 or 60 min, and cell counts were recorded before and after each incubation period. Data represent mean (n = 5) ± SD. Data were not significantly different (p <0.05).

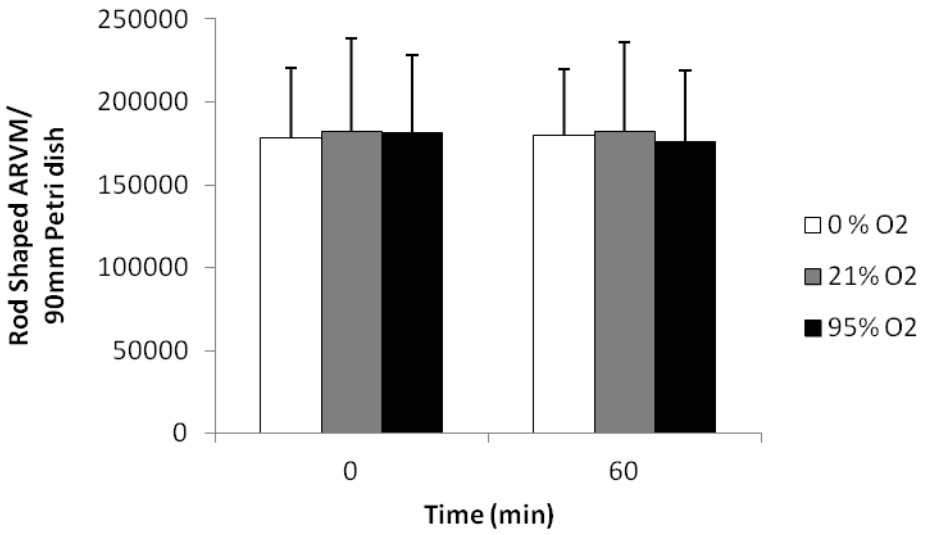

Figure 3.9. Total number of rod-shaped ARVM per 90mm Petri dish at the start (0 min) and end (60 min) of each experiment. Cell were exposed to 0, 21 or 95 % O_2. Data represent mean (n = 4) ± SD.

3.3.2.2.5 ^{64}Cu-ATSM Accumulation in ARVM in a Suspension of M199

The accumulation of ^{64}Cu-ATSM by ARVM maintained in a suspension of M199 is shown in figure 3.10. Data are expressed as a percentage of the total radioactivity in a 100 µl aliquot of the cell suspension. 1 min after the addition of ^{64}Cu-ATSM, the retained fraction was 31.8 ± 16.6 %, and 23.5 ± 4.9 % of the total radioactivity at 0 and 95 % O_2 respectively. These values increased to 63.2 ± 14.1 % and 53.4 ± 10.9% at 30 min respectively, ($p<0.05$). The amount of tracer that was associated with the cells then remained constant until the experiment was stopped at 60 min.

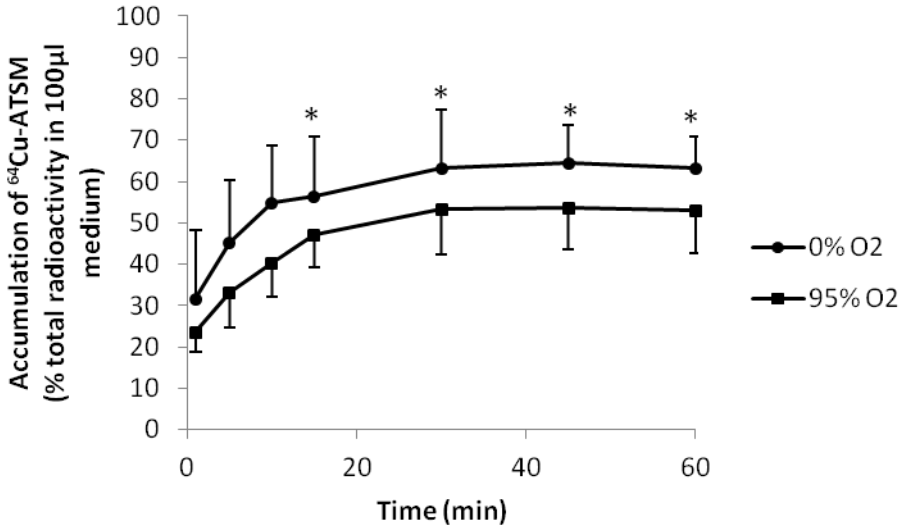

*Figure 3.10. Accumulation of ^{64}Cu-ATSM in ARVM maintained in suspension. Tracer retention was compared under oxygenated (square), or hypoxic (circle) conditions. Data represent mean (n = 5) ± SD. * = significantly different (p <0.05).*

When the data were normalised using the total protein content of cell pellets, similar patterns for ^{64}Cu-ATSM accumulation were observed. Under oxygenated conditions accumulation of ^{64}Cu-ATSM remained constant between 1- 60 min (~ 15 Bq/ µg protein). However under hypoxia the accumulation of ^{64}Cu-ATSM increased from 17 Bq/µg protein at 1 min, to 25 Bq/µg protein at 45 min (figure 3.11), reaching statistical significance after 30 min, ($p<0.05$).

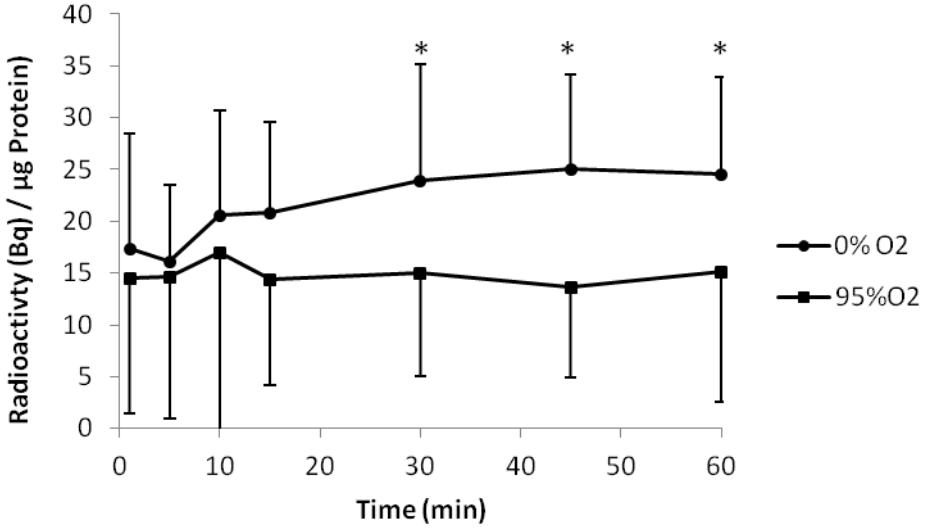

*Figure 3.11. Accumulation of ^{64}Cu-ATSM accumulation normalised for total protein. The total protein content of each of the ARVM cell pellets was ascertained using the BSA assay. Data represent mean (n = 5) ± SD. * = significantly different.*

3.4 Discussion and Conclusions

The purpose of these cell based experiments was to characterise the accumulation of ^{64}Cu-ATSM in ARVM under hypoxic and oxygenated conditions. The experiments were conducted to determine whether it would be possible to employ an ARVM based system, to characterise the hypoxia specificity and myocardial accumulation of novel ^{64}Cu-BTSC complexes. The results were also be used to determine whether the ARVM system could be scaled-down, and used as a high-throughput screening assay.

3.4.1 ATSM Radiolabelling Efficiency and Stability

Before starting our cell based experiments we assessed the radiolabelling efficiency and stability of ^{64}Cu-ATSM, in a solution of M199. This was to ensure that the constituents of the medium did not react with the complex and affect its stability. At 0 h the radiolabelling efficiency was 97 %. After adding M199 the stability of the complex remained stable for 6 h. However after 24 h the percentage of radiolabelled complex had decreased to 94 %. We therefore concluded that the efficiency of the initial ligand radiolabelling and the stability of the ^{64}Cu-ATSM in M199 were sufficient for our experiments.

3.4.2 Extraction of ^{64}Cu-ATSM from Culture Medium

We have assessed the extraction of ^{64}Cu-ATSM from cell culture medium by isolated cardiac myocytes incubated under oxygenated or hypoxic conditions. The results of these experiments (figure 3.3) demonstrated that tracer extraction was generally greater under hypoxic conditions, i.e. the amount of radioactivity in the culture medium during hypoxia

was lower than under oxygenated conditions, but at no point was the contrast between the two data-sets statistically significant. This was in part due to the large sample variance between replicate aliquots of medium. It is also likely that poor contrast that was observed between normoxic and hypoxic cells, was because only a small percentage of the total radioactivity was extracted. This high variability meant that it would not be possible to perform longitudinal uptake studies using a single culture. We therefore concluded that the tracer extraction method was too insensitive for the purpose of characterising our complexes. The only means of obtaining reliable longitudinal measurements would therefore be by directly measuring the intracellular accumulation of tracers. We achieved this by harvesting the cells at the end of each experiment, and measuring the amount of radioactivity associated with them. Unfortunately this required multiple ARVM cultures, one for each time point and experimental condition.

3.4.3 Accumulation of ^{64}Cu-ATSM: ARVM Attachment Culture

ARVM that were used during the ^{64}Cu-ATSM medium extraction study were harvested at the end of each experiment, after cell counting had been performed. The radioactivity associated with the cell pellets was measured, and ^{64}Cu-ATSM accumulation expressed as mBq per cell (figure 3.4). While the results of this first experiment were not significantly different, we did observe a contrast in tracer uptake between oxygenated and hypoxic cells. This suggested that direct measurement of radioactivity within cells may be more suitable for characterising ^{64}Cu-BTSC complexes. In this preliminary series of experiments, we observed a 1.5: 1 contrast ratio between hypoxic (2.6 ± 0.8 mBq/ cell) and oxygenated cells (1.7 ± 0.5 mBq/ cell) after 30 min, however the sample

variance was relatively large and this perhaps explains why the data-sets were not statistically different (these experiments were also only conducted in triplicate). We therefore chose to employ direct measurement of cell associated radioactivity for all future experiments.

3.4.3.1 Effect of Time of the Accumulation of ^{64}Cu-ATSM

For our next series of experiments we measured the cellular accumulation of ^{64}Cu-ATSM after 30, or 60 min. In this study we altered the way in which the culture medium was agitated, from stirring the cell incubation chamber to rocking. This was because during the first series of experiments we noticed that the centrifugal force generated by stirring the cultures forced the culture medium to edge of the Petri dish. This meant that at least 15 ml medium was required to submerge ARVM at the centre of the dish. By switching to rocking, and because aliquots of culture medium were no longer being removed in order to measured tracer extraction, we were able to reduce the volume of medium from 15 ml to 5 ml. However we continued to add 100 KBq of ^{64}Cu-ATSM to the culture medium, and because of this the concentration of ^{64}Cu-ATSM was higher than that used in the radiotracer extraction study. This was favourable because increasing the concentration of radiotracer could potentially lead to an increase in its accumulation, and potentially lead to a greater contrast between hypoxic and oxygenated cells. The results of the second series of experiments demonstrated that this was indeed the case (figure 3.5). Overall, radiotracer accumulation increased between ~5- 10-fold, depending upon the condition and incubation time. The results of these time-dependent experiments, demonstrated that the accumulation of ^{64}Cu-ATSM was always greater during hypoxia.

Furthermore the hypoxic to normoxic contrast increased to 2: 1 after 30 min, but again the data were not statistically different. After 60 min ^{64}Cu-ATSM accumulation had increased by 72.7 % and 64.1 % relative to the 30 min values, under oxygenated and hypoxic conditions respectively. While the hypoxic to normoxic contrast decreased to 1.6: 1 at 60 min, the sample variance was less that at 30 min and therefore the data sets were significantly different. Reducing the volume of medium and increasing the incubation time had therefore caused a concomitant increase in both radiotracer accumulation, and the hypoxic to normoxic contrast ratio. We therefore concluded that ARVM should be incubated with ^{64}Cu-BTSC complexes for a minimum of 1 h. However previous studies have demonstrated that ARVM exposed to anoxic conditions for more than 60-90 min are irreversibly damaged [265-267]. We therefore decided that in our experiments ARVM would not be incubated under any condition for more than 60 min to avoid cellular injury. We did this because damage to the cells could potentially have decreased the accuracy of our experiments.

3.4.3.2 Effect of Oxygen Concentration on the Accumulation of ^{64}Cu-ATSM

For the radiotracer extraction and time dependent experiments we employed a 95 % O_2/ 5 % CO_2 gas mixture, to generate and maintain oxygenated conditions. We employed such a high level of oxygen because we postulated that using these extremes (0% and 95 %) would provide the greatest hypoxic to normoxic contrast. However we were aware that in other cell based studies with Cu-ATSM and ^{18}FMISO had previously used gas mixtures at around room air saturation ~20 % [112, 119, 162, 167, 197, 208-209, 241]. While this is still hyperoxic relative to intravascular or interstitial pO_2, it is considerably closer to

physiological conditions when compared to 95 % oxygen. In our next series of experiments we therefore assessed ^{64}Cu-ATSM accumulation using a gas mixture that contained 21 % O_2, alongside the 0 % and 95 % O_2 mixtures, to allow us to compare our results with those of others. This also allowed us to assess whether decreasing the level oxygen had an effect on the accumulation of ^{64}Cu-ATSM.

During our oxygen level dependent ^{64}Cu-ATSM accumulation experiments we observed significantly greater tracer retention under hypoxic conditions, compared to either of the oxygenated conditions (figure 3.6). Contrast ratios of 1.3: 1 and 1.5: 1 were observed between hypoxic cells and those incubated under an atmosphere of 21 % O_2 and 95 % O_2 respectively. No difference was observed between the data sets from cells incubated under oxygenated conditions. However when the data sets were normalised for the total protein content of the respective cell pellets, only the 0 % and 21 % oxygen data sets were significantly different. This was most likely because the average value at 21 % O_2 (25.2 ± 5.6 Bq/ µg protein) was marginally lower than the value obtained at 95 % O_2 (25.9 ± 4.1 Bq/ µg protein). We can only speculate that this was due to the inherent sample variance.

The results of the time and oxygen level dependent experiments, demonstrated that while it was certainly possible to use a cell based assay to assess the myocardial accumulation of ^{64}Cu-BTSC complexes, it is unlikely that the assay could be scaled-down and used as a high-throughput screen for multiple tracers/ replicates. This is because both tracer accumulation and the hypoxic to normoxic cell contrast were low.

3.4.4 ^{64}Cu-ATSM Accumulation: ARVM Compared to Other Cell Types

In our time dependent ^{64}Cu-ATSM accumulation studies the average amount that was retained by ARVM was 4.5 ± 1.5 % (95 % O_2), and 8.2 ± 4.7 % (0 % O_2) of the total radioactivity added at the start of each experiment. When we assessed the effect of reducing the level of oxygen in our aerobic controls, the values were similar: 7.3 ± 0.8 % (0 % O_2), 5.6 ± 1.4 % (21 % O_2) and 4.9 ± 0.9 % (95 % O_2). These results demonstrate that the accumulation of ^{64}Cu-ATSM in ARVM was rather low, relative to the total amount of radioactivity added to the vessel. This is highlighted by comparing our data with those from other cell types (table 3.1).

Table 3.1. Maximum 64Cu-ATSM accumulation in other cell types.

	Cu-ATSM Accumulation (% total radioactivity)		
Cell Type	**Anoxia/ Hypoxia**	**Normoxia**	**Reference**
Chinese hamster ovary	~15	~9	[162]
EMT6	~60	~10	[163, 167]
MDA468	~45	~20	[241]
FaDu	~60	~15	[241]
R3327-AT	~27	~16	[241]
FSaII	~25	-	[241]
MCF7	~30/ 26 Bq/cell	~6 Bq/cell	[197, 241]
DU-145	~30	-	[241]
	^{64}Cu-ATSM Accumulation (% uptake)/ µg Protein		
LNCap	~0.40	~0.20	[242]
LAPC-4	~0.35	~0.30	[242]
PC-3	~0.35	~0.18	[242]
22Rv1	~1.0	~0.40	[242]

3.4.4.1 Metabolic Factors That May Affect ^{64}Cu-ATSM Accumulation

Due to the potential diagnostic, prognostic, and therapeutic applications of hypoxia tracers in oncology compared to cardiology, the majority of cell types that have been used to characterise ^{64}Cu-ATSM *in vitro* have been tumour cell lines [167, 197, 209, 241]. Chinese hamster ovary cells have also been used [162]. By comparing our data with those of others, we see that the accumulation of ^{64}Cu-ATSM in ARVM was much lower than in tumour cells, although it was comparable to uptake in CHO cells. One possible explanation for this is that ARVM are quiescent when cultured *in vitro*, and are therefore much less metabolically active than myocytes *in vivo*. White and Wittenberg demonstrated that the level of mitochondrial NAD(P)H was approximately ~2-fold higher in unpaced isolated cardiac myocytes, compared to those that were paced at 5 Hz [268]. Furthermore, they also demonstrated that oxygen utilisation was ~2-fold higher in cells paced at 5 Hz, compared to those that were paced at 0.5 Hz. In addition to this ARVM are terminally differentiated cells they do not divide, and this further reduces their energy requirements relative to tumour cells which vigorously proliferate *in vitro*. It is therefore likely that the tumours cells used by other groups would have had a higher demand for nutrients and oxygen, compared to our cultured ARVM. During our hypoxia experiments we noticed that while the pO_2 of the culture medium always fell below 0.8 mmHg, it never reached 0.0 mmHg. Other groups have also employed a 0 % oxygen gas mixture. It is feasible that the higher metabolic activity of tumour cells would cause them to utilise any residual oxygen that was dissolved in the culture medium, effectively making the cells more hypoxic than ARVM in our experiments. With respect to tracer accumulation, the effect of this would be to further decrease the rate at which reoxidation

of Cu(I)-ATSM occurs, which would therefore increase tracer trapping. This may explain why the retention of Cu-ATSM under hypoxic conditions was higher in tumour cells. Tumour cells down-regulate oxidative phosphorylation and increase the rate of glycolysis by a process known as the Warburg effect [269], so mitochondrial consumption of oxygen may not be responsible for this. However, it is possible that the consumption of residual oxygen may have occurred through another metabolic pathway, such as cholesterol synthesis [36-37]. Cholesterol is an integral membrane lipid that is required by all cells, especially those that are dividing. Rapidly dividing cells could perhaps have higher oxygen consumption through this process than terminally differentiate myocytes, which are not undergoing growth. This is supported by data from Gal *et al*, who investigated cholesterol metabolism in cervical cancer cell lines and non-cancerous fibroblasts, and observed a significantly higher rate of uptake and degradation of low-density lipoprotein by tumour cells compared to non-tumour cells [270].

3.4.4.2 Cell Number and Population Density

In our time- and oxygen-level dependent experiments the total number of ARVM, including rod-shaped, distorted, and rounded cells was in the range 2.0 x 10^5- 2.7 x 10^5 cells/ 90 mm Petri dish. Considering that we used 5 ml of culture medium in these experiments, the cell density was in the range 4.0 x 10^4- 5.2 x 10^4 cells/ ml. Dearling *et al* employed CHO cells at 2- 4 x10^5 cells/ ml in 50 ml medium [162]. Tumour cell lines were commonly used at a density of 1 x 10^6 cells/ ml (1- 5 x 10^7 cells in total) [167, 195, 208, 242], while Burgman *et al* characterised ^{64}Cu-ATSM accumulation in six tumour cell lines, seeded at 2x10^5 cell/ culture vessel with 0.5 ml culture medium [241]. The cell

numbers and population density that we were able to achieve with ARVM was therefore relatively low compared to these other studies. Furthermore because in our experiments ARVM were attached to the surface of the culture vessel, they were not evenly dispersed throughout the culture medium. These two factors combined may also explain why the accumulation of ^{64}Cu-ATSM was relatively low in ARVM, compared to other cell lines.

3.4.4.3 Concentration of ^{64}Cu-ATSM in the Culture Medium

The amount of radiotracer that was added to the culture medium is another factor that could affect the rate or amount of accumulation. Cu-BTSC complexes are thought to enter cells by passive diffusion. Increasing the concentration of radiotracer in the medium would therefore increase the number of potential interactions between molecules ^{64}Cu-ATSM and ARVM. It would also have the effect of increasing the rate of diffusion into cells, because there would be a larger concentration gradient between the extracellular and intracellular compartments, at least until the partitioning reached equilibrium. With the exception of Dearling *et al's* work with CHO cells, the concentration of ^{64}Cu-ATSM employed by other groups was ~2- 4-fold higher than the 20 KBq/ ml used in our experiments [162, 167, 208, 241-242]. It is therefore likely that if more ^{64}Cu-ATSM had been added to the culture medium, we may have observed greater tracer cellular accumulation and contrast between hypoxic and oxygenated cells.

3.4.4.4 Comparison of ^{64}Cu-ATSM accumulation with other Hypoxia Tracers

Martin *et al* [112] and Biskupiak *et al* [119], respectively assessed [^{3}H]FMISO and [^{131}I]IVM using ARVM based systems. After a 60 min incubation the hypoxic to

normoxic contrast ratio was 9.6: 1 for [^{3}H]FMISO, and 4.4:1 (hypoxia) and 8.4: (anoxia) for [^{131}I]IVM. We observed much lower contrast, with ratios between 1.3- 1.6: 1 after 60 min. This does not agree with previous data from isolated perfused hearts, obtained by Fujibayashi *et al* [174]. However both [^{3}H]FMISO and [^{131}I]IVM were exposed to ARVM at a concentration of 50 µM, which is at least two orders of magnitude greater than the ~15 nM ^{64}Cu-ATSM that we used. In our experiments we chose to restrict the concentration of ^{64}Cu-ATSM to reflect the nano/ pico molar quantities that are employed for clinical PET imaging.

3.4.4.5 ARVM Morphology after Exposure to Oxygenated and Hypoxic Conditions

Another way in which our experiments differed from those of Martin, and Biskupiak was that their experiments were run for up to 3 h. As already discussed we limited the incubation time to 60 min to avoid irreversible cellular injury. As part of their experimental protocol Martin *et al* monitored the morphology of ARVM before the start and at the end each experiment. After 60 min anoxic they observed a 10 % decrease in the number of rod-shaped ARVM, compared to control samples. Although the authors reported that the decrease in the percentage of rod-shaped ARVM was not statistically significant. After 180 min anoxic gassing the number of rod-shaped myocytes was 25 % less than control samples. We also assessed cell morphology as part of our experimental protocol. Our data show that after 30 or 60 min incubation the number of rod-shaped ARVM was comparable to the 0 min control values, regardless of the level of oxygenation (figures 3.8 and 3.9). Furthermore the number of rod-shaped ARVM was similar for all conditions. Our data show that the morphology, and therefore viability, of

ARVM was not affected by increasing or decreasing the level of oxygen. We can therefore be confident that the contrast that we observed between ^{64}Cu-ATSM retention in hypoxic cells compared to oxygenated cells was due to hypoxia selectivity, and not other factors which may be related to prolonged exposure to hypoxia or cellular injury.

3.4.4.6 Assessment of ^{64}Cu-ATSM accumulation in ARVM Maintained in Suspension

We made a final attempt to develop an ARVM based model for characterising ^{64}Cu-BTSC complexes, using cells maintained in a suspension of M199. As discussed previously this is not conducive to the medium to long term viability of ARVM. However both Rumsey *et al*, and Ramalingham *et al* have previously applied this method to demonstrate significant hypoxia-dependent uptake of BMS181321 [132], and ^{99m}Tc-BAPN [138] respectively. With the potential advantages that suspension culture has, such as high cell number, and lower cost because laminin is not required, it was an attractive approach that was worth investigating.

By using the cell suspension method we observed a maximum of 63.2 % retention of the total radioactivity, under hypoxic conditions. This is similar to the uptake that was observed in EMT6 [167], MDA468 [241], and FaDu [241] tumour cells, and considerably more than in CHO [163] cells, and other tumour cell lines [241]. However unlike these other studies we observed significant accumulation of ^{64}Cu-ATSM under oxygenated conditions, equating to 53.4 % of the total radioactivity. The contrast ratio between the two experimental conditions was therefore only 1.2: 1, compared to values

of generally 1.7- 6.0: 1 in other cell types, with the exception of LAPC-4 cells. With respect to the screening of other hypoxia tracers that were characterised using ARVM, Rumsey *et al* observed a hypoxic to normoxic cell contrast of was between ~2: 1 with BMS181321 [132], which was considerably higher than we observed for ^{64}Cu-ATSM.

In our cell suspension experiments we observed a 10-fold increase in radiotracer accumulation, compared to those where ARVM were allowed to attach to the culture vessel. While this approach lead to significantly greater retention of Cu-ATSM in ARVM, and also allowed us to discern a contrast in tracer uptake between our experimental conditions, once again we observed a large variance in the replicate samples. The amount of tracer that was retained under oxygenated conditions was also relatively high compared to other cell types, and tracers. Without further experiments it is not possible to determine why this occurred. However it is plausible that up-regulation of the bioreductive mechanism/s responsible for the Cu-ATSM accumulation may occur in ARVM that are undergoing apoptosis, as they are no longer attached to other cells or the extracellular matrix. This may be the reason why the retention of ^{64}Cu-ATSM retention was relatively high in these cells, even under oxygenated conditions.

3.4.5 Conclusions

During our experiments we observed considerable variation the number of cells that we obtained when isolating ARVM. We also observed large variance in the amount of ^{64}Cu-ATSM that accumulated within cells, even between replicates samples where cells had been incubated under the same condition. We therefore observed poor contrast in the

retention of ^{64}Cu-ATSM between our experimental conditions. This severely limited the potential usefulness of the ARVM based assays for the purposes that we had proposed. It was also unlikely that we would be able to scale-down our system, because lowering the cell number would further exacerbate these issues. We also planned to use an isolated myocyte approach to characterise the accumulation of our library of Cu-BTSC complexes at more physiologically relevant oxygen levels. However, as such poor contrast was observed under the extreme conditions that we tested, we concluded that this system was unlikely to be sensitive enough to monitor the accumulation of ^{64}Cu-BTSC complexes at low and intermediate levels of oxygenation. We therefore decided that the ARVM screening assay that we had developed was not suitable for characterising our library of ^{64}Cu-BTSC complexes, and we shifted our focus to another well established technique the Langendorff isolated perfused heart, as a means of characterising our tracers.

Chapter 4.

Calibration of Equipment Required for the for *Ex Vivo* Characterisation of Candidate Tracers

4.1 Introduction

This chapter will introduce the techniques and equipment that we employed to characterise ^{64}Cu-BTSC complexes, using Langendorff isolated perfused hearts. It will also describe the assembly, calibration, and optimisation of a purpose built Na/ I gamma radiation detector array for monitoring the flow of radioactivity into, through, and out of hearts in real-time. However before describing these experiments we will introduce the principles of *ex vivo* heart perfusion.

4.1.1 The Langendorff Isolated Perfused Heart

The isolated Langendorff perfused heart has been employed previously to characterise the myocardial tissue clearance/ accumulation of both perfusion and hypoxia targeting tracers. Before addressing how the method was previously employed it is pertinent to describe the principles of this widely used research tool, by first explaining how the heart is perfused *in vivo*.

4.1.1.1 The Coronary Vasculature

Blood carries with it not only oxygen but nutrients such as glucose, fatty acids and trace elements, as well as extra-cellular signalling molecules (e.g. insulin, glucagon). Blood also removes metabolic waste products such as CO_2 and lactate. The heart has a very limited store of nutrients, and because of its high work-rate nutrients need to be constantly replenished and waste products removed. The heart is therefore heavily vascularised.

At the very end of each cardiac contraction (end systole), the left ventricle has expelled most of the blood in its lumen into the aorta. Pressure in the aortic lumen is therefore high, while as the ventricular muscle begins to relax, the pressure within the ventricular lumen is relatively low. This rising back pressure forces the aortic valves to shut, thereby preventing the return of blood to the heart. The majority of the blood in the aortic lumen will follow the route of the aorta and great arteries. However, the pressure inside the ascending aorta and aortic arch at the time of systole, forces some of the blood through the coronary ostia, and into the right (RCA) and left main (LM) coronary arteries. The LM branches into the left anterior descending (LAD) and circumflex coronary arteries (CIRC). A fifth main coronary artery, the post descending artery (PDA) may branch off of either the RC or CIRC. These coronary arteries reside on the outer surface of the epicardium, and follow ridges formed where the chambers of the heart meet. Branches off of these arteries permeate into the tissue and perfuse the myocardium through a network of arterioles and capillaries. Blood returns to the chambers of the heart via veins that run parallel to the coronary arteries, and drains into the right atrium via the coronary sinus [11].

4.1.1.2 The Isolated Heart Perfusion Technique

Langendorff first described his method for the *ex vivo* perfusion of mammalian hearts in 1895 [271]. The technique allows the heart to be studied independently, without the affects of neuronal or hormonal stimuli. The heart is then perfused in a retrograde manner with a physiological salt solution, which usually also contains glucose, and is also saturated with oxygen. The pressure exerted by this retrograde perfusion closes the

aortic valves, causing the perfusate to flow through the coronary ostia and into the coronary arteries. The buffer flows through the coronary vasculature and bathes the tissue beds, continues to flows through the coronary veins and into the right ventricle via the coronary sinus. The perfusate then exits the heart via a small incision made in the pulmonary artery (figure 4.1).

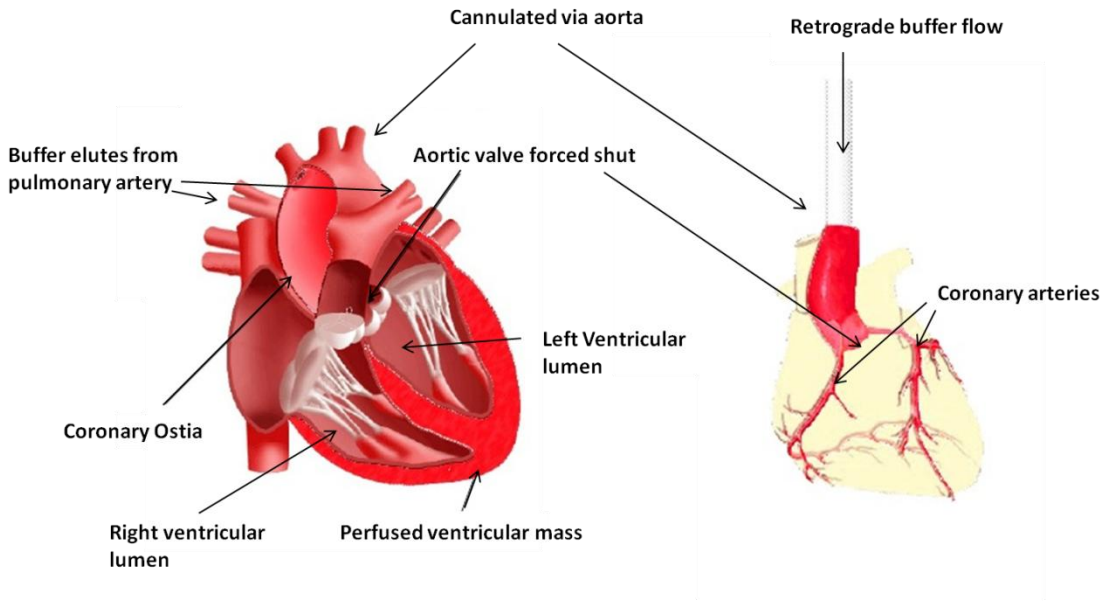

Figure 4.1. Langendorff isolated heart perfusion. Retrograde perfusion forces the aortic valve to close, and buffer then flows through the coronary ostia and into the coronary vasculature via the coronary arteries. Buffer then elutes from right ventricle via the pulmonary artery. Adapted from [272]

4.1.1.3 Langendorff Isolated Heart Perfusion: Advantages and Disadvantages

Although the Langendorff isolated heart technique has been and will no doubt continue to be used in cardiac research for many years, there are a number of limitations to the method that must be considered.

The advantages to using the Langendorff method are that the excision, cannulation and perfusion procedures are relatively quick and simple. The heart is then free from neuronal and hormonal stimuli, and more amenable to biochemical, physiological or morphological investigation than when *in situ*. The constituents of the perfusion buffer can be manipulated with ease, as can the perfusate flow rate, for example to induce ischaemia. The effect of any stimulus, condition, or pharmacological agent can then be directly monitored through changes in cardiac function or electrophysiology. These parameters can easily be measured by inserting a fluid filled balloon into the left ventricle, which is coupled to a pressure transducer and a data acquisition system, or by attaching an ECG monitor to the heart. The Langendorff isolated perfused heart technique is therefore most conducive to studies on radiotracer characterisation, as will be demonstrated in the following discussion.

The disadvantages of using isolated perfused hearts is that they are an *ex vivo* model that is constantly deteriorating from the moment the heart is excised from the donor. Although the heart is supplied with a variety of nutrients and minerals via the perfusion buffer, certain essential nutrients, for example amino- acids, are usually excluded and therefore the *ex vivo* conditions can do not exactly mimic those *in vivo*. Conversely the

isolated heart can withstand extreme conditions such prolonged anoxia, which in an *in vivo* scenario would cause the death of the animal. However the advantage of this is that it allows the study of these conditions. For these reasons the isolated perfused heart is considered to be one step further away from the physiological/ clinical setting.

Oxygenation is also an issue because Langendorff hearts are usually perfused with Krebs-Henseleit Buffer (KHB), a physiological salt solution. While gassing with 95% O_2/ 5% CO_2 achieves buffer saturations in excess of 500 mmHg, KHB does not have the oxygen carrying capacity of blood [273]. This is apparent in that the coronary flow through a blood-perfused rat heart at 74 mmHg perfusion pressure is typically 3 ml/ min, while flow rates of 12- 16 ml/ min are typically needed in constant flow systems, to achieve similar levels of cardiac function in a buffer perfused heart [273]. Southworth *et al* have demonstrated that when rat hearts are perfused with oxygenated KHB, the thickness of the ventricular walls doubles due to this vasodilation [274]. However whilst the isolated perfused heart may be considered "physiologically compromised" with respect to oxygen delivery, NMR studies have demonstrated that the buffer perfused Langendorff heart is energetically normal with respect to intracellular phosphocreatine and ATP levels [275].

4.1.2 Characterisation of Candidate Hypoxia Tracers Using Isolated Perfused Hearts

The Langendorff method of isolated heart perfusion has been widely employed as a model for characterising the myocardial retention of candidate perfusion and hypoxia

specific tracers. The nitroimidazole based tracers ^{18}F-MISO [127] and BMS181321 [115-116, 132-134], ^{99m}Tc labelled- HL91 [149, 151, 276], and the Cu-bis(thiosemicarbazones) ^{64,67}Cu-PTSM [75] and ^{62}Cu-ATSM [174], have all previously been assessed using this method. Invariably the washout/ accumulation of radiotracers in the heart has been measured and quantified using Na/I γ-detector systems. The radiotracer is either constantly infused or administered as a bolus, under oxygenated or ischaemic/ hypoxic conditions. The gamma detectors then measure radioactivity emitted from the heart in real-time. By using this method it is has been possible to determine the tissue retention, and potential normoxic to hypoxic tissue contrast of candidate hypoxia selective radiotracers. A number of studies have also used this method to produce kinetic analyses of radiotracer retention/ clearance. This was done in order to further quantify how changes to the structure and physiochemical properties, affect tracer performance [75, 115-116, 127, 134, 149, 151, 276].

4.1.2.1 The Gina star™ Data Acquisition System and Na/ I γ- Detector Array

For the radiotracer characterisation that we describe in this thesis, we designed and commissioned a purpose built Na/ I γ- radiation detector system from Raytest Isotopenmessgeräte GmbH (Straubenhardt, Germany) [277]. The Gina Star™ data acquisition system is a modified version of the company's standard GABI Star™ system, which is used for radio-HPLC. Our modified system was upgraded so that it was capable simultaneously receiving inputs from three Na/ I γ-detectors, instead of the two. The system was controlled by the Gina Star™ (version 4.0.2.75) software package, installed

on a laptop personal computer. Figure 4.2 provides a schematic representation of the combined γ-detector- isolated heart perfusion systems.

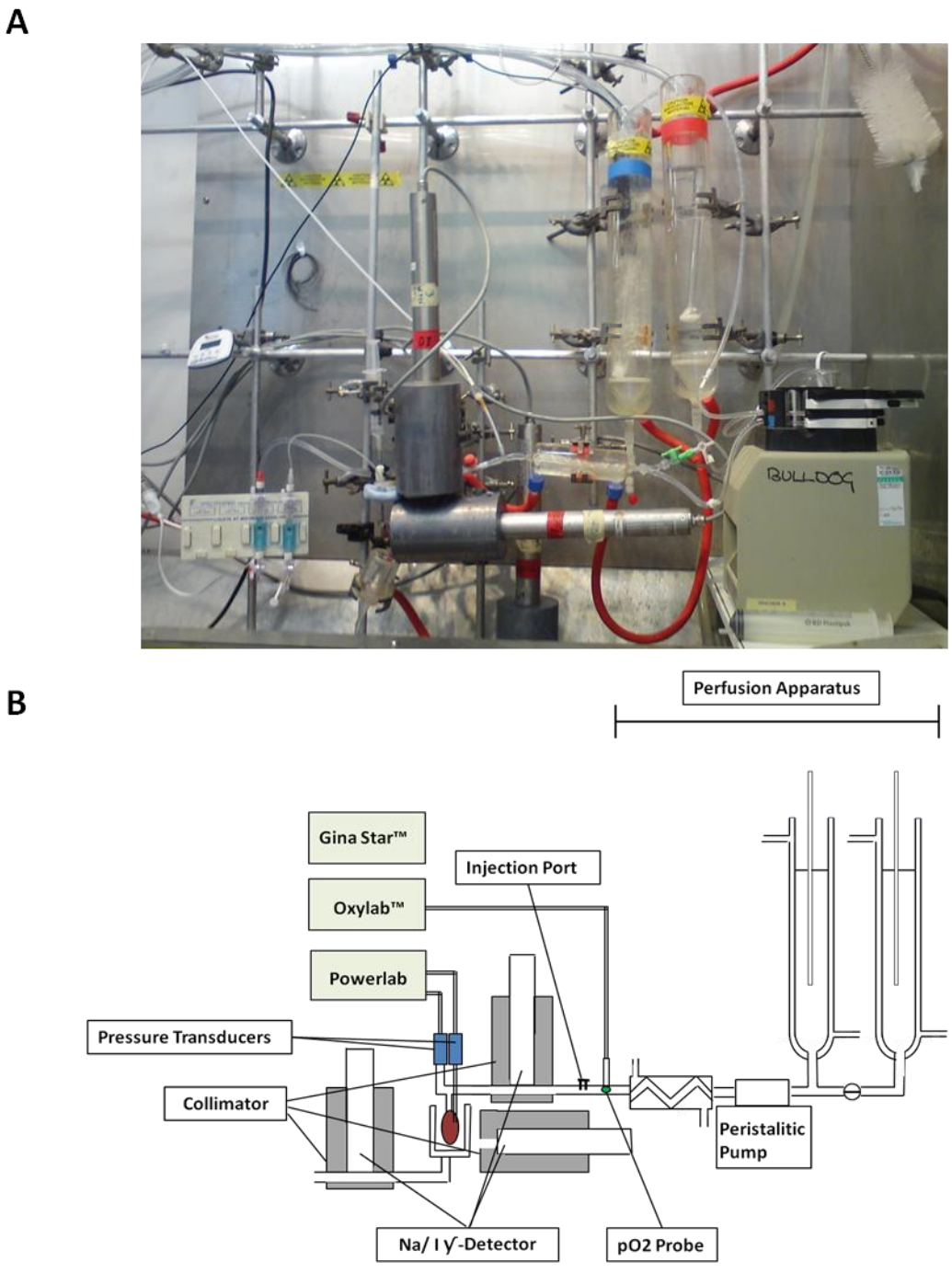

Figure 4.2. The triple γ-detector array (A), and schematic representation (B).

Previous studies have tended to employ a single γ-detector positioned close to the heart [115-116, 132, 149, 151, 174, 276], although occasionally two γ-detectors have been used to provide coincidence counts, in order to decrease the system error [75, 127, 134]. Our system employed Na/ I γ-detectors that were arrayed over the perfusion apparatus, allowing us to produce time-activity curves for the heart, as well as establishing both input and output functions. We hypothesised that these parameters could then be used to perform pharmacokinetic modelling on the time-activity curves that we obtained. Apart from providing valuable information regarding the rate of radiotracer clearance and tissue accumulation, compartmental pharmacokinetic modelling could potentially determine the rate at which reduction of the Cu(II)-complexes occurs, and perhaps give some insight into the fate of the ^{64}Cu- moiety. This information would allow for a more detailed and accurate characterisation, evaluation, and comparison of the ^{64}Cu-BTSC complexes, relative to what has previously been achieved with a single Na/ I detector, or cell based assays.

4.2 Materials and Methods

4.2.1 Chemical and Reagents

Unless stated otherwise all bulk chemicals were of analytical grade and were purchased from Sigma-Aldrich.

4.2.2 Gas mixtures

Gas mixtures used for this series of experiments were: oxygenated (95 % O_2/ 5 % CO_2), and anoxic (95 % N_2/ 5 % CO_2).

4.2.3 Isolated Heart Perfusion Apparatus

A schematic representation of the isolated heart perfusion rig is shown in figure 4.3. This particular set of perfusion apparatus was constructed as a constant flow system. The perfusion buffer flow rate was controlled via a peristaltic pump (Gilson, USA). All glassware was water-jacketed and supplied with warm water by a circulator/ heater, to maintain the perfusate at a temperature of 37.0- 37.4 ºC.

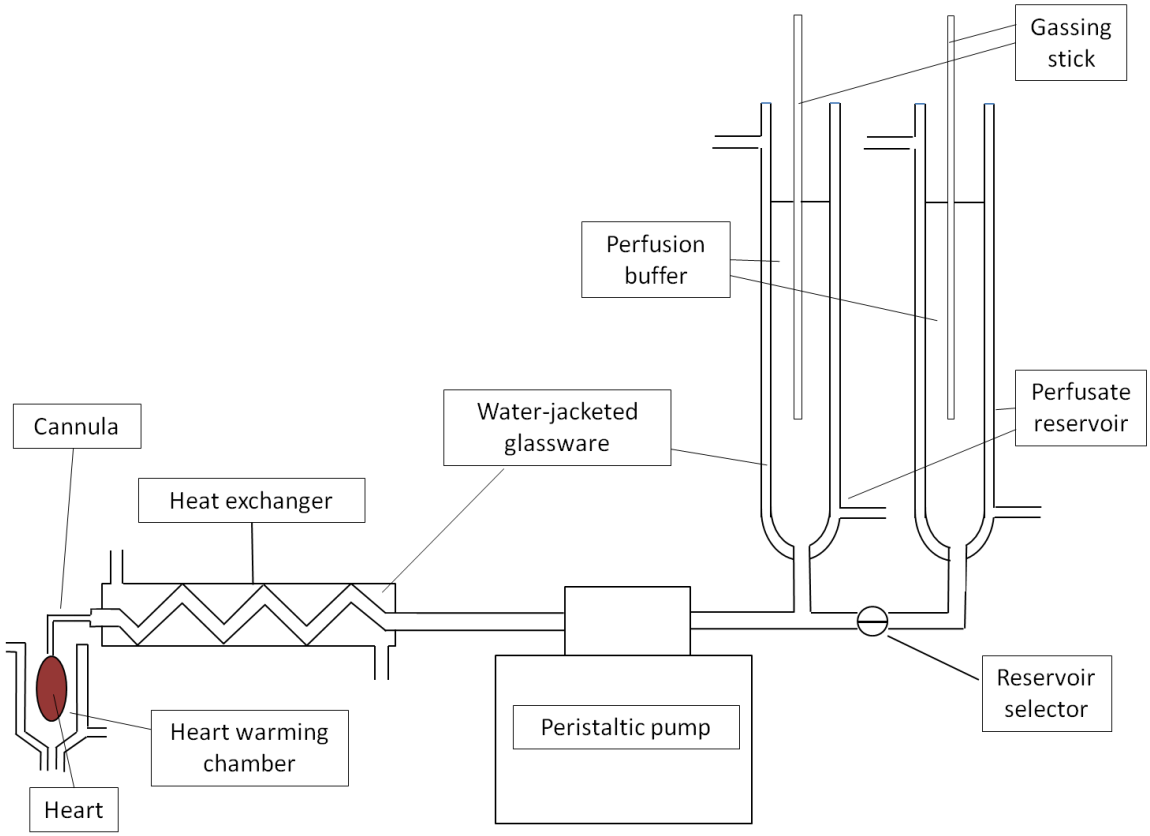

Figure 4.3. Schematic representation of Langendorff isolated heart perfusion apparatus.

4.2.3.1 Calibration of Perfusate Flow Rate

A peristaltic pump (Gilson, USA) was incorporated into the system in order to maintain a constant flow of perfusate. During the preliminary experiments described in this chapter the pump was calibrated and controlled manually. This calibration was performed by measuring the flow rate volumetrically, against the arbitrary values displayed on the pump control interface.

4.2.3.2 Calibration of Perfusion Buffer Temperature

At the time that the perfusion rig was built and then before the start of each experiment, the temperature of the perfusion buffer was measured using a thermocouple inserted into the perfusion cannula. This was performed regularly to ensure that the perfusate was at a temperature of between 37.0 and 37.4 ºC as it entered the coronary vasculature.

4.2.3.3 Measurement of Perfusion Buffer pO_2 During Deoxygenated Perfusion

The pO_2 of the perfusion buffer was measured every 60 seconds for 60 min, after switching from non-gassed to hypoxic (95% N_2/ 5%CO_2) perfusion buffer. The Oxylab pO_2™ combined with a pO_2 and temperature sensor (described in section 2.2.12.1), was then used to measure the pO_2 of the buffer as it flowed from the tip of the perfusion cannula.

4.2.3.4 Calibration of Pressure Transducers

In order to monitor cardiac function in isolated perfused hearts, and to assess the affects of perfusion with hypoxic buffer, a PowerLab/4SP data acquisition system and

LabChart® 7 (version 7.2) software package (ADInstruments, UK) were employed. This was coupled to two DTXPlus™ pressure transducers (BD, UK). One pressure transducer was positioned on a side-arm of the perfusion cannula to monitor perfusion pressure, while the second was attached to a small balloon that was inserted into the left ventricle of hearts, and was used to measure left ventricular pressure. From the left ventricular balloon input the LabChart® software was able to calculate left ventricular developed pressure (LVDP), left ventricular end diastolic pressure (LVEDP), and heart rate.

4.2.4 Langendorff Isolated Perfused Heart

4.2.4.1 Isolated Heart Perfusion Buffer

In this study isolated hearts were perfused with a modified Krebs-Henseleit buffer (mKHB) previously described by Cave and Garlick *et al* [278-279] (table 4.1). In our laboratory we use phosphate free KHB in all heart perfusion experiments to facilitate the analysis of cardiac phosphorus metabolism by ^{31}P NMR when necessary. The NMR signal from phosphate containing buffers would obscure the relatively weak intracellular ^{31}P signal. While none of the experiments described here employed ^{31}P NMR spectroscopy, we use the same perfusion medium is used in all studies in order to facilitate comparison of data across all experiments. Similarly EDTA is included to chelate any free heavy metal ions, which also potentially interfere with the NMR signal. Extra calcium was added compensate for the addition of EDTA, which also forms complexes with Ca^{2+}.

Table 4.1 Preparation of modified Krebs-Henseleit buffer, for the perfusion of isolated hearts in the Langendorff mode.

Chemical	Mol. Wt	Concentration (mM)	Amount (g)/ l
Sodium Chloride	58.4	118.5	6.925
Sodium Hydrogen Carbonate	84.0	25.0	2.01
Magnesium Sulphate	246.5	1.2	0.30
Potassium Chloride	74.6	6.0	0.44
Di-sodium EDTA.$2H_2O$	372.5	0.5	0.19
D-Glucose	180.2	11.0	1.98
Calcium Chloride	147.0	2.5	0.37

4.2.4.2 Excision and Cannulation of Hearts

Adult male Wistar rats (250-300 g) (B&K Universal, Hull, U.K.) were anaesthetised with pentobarbitone (Pentoject 1ml/ kg i.p.). When the animal was sedated to the point that no reflex actions were observed, heparin (200IU) was injected into the femoral vein. The heart was then rapidly excised and immersed in ice cold mKHB. Excess tissue was carefully removed and the heart was cannulated in the Langendorff mode. The heart was then perfused with mKHB (Table 4.1) under constant flow (14 ml/ min).

4.2.4.3 Conformation of Isolated Perfused Heart Preparation Stability

To establish the functional parameters upon which the heart preparations were to be accepted in any of our studies, we performed a stability study. By perfusing hearts at a constant flow (14 ml/ min), the perfusion apparatus and my cannulation technique were iteratively improved until the hearts were capable of developing a pressure 100- 140 mmHg. Criteria where established for heart rate, left ventricular developed pressure (LVDP), left ventricular end diastolic pressure (LVEDP) and coronary perfusion

pressure, whereby hearts meeting these requirements within 20 min of cannulation were entered into an experiment, while those that did not were rejected.

4.2.5 Preliminary Experiments with γ-Detection and Isolated Perfused Hearts

Before the Gina Star™ system was purchased a series of preliminary experiments were performed using a crude detector system, as proof of principle.

Hearts were cannulated as described above and a Na/ I γ-detector from a radio-HPLC was positioned ~1 cm from the heart. Hearts were first perfused with oxygenated mKHB (95% O_2/ 5% CO_2), which was then switched to deoxygenated buffer (95% N_2/ 5% CO_2). Under each condition a 2 MBq bolus of ^{64}Cu-ATSM, ^{64}Cu-PTSM or ^{18}F-MISO, diluted in mKHB), was administered via an injection port which was built into the perfusion line. Throughout each experiment the HLPC system software was used to record radioactive decay, to produce time-activity curves.

4.2.6 Gina Star™ Na/ I γ-Detector Calibration

The Gina Star™ data acquisition system was developed for the purpose of monitoring the accumulation and washout of radiotracers in isolated perfused hearts. In order to assess the relative sensitivity and response uniformity of three Na/I detectors, a series of calibration experiments were conducted before the system was used.

4.2.6.1 Detector Response Uniformity

Detector uniformity was tested to ensure that each of the three detectors responded equally to a given amount of radioactivity, and registered similar values for decay (counts per second). This was achieved by placing a vial containing 0.1- 50 MBq of ^{64}Cu in front of each detector at a distance of 68 mm, which we had previously found to give rise to 1000cps with 1 MBq ^{64}Cu. The decay was then measured for 1 min in triplicate, for each amount of radioactivity and each Na/ I γ-detector.

4.2.6.2 Detector Dead Time and Response Linearity

With the Gina Star™ system it was possible to amend the data sampling rate, allowing some control over the detector dead time or sample time. The system was setup to achieve the maximum sampling rate of 1 sample/ 0.2 sec. The linear range of the Na/I γ-detectors, in terms of counts per second registered, was also established from the detector uniformity data.

4.2.6.3 Shine Through

Injection of radioactivity in the perfusate line delivers tracers to the heart before it is either trapped or washes out. In our dynamic system, radioactivity flows past each of the three detectors in series, allowing us to monitoring the flow of radioactivity through the system in real-time. However the passage of radioactivity through the system, and the fact that there is likely to be activity in several regions simultaneously, may increase the effect of shine-through. This is caused by inappropriate registration of radioactive decay from proximal or distal regions of the system. Each detector therefore could potentially

register higher counts than expected, with erroneous flow past curves being superimposed onto the actual time-activity data. It was therefore essential to minimise this effect.

Shine-through was assessed after the construction of the perfusion rig and integration of the three Na/I detectors. A vial containing 1 or 10 MBq of ^{64}Cu was placed at the position of detector 1 (arterial) and the cps was recorded at detectors 2 (heart) and 3 (venous). The vial was then placed at the detector 2 position and cps measured by detector 1 and 3 was recorded. Finally the vial was placed at detector 3 and measurements were taken from detectors 1 and 2.

4.3 Results

4.3.1 Langendorff Rig Calibration

4.3.1.1 Calibration of Perfusate Flow Rate and Temperature

A plot for the calibration of the perfusion pump is shown in figure 4.4. Actual flow rate measured volumetrically is shown against the arbitrary flow displayed on the pump control interface. Using this example a displayed value of 24.0 would result in an actual flow rate of 12 ml/ min. This type of calibration was performed regularly (as pumping rate varies with tension on the peristaltic pump tubing), and flow rate was also confirmed at the start of each stabilisation period.

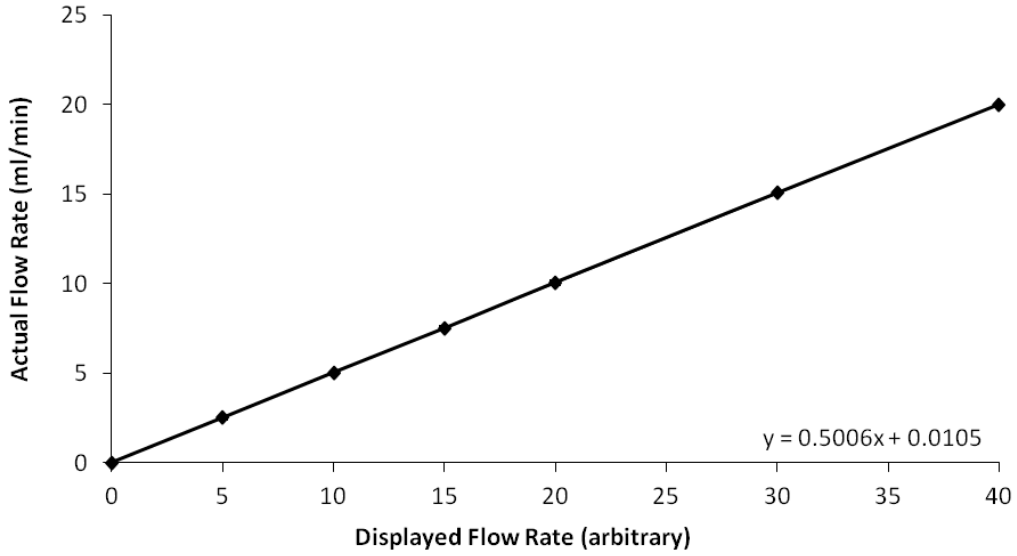

Figure 4.4. Calibration of the perfusate flow rate. Actual flow rate (ml /min) plotted against the arbitrary rate that was displayed on the pump control interface. Data represent mean (n = 3) ± SD.

The heater/circulator was used to supply warm water to the water-jacketed glassware, and was adjusted so that the temperature of mKHB was between 37.0 – 37.4 ºC as it exited the cannula. The results of this exercise (figure 4.5) demonstrate that the temperature of KHB as it exited the cannula remained constant over 2 h.

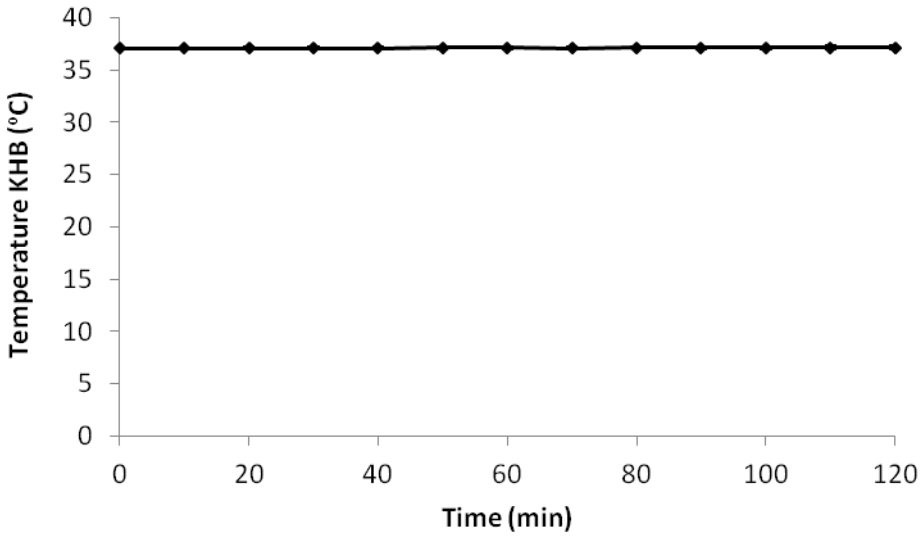

Figure 4.5. Temperature (ºC) of KHB exiting the perfusion cannula over a 2 h period. Data represent mean (n = 3) ± SD.

4.3.1.2 Perfusate pO_2

The partial pressure of dissolved oxygen in the perfusion buffer was monitored over 60 min after switching to hypoxic buffer (figure 4.6). At the start of the experiments the pO_2 of non-gassed KHB was ~140 mmHg. This buffer was not oxygenated so we were able to measure the pO_2 using the Oxylab pO_2™ system, which saturates at levels above 150 mmHg. After switching to hypoxic mKHB the perfusate pO_2 decreased in two distinct phases. The first was rapid with the average pO_2 falling from 144.3 ± 8.3 mmHg to 10.1 ± 4.1 mmHg within 10 min of switching to hypoxic buffer. The second phase was much slower with the level of oxygen steadily decreasing from 10.1 ± 4.1 mmHg to 5.8 ± 0.7 mmHg over 55 min.

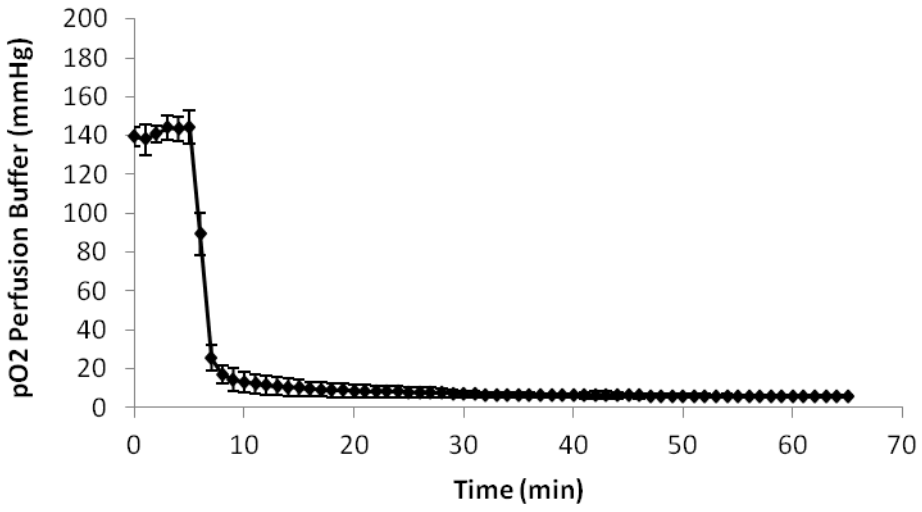

Figure 4.6. Partial pressure oxygen (pO2) of KHB over time, after switching from non-gassed to nitrogenated buffer. Data represent mean (n = 3) ± SD.

4.3.2 Conformation of Preparation Stability

To ensure that cardiac function and coronary perfusion pressure of isolated perfused hearts were within parameters previously defined by Hearse and Sutherland [273], and Skrzypiec-Spring *et al* [280] (Table 4.2), we conducted a series of preliminary experiments to assess my cannulation technique. Limits were set for left ventricular developed pressure (LVDP), left ventricular end diastolic pressure (LVEDP), heart rate and coronary perfusion pressure. Hearts were allowed a 20 min stabilisation period after cannulation, if during this time cardiac function failed to meet the established criteria they were discarded. Cardiac function was then monitored over 2 h.

Table 4.2. Criteria for Cardiac Function.

Cardiac Function (Parameter)	**Range**
Left Ventricular Developed Pressure	> 100 mmHg
Left Ventricular End Diastolic Pressure	4 – 8 mmHg
Heart Rate	> 280BPM
Perfusion Pressure	60 – 80 mmHg

Figure 4.7 displays the data for LVDP, LVEDP, heart rate, and coronary perfusion pressure that were used to establish exclusion criteria. On average over the 2 h perfusion period LVDP decreased by < 10 % per hour, as recommended by Sutherland and Hearse [273]. LVEDP rose from an average of 6 mmHg to ~11 mmHg during the same time. Heart rate slightly increased from 283 BPM to 293 BPM, and the coronary perfusion pressure rose from 57 mmHg to 68 mmHg.

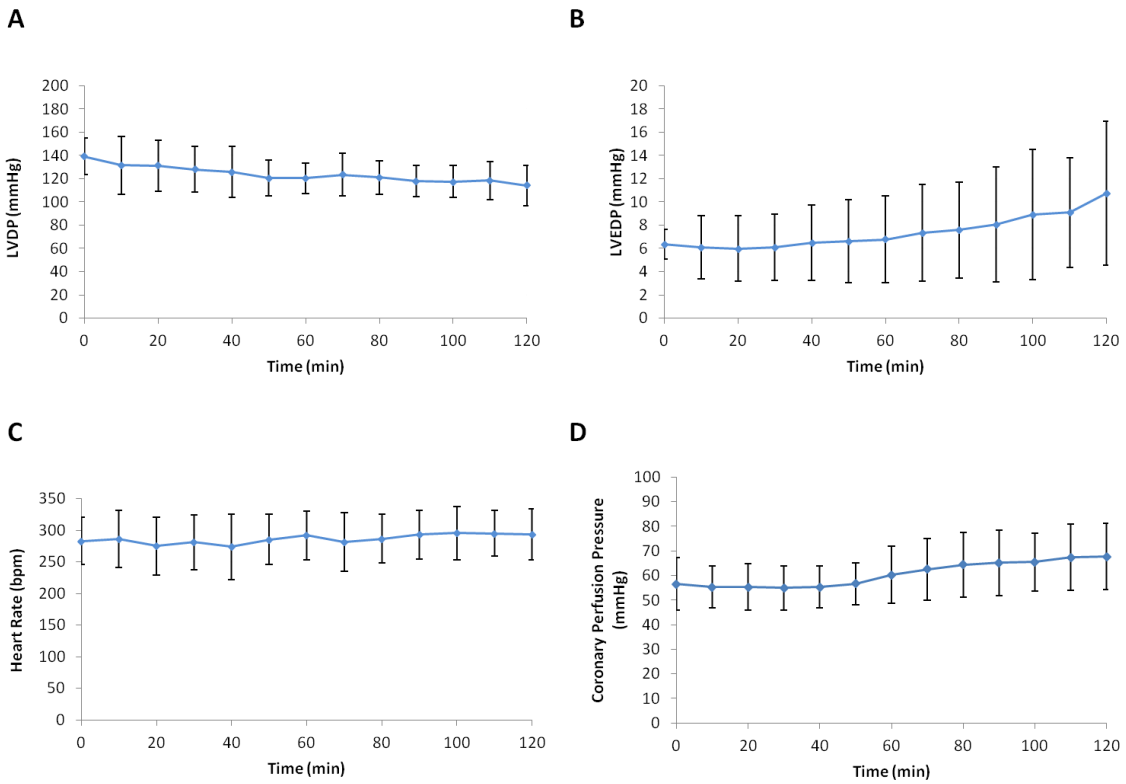

Figure 4.7. Establishment of exclusion criteria for cardiac function. LVDP (A), LVEDP (B), heart rate (C) and coronary perfusion pressure (D) over 2 h. Data represent mean (n = 6) ± SD.

4.3.3 Preliminary Hypoxia Tracer Retention Experiments

Time-activity curves from our preliminary *ex vivo* tracer characterisation experiments are shown in figure 4.8. Tissue retention was estimated as a proportion of the cps within the heart 10 min post injection, compared to the peak cps immediately after an injection. These data were considered as qualitative and not quantitative, because of the relatively simple system that was used for these initial experiments. ~5 % ID of ^{64}Cu-ATSM was retained during normoxia, but this increased to between ~45- 60 % ID under hypoxic conditions. Please note that during the first period of oxygenated perfusion, what appears to be 100 % retention of the first injection of ^{64}Cu-ATSM was actually due to an error where the detector was not in place, and the injection peak counts were missed. ^{18}F-MISO demonstrated negligible accumulation under oxygenated conditions, but ~5- 20 % ID was retained during hypoxia.

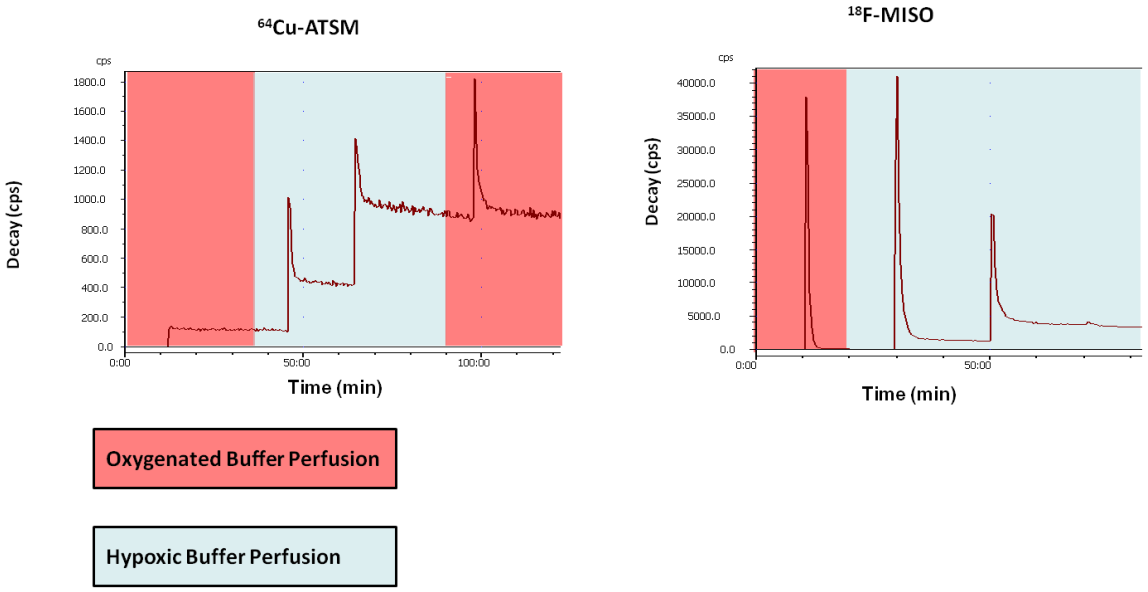

Figure 4.8. Time-activity curves from preliminary ex vivo tracer characterisation experiments for ^{64}Cu-PTSM, ^{64}Cu-ATSM and ^{18}F-MISO. Each peak is representative of a single bolus 2 MBq injection of radiotracer under oxygenated (red) or hypoxic (blue) conditions.

4.3.4 Gina Star™ Na/ I γ-Detector Calibration

4.3.4.1 Na/ I γ- Detector Response Uniformity

The results of the detector response uniformity exercise (figure 4.9) demonstrated that between 0 – 30000 cps (0- 50 MBq ^{64}Cu), each of the three detectors responded uniformly to a given amount of radioactivity. There was however some discrepancy between the detectors. With the exception of measurements taken when the detectors were exposed to 12.5 MBq, Detector 1 always registered the highest number of counts and detector 3 the lowest. From ~5000 – 30000 cps the difference was 2% of the mean counts (triplicate runs), between 500 - 2600 cps it was between to 1 - 4 %, but at ~100 cps there was 10 % discrepancy between the cps registered by detector 1 and detector 3. However with the exception of counts of ~30000 cps, the difference in the decay that was registered by detector 1 and 3 was less than standard deviation of the mean of the triplicates.

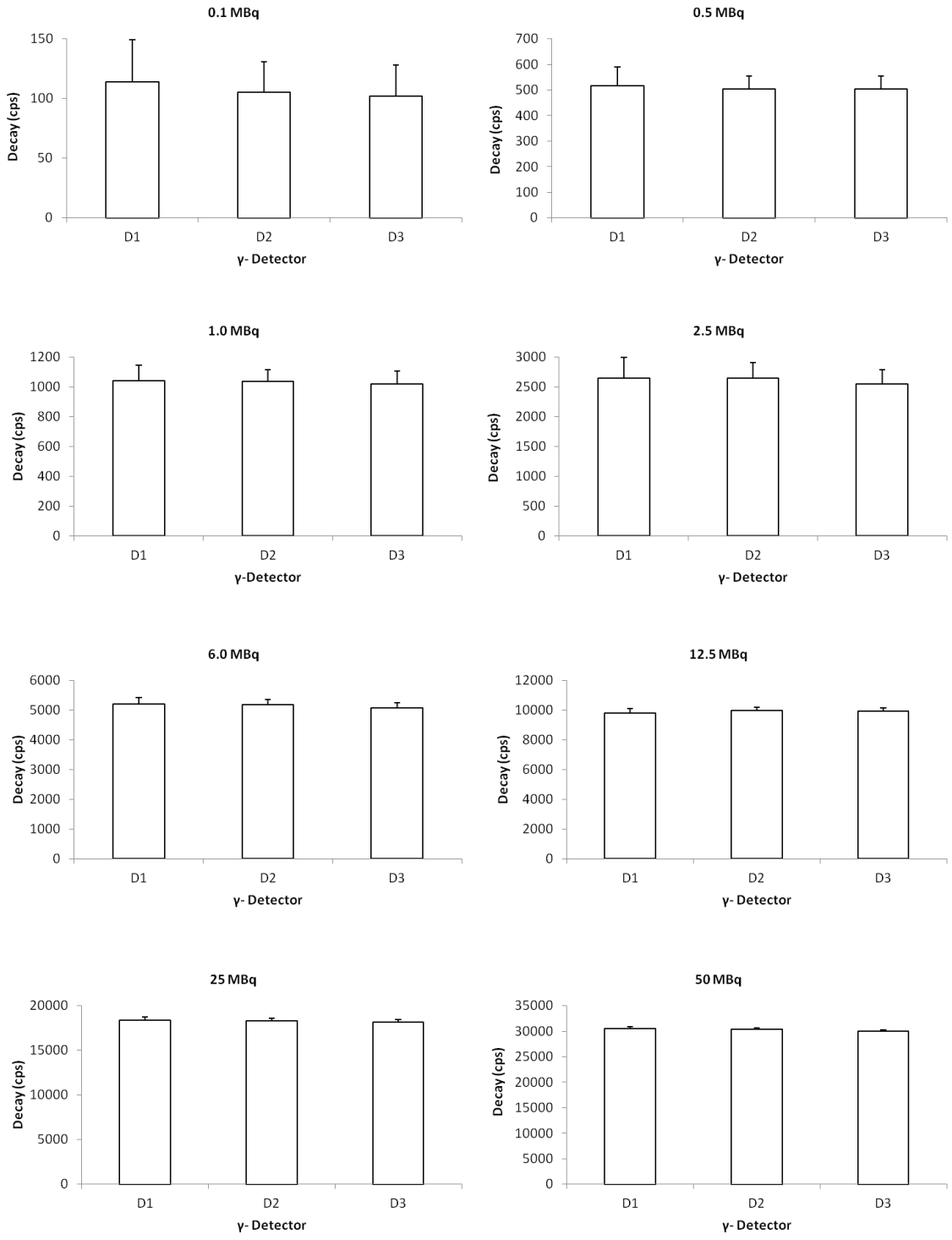

*Figure 4.9. Na/I Gamma-detector response uniformity. Decay (cps) registered by each of the detectors when 0.1- 50 MBq of ^{64}Cu was placed at a distance of 68mm. Data represent mean (n = 3) ± SD. * = significantly different (p <0.05).*

4.3.4.2 Na/ I γ-Detector Linearity

The detector linearity curves (figure 4.10) demonstrate that all three detectors displayed a good degree of linearity ($R^2 = 0.99$) over the range ~ 100 -30000 cps.

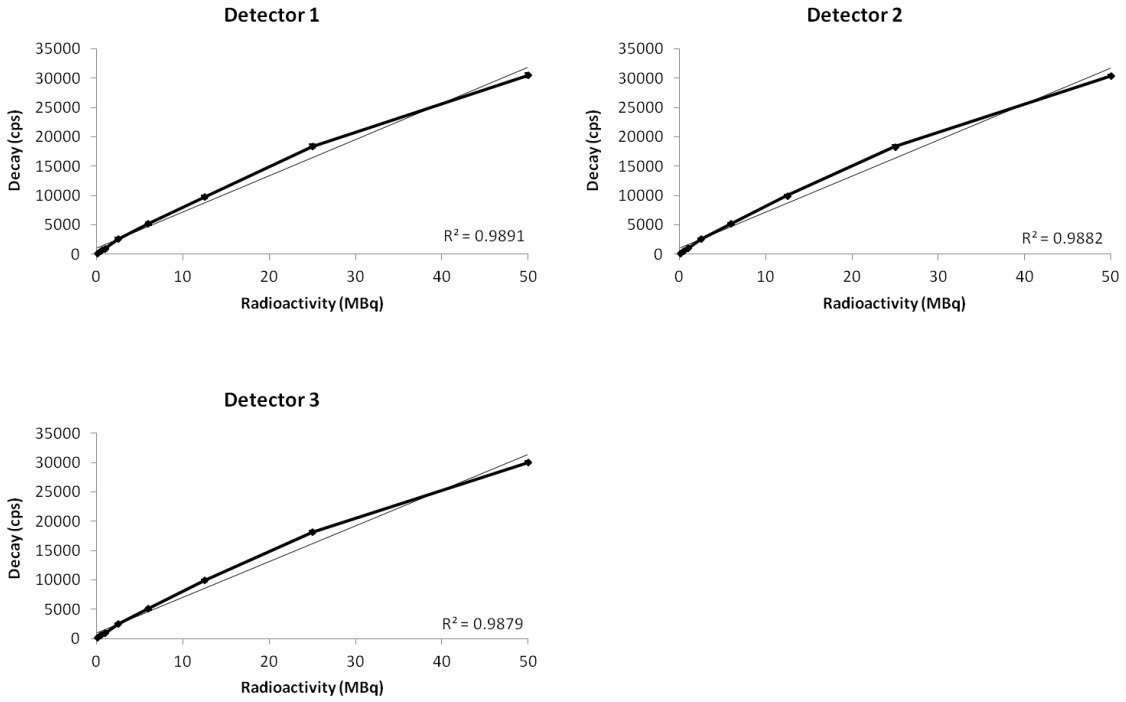

Figure 4.10. Gamma-detector linearity (0.1- 50 MBq/ 100- 30000 cps). Decay (cps) is plotted against radioactivity (MBq). Data represent mean (n = 3) ± SD.

Between 100- 18000 cps the relationship between the amount of radioactivity and decay counts was also linear ($R^2 = 1.0$) (figure 4.11).

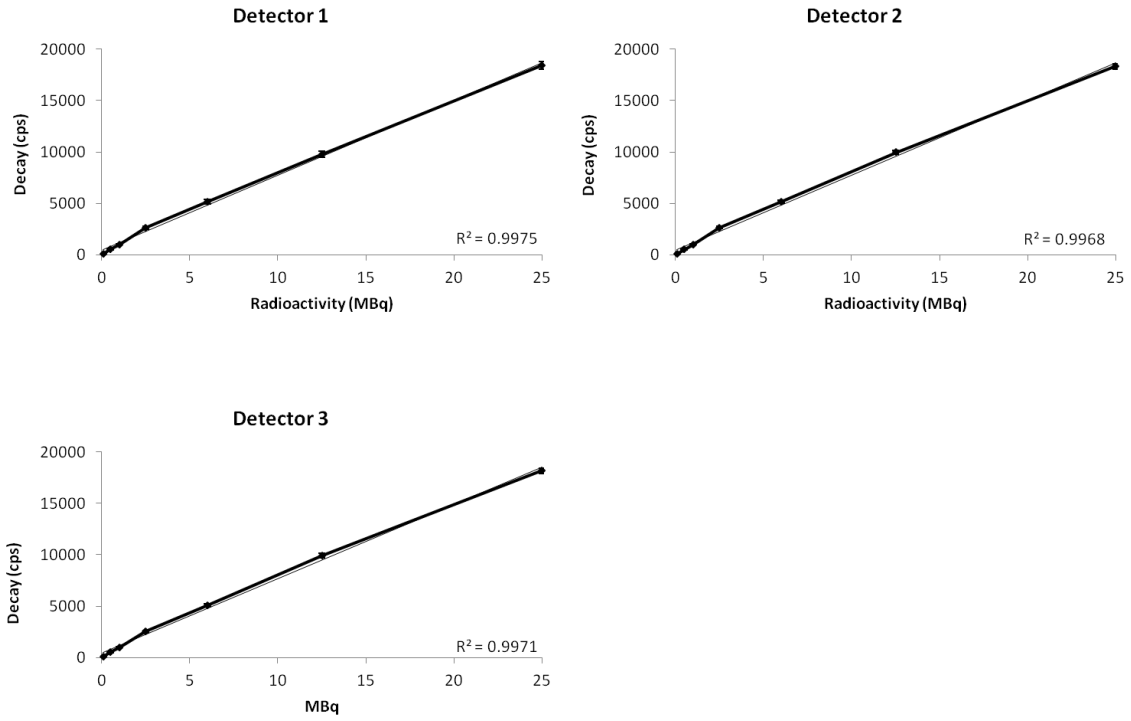

Figure 4.11. Gamma-detector linearity (0.1- 25 MBq/ 100- 18000 cps). Decay (cps) is plotted against radioactivity (MBq). Data represent mean (n = 3) ± SD.

Analysis of cps at the lower range of radioactivity, between 0 – 2600cps (figure 4.12), demonstrated that the sensitivity of all three of the detectors remained linear ($R^2 = 1.0$).

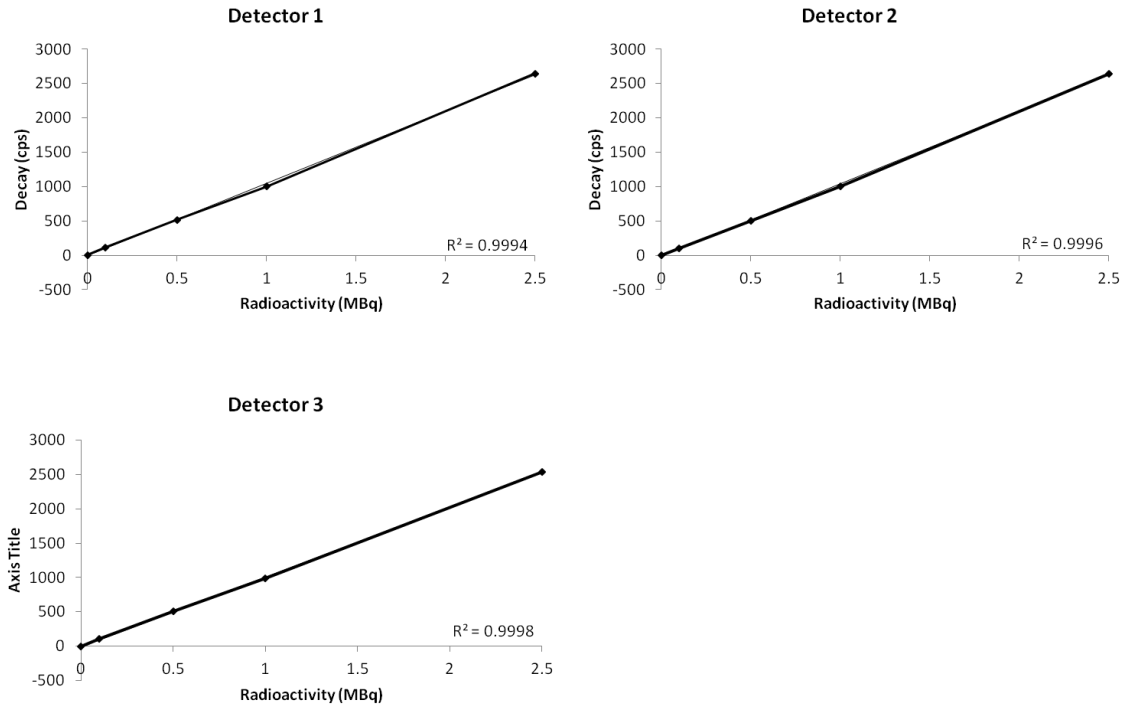

Figure 4.12. Gamma-detector linearity (0.1- 2.5 MBq/ 100- 2600 cps). Decay (cps) is plotted against radioactivity (MBq). Data represent mean (n = 3) ± SD.

4.3.4.3 Shine Through

Each of the three detectors was shielded by a custom built 2 cm thick lead collimator to reduce shine-through. As a result of shielding exposure to 1 MBq of ^{64}Cu resulted in a slight but insignificant increase of 15 cps above the background counts. When 10MBq was used the number of disintegrations registered also increased slightly, by 48 cps above background counts.

4.4 Discussion and Conclusions

4.4.1 Calibration of Perfusion Apparatus and Perfusion Buffer pO_2

The perfusion pump was calibrated and least squares regression was used to determine the relationship between arbitrary flow and actual flow rate (figure 4.4). We also established that the temperature of the perfusion buffer was constant, and within the range 37.0- 37.4 ºC (figure 4.5). We were therefore confident that our perfusion apparatus was suitable for our experiments.

Measurements of the pO_2 of mKHB taken after switching to the perfusate pO_2 decreased in two distinct phases (figure 4.6). This observation presented the opportunity to assess radiotracer performance at two levels of hypoxia; early and late. This will be discussed further in Chapter 5.

4.4.2 Confirmation Isolated Perfused Heart Preparation Stability

Exclusion criteria for cardiac function and coronary perfusion pressure were established (Table 4.2). These criteria were then used to determine whether the function of isolated perfused hearts was acceptable for experimental purposes, and also ensured that all hearts were of equal viability. The results of these preliminary experiments demonstrated that we were capable of isolating hearts and maintaining their cardiac function within previously defined parameters [273, 280].

4.4.3 Preliminary *Ex Vivo* Tracer Characterisation Experiments using γ-Detection

It was not possible to properly quantify these data in terms of tissue retention, because this crude system was not capable of recording the time-activity data in a list form, for exporting into spreadsheet applications. The tissue retention of each of the tracers was therefore estimated from the time-activity curves.

4.4.3.1 What Was Learnt from Preliminary *Ex Vivo* Experiments?

Preliminary *ex vivo* experiments were performed in order to further assess the feasibility of using a combination of the isolated perfused heart and γ-radiation detectors, to characterise the candidate hypoxia tracers. As already discussed in section 4.1.2, this approach had been employed previously by other groups. However, it was thought necessary to repeat some of their work ourselves before purchasing dedicated perfusion apparatus and a γ-detector system.

From our preliminary experiments we observed ^{64}Cu-PTSM [75] accumulation in both oxygenated and hypoxic hearts, and hypoxia selective retention of both ^{64}Cu-ATSM [174] and ^{18}F-MISO [127] (figure 4.8), as previously reported. Our crude reproduction of previous experiments and results, demonstrated to us that the isolated heart perfused heart combined with γ-radiation detectors, would provide an excellent model for characterising the myocardial retention and hypoxia avidity of our tracers. Furthermore these experiments demonstrated that when ^{64}Cu-BTSC complexes are administered as a single bolus, the first pass extraction of radioactivity is sufficient to allow measurements by Na/ I γ- detectors.

4.4.4 Calibration of Gina Star™ Data Acquisition System and Na/ I γ-Detectors

4.4.4.1 Detector Uniformity

It was necessary to confirm that the sensitivity of the three γ-detectors was equal, as a large variation could potentially hinder our attempt to analyse the time-activity data using kinetic modelling. The detector uniformity data demonstrated some discrepancy between the counts that were registered by each of the detectors, but the error was still less than that of the triplicate measurements for a single detector (figure 4.9). We therefore considered this to be an acceptable level of error.

4.4.4.2 Detector Linearity

At a sampling rate of 0.2 sec/ sample the Gina™ data acquisition system was capable of accurately measuring the count rate in the range 0 – 30000 cps (Figures 4.10- 4.12). However, to maintain the highest degree of accuracy we decided to limit the amount of radioactivity, so that the counts would not exceed 18000 cps. We therefore chose to inject 1 MBq of radiotracer per bolus in our experiments, because of the excellent sensitivity of the γ-detectors. Nevertheless it was useful to know that larger amounts radioactivity could be used if necessary. This was particularly welcome with respect to minimising shine-through, and for personal radiation protection throughout the rest of the study.

4.4.5 Construction of the Triple γ-Detector Array

As the result of our positive preliminary experiments we designed and commissioned the Gina Star™ system. Following the calibration of the perfusion equipment, the

establishment of exclusion criteria, and after assessing the uniformity and linearity of the three Na/ I γ-detectors, we then integrated the Gina Star™ and isolated heart perfusion systems. This integrated system was referred to in-house as the 'Triple γ- Detector Array' (Figure 4.1). Of the three detectors, one was positioned on the perfusion line immediately after the radiotracer injection port, to provide an input function. The second detector was placed 4 cm from the heart. The third detector was positioned on the perfusion line after the heart, to monitor radioactivity in the coronary effluent. All of the detectors were shielded with a custom built 2 cm thick lead collimator. To allow detection of radioactivity in the heart a 2 cm diameter hole was drilled into the collimator, to expose the γ-detector. The perfusion line was threaded through holes drilled through the base of the other two collimators, and the detectors rested on the perfusion line.

This completed our preliminary work, which had demonstrated the stability, sensitivity, and reproducibility of our purpose built radiotracer characterisation system. The proceeding chapter will discuss the application of the triple γ-detector array.

Chapter 5.

Characterisation of ^{64}Cu-Bis(thiosemicarbazones) in Isolated Perfused Hearts

5.1 Introduction

After calibrating the heart perfusion apparatus, establishing exclusion criteria for isolated heart preparations, and assessing the sensitivity of the Gina Star™ γ-detector system, we began to utilise the triple detector array to characterise our library of Cu-BTSC complexes. This chapter will discuss why specific ^{64}Cu-BTSC complexes were chosen, and how they performed during the characterisation experiments. The results of our experiments will then be compared to data from other groups, who have characterised Cu-BTSC complexes or other hypoxia selective tracers.

5.1.1 Selection of Cu-BTSC Complexes for Characterisation

The general structure of a Cu-BTSC complex is shown in figure 5.1, while table 5.1 provides a summary of the ^{64}Cu-BTSC complexes which we selected to further assess their hypoxia selectivity, and to evaluate them as myocardial hypoxia imaging agents.

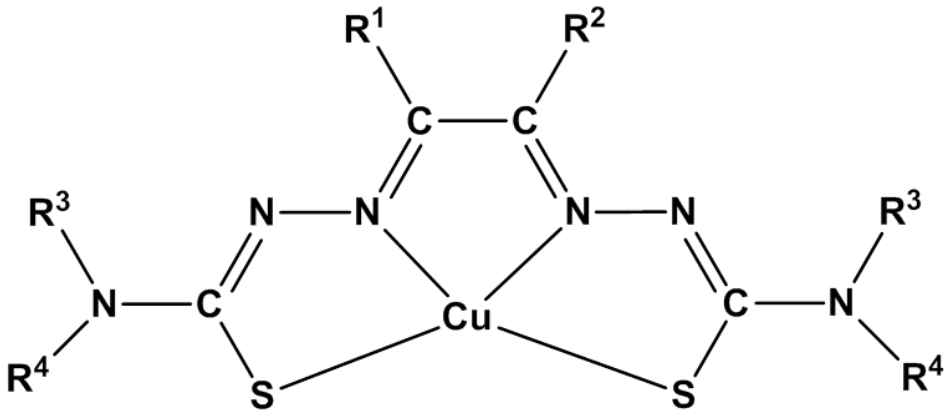

Figure 5.1. General structure of Cu-bisthiosemicarbazone complexes [162-163].

Table 5.1. Name, R^{1-4} –group substitution, and molecular weight and of Cu-BTSC complexes that were investigated during this study. Abbreviations: 2,3-butanedione bis(thiosemicarbazone) (ATS), Diacetyl bis(N^4-ethlythiosemicarbazone) (ATSE), Diacetyl bis(N^4-methlythiosemicarbazone) (ATSM), 2,3-pentanedione bis(thiosemicarbazone) (CTS), 2,3-pentanedione bis(N^4-methylthiosemicarbazone) (CTSM), 3,4-hexanedione bis(thiosemicarbazone) (DTS), 3,4-hexanedione bis(N^4-methylthiosemicarbazone) (DTSM), Pyruvaldehyde bis(N^4ethylthiosemicarbazone) (PTSE), Pyruvaldehyde bis(N^4-methylthiosemicarbazone) (PTSM)

Ligand	**R^1**	**R^2**	**R^3**	**R^4**	**Mol Wt Cu-Complex**	**Selected References**
ATS	CH_3	CH_3	H	H	293.86	[162-163, 167, 281-282]
ATSE	CH_3	CH_3	C_2H_5	H	349.97	[208]
ATSM	CH_3	CH_3	CH_3	H	321.91	[162-163, 167, 174, 209]
CTS	C_2H_5	CH_3	H	H	307.89	[162-163, 167]
CTSM	C_2H_5	CH_3	CH_3	H	335.94	[162-163, 167]
DTS	C_2H_5	C_2H_5	H	H	321.91	[162-163, 167]
DTSM	C_2H_5	C_2H_5	CH_3	H	349.97	[162-163, 167]
PTSE	CH_3	H	C_2H_5	H	335.94	[162-163, 171]
PTSM	CH_3	H	CH_3	H	307.89	[75, 129, 162-163, 167, 281]

All novel Cu-BTSC complexes where chosen because Dearling *et al* [162-163, 167], and McQuade *et al* [208] have previously demonstrated that they display some degree of hypoxia selectivity, but to date none of the novel tracers have been assessed in cardiac tissue. Cu-PTSM has previously been shown to accumulate in myocardial tissue regardless of the intracellular oxygen status, and is widely regarded as a perfusion tracer [75-76] . It was therefore included in this study as a positive control. ^{64}Cu-ATSM was included as the 'gold standard' hypoxia imaging tracer, against which all other ^{64}Cu-BTSCs would be compared. We also included $^{64}CuCl_2$ as a negative control, as this is the form in which ^{64}Cu is supplied for radiolabelling.

5.1.2 Isolated Heart Perfusion and Tracer Administration

5.1.2.1 Langendorff Isolated Heart Perfusion Protocol

The application Langendorff perfused heart models for the characterisation of hypoxia imaging tracers is reasonably well reported, as discussed in Chapter 4. A variety of heart perfusion and tracer administration protocols have been employed. Studies with the nitroimidazole based tracers have generally used both low flow ischaemia, and/ or normal flow hypoxic buffer perfusion protocols [115-116, 127, 134, 151-152, 276]. The myocardial accumulation of ^{62}Cu-PTSM was also evaluated using ischaemia, and hypoxia protocols [75]. The rationale for employing an ischaemia protocol is that it reflects most cardiac pathophysiologies that we are interested in imaging clinically. However to be able to directly compare radiotracer washout and retention under oxygenated or hypoxic conditions, it was advantageous to perfuse hearts at a constant flow rate. By negating the effects of flow on tracer accumulation (both with respect to delivery and washout), we could address whether ^{64}Cu-BTSC retention is flow dependent

or due to hypoxia specificity alone. We therefore decided to employ hypoxia with a constant flow rate.

5.1.2.2 Tracer Administration Protocol

It was also important to identify the most appropriate method of tracer delivery. Both constant infusion and bolus delivery are conducive to assessing radiotracer performance. Constant infusion has often been employed for characterising nitroimidazole based tracers, because they demonstrate low single pass tissue accumulation. However, we and others [75, 174] have demonstrated that Cu-BTSC display rapid extraction from the perfusate, and high myocardial tissue accumulation using bolus administration. We therefore chose to employ the bolus method of tracer delivery for our experiments, as this is also more representative of the ultimate clinical application.

5.1.3 Aims

The purpose of these experiments was to assess how the structure of ^{64}Cu-BTSC complexes affects their accumulation in cardiac tissue. To achieve this we determined the relative lipophilicity of our library of ^{64}Cu-BTSC complexes, using radio-ITLC and octanol extraction, before characterising them using our isolated perfused heart model. In doing this we aimed to confirm whether these novel complexes (table 5.1) selectively accumulated in hypoxic cardiac tissue. The retention profiles of these radiotracers would then be compared to those of ^{64}Cu-ATSM, to ascertain whether any of them performed better than the current "gold standard" tracer.

5.2 Materials and Methods

5.2.1 Synthesis of BTSC ligands and Confirmation of Structure

All BTSC ligands were kindly provided by Prof. P Blower and Dr R. Paul (Dept. Imaging Sciences and Medical Engineering, King's College, London). Ligands were synthesised as previously reported [172, 264].

The molecular mass of each of the BTSC ligands was ascertained by Mr Levente Meszaros (Division of Imaging Sciences and Molecular Engineering, King's College, London) using LC/MS as follows: the HPLC system was a 1200 system with degasser, quaternary pump, UV-visible variable wavelength detector, and an autosampler (Agilent, USA). The mass spectrometer was a 6520 Accurate-Mass Q-TOF LC/MS (Agilent, USA). Samples were acquired using Agilent Masshunter workstation acquisition software and data was analysed using Masshunter Qualitative analysis software (Agilent, USA).

Dr Karen Shaw (Division of Imaging Sciences and Molecular Engineering, King's College, London) confirmed the structure of each BTSC ligand by ^{1}H NMR spectroscopy, using a Bruker widebore ultrashield plus with Avance III console operating at a ^{1}H frequency of 400 MHz probe, a 5 mm BBO probe with ^{1}H, ^{2}H and broadband-xchannels (Bruker, Germany). Data were analysed using Topspin v2.1 software (Bruker, Germany). Key acquisition parameter were as follows: pulse sequence: zg30, number of scans (ns): 16, dummy scans (ds): 2, sweep width (swh):8223.685 Hz, Acquisition time: 3.98 sec, D1: 1 sec ^{1}H frequency: 399.47MHz, solvent: DMSO-d6.

5.2.2 Radiolabelling of Bis(thiosemicarbazone) Ligands with ^{64}Cu

Radiolabelling of all BTSC ligands with ^{64}Cu was performed using a common protocol described in Section 3.2.3.1, using 40 MBq ^{64}Cu for labelling. Once eluted from the Sep-Pak column with 500 µl ethanol, stock solutions of ^{64}Cu-BTSC complexes were then diluted to 10 MBq/ ml with mKHB. The radiolabelling efficiency was then assessed by radio-ITLC, as described in section 3.2.3.2.

5.2.3 ^{64}Cu-bis(thiosemicarbazone) Stability

Radio-ITLC was employed to monitor the stability of each of the ^{64}Cu complexes over 24 h, to determine whether the ^{64}Cu-complexes remained stable throughout the course of a day's experiments. Ligands were radiolabelled with 40 MBq ^{64}Cu, according to the common protocol, and the volume was adjusted to 10MBq/ ml mKHB. Samples were then stored on the bench throughout the day, and in a refrigerator over-night. At 0, 1, 3, 6 and 24 h, 2 µl aliquots were removed and assessed by radio-ITLC.

5.2.4 Retention Factors of ^{64}Cu-bis(thiosemicarbazones)

Retention factor (Rf) values were obtained from radio-ITLC traces, and were used to compare the relative lipophilicities of ^{64}Cu-BTSC complexes.

Rf values were calculated using data from radiolabelling quality control, and ^{64}Cu complex stability experiments. These data were also obtained using the Laura (v. 4.0.3.75) software package (LabLogic, UK).

5.2.5 Partition Ratio of ^{64}Cu-bis(thiosemicarbazones)

The partition ratio of a substance also provides a quantitative index of hydrophilicity/ lipophilicity. Octanol extraction was employed to determine the partition ratio of the ^{64}Cu-BTSC complexes. John and Green previously used a similar method when they assessed a library of ^{67}Cu-BTSC complexes as perfusion tracers [171]. The partition ratio of the complexes was determined using both ultrapure water, and mKHB as the aqueous phase. Ultrapure water is commonly used as the aqueous phase for octanol extraction experiments, and was therefore included to allow comparisons with data from other groups. Unlike water, mKHB is a physiological salt solution and this could potentially alter the partition ratio of Cu-BTSC complexes, relative to those obtained using water. An aqueous phase of mKHB was therefore also included as it is this solution that would deliver the ^{64}Cu-BTSC complexes to the heart.

500 µl ultrapure water or mKHB and 500 µl octanol were pipetted into three 2 ml vials. 200 KBq (~20 µl) of each ^{64}Cu-complex was added to separate vials. The vials were vortexed for 1 min and allowed to settle for 1 min. The vials were then centrifuged at 3000 g for 5 min, to ensure complete separation of the organic and aqueous phases. 3x 100 µl aliquots were then carefully removed from each of the layers, before the radioactivity in each of the fractions was measured by gamma well counting. This was repeated in triplicate for each ^{64}Cu complex. Partition ratios were calculated using the equation:

$$LogP = \log_{10} (cpm\ octanol / cpm\ water\ or\ modified\ KHB) \qquad (eqn\ 5.1)$$

5.2.6 Characterisation of ^{64}Cu-bis(thiosemicarbazones) in Isolated Perfused Rat Hearts

The next stage in the characterisation of the ^{64}Cu-BTSC complexes was to investigate their cardiac tissue clearance and tissue retention in isolated perfused rat hearts, using the triple γ-detector array.

Hearts of male Wistar rats were excised, cannulated, and prepared for experiments, according the protocol described in section 4.2.4.2. Hearts were perfused with mKHB buffer gassed with 95 % O_2/ 5% CO_2, and allowed to stabilise for 20 min. During this time cardiac function (Heart rate, LVDP and LVEDP) and perfusion pressure were expected to remain within the range criteria that we had established in section 4.3.2. If these parameters were not attained during the stabilisation period the heart was discarded. Figure 5.2 provides a schematic representation of our experimental protocol.

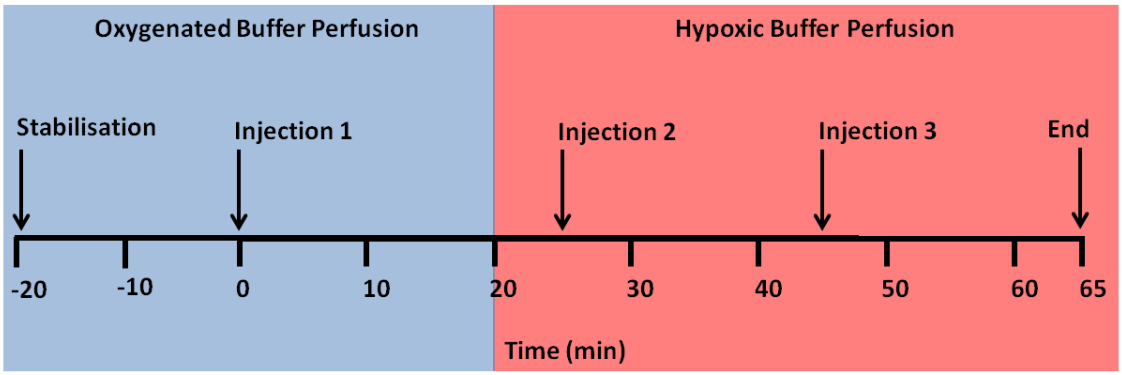

Figure 5.2. Schematic representation of the experimental protocol that was employed for the characterisation of ^{64}Cu-BTSC clearance/ tissue retention, in isolated perfused rat hearts.

In brief, at the end of a 20 min stabilisation period the experiments were initiated by administrating a 1 MBq bolus (100- 160 µl) of radiotracer, diluted in mKHB (10 MBq/

ml). At 20 min the perfusate was switched to hypoxic buffer, which was achieved by gassing with 95% N_2/ 5% CO_2. This continued until the end of each experiment at 65 min. A second bolus was administered at 25 min (5 min hypoxia), followed by a final bolus at 45 min (25 min hypoxia).

5.2.6.1 Determining Percentage Tissue Retention of Radiotracers

The retained fraction of each bolus of ^{64}Cu-BTSC complexes was determined using a similar method to that employed by Fujibayashi *et al* [174].

Background counts were recorded by the Gina data acquisition system before the start of each experiment. The initial background (iBkG) was determined by averaging the cps over 30 sec, just prior to the first injection. The iBkG was then subtracted from all subsequent measurements, and also served as the baseline cps for the first injection of radiotracer. For the second and third injections, by which time radioactivity had accumulated within the heart, the baseline was the sum of the iBkG and residual radioactivity (Rcps). Rcps was derived by averaging the number of counts recorded over 1 sec (at a sample rate of 5 measurements/ sec) immediately before an injection of radiotracer, such that at 0 min Rcps was equal to iBKG. In order to determine the accumulated cps (Acps) at 20 min post-injection, measurements were again averaged over 1 sec. The tissue retention factor (TRF) was then calculated as follows:

$$TRF = (Acps - iBkG)_{decay\ corrected} - (Rcps - iBkG)_{decay\ corrected} \quad \text{(eqn. 5.2)}$$

Following each injection of radiotracer the decay counts that were registered increased rapidly. In order to determine the amount of tissue retention (TR) of each tracer, the five highest recorded cps measurements were averaged to obtain the mean peak cps (Pcps). Tissue retention was expressed as the percentage of each bolus that was retained in the heart, and was determined by the following equation:

$$TR\ (\%) = (100 / Pcps) \times TRF \qquad (eqn.\ 5.3)$$

With the exception of iBKG, and Rcps at 0 min all data were corrected for decay.

5.2.6.2 Lactate Release from Isolated Perfused Hearts

The production and release of lactate from isolated perfused hearts was used as further index of cardiac hypoxia, as the heart switches from the β-oxidation of fatty acids to anaerobic glycolysis. For measuring the concentration of lactate in the coronary effluent a 2300 STAT Plus™ glucose and lactate analyser (YSI UK Ltd, UK), fitted with an immobilised L-lactate oxidase membrane was used (YSI 2329). L-lactate oxidase converts lactate to pyruvate and hydrogen peroxide. Hydrogen peroxide is then oxidised at a platinum electrode to form O_2, $2H^+$ and $2e^-$. The current produced by these electrons is proportional to the amount of lactate in the initial sample.

At 0, 10, 20-25, 35, 45 55 and 65 min, 0.5 ml of the coronary effluent was collected. The analyser was first calibrated using 15 and 30 mMol/ l lactate standard solutions, before the concentration of lactate in the aliquots of coronary effluent was measured.

5.2.7 Data and Statistical Analysis

Data analysis was performed using Microsoft Office Excel® 2007. Statistical analyses were performed using GraphPad Prism® (Version 5.04) (GraphPad Software Inc, USA). All values are expressed as the mean ± SD. A paired t-test was used for all pair-wise comparisons. For multiple tests a one way ANOVA with the Bonferroni correction was applied. The Dunnett's post analysis test was applied when multiple comparisons were made to a control group.

5.3 Results

5.3.1 Stability of ^{64}Cu-BTSC Complexes

The stability of ^{64}Cu-BTSC complexes was monitored over 24 h using radio-ITLC (figure 5.3). At 0 h the labelling efficiency for each of the BTSC ligands was greater than 97 %. After 24 h the percentage of radiolabelled complex was greater than 96 % for all complexes, with the exception of ^{64}Cu-ATSM which decreased to 94 %. However at 3 h the amount of ^{64}Cu-ATS that was radiolabelled was to 92 %, and at 3 and 6 h post-labelling ^{64}Cu-PTSM was recorded at 94 %. The fluctuations in the stability of ^{64}Cu-ATS, and ^{64}Cu-PTSM and perhaps ^{64}Cu-ATSM were possibly due to operator, when loading and running the samples.

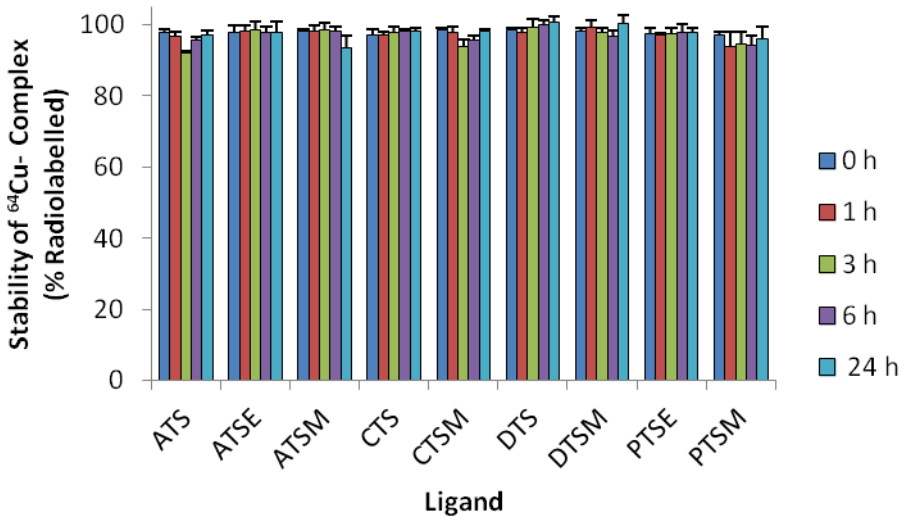

Figure 5.3. Stability of ^{64}Cu- bis(thiosemicarbazone) complexes over 24 h determined by radio-ITLC, using an ethanol mobile and silica sorbent phase. Data are expressed as mean (n = 3) ± SD.

5.3.2 Physicochemical Properties of ^{64}Cu-BTSC Complexes

5.3.2.1 Retention Factor of ^{64}Cu-BTSC Complexes Determined by Radio-ITLC

All ^{64}Cu-BTSCs migrated with the ethanol solvent phase, but $^{64}Cu^{2+}$ remained at the origin (figure 5.4). The Rf values of each of the ^{64}Cu-complexes were compared to that of ^{64}Cu-ATSM (0.79 ± 0.01). Values for the ^{64}Cu-complexes of: ATS (0.70 ± 0.001), PTSM (0.74 ± (0.01), CTS (0.78 ± 0.01), and DTS (0.78 ± 0.01) were lower, while those of PTSE (0.80 ± 0.01), CTSM (0.82 ± 0.01) and ATSE (0.83 ± 0.01) and DTSM (0.85 ± 0.01) were higher.

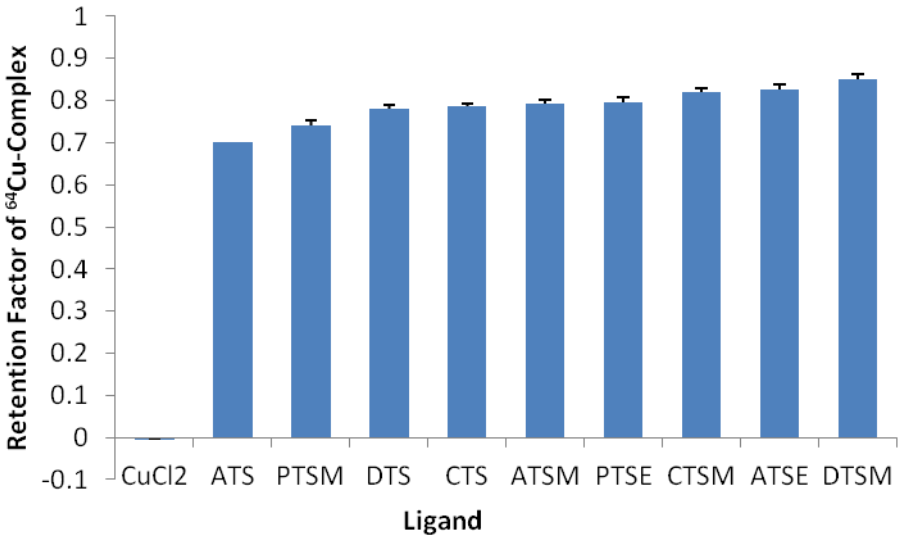

Figure 5.4. Retention factors of ^{64}Cu-BTSC complexes, shown in order of increasing lipophilicity with $^{64}CuCl_2$ included for comparison. Data were obtained by radio-ITLC and are expressed as mean (n=3)± SD.

Rf values were then plotted against the molecular weight of the corresponding ^{64}Cu-BTSC (figure 5.5). The results demonstrate that the relationship (R^2= 0.87) between these two parameters.

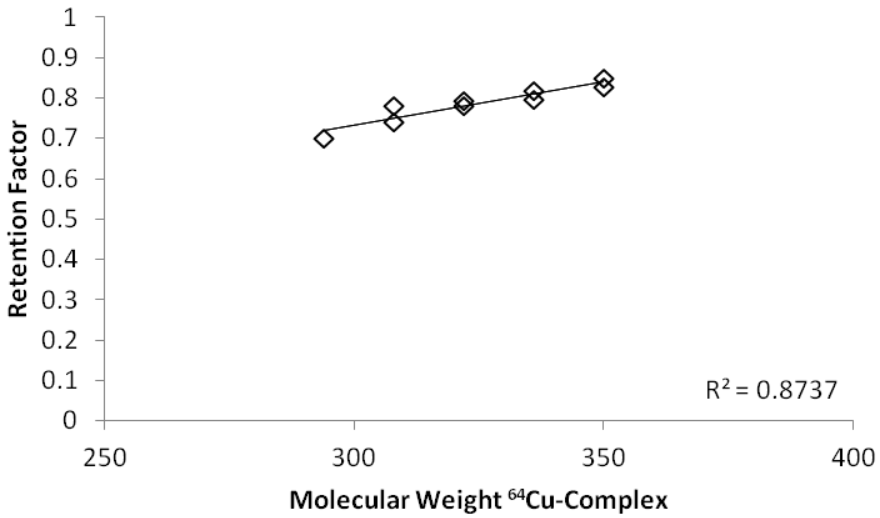

Figure 5.5. Retention factor of ^{64}Cu-BTSC complexes plotted against corresponding molecular weight.

5.3.2.2 Partition Ratios of ^{64}Cu-BTSC Complexes

For conventional purposes logP values are summarised in table 5.2. Our values were similar to those reported by Dearling *et al* [162, 167].

Table 5.2. LogP values of $^{64}CuCl_2$ and ^{64}Cu-BTSC complexes, determined by octanol extraction, with an aqueous phase of either water or mKHB. Data represent mean (n= 3) ± SD.

^{64}Cu-Complex	Log p (Octanol/ Water)	Log p (Octanol/ mKHB)
$^{64}CuCl_2$	-1.52 ± 1.09	-1.86 ± 0.71
ATS	0.88 ± 0.01	0.91 ± 0.01
ATSE	1.86 ± 0.17	1.85 ± 0.13
ATSM	1.69 ± 0.01	1.72 ± 0.11
CTS	1.31 ± 0.14	1.45 ± 0.05
CTSM	1.97 ± 0.04	1.94 ±0.06
DTS	1.70 ± 0.07	1.77 ± 0.07
DTSM	2.01 ± 0.17	2.02 ± 0.10
PTSE	1.74 ± 0.21	1.68 ± 0.25
PTSM	1.52 ± 0.14	1.56 ± 0.12

Partition ratios were then used to compare the relative lipophilicity of the ^{64}Cu-BTSC complexes, theses are summarised in table 5.3.

Table 5.3. Partition ratios for $^{64}CuCl_2$ and ^{64}Cu-BTSC complexes, determined by octanol extraction. An aqueous phase of either water or mKHB was used. Data represent mean (n= 3) ± SD.

^{64}Cu-Complex	**Partition Ratio (p) (Octanol/ Water)**	**Partition Ratio (p) (Octanol/ mKHB)**
$^{64}CuCl_2$	0.17 ± 0.30	0.04 ± 0.04
ATS	7.60 ± 0.17	8.19 ± 0.23
ATSE	96.31 ± 14.81	90.75 ± 20.63
ATSM	51. 68 ± 7.80	54.08 ± 14.62
CTS	21.14 ± 6.42	28.10 ± 3.10
CTSM	93.38 ± 7.55	88.38 ± 11.31
DTS	50.68 ± 8.80	59.45 ± 10.39
DTSM	116.33 ± 39.74	106.51 ± 24.97
PTSE	65.25 ± 20.56	54.94 ± 26.79
PTSM	34.42 ± 10.70	37.86 ± 10.99

For each of the ^{64}Cu-BTSC complexes the partition ratios that were obtained using water were compared to values obtained using mKHB (figure 5.6). The corresponding values were similar regardless of the aqueous phase that was used. The partition ratios for each of complexes were then compared to those of ^{64}Cu-ATSM. The ^{64}Cu-Complexes of ATS, CTS, PTSM and DTS were less lipophilic, but those of PTSE, CTSM, ATSE and DTSM demonstrated greater distribution into the organic phase.

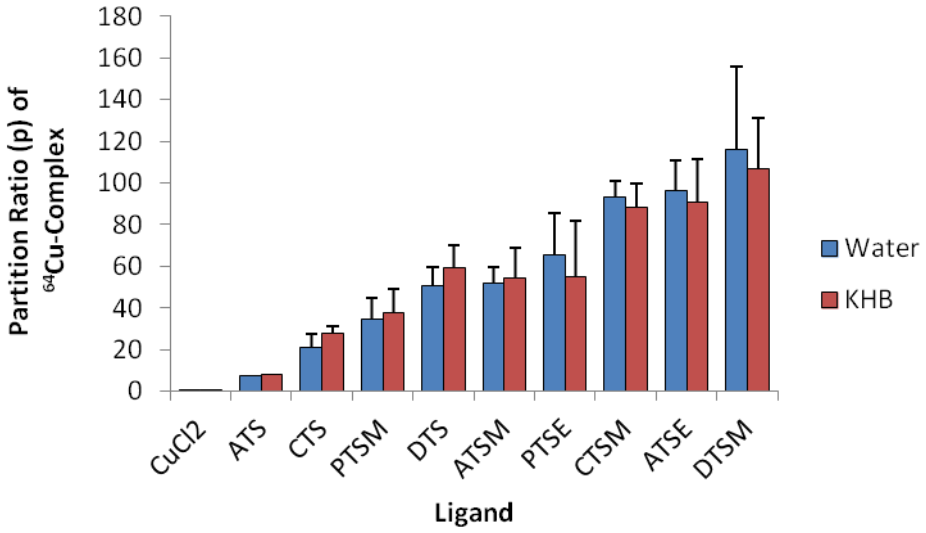

Figure 5.6. Partition ratio (octanol/ water or KHB) of $^{64}CuCl_2$ and ^{64}Cu-BTSC complexes. Data are shown in order of increasing lipophilicity, and compare partition ratios obtained using water to those obtained using KHB as the aqueous phase. Data represent mean (n = 3) ± SD.

Partition ratios (octanol/ mKHB) were then plotted against the molecular weight of the corresponding ^{64}Cu-BTSC complex (figure 5.7). A relationship (R^2 = 0.80) was also observed between these parameters.

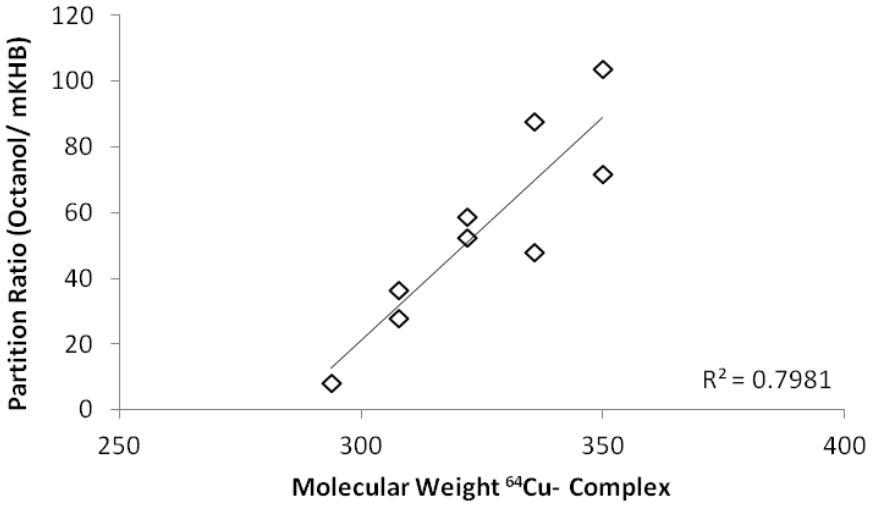

Figure 5.7. Partition ratio (octanol/ KHB) plotted against the molecular weight of ^{64}Cu-BTSC complexes. Data for partition ratios represent mean (n = 3).

5.3.3 Parameters Recorded Throughout ^{64}Cu-BTSC Characterisation in Isolated perfused Hearts

During all of our ^{64}Cu-BTSC characterisation experiments where isolated perfused hearts were employed, the pO_2 of the perfusate, heart rate, LVDP, LVEDP and perfusion pressure were monitored in real-time. This was to ensure that cardiac function was within the range of the exclusion criteria established in section 4.3.2. However these parameters were also monitored to confirm that hearts received an adequate supply of oxygen during normal perfusion, but were deprived of oxygen under hypoxic conditions.

5.3.3.1 Partial Pressure of Oxygen of Coronary Perfusate

The graphs presented in figure 5.8 demonstrate that the pO_2 of the perfusate was measurable after 22 min (2 min hypoxia), and was in the range 92.4- 61.3 mmHg. At 25 min, when the second bolus of tracer was administered, the buffer pO_2 had decreased to between 31.5- 40 .6 mmHg. At 45 min, when the final bolus was administered, the pO_2 had further decreased to between 9.8 and 14.4 mmHg. By the end of the experiments at 65 min the perfusate pO_2 was between 6.6 and 10.2 mmHg. This was consistent and reproducible across all treatment groups.

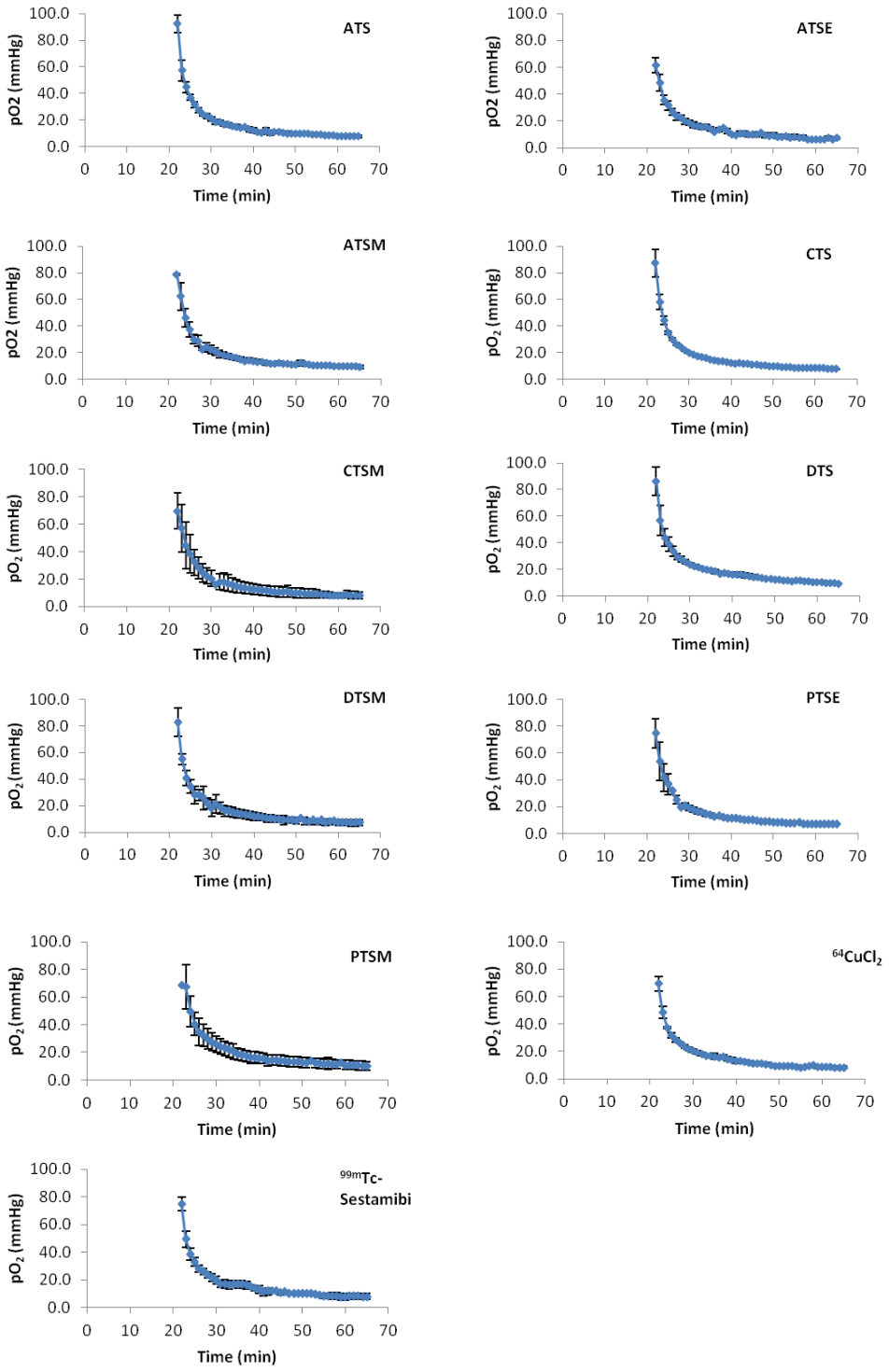

Figure 5.8. Partial pressure of dissolved oxygen in coronary perfusate during deoxygenated buffer perfusion. Values were measured using the OxyLab™ system. Values shown are from 22-65 min, as readings taken before this time were above the accurate measurement range of the oxygen sensor. Data represent mean (n = 3 – 5) ± SD.

5.3.3.2 Release of Lactate from Isolated Perfused Rat Hearts

From 0- 20 min the average concentration of lactate was 0.036- 0.078 mMol/ l. Within 1-2 min of switching to hypoxic mKHB the concentration of lactate increased significantly. The highest concentrations of lactate were observed at 21- 25 min (0.42- 1.01 mMol/ l). In all experiments the lactate concentration then steadily decreased up to 65 min (0.10-0.21 mMol/ l), but values were always higher than was observed when hearts were perfused with oxygenated KHB (figure 5.9).

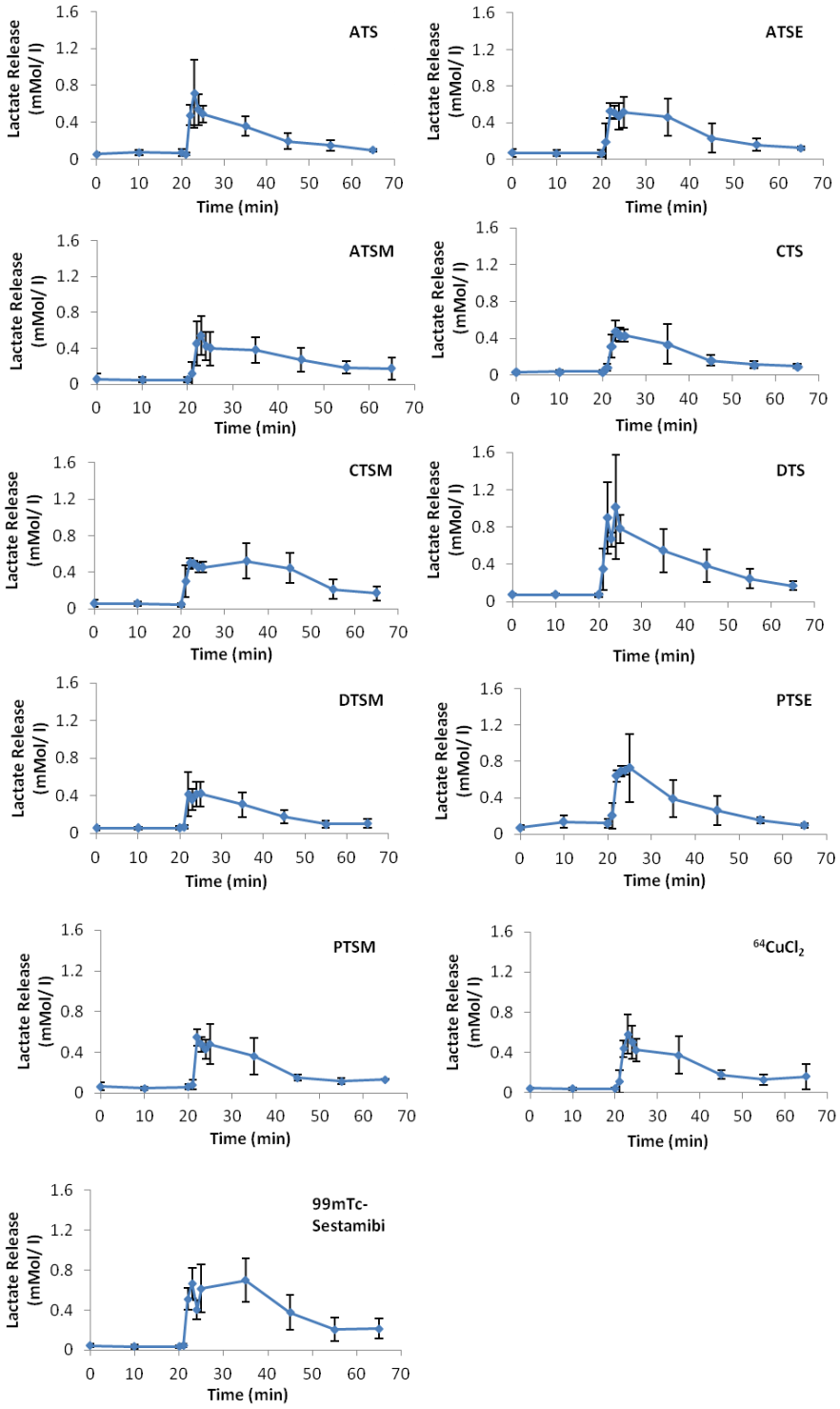

Figure 5.9. Concentration of lactate (mMol/ l) in coronary effluent, for all data sets. Data represent mean (n = 3 – 5) ± SD.

5.3.3.3 Coronary Perfusion Pressure

During the stabilisation period and for the first 20 min of each experiment the coronary perfusion pressure was in the range 60- 80 mmHg. All hearts reacted similarly when the perfusate was switched to hypoxic mKHB at 20 min. There was a small decrease in perfusion pressure of between 4.3- 9.9 mmHg for the first 3- 4 min. Then from 24 - 65 min the perfusion pressure steadily increased. At 65 min the average perfusion pressure for all data sets was between 83.6- 158.1 mmHg (figure 5.10).

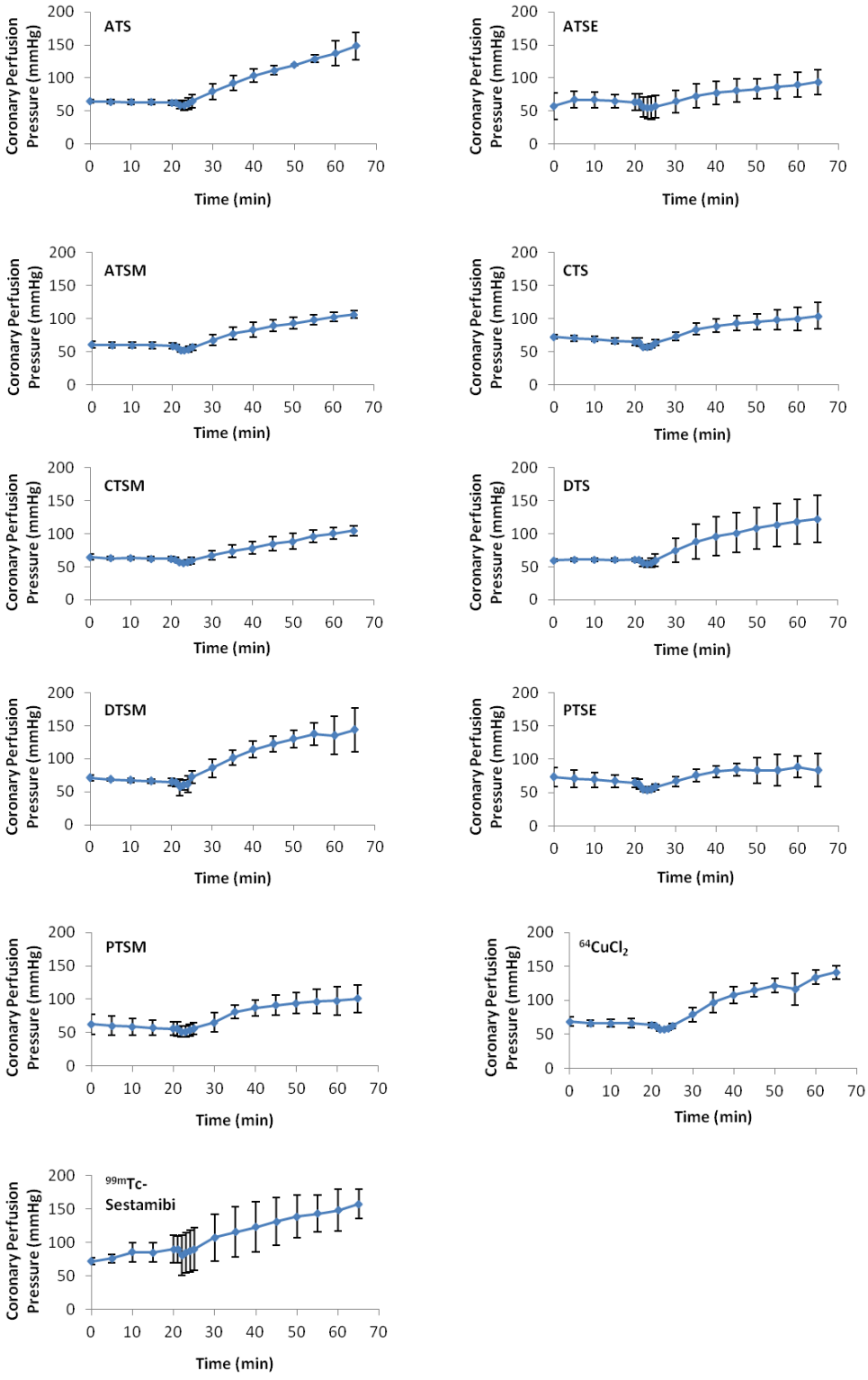

Figure 5.10. Coronary perfusion pressure. Data represent mean (n = 3 – 5) ± SD.

5.3.3.4 Left Ventricular Developed Pressure

Left ventricular developed pressure (LVDP) was calculated automatically by the LabChart® 7 (version 7.2) software package, as a function of the left ventricular systolic pressure minus left ventricular diastolic pressure. These data are shown in figure 5.11.

Under oxygenated conditions the LVDP fluctuated slightly between each heart, and each data set. During the first 20 min LVDP for all hearts was in the range 130- 180 mmHg. The switch to deoxygenated mKHB perfusion was marked by a sharp decrease in LVDP for all data sets that continued until 25- 30 min. Between 30 and 35 min there was a slight recovery in LVDP for up to 5 min. However after this period the LVDP began to decrease once again, and this continued up until the experiments were terminated at 65 min. During experiments with ^{99M}Tc-Sestamibi the recovery phase was absent and the LVDP consistently decreased between 20 and 65 min.

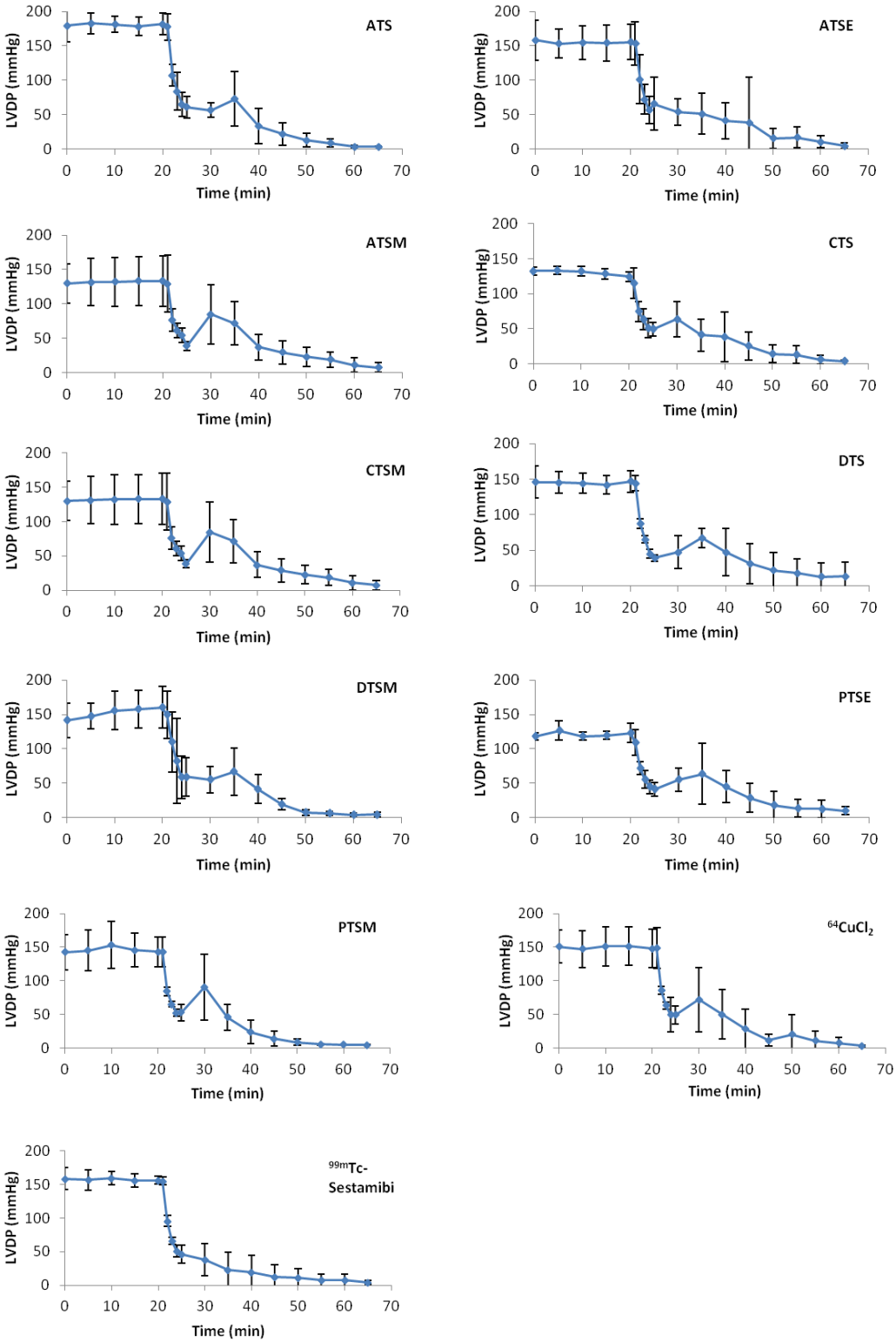

Figure 5.11. Left ventricular developed pressure for all data sets. Data represent mean (n = 3 – 5) ± SD.

5.3.3.5 Left Ventricular End Diastolic Pressure

During the stabilisation period and at the start of each experiment the LVEDP of all hearts was between 5 and 8 mmHg. By 20 min this average LVEDP for all data sets was in the range 4- 13 mmHg. Upon initiating hypoxia the LVEDP began to increase steadily, which continued until the end of each experiment. By 65 min LVEDP was markedly higher than the initial 5- 8 mmHg, with the LVEDP of all hearts in the range 85- 136 mmHg (figure 5.12).

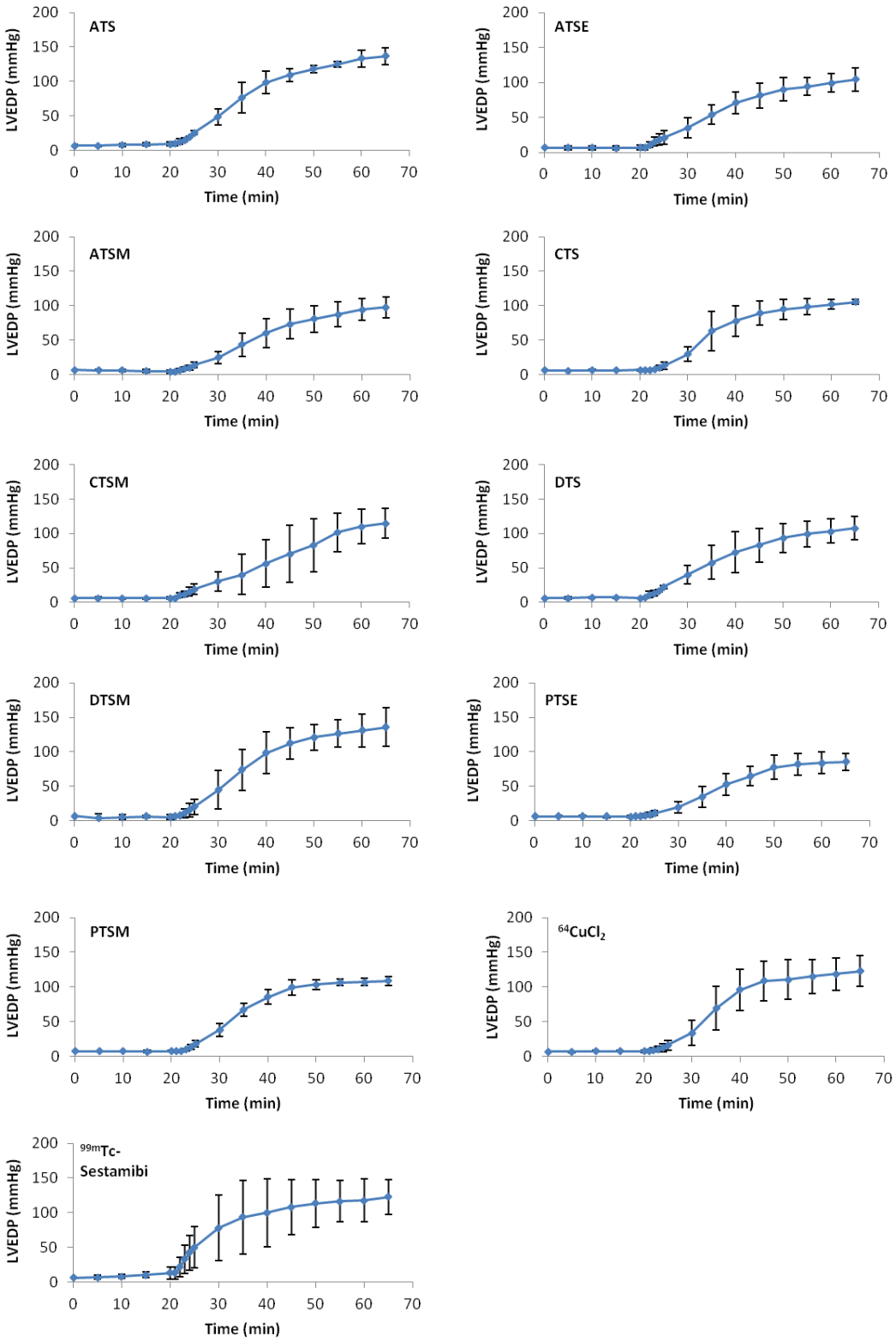

Figure 5.12. Average left ventricular end diastolic pressure (LVEDP) for all data sets. Data represent mean (n = 3 – 5) ± SD.

5.3.3.6 Heart Rate

During normoxic perfusion the average heart rate for all data sets was 280- 300 BPM. After 1- 2 min of deoxygenated buffer perfusion, heart rate began to decrease rapidly. After 35 min, heart rate no longer responded to sinus rhythm and the heart began to fibrillate, causing large variation in the sampling values. For this reason only time points up to 35 min are shown (figure 5.13).

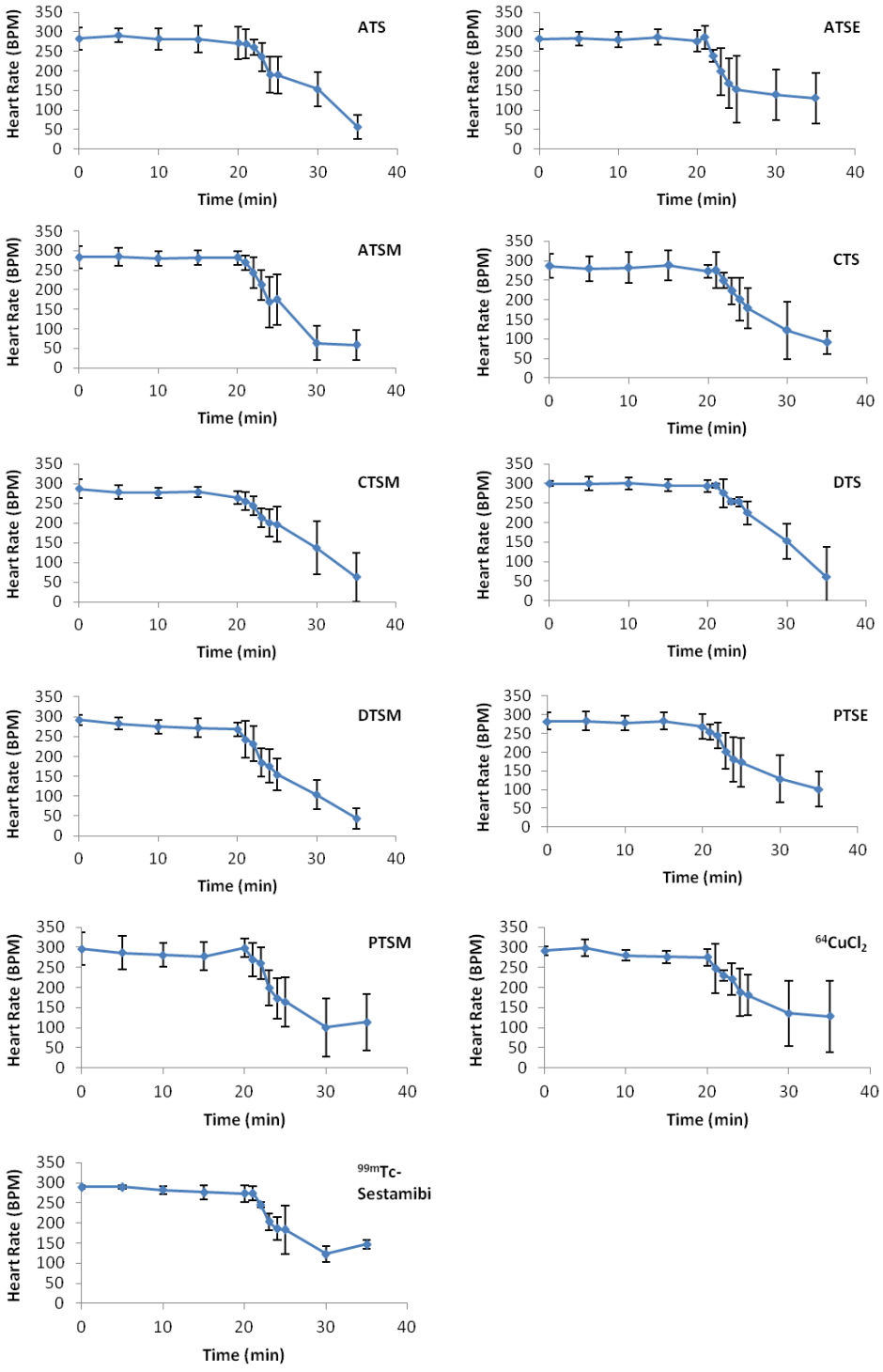

Figure 5.13. Heart rate (BPM) of all data sets over the first 35 min of each experiment. Data represent mean (n = 3 – 5) ± SD.

5.3.4 Characterisation of ^{64}Cu-Complexes in Isolated Perfused Rat Hearts

5.3.4.1 Triple γ-Detector Raw Data

An example of a set of traces acquired using the triple γ-detector array, are shown in figure 5.14. All of these traces were acquired simultaneously and in real-time. Immediately after administrating 1 MBq of radiotracer into the perfusion line, the cps registered by detector 1 (arterial) began to increase rapidly. This was followed within 8 sec by an increase in cps by detector 2 (heart), and 17 sec post-injection by detector 3 (venous). Focusing on detector 2 and using ^{64}Cu-ATSM as an example hypoxia avid tracer, a clear distinction can be made between tracer retention under oxygenated (injection 1) and deoxygenated (injections 2 and 3) conditions (figure 5.14).

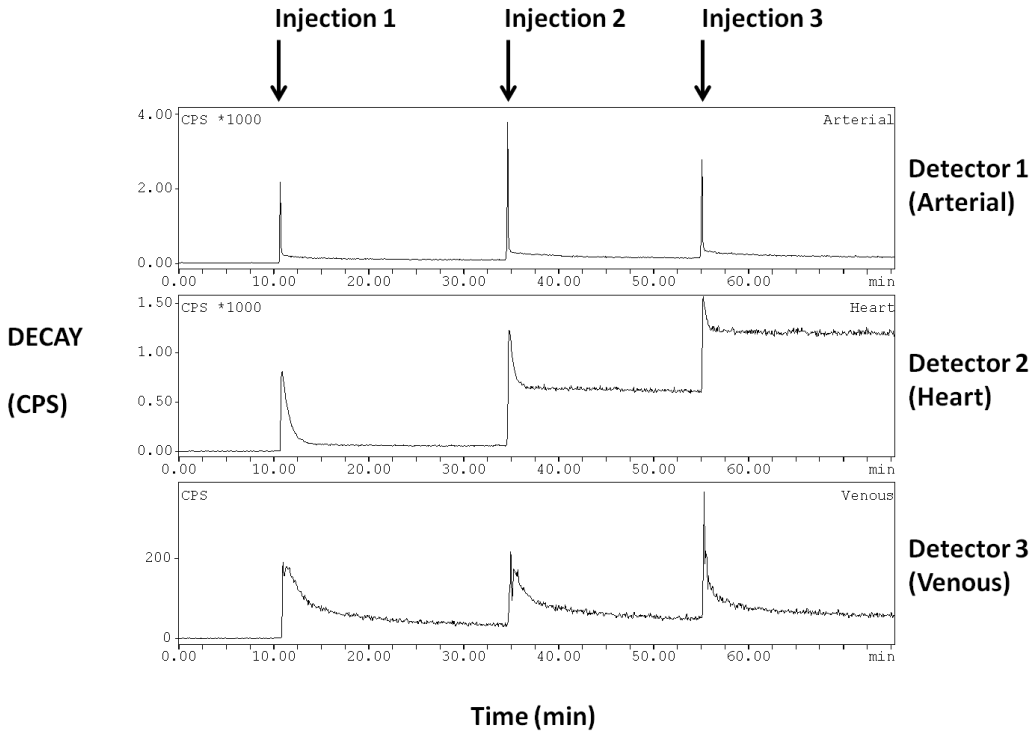

Figure 5.14. A typical set of time-activity curves from the Triple γ-detector array, displaying cps against time for the three Na/I γ-detectors. Acquired using the triple γ-detector array, Gina data acquisition and control interface, and produced by the Gina Star™ (v. 5.01) software package. Each peak represents a 1MBq bolus injection of ^{64}Cu-ATSM, under oxygenated (injection 1) and deoxygenated (injections 2 and 3) conditions.

The qualitative time—activity curves data that were obtained using the triple γ-detector array are shown in figure 5.15. Only traces obtained from detector 2 (heart) are displayed. From these curves we see that ^{64}Cu-complexes of: ATS, ATSE, ASTM, CTS, CTSM, DTS, and DTSM display hypoxia selective tissue retention. ^{64}Cu-PTSE and ^{64}Cu-PTSM were retained regardless of the oxygen status, while retention of the negative control $^{64}CuCl_2$ was negligible under all conditions. However the perfusion tracer ^{99m}Tc-sestamibi accumulated in well oxygenated tissue, but eluted from hearts during hypoxia to almost background levels.

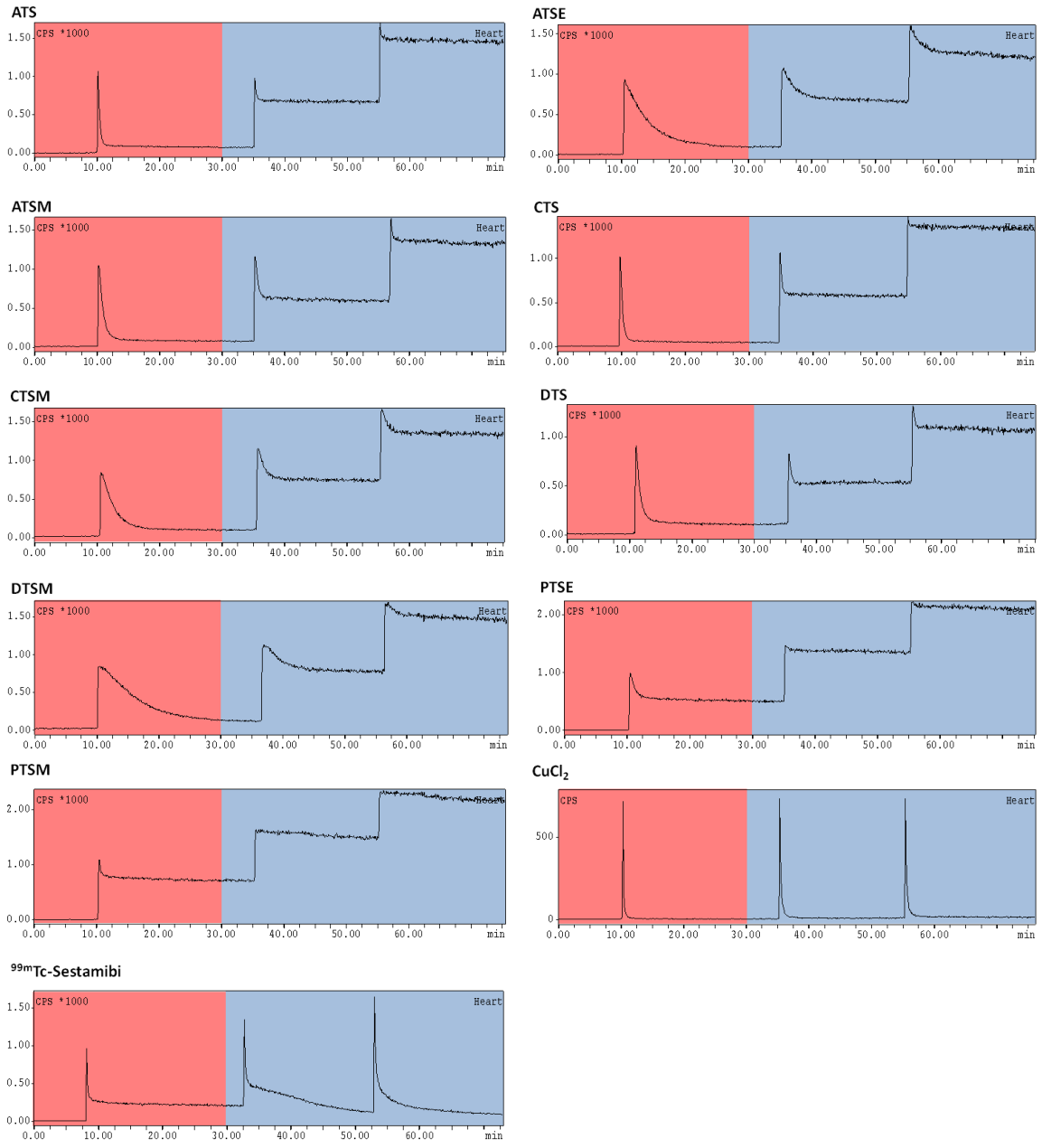

Figure 5.15. Example of time-activity curves that demonstrate the myocardial clearance/ accumulation of ^{64}Cu-BTSC complexes, $^{64}CuCl_2$ and ^{99m}Tc. Regions highlighted in pink represent periods of oxygenated buffer perfusion, those shown blue represent perfusion with deoxygenated buffer. Each peak represents the administration of a 1 MBq bolus of radiotracer .Curves were recorded by detector 2 (heart) of the triple γ-detector array.

5.3.4.2 ^{64}Cu-BTSC Accumulation in Isolated Perfused Rat Hearts

5.3.4.2.1 Comparison between Oxygenated and Hypoxic Tissue Retention

The initial qualitative observations made in section 5.2.1 were confirmed by manually analysing the time-activity data (available in a list form), that were recorded and stored by the Gina Star™ software. Figure 5.16 demonstrates the tissue retention of each tracer. Results were calculated as described in section 5.2.6.1, and expressed as a percentage of the total radioactivity injected (% ID). The accumulation of ^{64}Cu-BTSC complexes are shown under oxygenated conditions, and following 5 or 25 min perfusion with hypoxic buffer.

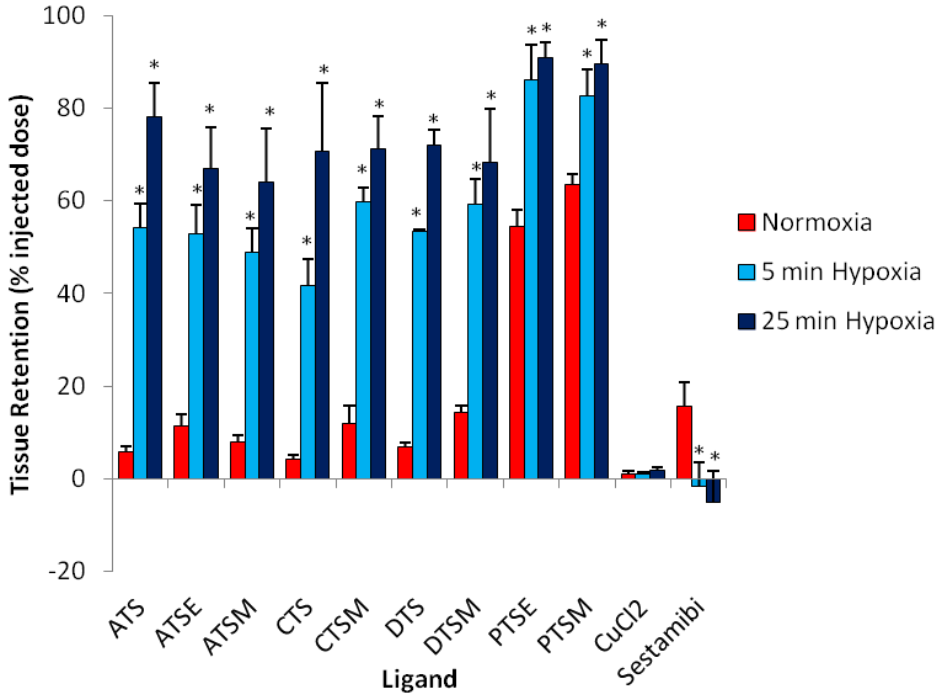

*Figure 5.16. Percent retention of ^{64}Cu-BTSC complexes, $^{64}CuCl_2$, and ^{99m}Tc-Sestamibi 20 min post-injection. Experiments were performed using isolated perfused rat hearts, under oxygenated conditions (red) and after 5 min (light blue) and 25 (dark blue) min hypoxia. Data represent mean (n = 3 – 5) ± SD. * = significantly different from control (normoxia) ($p<0.05$).*

Under oxygenated conditions ^{64}Cu-PTSE and ^{64}Cu-PTSM (complexes with a single methyl group on the di-imine backbone at the R^1 position), displayed significantly higher tissue retention than ^{64}Cu-ATSM, ($p<0.05$) with 54.5 ± 3.5 % ID and 63.6 ± 2.1 % ID respectively. Under hypoxic conditions the retained fraction increased to 86.2 ± 7.5 % ID and 90.1 ± 3.3 % ID after 5 min, and 90.1 ± 3.3 % ID and 89.5 % ID after 25 min, also respectively.

When compared to ^{64}Cu-PTSE and ^{64}Cu-PTSM, ^{64}Cu-BTSC complexes that were alkylated at the R^1 and R^2 positions displayed significantly different retention profiles. Under oxygenated condition the retention of these tracers ranged from 4.3 ± 0.7 % ID (^{64}Cu-CTS) to 14.4 ± 1.4 % ID (^{64}Cu-DTSM). However after 5 min hypoxia the retained fraction increased significantly to between 41.8 ± 5.7 % ID (^{64}Cu-CTS) and 59.4 ± 5.5 % ID (^{64}Cu-DTSM) ($p<0.05$). After 25 min hypoxia this increased further still, to between 64.0 ± 11.65 ID (^{64}Cu-ATSM) and 78.2 ± 7.2 % ID (^{64}Cu-ATS).

Accumulation of $^{64}CuCl_2$ in myocardial tissue was negligible regardless of the level of oxygenation. On average 0.9 ± 0.7 % ID was retained during normoxia. Under hypoxic conditions retention increased marginally, to 1.0 ± 0.4 % ID after 5 min, and 1.7 ± 0.7 % ID after 25 min. However the slight increase in the retention of $^{64}CuCl_2$ was not statistically significant.

For ^{99m}Tc-Sestamibi an average of 15.8 ± 5.4 % ID was retained under oxygenated conditions. However under hypoxic conditions the retained fraction decreased

significantly to -1.5 ± 5.0 % ID after 5 min, and -5.2 ± 6.8 % ID after 25 min. ^{99m}Tc-Sestamibi therefore did not accumulate during hypoxia; moreover, the fraction that had previously been retained under oxygenated conditions eluted from the heart during hypoxia.

5.3.4.2.2 Comparison of ^{64}Cu-BTSC Accumulation after 5 and 25 Minutes Hypoxia

When the tissue retention after 5 min hypoxia was compared to the corresponding 25 min values (figure 5.17), the accumulation of the ^{64}Cu-complexes of ATS, ATSE, ATSM, CTS, CTSM and DTS increased significantly ($p<0.05$). For all other ^{64}Cu-BTSCs, $^{64}CuCl_2$ and ^{99m}Tc-Sestamibi, tissue retention values were similar at these times.

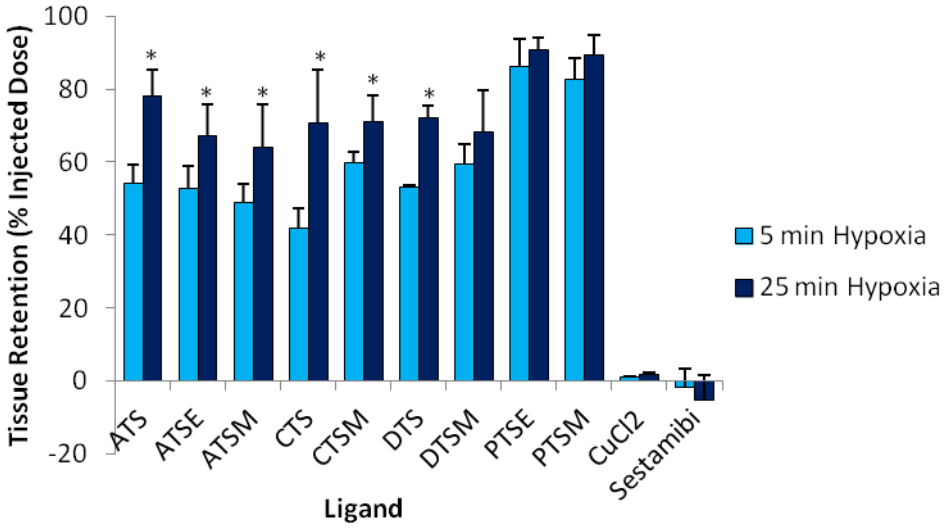

*Figure 5.17. Comparison of tissue retention after 5 and 25 min hypoxia. Tissue retention (% injected dose) of each tracer after 5 min hypoxia (light blue), are compared to the corresponding uptake values after 25 min (dark blue) hypoxia. Data represent mean (n = 3 – 5) ± SD. * = significantly different.*

5.3.4.2.3 Comparison between the Retention of Novel ^{64}Cu-BTSC Complexes and ^{64}Cu-ATSM

The tissue retention of ^{64}Cu-BTSCs with a ligand that is alkylated at the R^1 and R^2 positions (hypoxia selective) were compared to ^{64}Cu-ATSM, under oxygenated conditions (Fig. 5.18), and after 5 min (Fig. 5.19) and 25 min (Fig. 5.20) hypoxia. Please note that in these figures the complexes are in order of increasing partition ratio (octanol/ mKHB). Under oxygenated conditions there was less accumulation of ^{64}Cu-ATS (5.8 ± 1.1 % ID), ^{64}Cu-CTS (4.3 ± 5.7 % ID) and ^{64}Cu-DTS (6.9 ± 0.8 % ID), compared to ^{64}Cu-ATSM (8.0 ± 1.7 % ID). Conversely, accumulation of ^{64}Cu-CTSM (11.9 ± 3.8 % ID), ^{64}Cu-ATSE (11.4 ± 2.6 % ID), and ^{64}Cu-DTSM (14.3 ± 1.4 % ID) was higher. However, the tissue retention values were only statistically significant for the ^{64}Cu-complexes of CTS, CTSM and DTSM ($p<0.05$) (figure 5.18).

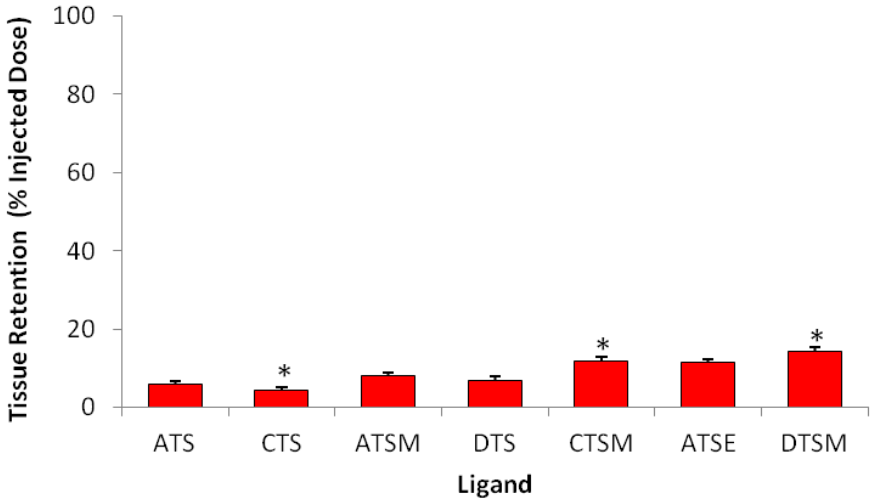

*Figure 5.18. Comparison of tissue retention values for hypoxia selective ^{64}Cu-BTSCs under oxygenated conditions. The tissue retention (% injected dose) of novel ^{64}Cu-BTSC complexes that displayed hypoxia selectivity were compared to ^{64}Cu-ATSM. Complexes are shown in order of increasing lipophilicity (octanol/ mKHB) Experiments were performed using isolated perfused hearts. Data represent mean (n = 3 – 5) ± SD. * = significantly different.*

After 5 min hypoxia all novel ^{64}Cu-BTSC complexes, with the exception of ^{64}Cu-CTS (41.8 ± 5.7 % ID), demonstrated greater tissue retention compared to ^{64}Cu-ATSM (48.9 ± 5.2 % ID). Values were as follows: ^{64}Cu-ATS (54.2 ± 5.2 % ID), ^{64}Cu-DTS (53.2 ± 0.5.), ^{64}Cu-CTSM (59.7 ± 3.2 %ID), ^{64}Cu-ATSE (52.9 ± 6.2 % ID), and ^{64}Cu-DTSM (59.3 ± 5.5% ID) (figure 5.19). However, only the tissue retention values for ^{64}Cu-CTSM and ^{64}Cu-DTSM were significantly different to ^{64}Cu-ATSM ($p<0.05$).

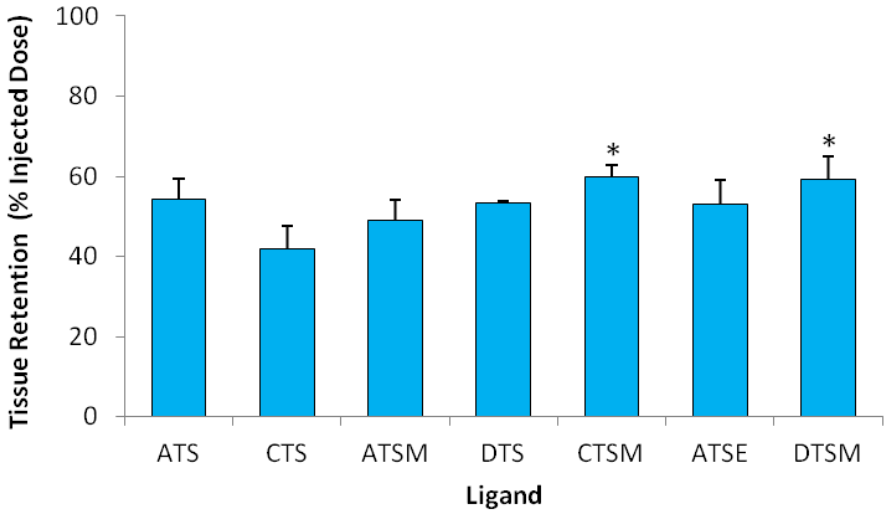

*Figure 5.19. Comparison of the tissue retention values for hypoxia selective ^{64}Cu-BTSC after 5 min hypoxia. The tissue retention (% injected dose) of novel ^{64}Cu-BTSC complexes that displayed hypoxia selectivity were compared to ^{64}Cu-ATSM. Complexes are shown in order of increasing lipophilicity (octanol/ mKHB). Experiments were performed using isolated perfused hearts. Data represent mean (n = 3 – 5) ± SD. * = significantly different.*

After 25 min hypoxia the tissue retention values of all complexes were statistically comparable to that of ^{64}Cu-ATSM (63.9 ± 11. 7 % ID). For each ^{64}Cu-complex the retained fraction was as follows: ATS (78.2 ± 7.2 % ID), CTS (70.7 ± 14.5 % ID), DTS (72.1 ± 3.2 % ID), CTSM (71.2 ± 7.1 % ID), ATSE (67.0 ± 8.9 % ID), and DTSM (68.2 ± 11.6 % ID) (figure 5.20).

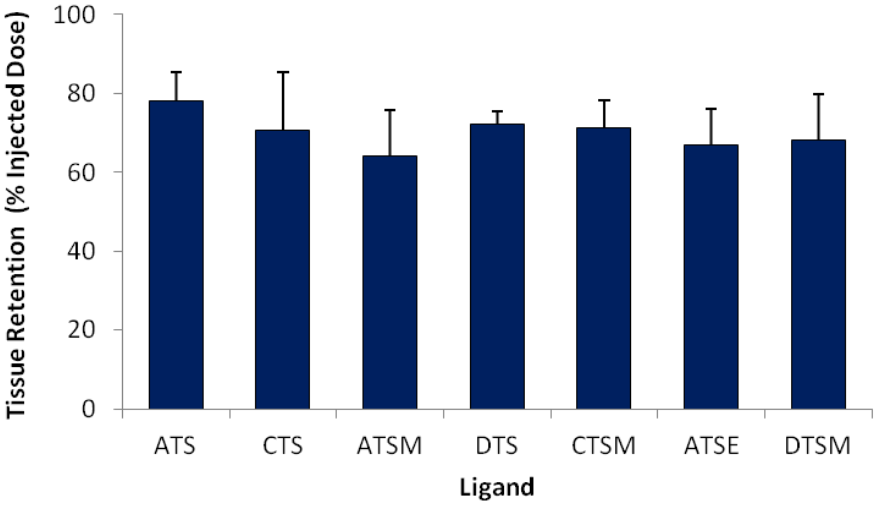

*Figure 5.20. Comparison of the tissue retention values for hypoxia selective ^{64}Cu-BTSC after 25 min hypoxia. The tissue retention (% injected dose) of novel ^{64}Cu-BTSC complexes that displayed hypoxia selectivity were compared to ^{64}Cu-ATSM. Complexes are shown in order of increasing lipophilicity (octanol/ mKHB). Experiments were performed using isolated perfused hearts. Data represent mean (n = 3 – 5) ± SD. * = significantly different (p<0.05).*

5.3.4.2.4 Contrast between Hypoxic and Oxygenated Tissue Retention

The hypoxic to normoxic tissue retention ratios of ^{64}Cu-BTSC complexes are summarised in table 5.4, and shown in figure 5.21. The ^{64}Cu-complexes of PTSE and PTSM displayed significantly lower contrast than ^{64}Cu-ATSM. The ^{64}Cu-complexes of ATSE, CTS, DTS and DTSM displayed contrast ratios that were comparable to ATSM. However ^{64}Cu-ATS and ^{64}Cu-CTS displayed significantly higher hypoxic tissue retention ratios ($p<0.05$).

*Table 5.4. Hypoxic to normoxic tissue retention ratios of ^{64}Cu-complexes. Data represent mean (n = 3 – 5) ± SD. * denotes significantly different from ^{64}Cu-ATSM.*

Ligand	5 min Hypoxia	25 min Hypoxia
ATS	*9.5 ± 1.7	*13.9 ±3.6
ATSE	4.9 ± 1.1	6.1 ± 1.5
ATSM	6.2 ± 1.2	8.2 ± 2.0
CTS	*9.8 ± 1.6	*16.6 ± 2.9
CTSM	5.5 ± 2.0	6.5 ± 2.1
DTS	8.2 ± 2.7	11.5 ± 4.8
DTSM	4.2 ± 0.4	4.8 ± 1.1
PTSE	*1.6 ± 0.2	*1.7 ± 0.1
PTSM	*1.3 ± 0.1	*1.4 ± 0.1

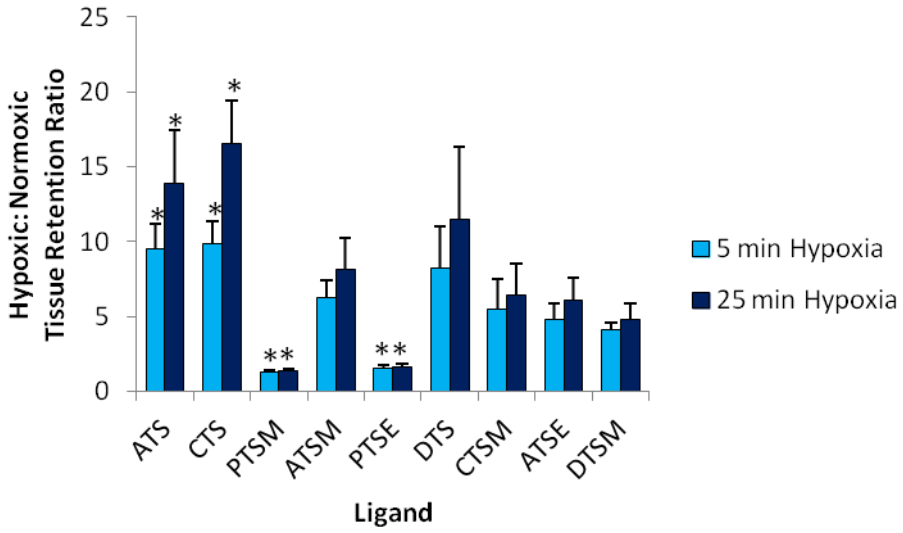

*Figure 5.21. Contrast between the tissue retention of ^{64}Cu-BTSC complexes under oxygenated and hypoxic conditions. Ratios are for injections administered after 5 (light blue) and 25 min (dark blue) hypoxic buffer perfusion. A comparison was made between ^{64}Cu-ATSM and all other ^{64}Cu-BTSCs, at 5 and 25 min post- hypoxia. Complexes are shown in order of increasing lipophilicity (octanol/ mKHB). Data represent mean ± SD. * = significantly different (p = 0.05).*

5.3.4.2.5 Comparison between ^{64}Cu-BTSC Molecular Weight, Partition Ratio, and Tissue Retention

In this section the results demonstrated thus far will be compared graphically, to ascertain whether there are any relationships between the physicochemical properties and accumulation of the ^{64}Cu-BTSC complexes, which demonstrated a hypoxic to normoxic tissue retention ratio of greater than 3: 1.

Under oxygenated conditions a positive relationship (R^2= 0.81) was observed between the molecular weight of ^{64}Cu-BTSC complexes, and the amount of radiotracer that was retained within the heart. However during hypoxia these parameters did not correlate. R^2 values during hypoxia were as follows: 5 min (0.26), and 25 min (0.41) (figure 5.22).

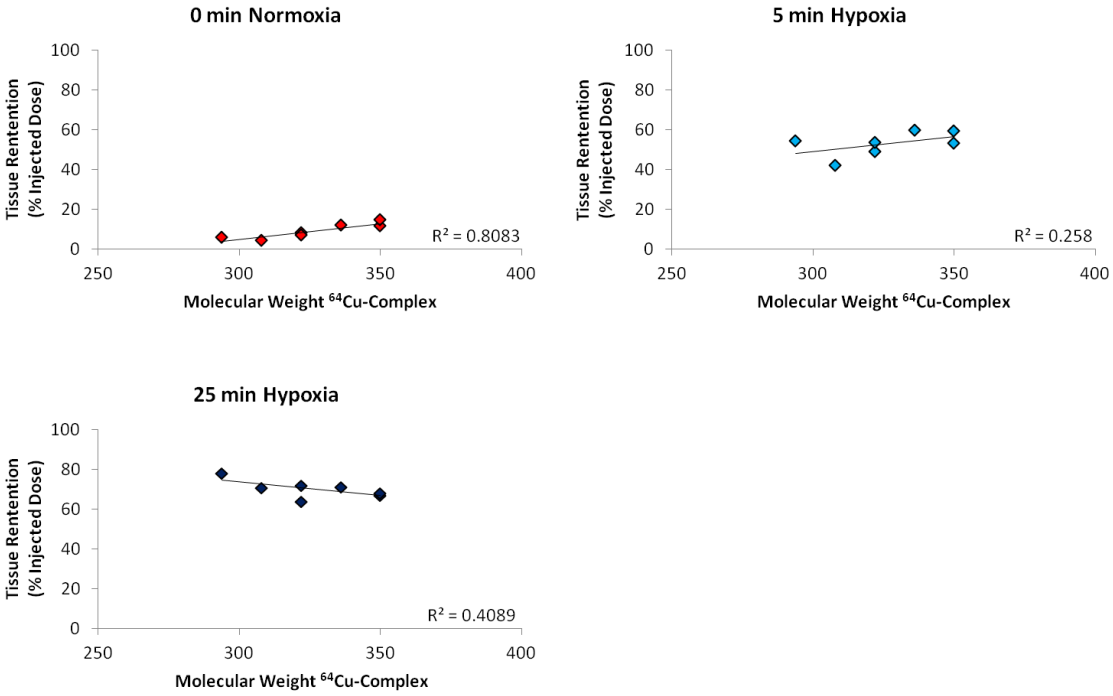

Figure 5.22. Comparison between the molecular weight and tissue retention (% injected dose) of hypoxia selective ^{64}Cu-BTSC complexes during normoxia, and after 5 min, and 25 min hypoxia. Data represent mean (n= 3 – 5).

Under oxygenated conditions there was a positive relationship (R^2 = 0.84) between the partition ratio and tissue retention of this class of tracers (figure 5.23). However after 5 min (R^2 = 0.41), and 25 min hypoxia (R^2 = 0.29) no relationship was observed between these parameters (figure 5.23).

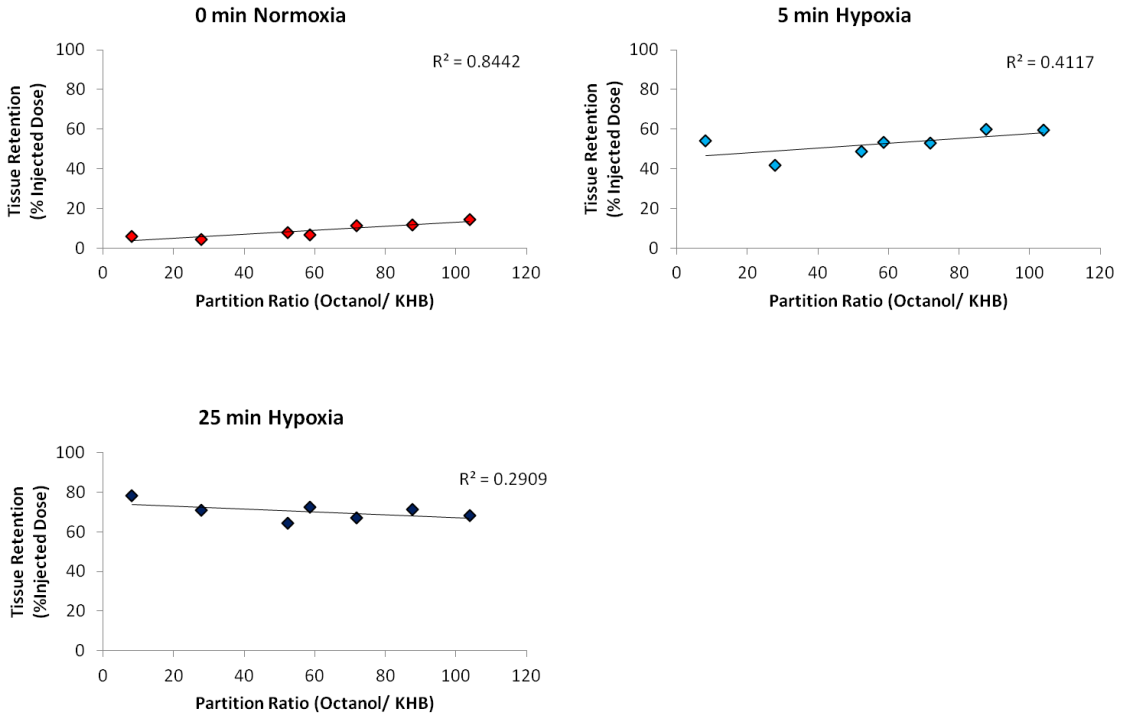

Figure 5.23. Comparison between the partition ratio (octanol/ mKHB) and tissue retention (% injected dose) of hypoxia selective ^{64}Cu-BTSC complexes during normoxia, and after 5 min and 25 min hypoxia. Data represent mean (n= 3 – 5).

A relationship was observed between the hypoxic to normoxic tissue retention ratios and the molecular weight of the corresponding ^{64}Cu-BTSC complex, with R^2 values of 0.87 and 0.79, after 5 min and 25 min hypoxia respectively (figure 5.24).

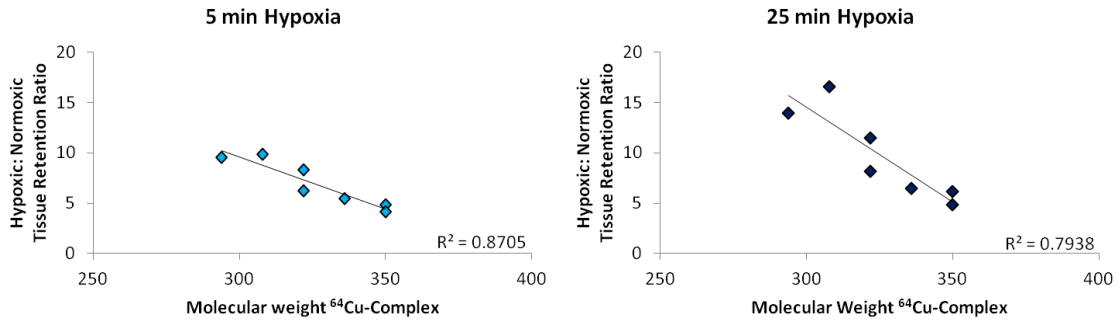

Figure 5.24. Comparison between the hypoxic to normoxic tissue retention ratio and molecular weight of hypoxia selective ^{64}Cu-BTSC complexes after 5 min, and 25 min hypoxia. Data represent mean (n= 3 – 5).

A relationship was also observed between the hypoxic to normoxic tissue retention ratios and the molecular weight of the corresponding Cu-BTSC complex, with R^2 values of 0.81 and 0.78, after 5 min and 25 min hypoxia respectively (figure 5.25).

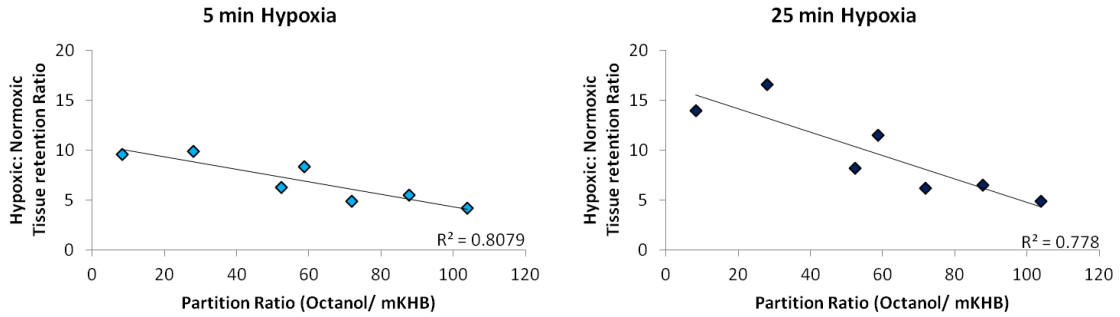

Figure 5.25. Comparison between the hypoxic to normoxic tissue retention ratio and partition ratio (octanol/ mKHB) of hypoxia selective ^{64}Cu-BTSC after 5 min, and 25 min hypoxia. Data represent mean (n= 3 – 5).

5.4 Discussion and Conclusions

5.4.1 BTSC Radiolabelling efficiency and ^{64}Cu-Complex Stability

The radiolabelling efficiency of all BTSC ligands was always greater than 97%. In a solution of mKHB the radiolabelled complexes displayed a high degree of stability over 24 h (figure 5.3). With the exception of ^{64}Cu-ATSM (94 % radiolabelled), less than 4 % free ^{64}Cu was present in each of the tracer stocks at 24 h. It was therefore decided that complexes that were radiolabelled in the morning could be used for the entire day's experiments.

5.4.2 Retention Factor of ^{64}Cu-BTSC

Rf values were determined to ascertain how the alkylation pattern of a particular ligand affects the relative lipophilicity of the corresponding ^{64}Cu-complex. The values that we obtained were somewhat higher than those reported by Dearling *et al* [162, 167], which is likely due to the fact that they used ethyl acetate as the mobile phase, while we employed ethanol. However, although the solvent phase and therefore the actual Rf values reported here are higher than previously reported values, the relative order of lipophilicity is comparable (Fig. 5.4), and we also observed a positive relationship (R^2= 0.87) between molecular weight and the Rf values of the Cu-complexes (figure 5.5).

5.4.3 LogP Values and Partition Ratios

Octanol extraction was also employed to assess the relative lipophilicity of ^{64}Cu-BTSC complexes, in order to allow us to draw comparisons with data from Dearling *et al* [162, 167] and McQuade *et al* [208]. When ultrapure water was used as the aqueous phase, the

logP values that we obtained (table 5.2) were similar to those previously reported. We then replaced water with aqueous phase of mKHB, to assess whether this would have an effect on the partition ratio, or relative lipophilicity of the complexes. The values were largely unaffected (table 5.3 and figure 5.6), and we again observed a positive relationship (R^2= 0.80), between the molecular weight of the ^{64}Cu-BTSC complexes and their partition ratios (octanol/ mKHB) (figure 5.7).

5.4.4 Perfusate pO_2, Cardiac Function and Lactate Release

The Oxylab pO_2™ system and oxygen probes are extremely sensitive, but the measurement range is limited to $pO_2 \leq$ 100mmHg. In a personal communication, a representative of the manufacturer stated that the Oxylab™ system can detect and measure up to a pO_2 of 150 mmHg, but when 100 mmHg is exceeded the error can be as much as ± 15 %. The pO_2 of oxygenated KHB typically exceeds 500 mmHg [283], in excess of the Oxylab pO_2™'s operating range. Measurements of buffer oxygen saturation were therefore only taken upon commencement of gassing with anoxic gas mixtures. After switching to hypoxic buffer the decrease pO_2 was biphasic. The initial rapid phase lasted ~5 min, before it slowed. However, the pO_2 continued to decrease for the duration each experiment (figure 5.8).

At the start of each experiment, cardiac function and perfusion pressure were within the ranges defined in section 4.3.2. These parameters then remained stable for the 20 min of oxygenated buffer perfusion, which followed the first injection of radiotracer (figures 5.10- 5.13). During this time the efflux of lactate into the coronary effluent was stable, at

a concentration of between 0.036- 0.078 mMol/ l (figure 5.9). Cardiac function was therefore considered normal while hearts were perfused with oxygenated mKHB.

Within 2 min of switching perfusion to hypoxic mKHB, the buffer pO_2 fell to within the detection range of the Oxylab pO_2™ (92.4- 61.3 mmHg) (figure 5.8). However, after just 1 min of commencing perfusion with hypoxic mKHB, LVDP (figure 5.11) and heart rate (figure 5.13) began to decrease, and LVEDP (figure 5.12) and lactate efflux (figure 5.9) began to rise. The rise in lactate release demonstrated that by perfusing the hearts with hypoxic buffer they lost the capacity to metabolise energy substrates via the electron transport chain, and upregulated their metabolism of glucose via anaerobic glycolysis. Contractility concomitantly decreased because glycolysis alone cannot supply enough ATP to maintain cardiac contractility, as discussed in sections 1.4.3 and 1.5.

From the onset of hypoxia LVEDP (figure 5.12) gradually increased, but heart rate continuously decreased. Conversely LVDP initially decreased for all hearts (except inexplicably those that were administered with ^{99m}Tc-Sestamibi). There was a brief recovery in LVDP which occurred after 5- 10 min perfusion with hypoxic mKHB, and which lasted between 1- 10 min. In general, other researchers who have also characterised hypoxia tracers have not included cardiac function data in their reports, as we did. We are therefore unaware of whether they observed a similar recovery in cardiac function during their hypoxia protocols. However, Kusuoka *et al* also observed a decrease in LVDP and a rise in LVEDP in isolated rat hearts subject to hypoxia [115]. In a more recent study Suner and Jay compared the effects on cardiac function of hypoxia

and carbon monoxide poisoning, using isolated perfused hearts [284]. They also observed a decrease in LVDP and heart rate, and a rise in LVEDP and lactate release. However, they did not observe a recovery of LVDP during their hypoxia protocol (perfusion with KHB gassed with 30 % N_2 70 % O_2, for 15 min). While the period of hypoxia employed by Sun and Jay was longer than the time-frame within which we observed a recovery of LVDP, neither they or other researchers have observed this [284-286]. In contrast to our experiments, others have generally paced hearts using an externally applied electrical stimulus. We on the other hand did not use pacing, and therefore contractility was allowed to match the delivery of oxygen, at least in the early stages of hypoxia. We postulate that the brief period of recovery of LVDP was due to a transient recovery of ATP, following the rapid cessation of contractility that occurred immediately upon perfusing hearts with hypoxic buffer. This overshoot perhaps led to a temporary ATP surplus, which allowed a short functional recovery before metabolism and contractility became more closely matched, and the decline in contractile function resumed.

Heart rate began to decrease from the onset of hypoxia, and after just 15 min hearts began to fibrillate and all contractility effectively ceased, which led to large variations in the average heart rate interpreted by the PowerLab™ system, between each replicate. We therefore omitted all measurements of heart rate that were recorded after 15 min hypoxia (35 min total experiment time).

Although it was not possible to measure the intracellular pO_2 of cardiac cells during tracer characterisation experiments, the results presented in section 5.3.3 demonstrate that the hearts were severely oxygen deprived. Significant decreases in heart rate and LVDP, and increases in perfusion pressure, LVEDP, and lactate release all serve to confirm this. Our observations of cardiac function, coronary perfusion pressure, and lactate release are in accordance with those of Serizawa *et al*, who investigated the effects of 3 min ischaemia or hypoxia on left ventricular relaxation time and diastolic stiffness [287]. They demonstrated that in isolated rabbit hearts subject to low flow ischaemia (~35 % normal flow) for 3 min, LVDP, LVEDP, and coronary perfusion pressure decreased, but efflux of lactate into the coronary perfusate increased. However, while ischaemia caused a decrease in LVEDP, it increased during hypoxia, which we also observed. Similarly we observed a slight decline in the coronary perfusion pressure after switching to hypoxic buffer, which lasted for between 2- 4 min, before it then began to rise. The authors suggested that the initial decline in perfusion pressure was due to coronary vasodilation, to counteract decreased oxygen delivery. Of particular interest and relevance to our study is the fact that they observed an increase in LVEDP during hypoxia, but not during low flow ischaemia. Serizawa *et al* also observed ~4-fold increase in the diastolic relaxation time and incomplete relaxation of the myocardial contractile apparatus, which they suggested caused a rise in LVEDP in hypoxic hearts. They proposed that this occurred because the sarcoplasmic reticulum became saturated with Ca^{2+}, but that there was still sufficient Ca^{2+} within the cytosol to prevent complete relaxation. However, during ischaemia the effect of this is somewhat masked by the loss of coronary turgor pressure. This agrees with observations made by Kihara *et al*, who

demonstrated that the cytoplasmic concentration of Ca^{2+} increases during hypoxia [285]. While this explains why in our experiments LVEDP rose during hypoxia, it also highlights how more physiologically relevant ischaemia protocols differ from hypoxic buffer perfusion. As we already discussed in section 5.1.2.1, we chose to use a hypoxic buffer to confirm that the retention of our complexes was due to hypoxia alone, maintaining constant flow perfusion to avoid variations in the rate of tracer delivery, which would interfere with modelling of our tracer time-activity curves. Our observations were similar to those of Serizawa *et al*, although we exposed hearts to hypoxia for considerably more time (45 min compared 2 min). Furthermore, Wardle *et al* exposed isolated rat hearts to hypoxia for 30 min and also observed a marked increase in the release of lactate from hearts [288], with profiles similar to our own. Our own data in conjunction with data from these other studies provide supportive evidence that the hearts used in our experiments were severely oxygen deprived when perfused with hypoxic mKHB.

Finally, we are aware that the extremely low level of hypoxia that we employed during our experiments may not necessarily reflect that which is observed *in vivo*. This series of experiments was a screening process, which was conducted to identify candidate tracers which shall be taken forward into a more in depth study, where we will first determine the level of oxygenation that is clinically relevant. This will be done using ^{31}P NMR to measure transitions in cardiac ATP levels, and tracer retention will then be determined at these levels of oxygenation. We will discuss these future experiments in Chapter 6. While we measured cardiac function during our tracer washout/ accumulation

experiments we did not determine myocardial viability, for example by tissue sectioning and staining or by measuring cardiac function upon reoxygenation. We are therefore unaware of whether there was tissue infarction or necrosis during hypoxia. However as discussed in Chapter 1, Cu-BTSC complexes are only retained in cells that are able to synthesise the bioreductants necessary for tracer trapping. We therefore concluded by inference, that while the hearts were severely oxygen deprived during hypoxia, and some degree of infarction may have been present in the tissue, the majority of the myocardium must still have been viable. This is because the retention of all ^{64}Cu-BTSC increased following the switch to hypoxic buffer perfusion. Furthermore, tracer retention was always greater after 25 min hypoxia compared values obtained at 5 min.

5.4.5 Characterisation of ^{64}Cu-BTSC complexes in Isolated Perfused Rat Hearts

While not able to provide quantitative data regarding tracer washout/ retention, the time-activity curves from hearts (figure 5.15) were able to indicate whether a tracer displayed hypoxia selectivity. From these traces it is clear that $^{64}CuCl_2$, which was used as a negative control, demonstrated negligible accumulation under both normoxia and hypoxia. ^{64}Cu-PTSM has previously been reported as a potential perfusion agent, for monitoring myocardial and cerebral blood flow because it is retained in tissue irrespective of their oxygenation status [73, 165, 170]. Using our system we confirm that ^{64}Cu-PTSE and ^{64}Cu-PTSM, both of which are protonated at the R^2 position, displayed significant tissue accumulation under oxygenated conditions. In contrast, the time activity curves for the ^{64}Cu complexes of ATS, ATSE, ATSM, CTS, CTSM, DTS and DTSM demonstrated that all of these complexes exhibit hypoxia selectivity.

By manually analysing the time-activity curve raw data, using the method described in Section 5.2, it was possible determine the actual tissue retention of each tracer. The tissue retention values (figure 5.16) proved that the initial observations of the real-time time-activity curves were correct, but also allowed us to quantify tracer retention.

When using the bolus method of tracer delivery it is important to obtain a true peak in the decay counts emitted from the heart [134]. Otherwise because of the rapid kinetics that these tracers display, their retention within the myocardium as a percentage of the injected dose cannot be accurately determined. In our experiments the Gina Star™ system was set up to acquire cps measurements every 0.2 seconds, which is considerably higher than the sampling rates of 1 sample/ sec used by Ng *et al* [134], and 1 sample/ 5 sec used by Rumsey *et al* [132]. To ensure that the Gina Star™ system was able to detect the peak counts we considered the time-activity curves of $^{64}CuCl_2$. This tracer cleared from the heart faster than any of the ^{64}Cu-BTSC complexes. It was therefore rational to assume that if the Gina Star system could detect a true peak for $^{64}CuCl_2$, then it would be able to do so for the ^{64}Cu-BTSC complexes. Upon injecting $^{64}CuCl_2$ into the perfusion line the decay counts registered from the heart (detector 2) began to increase, and the cps peaked after ~3 sec. The majority if not all of the bolus had therefore entered the heart within this time. The cps peak was also very sharp, lasting only 1 sec before the counts began to fall, reflecting the rapidity with which the tracer then distributed through the coronary vasculature. If $^{64}CuCl_2$ had entered the heart at a slower rate then one would perhaps have expected the cps gradually increase over time before reaching a plateau, as

the concentration of radiotracer entering the heart would equal that which was eluting from it, before it began to decrease. The total time taken for the counts to go from the background level, up to maximum counts, and then back down once again to a steady state was ~27 sec, after $^{64}CuCl_2$ first entered the heart. As the majority if not all of the radioactivity had entered the heart within ~3 sec, and because it took ~27 sec for a bolus of $^{64}CuCl_2$ to completely pass through the heart, we can be confident that the Gina Star™ system was able to detect the true cps peak, especially considering the rate at which measurements were acquired. We were therefore also confident that our calculations of percentage tissue retention were accurate.

5.4.6 Retention of Radiotracers in Isolated Perfused Hearts

5.4.6.1 ^{99m}Tc-Sestamibi

^{99m}Tc-Sestamibi is SPECT imaging tracer that is used to assess myocardial perfusion. It is a lipophilic cation that passively diffuses into cells, and accumulates within the mitochondrial matrix. As ^{99m}Tc-Sestamibi is positively charged it is only retained in the negatively charged matrix of mitochondria with an active electron transport chain. ^{99M}Tc-Sestamibi is therefore used clinically as a negative contrast imaging agent that accumulates within normally perfused tissue, but is not retained in regions of the myocardium where blood or oxygen is supply is restricted. In our experimental model of hypoxia with constant flow, loss of ^{99m}Tc-Sestamibi retention in the myocardium cannot be due to lack of tracer delivery, must be due to a loss of mitochondrial membrane potential [289]. For this reason ^{99m}Tc-Sestamibi retention was used in conjunction with measurements of the perfusion buffer pO_2 and lactate release, to demonstrate that hearts

were subjected to severe oxygen deprivation during hypoxia. ^{99m}Tc-Sestamibi accumulated in hearts perfused with oxygenated mKHB but cleared from those perfused with hypoxic buffer. It is interesting to note that the rate of washout of the bolus that was administered during early hypoxia was higher than observed during normoxia. Even at this early hypoxia time point, it seems that the mitochondrial membrane potential is compromised. From this point on the myocardium seems unable to retain ^{99m}Tc-Sestamibi, and there was even washout of tracer that was originally retained during normoxia.

5.4.6.2 $^{64}CuCl_2$

$^{64}CuCl_2$ is the form in which ^{64}Cu(II) is supplied for radiolabelling, it has also been employed previously as a negative control during ^{64}Cu-BTSC characterisation studies [162]. We therefore also included $^{64}CuCl_2$ in this study as a negative control. In an aqueous solution $^{64}CuCl_2$ dissociates into $^{64}Cu^{2+}$ and $2Cl^-$ ions. Due to its positive charge $^{64}Cu^{2+}$ is unable to passively diffuse across cell membranes. It should not therefore be able accumulate within hearts to the same degree as the lipophilic Cu-BTSC complexes. Moreover, if we were to observe accumulation of $^{64}Cu^{2+}$ it should be independent of the level of oxygenation. As discussed previously, in our experiments a bolus of $^{64}CuCl_2$ passed through the heart in ~27 sec, which suggests that the tracer does not get taken up by cells, but rather it passes directly through the coronary vasculature, and elutes from the heart. However, we did observe a relatively small amount of $^{64}Cu^{2+}$ uptake (normoxia (0.9 % ID), 5 min hypoxia (1.0 % ID), and 25 min hypoxia (1.7 % ID)), and the accumulation of $^{64}Cu^{2+}$ was 2-fold higher after 25 min hypoxia, compared to normoxic

retention. The reason for this is unknown, but it is feasible that during hypoxia the biological mechanisms responsible for importing copper into the heart may be upregulated. It also feasible that prolonged exposure to hypoxia may have led to damage being caused to the membranes of cells with the heart. This may have caused some damage to the vasculature, and allowed a small percentage of $^{64}Cu^{2+}$ to enter the interstitial space [290]. Nevertheless the relatively low uptake of $^{64}Cu^{2+}$ compared to the ^{64}Cu-BTSCs suggests that copper is not removed from the complex, and then transported into the cells via a receptor or transporter protein mediated mechanism, but rather that it is the ligand that is responsible for transporting copper moiety through the cell membrane and into the cytoplasm.

5.4.6.3 ^{64}Cu-PTSM

$^{62, 67}$Cu-PTSM has previously been investigated as a perfusion agent, for monitoring myocardial, cerebral [73, 75, 165, 170] and renal [76, 291] blood flow. It has been proposed that its relatively low redox potential (-0.51 V) compared to Cu-ATSM (-0.59 V), allows the intracellular reduction of Cu(II)-PTSM to Cu(I)-PTSM in normoxic tissue. This in turn leads to the dissociation of the complex, and the intracellular accumulation of radiocopper [165].

In our study the single pass extraction of ^{64}Cu-PTSM under oxygenated conditions was 63.6 % ± 2.1 % ID. During hypoxia this increased significantly to 82.7 ± 5.7 % ID and 89.5 ± 5.2 % ID, after 5 min and 25 min hypoxia respectively. However while ^{64}Cu-PTSM accumulation increased during hypoxia, the maximum hypoxic to normoxic tissue

contrast was only 1.4: 1, which as other have suggested precludes the use of ^{64}Cu-PTSM as a hypoxia imaging agent. The tissue retention values that we obtained for ^{64}Cu-PTSM are higher than those reported by Shelton *et al*, as they did not observe any difference in retention between oxygenated and hypoxic conditions [75]. Using isolated perfused rabbit hearts Shelton *et al* characterised ^{67}Cu-PTSM under a variety of conditions. The tracer was administered as a bolus during ischaemia (10 % control flow) (46 % ID), hypoxia (perfusion without erythrocytes) (49 % ID), and hyperaemia (200 % control flow) (51 % ID), but under each of these conditions the fraction of tracer that was retained was comparable to normally perfused control hearts (48 % ID). There are two possible explanations for this. Firstly, the method that we used for initiating and maintaining hypoxia, may have been more severe than that employed by Shelton *et al*. Secondly, we used much smaller hearts and perfused them at a higher flow rate. Instead of gassing the perfusion buffer as we did, Shelton *et al* chose to use isolated erythrocytes to deliver oxygen to the hearts, and during their hypoxia protocol they simply omitted erythrocytes from the perfusate. We on the other hand continually gassed the perfusion buffer with either an oxygenated or anoxic gas mixture. As the results in figure 5.8 show, after perfusing hearts with hypoxic buffer for 45 min the pO_2 of mKHB dropped to between 10 -15 mmHg. Furthermore, in a set of preliminary experiments we attempted to measure the pO_2 of non-gassed mKHB but it was still above 150 mmHg, too high to be measured using the Oxylab pO_2™ system. Is it therefore likely the 'hypoxic' buffer used by Shelton *et al* had a higher pO_2 than our corresponding buffer. As our data shows, while ^{64}Cu-PTSM is not hypoxia selective its accumulation within the heart certainly appears to be oxygen sensitive, with the retention profile of ^{64}Cu-PTSM inversely related

to the pO_2 of the perfusion buffer. Shelton *et al* used hearts from rabbits (1.5- 2.0 kg) which would have been considerably larger hearts than the rat hearts that we used in our study. However, this group perfused hearts at only 6 ml/ min, whereas we perfused at 14 ml/ min. It is therefore feasible that although the hearts used by Shelton's group were perfused with erythrocytes, even the control hearts may not have been sufficiently oxygenated. Unfortunately this group did not report the concentration of erythrocytes in their perfusion buffer, but it is likely to have been lower than the *in vivo* concentration. This combined with a relatively low flow rate is perhaps why they did not observe a contrast between control and test conditions.

Results from Dearling *et al* have also suggested that the accumulation of ^{64}Cu-PTSM may be sensitive to the level of oxygenation, as they observed an hypoxic to normoxic contrast of ~1.3: 1 using CHO cells [162]. As both Dearling's group and our own have observed oxygen level-dependent retention of Cu-PTSM, it suggests that once inside the cell the tracer may be more stable than previously thought. Minkel *et al* [173] and Fujibayashi *et al* [169, 174] have suggested that Cu-PTSM dissociates even in normoxic cells. However both our own and Dearling *et al*'s data suggest that the intracellular bioreduction of Cu-PTSM may be reversible in the presence of oxygen, as is thought to occur with Cu-ATSM, otherwise we would also have observed a hypoxic to normoxic contrast of 1: 1. While this is an interesting observation, the contrast for ^{64}Cu-PTSM is still insufficient for delineating hypoxic tissue, and Cu-PTSM should still only be considered as a perfusion tracer.

5.4.6.4 ^{64}Cu-PTSE

Our data show that the time-activity curves and therefore myocardial accumulation of ^{64}Cu-PTSE were similar to those of ^{64}Cu-PTSM. Under oxygenated conditions 54.5 ± 3.5 % ID was retained, which rose to 86.2 ± 7.5 % ID after 5 min hypoxia, and 90.9 ± 3.3 % ID after 25 min. ^{64}Cu-PTSE was first described and investigated as a perfusion tracer by John and Green [171], before being studied further as a hypoxia tracer by Dearling *et al*, using CHO and EMT6 tumour cells [162-163, 167]. Dearling and co-workers observed low hypoxic to normoxic tissue contrast of ~1.3: 1 with ^{64}Cu-PTSE. However, when they employed a mathematical model termed the 'hypoxia selectivity index (HSI)', which compared the logarithm of the intracellular to extracellular concentration of radiotracers, under oxygenated and hypoxic conditions [163, 167], they showed that Cu-PTSE displayed some degree of hypoxia selectivity. In fact when the mean HSI 5- 60 min was plotted against redox potential, the HSI of Cu-PTSE (~0.45) was comparable to Cu-ATSM and the other novel Cu-BTSC complexes that we have assessed. However, by using isolated hearts to assess the single pass extraction of ^{64}Cu-PTSE in oxygenated or hypoxic tissue, we have shown that although the accumulation of this tracer appears to be oxygen sensitive it is poorly hypoxia selective, much like Cu-PTSM. This is not surprising considering that the redox potential of Cu-PTSE (-0.52 V) is similar to that of Cu-PTSM (-0.51 V) [167]. We can therefore confirm that because of its high uptake in normoxic tissue, and low hypoxic to normoxic tissue contrast (1.7: 1), ^{64}Cu-PTSE is not hypoxia selective, and was therefore excluded as a candidate hypoxia tracer.

5.4.6.5 ^{64}Cu-ATSM and the Novel Hypoxia Selective ^{64}Cu-BTSC Complexes

The remaining ^{64}Cu-BTSC complexes that were included in this study were all alkylated at the R^1 and R^2 positions, and demonstrated very different tissue retention profiles from the tracers that have already been discussed.

Under oxygenated conditions the retention of the ^{64}Cu complexes of ATS, ATSE, ATSM, CTS, CTSM, DTS, and DTSM was between 4.3- 14.3 % ID. ^{64}Cu-CTS (4.3 ± 5.7 % ID) demonstrated significantly lower retention than ^{64}Cu-ATSM (8.0 ± 1.7 % ID), while the accumulation of ^{64}Cu-CTSM (11.9 ± 3.8 % ID) and ^{64}Cu-DTSM (14.3 ± 1.4 % ID) was significantly higher ($p<0.05$). The tissue retention values for all other tracers were comparable to that of ^{64}Cu-ATSM. Following the switch from oxygenated to hypoxic buffer, a 38- 49 % increase in tissue retention was observed for the ^{64}Cu-complexes of ATS, ATSE, ATSM, CTS, CTSM, DTS and DTSM compared to normoxic values. With the exception of the ^{64}Cu-DTSM (59.3 ± 5.5% ID) and ^{64}Cu-CTSM (59.7 ± 3.2 % ID), after 5 min hypoxia the tissue retention of all other tracers was statistically comparable to ^{64}Cu-ATSM (48.9 ± 5.2 % ID). After 25 min hypoxia, the tissue retention values of all of these complexes increases by a further 9- 24 % ID. However, at this late hypoxia time point the values for all tracers were statistically comparable to ^{64}Cu-ATSM.

After 5 min hypoxia the significant increase in tissue retention of these tracers, gave rise to hypoxic to normoxic tissue contrast ratios of between 4.2: 1 (^{64}Cu-DTSM) and 9.8: 1 (^{64}Cu-CTS), with a ratio of 6.2: 1 for ^{64}Cu-ATSM. Interestingly the contrast ratio for ^{64}Cu-ATS (9.5: 1) was also higher than that of ^{64}Cu-ATSM. After 25 min hypoxia the

contrast was greater still. A ratio of 4.8: 1 was observed for ^{64}Cu -DTSM, 13.9: 1 for ^{64}Cu-ATS and 16.6: 1 for ^{64}Cu-CTS, with a ratio of 8.2: 1 for ^{64}Cu-ATSM. In this study all complexes that possessed an alkyl group at both the R^1 and R^2 positions demonstrated hypoxia selectivity. Furthermore, all of them displayed hypoxic to normoxic tissue retention ratios of greater than 3: 1, which Nunn *et al* suggested was the minimum requirement for a hypoxia imaging agent [105]. We have therefore identified two compounds ^{64}Cu-ATS and ^{64}Cu-CTS, which demonstrated lower accumulation in oxygenated tissue, and significantly greater hypoxic to normoxic tissue contrast compared to the current "gold standard" tracer ^{64}Cu-ATSM.

In terms of how these data fit in with previous reports there is much to compare and contrast, and a discussion of the hypoxia selective radiotracers should begin with the lead compound Cu-ATSM. This tracer was introduced by Wada *et al* in 1994 [205], and since then reports have shown that Cu-ATSM displays selective retention in isolated hearts [174], and cells [162-163, 167, 209, 241] exposed to hypoxic conditions. As we have demonstrated, our data from this study concur with these reports.

Fujibayashi and co-workers were the first group to demonstrate the hypoxia selectivity of ^{62}Cu-ATSM, also employing the isolated perfused rat heart model [174]. They observed 20 % retention of the injected dose under normoxic conditions, but more than 80 % during hypoxia. Their normoxic value is a slightly higher than we observed in our study (8.0 ± 1.5 % ID), but during hypoxia our value was slightly lower (64.0 ± 11.7 % ID). Nonetheless in our study the hypoxic to normoxic contrast was 8.2: 1, which was higher

than the 4: 1 ratio observed by Fujibayashi [174]. This was mostly likely due to fact that the hearts used by the Fujibayashi group were excised from larger animals (350- 450 g) than those that we used (250- 300 g), and theirs were perfused at a lower flow rate of 6 ml/ ml, in contrast to 14ml /min that we used. The 14 ml/ min flow rate that we employed ensured that the coronary perfusion pressure was ~70 mmHg, comparable to the aortic pressure *in vivo*. For a larger heart the flow rate required to achieve this pressure would be even higher. It is therefore likely that at 6ml/ min their larger hearts were under perfused and on the cusp of low flow ischaemia, even in their control group. This may explain why the control tissue retention values were greater than we observed in our study. Unfortunately the authors did not provide any data regarding the pO_2 of the perfusion buffer or contractile function data, so we were unable to compare these parameters.

One of purposes of conducting this research was to further characterise a number of novel Cu-BTSC complexes, which have previously demonstrated hypoxia selectivity, but which are at the moment poorly represented in the scientific literature. Studies by Dearling *et al* were the first to report on the screening of these novel ^{64}Cu-labelled BTSC complexes, to assess them as candidate hypoxia selective tracer [162-163, 167]. Using both CHO and EMT cells in conjunction with their HSI model, they showed that the ^{64}Cu-complexes of: ATS, ATSM, CTS, CTSM, DTS, DTSM, PTSE, and PTSM demonstrated some degree of hypoxia selective accumulation. However they also assessed a number of other complexes which we did not. This was because the HSI values for these complexes were comparable to or lower than that of Cu-PTSM. We also

characterised the myocardial retention of Cu-ATSE, which was first described by McQuade *et al* [208], but which also had yet to be screened in cardiac tissue.

The results of Dearling *et al* suggested that a number of their novel Cu-BTSC complexes were hypoxia selective. However the cell based methods that have been used thus far to characterise Cu-BTSC complexes, have generally only given a rough indication of whether a particular complex is in fact hypoxia selective. Our own data from ARVM, which is described in chapter 3, is testament to this. As discussed above, even though the uptake of Cu-PTSE in hypoxic cells was lower than in normoxic cells, the HSI method used by Dearling's group suggested that Cu-PTSE may be hypoxia selective, however our data do not agree with this. The accumulation of Cu-CTSM in CHO cells is another example of how unreliable cell based assays can be. In these cells the uptake of Cu-CTSM was only marginally higher under hypoxic compared to normoxic conditions, although the HSI did correctly predict that this tracer would be hypoxia selective. However by employing a more robust and dynamic system, which monitored radioactivity as it passed through the heart in real-time, we were able to assess the first pass extraction of ^{64}Cu-BTSC complexes. This method enabled us to demonstrate with greater confidence than was achieved previously using cell based systems, that alongside ^{64}Cu-ATSM the ^{64}Cu-complexes of ATS, ATSE, CTS, CTSM, DTS, and DTSM all display significant hypoxic tissue selectivity. We also demonstrated that during hypoxia the fraction of radioactivity that was retained in the heart, was similar for all of these tracers. This suggests that the greater improvements in hypoxic to normoxic tissue contrast of this series of radiotracers, was largely gained by decreasing the non-specific

retention during normoxia, which as we will now show was governed not by redox potential but by the relative lipophilicity of the complex.

For ^{64}Cu-BTSC complexes a positive relationship between molecular weight and lipophilicity has been demonstrated by John and Green [171], Green *et al* [170] and Dearling *et al* [167]. We also report similar findings in this study (Figure 5.5 and 5.7 Partition)**.** Earlier work by Minkel *et al* [173] and Dearling and co-workers [167], did not show a relationship between the cellular uptake of Cu-BTSC complexes and their relative lipophilicity. Our data on the other hand suggest that there is in fact an important relationship between these two parameters. By employing a more robust and dynamic system, and by assessing the first pass extraction of ^{64}Cu-BTSC complexes by administering a bolus of tracer, we demonstrate that under oxygenated conditions there is a relationship between the tissue retention of these tracers and their molecular weight or partition ratio, with R^2 values of 0.81 and 0.84 respectively (figures 5.22 and 5.23). We also observed a relationship between the molecular weight or partition ratio, and the hypoxic to normoxic tissue contrast ratio of hypoxia selective ^{64}Cu-BTSCs (figures 5.24 and 5.25), with R^2 values for these comparisons of 0.87 and 0.81 (5 min hypoxia), and 0.79 and 0.78 (25 min hypoxia) respectively. This suggests that the relative lipophilicity of Cu-BTSC complexes also governs their hypoxic to normoxic tissue contrast. However for data that were obtained under hypoxic conditions, when we plotted values for tissue retention or hypoxic to normoxic contrast against either molecular weight or partition ratio, we did not observe a relationship between any of these parameters. Thus while lipophilicity may govern the accumulation of Cu-BTSC during normoxia, lipophilicity is

certainly not the mechanism for hypoxia selectivity. Rather complexes with relatively high partition ratios may interact more with the cell membrane, this would have the effect of slowing their rate of elution from cells, or possibly lead to irreversible trapping within the membrane. Thus, as the relative lipophilicity of the complexes increase they take longer to clear from normoxic tissue, which in turn decreases the hypoxic to normoxic tissue contrast. This has previously been suggested by Minkel *et al* [173], but we are the first to demonstrate it experimentally.

Another important observation that we made, was that during hypoxia the tissue retention of the all Cu-BTSC complexes increased from 5 to 25 min hypoxia. Of the hypoxia selective complexes only ^{64}Cu-DTSM did not display a significant difference between 5 and 25 min hypoxia, although the average retention at 25 min was 8.8 % higher than at 5 min. This indicates that these tracers should not be considered as 'all or nothing' markers of hypoxia, but that they may demonstrate graded hypoxia selectivity. When we consider the intracellular retention mechanisms proposed for these tracers [167, 174, 241, 292], a number of observations that we have made during this study, may add extra insight into intracellular fate of Cu-BTSC complexes. It has been suggested that Cu-PTSM dissociates rapidly once taken up by cells, irrespective of their oxygenation status [174]. However we have shown that retention of Cu-PTSM and similarly Cu-PTSE is oxygen sensitive, although these tracers are poorly hypoxia selective. If we consider that after a bolus of tracer is administered, an equal amount of tracer should enter the cells of the heart, regardless of whether it is receiving oxygenated or hypoxic buffer. Once Cu-PTSM or Cu-PTSE have traversed the cell membrane and been reduced, if they rapidly

dissociate to form free ligand and Cu(I), one would expect their retention during normoxia and hypoxia to be equal. However if these complexes do not rapidly dissociate they could be reoxidised back to the Cu(II) form, and be free to traverse the cell membrane and elute from the heart. This would explain why the retention of Cu-PTSM increased during hypoxia. The retention mechanism for Cu-PTSM is therefore likely to be that same as that of Cu-ATSM (figure 1.15). The only difference being that because Cu-PTSM has a lower redox potential (relative to hypoxia selective Cu-BTSCs), it is more likely to dissociate or have the copper moiety removed by biomolecules before it can be reoxidised, which would increase its retention compared to more hypoxia selective Cu-BTSCs. This is further supported by the slight increase in tracer retention at 5 and 25 min hypoxia when the buffer pO_2 was ~20- 30 mmHg lower. Furthermore, similar but more conclusive observations were made for the hypoxia selective complexes. This agrees with the observation made by Maurer *et al*, who proposed that in cells Cu-BTSC are reduced to the Cu(I) form regardless of the level of oxygenation, but in the presence of oxygen they can be oxidised back to the Cu(II) form [293]. This suggests that all ^{64}Cu-BTSC complexes share the same retention mechanism, and while not all of them are hypoxia specific, they are all oxygen sensitive.

It was originally thought that Cu-BTSCs enter cells by passively diffusing across the cell membrane [164-165, 174]. However the results of a recent study by Price *et al*, have suggested that Cu-BTSC complexes may also be transported into cells by membrane protein mediated mechanisms [294], as well as by passive diffusion. Price and co-workers demonstrated that the accumulation of Cu-GTS and Cu-ATSM in M17 (human

neuronal) and U87MG (glial) cells was dependent up on temperature and the availability of ATP, as well as the presence of membrane proteins. Tracer accumulation was not saturated by increasing concentration, which supports the hypothesis that passive diffusion also takes place. With respect to our study, the relationship that we observed between lipophilicity/ molecular weight and tracer retention, further suggests that passive diffusion is the predominate method by which these tracers enter cells. The Price group also suggested that the efflux of Cu from cells is facilitated by ATP dependent transport proteins. Furthermore Cu efflux also decreased when protein synthesis was inhibited. While we did not investigate Cu efflux directly during our experiments our results support this proposal, as we did not observe a relationship between lipophilicity/ molecular weight and percentage tracer retention during hypoxia.

Chapter 6.

Summary and Further Work

6.1 Summary of Major Findings

The aim of this thesis was to build upon the structure activity work of Dearling, Lewis, Blower, McQuade *et al*, focusing on whether any of the novel Cu-BTSC complexes that they synthesised were suitable for cardiac imaging, or more specifically showed greater promise than Cu-ATSM. We initially set out to develop an ARVM based high-throughput screen for characterising ^{64}Cu-BTSC complexes. After designing and calibrating a novel cell incubation chamber, and determining the optimum ARVM culture conditions, we applied our relatively large scale system. In doing so we successfully demonstrated for the first time, the hypoxia selective accumulation of ^{64}Cu-ATSM in ARVM. Unfortunately, for a number of reasons this system had a large inherent variability, i) the number of cells that is obtained when isolating ARVM can vary considerably between isolations, and is difficult to control for, ii) the accumulation of ^{64}Cu-ATSM within cells was also extremely variable. These factors gave rise to a poor contrast between ^{64}Cu-ATSM uptake in hypoxic and normoxic cells. While there are a number of parameters that may have improved this contrast, for example increasing the concentration of radiotracer or incubating the cells for longer, our data suggested that it would not be possible to downscale the system to allow us to screen multiple tracers or replicates simultaneously. Furthermore, the ARVM isolation and purification process was relatively long and costly compared to using isolated perfused hearts, which can be excised rapidly and have to be used immediately. We therefore concluded that the cell based screen would not be suitable for characterising the myocardial tissue accumulation of our library of ^{64}Cu-BTSC complexes. In light of this we decided to focus our efforts on developing a more dynamic system that could model the single pass extraction of

these tracers. For this purpose we chose to employ isolated perfused hearts in combination with γ-radiation detectors.

The "triple detector array" proved to be a considerably more reliable, accurate, and reproducible method for characterising the hypoxia specificity and myocardial accumulation of our complexes. Although the isolated perfused heart is an *ex vivo* preparation, by using the bolus method of tracer delivery we were able, to a certain degree, to mimic the first pass extraction of radiotracers as would occur *in vivo*. For our initial experiments we used a single γ-detector from a radio-HPLC with promising results, similar to those obtained for ^{62}Cu-ATSM by Fujibayashi *et al* [174], and for ^{67}Cu-PTSM and ^{18}FMISO by Shelton *et al* [75-76]. This preliminary work suggested that the isolated perfused heart-γ-detector method would be a superior means of assessing our tracers. We therefore designed and commissioned the purpose built "triple detector array". After carefully calibrating and optimising this system, as well as establishing exclusion criteria for cardiac function we began to screen and characterise our library of tracers.

The results from our experiments using isolated hearts have provided further insight into the structure activity relationships within the class of Cu-BTSC complexes, and demonstrated how the physicochemical properties of these tracers affect their accumulation in cardiac tissue. The first major finding from our work is that all of the ^{64}Cu-BTSCs were able to readily accumulate within cardiac tissue, and that the retention profiles of these tracers are dependent upon their redox potential, as well as the

oxygenation status of the heart. We have also shown that Cu-PTSE like Cu-PTSM is not hypoxia selective. While Fujibayashi *et al* and Dearling *et al* have previously suggested that complexes with only a single alkyl group on the di-imine backbone are less likely to be hypoxia selective, we have shown this without ambiguity. However as we observed that the percentage tissue retention of these tracers was inversely related to the level of oxygenation, our data also suggest that Cu-PTSM and Cu-PTSE display a degree of oxygen sensitivity. We also observed this for ^{64}Cu-BTSCs where the ligand was alkylated at both the R^1 and R^2 positions (strongly hypoxia selective). This may explain why Dearling *et al* observed some degree of hypoxia selectivity with Cu-PTSM, and mid-range selectivity for Cu-PTSE when they applied the HSI model [167]. Our data suggest that the mechanism of retention of Cu-PTSM that was proposed by Fujibayashi *et al* [174], whereby Cu-PTSM enters the cell and is reduced and trapped regardless of the oxygenation status, may not accurately portray the intracellular fate of this complex. Our observations that Cu(I)-PTSM (and Cu(I)-PTSE) retention does increase under hypoxia, suggest that once reduced these tracers can also undergo reoxidation back to the uncharged Cu(II) species, which is then free to elute from the cell. It is therefore more likely that the trapping mechanism proposed for Cu-ATSM by Dearling *et al* and Maurer *et al*, better reflects the true mechanism by which all Cu-BTSC complexes are retained within cells. They proposed that the retention of Cu-ATSM may not just be dependent upon the rate at which the complex is reduced, but that the trapping of the copper moiety is dependent upon an interplay between the rate at which the complex dissociates, and the rate at which reoxidation of the Cu(I)-complex occurs [167]. Our data do not entirely agree with Dearling *et al*, as they also suggested that because of its relatively high redox

potential Cu-PTSM is unlikely to undergo reoxidation, and will be irreversibly trapped within the cell .

In this thesis we have provided further evidence in support of observations that were made by Dearling *et al* [162-163, 167] and McQuade *et al* [208], that Cu-BTSC complexes which posses alkyl groups at both the R^1 and R^2 positions invariably display hypoxia selectivity. Furthermore the retention of these compounds in hypoxic cardiac tissue was very similar (42- 59 % ID after 5 min, and 64- 78 %ID after 25 min hypoxia), which is not surprising considering that they have similar redox potentials of between (-0.58- -0.59 V) [167]. Dearling's data combined without ours suggest that it will not be possible to further refine the redox potential, and therefore hypoxia selectivity of Cu-BTSCs, beyond the change that occurs between Cu-PTSM and Cu-ATSM, by merely altering the alkylation pattern at the R^1 and R^2 positions. Our data from well oxygenated hearts suggest that the relative lipophilicity of these complexes may also be an important factor to consider, when developing and assessing this class of tracers. The importance of lipophilicity to the biological activity of Cu-BTSC complexes is widely reported [162, 167, 171, 173], but we have demonstrated for the first time that there is a relationship between their first pass extraction and relative lipophilicity. We have also shown that the least lipophilic and lowest molecular weight complexes Cu-ATS and Cu-CTS, demonstrate the lowest uptake in normoxic tissue but greater accumulation in hypoxic tissue compared Cu-ATSM, which led to them displaying the highest degree of hypoxic to normoxic tissue contrast. We have therefore identified from a library of Cu-BTSC complexes, two tracers that warrant further investigation not only as imaging radiotracers

for cardiac hypoxia but also in oncology, as we believe these tracers have the potential to supersede Cu-ATSM, because of the superior pharmacokinetics that they have demonstrated in our *ex vivo* model. However we should note that we are aware that Cu-ATS does not cross the blood brain barrier [282], while biodistribution of Cu-CTS has yet to be assessed.

6.2 Further Work

In our recent review we described what needs to be done in order to develop and further validate the Cu-BTSC complexes as hypoxia tracers [106], these were as follows:

- Screening of the current Cu-BTSC library and new Cu-BTSC-like complexes
- Assessing the role of oxygen
- Assessing the effect of acidosis
- Assessing the effect of perfusion
- Identifying the intracellular bioreductants
- Determining the fate of radio-copper once removed from the ligand

Addressing these issues now represents the core of the research in our group. The research that is described in this thesis was just the first step towards characterising our library of Cu-BTSC complexes. In the "triple detector array" we have established a model system, which is capable of assessing the first pass extraction and hypoxia specificity of candidate hypoxia tracers. We then used this system to identify novel tracers that could potentially display more desirable pharmacokinetics, and better hypoxic to normoxic tissue contrast *in vivo*, compared to the lead complex Cu-ATSM.

With respect to work which directly follows on from the research that has been presented in this thesis, our suggestions for future work are as follows:

By determining the redox potentials of the Cu-BTSC complexes that we also assessed during our study, Dearling *et al* demonstrated that it may not be possible to refine the redox potential of Cu-BTSC complexes, beyond the change that occurs between Cu-PTSM and Cu-ATSM. With the exception of the more lipophilic complexes Cu-CTSM and Cu-DTSM during early hypoxia, our data from isolated hearts subjected to hypoxia support this proposal, because we did not observe a significantly different amount of retention for any of hypoxia selective the tracers relative to Cu-ATSM. Our next series of experiments should therefore address the effect of oxygenation, to determine whether any of the complexes screened in this study are retained at more pathophysiologically relevant pO_2 levels. This would involve using a gas mixer to carefully moderate the level of oxygen in the coronary perfusate. The pO_2 would then be gradually titrated down, and at each level of oxygenation an injection of tracer would be administered. The percentage retention of each tracer at each level of oxygen should then be compared to ascertain if there are any differences or improvements over that of Cu-ATSM.

In addition to screening the complexes at pathophysiologically relevant oxygen levels, it is also necessary to compare the percentage tissue retention of these tracers with the level of energy substrates, such as ATP and creatine kinase, within the heart using ^{31}P NMR spectroscopy. This would allow us to establish the biological relevance of the

accumulation of any given tracer within the heart, and perhaps provide greater diagnostic or prognostic insight clinically.

We designed the "triple detector array" specifically so that it was able to acquire an input and output function as well as measuring the radioactivity within the heart, with a view to allowing us to perform pharmacokinetic compartmental modelling on the radiotracer time-activity curves. We should therefore focus on developing these pharmacokinetic models incorporating these input and output functions, to ascertain whether they can provide further evidence of structure activity relationships that we have indentified during this present study. Pharmacokinetic modelling in this manner may also provide further information on the rate of uptake, bioreduction, and dissociation of Cu-BTSC complexes, as well as the fate of the ^{64}Cu-moiety.

The work described in this thesis has been solely based on *in vitro*, and *ex vivo* models, we should therefore aim to employ or develop suitable *in vivo* models of cardiac ischaemia. This would include performing biodistribution studies on all of the complexes, as well as using microPET imaging to asses their cardiac accumulation. This should be done using normal animals and also the wide variety of animal models of cardiovascular disease, which available to us within our own division and the adjacent Division of Cardiovascular Research at King's.

Finally we would hope that larger in-patient trials are conducted with Cu-ATSM or other candidate hypoxia tracers that we have identified. This would perhaps be in combination

with ^{99m}Tc-Sestamibi imaging as suggested in chapter 1. Such trials would be able to determine whether any member of this class of tracers is suitable for delineating myocardial hypoxia in its many guises in the clinical setting.

References

1. Mathers, C.D. and D. Loncar. *Projections of Global Mortalilty and Disease from 2002-2030*. 2007; Available from: http://medicine.plosjournals.org/perlserv/?request+get-document&doi=10.1371/journal.pmed.0030442.

2. Coetzee, A., P. Foex, D. Holland, A. Ryder, and L. Jones, Effect of hypoxia on the normal and ischemic myocardium. Crit Care Med, 1984. 12(12): p. 1027-31.

3. Nakamura, Y., M. Nagata, H. Mori, K. Sakurai, M. Takahashi, and S. Hattori, Different effects of acute ischemia and anoxia on the canine myocardium. Jpn Heart J, 1984. 25(5): p. 783-92.

4. Yatsu, F.M. and S.A. Moss, Brain lipid changes following hypoxia. Stroke, 1971. 2(6): p. 587-93.

5. Meyer, J.A., Potentiation of solid-tumor chemotherapy by metabolic alteration. Ann Surg, 1974. 179(1): p. 88-93.

6. Doust, J.W., Differential tissue and organ anoxia in disease: the measurement of periarticular oxygen saturation levels in patients with arthritis. Ann Rheum Dis, 1951. 10(3): p. 269-76.

7. Capla, J.M., R.H. Grogan, M.J. Callaghan, R.D. Galiano, O.M. Tepper, D.J. Ceradini, and G.C. Gurtner, Diabetes impairs endothelial progenitor cell-mediated blood vessel formation in response to hypoxia. Plast Reconstr Surg, 2007. 119(1): p. 59-70.

8. Young, T., J. Skatrud, and P.E. Peppard, Risk factors for obstructive sleep apnea in adults. JAMA, 2004. 291(16): p. 2013-6.

9. Airley, R., J. Monaghan, and J. Stratford, Hypoxia and disease: opportunities for novel diagnostic and therapeutic prodrug strategies. The Pharmaceutical Journal, 2000. 264: p. 666-673.

10. Raichle, M.E., The pathophysiology of brain ischemia. Ann Neurol, 1983. 13(1): p. 2-10.

11. Katz, A.M., *Physiology of the Heart*. 4th ed. 2005, Philadelphia: Lippincott Williams and Walker.

12. Sabbah, H.N., V.G. Sharov, and S. Goldstein, Cell death, tissue hypoxia and the progression of heart failure. Heart Fail Rev, 2000. 5(2): p. 131-8.

13. Crossman, D.C., The pathophysiology of myocardial ischaemia. Heart, 2004. 90(5): p. 576-80.

14. Reimer, K.A. and R.B. Jennings, The "wavefront phenomenon" of myocardial ischemic cell death. II. Transmural progression of necrosis within the framework of ischemic bed size (myocardium at risk) and collateral flow. Lab Invest, 1979. 40(6): p. 633-44.

15. Jennings, R.B. and K.A. Reimer, Factors involved in salvaging ischemic myocardium: effect of reperfusion of arterial blood. Circulation, 1983. 68(2 Pt 2): p. I25-36.

16. Heusch, G., Hibernating myocardium. Physiol Rev, 1998. 78(4): p. 1055-85.

17. Shivalkar, B., A. Maes, M. Borgers, J. Ausma, I. Scheys, J. Nuyts, L. Mortelmans, and W. Flameng, Only hibernating myocardium invariably shows early recovery after coronary revascularization. Circulation, 1996. 94(3): p. 308-15.

18. Braunwald, E. and J.D. Rutherford, Reversible ischemic left ventricular dysfunction: evidence for the "hibernating myocardium". J Am Coll Cardiol, 1986. 8(6): p. 1467-70.

19. Vanoverschelde, J.L., C. Depre, B.L. Gerber, M. Borgers, W. Wijns, A. Robert, R. Dion, and J.A. Melin, Time course of functional recovery after coronary artery bypass graft surgery in patients with chronic left ventricular ischemic dysfunction. Am J Cardiol, 2000. 85(12): p. 1432-9.

20. Rahimtoola, S.H., A perspective on the three large multicenter randomized clinical trials of coronary bypass surgery for chronic stable angina. Circulation, 1985. 72(6 Pt 2): p. V123-35.

21. Ross, J., Jr., Myocardial perfusion-contraction matching. Implications for coronary heart disease and hibernation. Circulation, 1991. 83(3): p. 1076-83.

22. Braunwald, E. and R.A. Kloner, The stunned myocardium: prolonged, postischemic ventricular dysfunction. Circulation, 1982. 66(6): p. 1146-9.

23. Rahimtoola, S.H., The hibernating myocardium. Am Heart J, 1989. 117(1): p. 211-21.

24. Bolli, R., W.X. Zhu, C.J. Hartley, L.H. Michael, J.E. Repine, M.L. Hess, R.C. Kukreja, and R. Roberts, Attenuation of dysfunction in the postischemic 'stunned' myocardium by dimethylthiourea. Circulation, 1987. 76(2): p. 458-68.

25. Camici, P.G. and F. Crea, Coronary microvascular dysfunction. N Engl J Med, 2007. 356(8): p. 830-40.

26. Kemp, H.G., R.A. Kronmal, R.E. Vlietstra, and R.L. Frye, Seven year survival of patients with normal or near normal coronary arteriograms: a CASS registry study. J Am Coll Cardiol, 1986. 7(3): p. 479-83.

27. Arthur, H.M., P. Campbell, P.J. Harvey, M. McGillion, P. Oh, E. Woodburn, and C. Hodgson, Women, cardiac syndrome X, and microvascular heart disease. Can J Cardiol, 2012. 28(2 Suppl): p. S42-9.

28. Arbogast, R. and M.G. Bourassa, Myocardial function during atrial pacing in patients with angina pectoris and normal coronary arteriograms. Comparison with patients having significant coronary artery disease. Am J Cardiol, 1973. 32(3): p. 257-63.

29. Kemp, H.G., Jr., Left ventricular function in patients with the anginal syndrome and normal coronary arteriograms. Am J Cardiol, 1973. 32(3): p. 375-6.

30. Iemitsu, M., T. Miyauchi, S. Maeda, S. Sakai, T. Kobayashi, N. Fujii, H. Miyazaki, M. Matsuda, and I. Yamaguchi, Physiological and pathological cardiac hypertrophy induce different molecular phenotypes in the rat. Am J Physiol Regul Integr Comp Physiol, 2001. 281(6): p. R2029-36.

31. Drazner, M.H., The progression of hypertensive heart disease. Circulation, 2011. 123(3): p. 327-34.

32. Brette, F. and C. Orchard, T-tubule function in mammalian cardiac myocytes. Circ Res, 2003. 92(11): p. 1182-92.

33. Lopaschuk, G.D., D.D. Belke, J. Gamble, T. Itoi, and B.O. Schonekess, Regulation of fatty acid oxidation in the mammalian heart in health and disease. Biochim Biophys Acta, 1994. 1213(3): p. 263-76.

34. Lopaschuk, G.D. and M. Saddik, The relative contribution of glucose and fatty acids to ATP production in hearts reperfused following ischemia. Mol Cell Biochem, 1992. 116(1-2): p. 111-6.

35. Randle, P.J., P.B. Garland, C.N. Hales, and E.A. Newsholme, The glucose fatty-acid cycle. Its role in insulin sensitivity and the metabolic disturbances of diabetes mellitus. Lancet, 1963. 1(7285): p. 785-9.

36. Stryer, L., *Biochemistry*. Fourth ed. 1995, New York: W. H. Freeman and Company. 1064.

37. Voet, D. and J. Voet, *Biochemistry*. Second ed. 1995, New York: John Wiley & Sons INC. 1360.

38. Stremmel, W., Fatty acid uptake by isolated rat heart myocytes represents a carrier-mediated transport process. J Clin Invest, 1988. 81(3): p. 844-52.

39. van der Vusse, G.J., M. van Bilsen, and J.F. Glatz, Cardiac fatty acid uptake and transport in health and disease. Cardiovasc Res, 2000. 45(2): p. 279-93.

40. Jennings, R.B., K.A. Reimer, and C. Steenbergen, Myocardial ischemia revisited. The osmolar load, membrane damage, and reperfusion. Journal of Molecular and Cellular Cardiology, 1986. 18(8): p. 769-780.

41. Jennings, R.B., K.A. Reimer, and C. Steenbergen, Effect of inhibition of the mitochondrial ATPase on net myocardial ATP in total ischemia. J Mol Cell Cardiol, 1991. 23(12): p. 1383-95.

42. Buja, L.M., Myocardial ischemia and reperfusion injury. Cardiovasc Pathol, 2005. 14(4): p. 170-5.

43. Gustafsson, A.B. and R.A. Gottlieb, Heart mitochondria: gates of life and death. Cardiovasc Res, 2008. 77(2): p. 334-43.

44. Lemasters, J.J., T.P. Theruvath, Z. Zhong, and A.L. Nieminen, Mitochondrial calcium and the permeability transition in cell death. Biochim Biophys Acta, 2009. 1787(11): p. 1395-401.

45. Halestrap, A.P. and P. Pasdois, The role of the mitochondrial permeability transition pore in heart disease. Biochim Biophys Acta, 2009. 1787(11): p. 1402-15.

46. Desagher, S. and J.C. Martinou, Mitochondria as the central control point of apoptosis. Trends Cell Biol, 2000. 10(9): p. 369-77.

47. Krohn, K.A., J.M. Link, and R.P. Mason, Molecular imaging of hypoxia. J Nucl Med, 2008. 49 Suppl 2: p. 129S-48S.

48. Lapi, S.E., T.F. Voller, and M.J. Welch, Positron Emission Tomography Imaging of Hypoxia. PET Clin, 2009. 4(1): p. 39-47.

49. Pijls, N.H.J. and J.-W.E.M. Sels, Functional Measurement of Coronary Stenosis. Journal of the American College of Cardiology, 2012. 59(12): p. 1045-1057.

50. Neishi, Y., T. Akasaka, Y. Koyama, M. Akiyama, N. Watanabe, N. Kamiyama, S. Kaji, Y. Saito, R. Suetsuna, and K. Yoshida, [Measurement of coronary flow reserve by pressure/temperature sensor guide wire-based thermodilution in experimental models]. J Cardiol, 2002. 40(6): p. 249-57.

51. Claessen, B.E., M. Bax, R. Delewi, M. Meuwissen, J.P. Henriques, and J.J. Piek, The Doppler flow wire in acute myocardial infarction. Heart, 2010. 96(8): p. 631-5.

52. Wipper, S., C. Detter, C. Lohrenz, and E.S. Debus, Intraoperative quality control in vascular surgery. J Cardiovasc Surg (Torino), 2012. 53(1 Suppl 1): p. 145-9.

53. Gu, Y., V.A. Bourke, J.G. Kim, A. Constantinescu, R.P. Mason, and H. Liu, Dynamic response of breast tumor oxygenation to hyperoxic respiratory challenge monitored with three oxygen-sensitive parameters. Appl Opt, 2003. 42(16): p. 2960-7.

54. Optronix, O. *Oxylite 2000 Instrument*. [cited 2009 22 January]; Available from: www.oxfordoptronix.com.

55. Zhao, D., A. Constantinescu, E.W. Hahn, and R.P. Mason, Tumor oxygen dynamics with respect to growth and respiratory challenge: investigation of the Dunning prostate R3327-HI tumor. Radiat Res, 2001. 156(5 Pt 1): p. 510-20.

56. Eastwood, J.D., M.H. Lev, and J.M. Provenzale, Perfusion CT with iodinated contrast material. AJR Am J Roentgenol, 2003. 180(1): p. 3-12.

57. Mather, A.N., T. Lockie, E. Nagel, M. Marber, D. Perera, S. Redwood, A. Radjenovic, A. Saha, J.P. Greenwood, and S. Plein, Appearance of microvascular obstruction on high resolution first-pass perfusion, early and late gadolinium enhancement CMR in patients with acute myocardial infarction. J Cardiovasc Magn Reson, 2009. 11: p. 33.

58. Schaefer, S., C.R. Malloy, J. Katz, R.W. Parkey, L.M. Buja, J.T. Willerson, and R.M. Peshock, Gadolinium-DTPA-enhanced nuclear magnetic resonance imaging of

reperfused myocardium: identification of the myocardial bed at risk. J Am Coll Cardiol, 1988. 12(4): p. 1064-72.

59. de Roos, A., A.C. van Rossum, E. van der Wall, S. Postema, J. Doornbos, N. Matheijssen, P.R. van Dijkman, F.C. Visser, and A.E. van Voorthuisen, Reperfused and nonreperfused myocardial infarction: diagnostic potential of Gd-DTPA--enhanced MR imaging. Radiology, 1989. 172(3): p. 717-20.

60. Platts, D.G. and J.F. Fraser, Contrast echocardiography in critical care: echoes of the future? A review of the role of microsphere contrast echocardiography. Crit Care Resusc, 2011. 13(1): p. 44-55.

61. Porter, T.R. and F. Xie, Myocardial perfusion imaging with contrast ultrasound. JACC Cardiovasc Imaging, 2010. 3(2): p. 176-87.

62. Neumann, G., J. Wagner, W. Pensky, R. Felix, A. Schaede, H. Simon, and C. Winkler, [Proceedings: The 201 thallium scintigram of the heart as an indicator for the distribution of vital myocardium]. Z Kardiol, 1975. Suppl 2: p. 41.

63. Sebening, H., H. Lichte, E. Sauer, L. Lutilsky, G. Hor, W. Delius, and A. Wirtzfeld, [Proceedings: Myocardial scintigraphy with 201 thallium]. Z Kardiol, 1975. Suppl 2: p. 42.

64. Gerundini, P. and L. Maffioli, Cationic complexes of technetium for myocardial imaging. J Nucl Med, 1989. 30(8): p. 1415-9.

65. Sinusas, A.J., G.A. Beller, and D.D. Watson, Cardiac imaging with technetium 99m-labeled isonitriles. J Thorac Imaging, 1990. 5(3): p. 20-30.

66. Phelps, M.E., E.J. Hoffman, R.E. Coleman, M.J. Welch, M.E. Raichle, E.S. Weiss, B.E. Sobel, and M.M. Ter-Pogossian, Tomographic images of blood pool and perfusion in brain and heart. J Nucl Med, 1976. 17(7): p. 603-12.

67. Shah, A., H.R. Schelbert, M. Schwaiger, E. Henze, H. Hansen, C. Selin, and S.-C. Huang, Measurement of regional myocardial blood flow with N-13 ammonia and positron-emission tomography in intact dogs. Journal of the American College of Cardiology, 1985. 5(1): p. 92-100.

68. Knabb, R.M., K.A. Fox, B.E. Sobel, and S.R. Bergmann, Characterization of the functional significance of subcritical coronary stenoses with H(2)15O and positron-emission tomography. Circulation, 1985. 71(6): p. 1271-8.

69. Higuchi, T., S.G. Nekolla, M.M. Huisman, S. Reder, T. Poethko, M. Yu, H.J. Wester, D.S. Casebier, S.P. Robinson, R.M. Botnar, *et al.*, A new 18F-labeled myocardial PET tracer: myocardial uptake after permanent and transient coronary occlusion in rats. J Nucl Med, 2008. 49(10): p. 1715-22.

70. Nekolla, S.G., S. Reder, A. Saraste, T. Higuchi, G. Dzewas, A. Preissel, M. Huisman, T. Poethko, T. Schuster, M. Yu, *et al.*, Evaluation of the novel myocardial perfusion positron-emission tomography tracer 18F-BMS-747158-02: comparison to 13N-

ammonia and validation with microspheres in a pig model. Circulation, 2009. 119(17): p. 2333-42.

71. Yalamanchili, P., E. Wexler, M. Hayes, M. Yu, J. Bozek, M. Kagan, H.S. Radeke, M. Azure, A. Purohit, D.S. Casebier, *et al.*, Mechanism of uptake and retention of F-18 BMS-747158-02 in cardiomyocytes: a novel PET myocardial imaging agent. J Nucl Cardiol, 2007. 14(6): p. 782-8.

72. Yu, M., M.T. Guaraldi, M. Mistry, M. Kagan, J.L. McDonald, K. Drew, H. Radeke, M. Azure, A. Purohit, D.S. Casebier, *et al.*, BMS-747158-02: a novel PET myocardial perfusion imaging agent. J Nucl Cardiol, 2007. 14(6): p. 789-98.

73. Green, M.A., A potential copper radiopharmaceutical for imaging the heart and brain: copper-labeled pyruvaldehyde bis(N4-methylthiosemicarbazone). Int J Rad Appl Instrum B, 1987. 14(1): p. 59-61.

74. Green, M.A., C.J. Mathias, M.J. Welch, A.H. McGuire, D. Perry, F. Fernandez-Rubio, J.S. Perlmutter, M.E. Raichle, and S.R. Bergmann, Copper-62-labeled pyruvaldehyde bis(N4-methylthiosemicarbazonato)copper(II): synthesis and evaluation as a positron emission tomography tracer for cerebral and myocardial perfusion. J Nucl Med, 1990. 31(12): p. 1989-96.

75. Shelton, M.E., M.A. Green, C.J. Mathias, M.J. Welch, and S.R. Bergmann, Kinetics of copper-PTSM in isolated hearts: a novel tracer for measuring blood flow with positron emission tomography. J Nucl Med, 1989. 30(11): p. 1843-7.

76. Shelton, M.E., M.A. Green, C.J. Mathias, M.J. Welch, and S.R. Bergmann, Assessment of regional myocardial and renal blood flow with copper-PTSM and positron emission tomography. Circulation, 1990. 82(3): p. 990-7.

77. Knapp, F.F., Jr., K.R. Ambrose, and M.M. Goodman, New radioiodinated methyl-branched fatty acids for cardiac studies. Eur J Nucl Med, 1986. 12 Suppl: p. S39-44.

78. Underwood, S.R., J.J. Bax, J.v. Dahl, M.Y. Henein, A.C. van Rossum, E.R. Schwarz, J.-L. Vanoverschelde, E.E.v.d. Wall, and W. Wijns, Imaging techniques for the assessment of myocardial hibernation: Report of a Study Group of the European Society of Cardiology. Eur Heart J, 2004. 25(10): p. 815-836.

79. Barrington, S.F., J. Chambers, W.A. Hallett, M.J. O'Doherty, J.C. Roxburgh, and T.O. Nunan, Comparison of sestamibi, thallium, echocardiography and PET for the detection of hibernating myocardium. European Journal of Nuclear Medicine and Molecular Imaging, 2004. 31(3): p. 355-361.

80. DeGrado, T.R., H.H. Coenen, and G. Stocklin, 14(R,S)-[18F]fluoro-6-thia-heptadecanoic acid (FTHA): evaluation in mouse of a new probe of myocardial utilization of long chain fatty acids. J Nucl Med, 1991. 32(10): p. 1888-96.

81. Ebert, A., H. Herzog, G.L. Stocklin, M.M. Henrich, T.R. DeGrado, H.H. Coenen, and L.E. Feinendegen, Kinetics of 14(R,S)-fluorine-18-fluoro-6-thia-heptadecanoic acid in normal human hearts at rest, during exercise and after dipyridamole injection. J Nucl Med, 1994. 35(1): p. 51-6.

82. Schulz, G., J. von Dahl, H.J. Kaiser, K.C. Koch, O. Sabri, L. Banneitz, U. Cremerius, and U. Buell, Imaging of beta-oxidation by static PET with 14(R,S)-[18F]-fluoro-6-thiaheptadecanoic acid (FTHA) in patients with advanced coronary heart disease: a comparison with 18FDG-PET and 99Tcm-MIBI SPET. Nucl Med Commun, 1996. 17(12): p. 1057-64.

83. Weiss, E.S., E.J. Hoffman, M.E. Phelps, M.J. Welch, P.D. Henry, M.M. Ter-Pogossian, and B.E. Sobel, External detection and visualization of myocardial ischemia with 11C-substrates in vitro and in vivo. Circ Res, 1976. 39(1): p. 24-32.

84. Goldstein, R.A., M.S. Klein, M.J. Welch, and B.E. Sobel, External assessment of myocardial metabolism with C-11 palmitate in vivo. J Nucl Med, 1980. 21(4): p. 342-8.

85. Weiss, E.S., S.A. Ahmed, M.J. Welch, J.R. Williamson, M.M. Ter-Pogossian, and B.E. Sobel, Quantification of infarction in cross sections of canine myocardium in vivo with positron emission transaxial tomography and 11C-palmitate. Circulation, 1977. 55(1): p. 66-73.

86. Buxton, D.B., M. Schwaiger, A. Nguyen, M.E. Phelps, and H.R. Schelbert, Radiolabeled acetate as a tracer of myocardial tricarboxylic acid cycle flux. Circ Res, 1988. 63(3): p. 628-34.

87. Maes, A.F., F. Van de Werf, L.V. Mesotten, P.B. Flamen, R.S. Kuzo, J.L. Nuyts, and L. Mortelmans, Early assessment of regional myocardial blood flow and metabolism in thrombolysis in myocardial infarction flow grade 3 reperfused myocardial infarction using carbon-11-acetate. J Am Coll Cardiol, 2001. 37(1): p. 30-6.

88. Tadamura, E., N. Tamaki, A. Matsumori, Y. Magata, Y. Yonekura, R. Nohara, S. Sasayama, M. Yoshibayashi, T. Kamiya, and J. Konishi, Myocardial metabolic changes in hypertrophic cardiomyopathy. J Nucl Med, 1996. 37(4): p. 572-7.

89. Egred, M., G.D. Waiter, A. Al-Mohammad, S.I. Semple, T.W. Redpath, and S. Walton, Blood oxygen level dependent (BOLD) MRI: A novel technique for the detection of myocardial ischemia. Eur J Intern Med, 2006. 17(8): p. 551-5.

90. Egred, M., G.D. Waiter, T.W. Redpath, S.K. Semple, A. Al-Mohammad, and S. Walton, Blood oxygen level-dependent (BOLD) MRI: A novel technique for the assessment of myocardial ischemia as identified by nuclear imaging SPECT. Eur J Intern Med, 2007. 18(8): p. 581-6.

91. Carlier, P.G., D. Bertoldi, C. Baligand, C. Wary, and Y. Fromes, Muscle blood flow and oxygenation measured by NMR imaging and spectroscopy. NMR Biomed, 2006. 19(7): p. 954-67.

92. Southworth, R. and P.B. Garlick, Dobutamine responsiveness, PET mismatch, and lack of necrosis in low-flow ischemia: is this hibernation in the isolated rat heart? Am J Physiol Heart Circ Physiol, 2003. 285(1): p. H316-24.

93. Meyer, M.D.C. and M.D.M. Schwaiger, Myocardial Blood Flow and Glucose Metabolism in Diabetes Mellitus. The American Journal of Cardiology, 1997. 80(3, Supplement 1): p. 94A-101A.

94. Vitale, G.D., R.A. deKemp, T.D. Ruddy, K. Williams, and R.S.B. Beanlands, Myocardial Glucose Utilization and Optimization of 18F-FDG PET Imaging in Patients with Non–Insulin-Dependent Diabetes Mellitus, Coronary Artery Disease, and Left Ventricular Dysfunction. Journal of Nuclear Medicine, 2001. 42(12): p. 1730-1736.

95. Kim, J.G., D. Zhao, Y. Song, A. Constantinescu, R.P. Mason, and H. Liu, Interplay of tumor vascular oxygenation and tumor pO2 observed using near-infrared spectroscopy, an oxygen needle electrode, and 19F MR pO2 mapping. J Biomed Opt, 2003. 8(1): p. 53-62.

96. Raichle, M.E., Behind the scenes of functional brain imaging: a historical and physiological perspective. Proc Natl Acad Sci U S A, 1998. 95(3): p. 765-72.

97. Tjandra, T., J.C. Brooks, P. Figueiredo, R. Wise, P.M. Matthews, and I. Tracey, Quantitative assessment of the reproducibility of functional activation measured with BOLD and MR perfusion imaging: implications for clinical trial design. Neuroimage, 2005. 27(2): p. 393-401.

98. Carlier, P.G., D. Bertoldi, C. Baligand, C. Wary, and Y. Fromes, Muscle blood flow and oxygenation measured by NMR imaging and spectroscopy. NMR in Biomedicine, 2006. 19(7): p. 954-967.

99. Kuhl, D.E. and R.Q. Edwards, CYLINDRICAL AND SECTION RADIOISOTOPE SCANNING OF THE LIVER AND BRAIN. Radiology, 1964. 83: p. 926-36.

100. Jaszczak, R.J., L.T. Chang, N.A. Stein, and F.E. Moore, Whole-body single-photon emission computed tomography using dual, large-field-of-view scintillation cameras. Phys Med Biol, 1979. 24(6): p. 1123-43.

101. Ter-Pogossian, M.M., M.E. Phelps, E.J. Hoffman, and N.A. Mullani, A positron-emission transaxial tomograph for nuclear imaging (PETT). Radiology, 1975. 114(1): p. 89-98.

102. NHS. Available from: http://www.nhspetctsouth.com/clinicians/about-this-service.

103. Wikipedia. Available from: http://www.wikipedia.org/.

104. Strauss, H.W., A. Nunn, and K. Linder, Nitroimidazoles for imaging hypoxic myocardium. J Nucl Cardiol, 1995. 2(5): p. 437-45.

105. Nunn, A., K. Linder, and H.W. Strauss, Nitroimidazoles and imaging hypoxia. Eur J Nucl Med, 1995. 22(3): p. 265-80.

106. Handley, M.G., R.A. Medina, E. Nagel, P.J. Blower, and R. Southworth, PET imaging of cardiac hypoxia: opportunities and challenges. J Mol Cell Cardiol, 2011. 51(5): p. 640-50.

107. Nakamura, S., Structure of Azomycin, a new antibiotic. Pharm Bull, 1955. 3(5): p. 379-83.

108. Adams, G.E., I. Ahmed, E.D. Clarke, P. O'Neill, J. Parrick, I.J. Stratford, R.G. Wallace, P. Wardman, and M.E. Watts, Structure-activity relationships in the development of hypoxic cell radiosensitizers. III. Effects of basic substituents in nitroimidazole sidechains. Int J Radiat Biol Relat Stud Phys Chem Med, 1980. 38(6): p. 613-26.

109. Adams, G.E., E.D. Clarke, I.R. Flockhart, R.S. Jacobs, D.S. Sehmi, I.J. Stratford, P. Wardman, M.E. Watts, J. Parrick, R.G. Wallace, *et al.*, Structure-activity relationships in the development of hypoxic cell radiosensitizers. I. Sensitization efficiency. Int J Radiat Biol Relat Stud Phys Chem Med, 1979. 35(2): p. 133-50.

110. Adams, G.E., E.D. Clarke, P. Gray, R.S. Jacobs, I.J. Stratford, P. Wardman, M.E. Watts, J. Parrick, R.G. Wallace, and C.E. Smithen, Structure-activity relationships in the development of hypoxic cell radiosensitizers. II. Cytotoxicity and therapeutic ratio. Int J Radiat Biol Relat Stud Phys Chem Med, 1979. 35(2): p. 151-60.

111. Shelton, M.E., C.S. Dence, D.-R. Hwang, P. Herrero, M.J. Welch, and S.R. Bergmann, In vivo delineation of myocardial hypoxia during coronary occlusion using fluorine-18 fluoromisonidazole and positron emission tomography: A potential approach for identification of jeopardized myocardium. Journal of the American College of Cardiology, 1990. 16(2): p. 477-485.

112. Martin, G.V., M.D. Cerqueira, J.H. Caldwell, J.S. Rasey, L. Embree, and K.A. Krohn, Fluoromisonidazole. A metabolic marker of myocyte hypoxia. Circ Res, 1990. 67(1): p. 240-4.

113. Kaneta, T., Y. Takai, Y. Kagaya, Y. Yamane, H. Wada, M. Yuki, R. Iwata, M. Tsujitani, S. Takahashi, and S. Yamada, Imaging of ischemic but viable myocardium using a new 18F-labeled 2-nitroimidazole analog, 18F-FRP170. J Nucl Med, 2002. 43(1): p. 109-16.

114. Jette, D.C., L.I. Wiebe, and J.D. Chapman, Synthesis and in vivo studies of the radiosensitizer 4-[82Br]bromomisonidazole. Int J Nucl Med Biol, 1983. 10(4): p. 205-10.

115. Kusuoka, H., K. Hashimoto, K. Fukuchi, and T. Nishimura, Kinetics of a putative hypoxic tissue marker, technetium-99m-nitroimidazole (BMS181321), in normoxic, hypoxic, ischemic and stunned myocardium. J Nucl Med, 1994. 35(8): p. 1371-6.

116. Okada, R.D., K.N. Nguyen, H.W. Strauss, and G. Johnson, 3rd, Effects of low flow and hypoxia on myocardial retention of technetium-99m BMS181321. Eur J Nucl Med, 1996. 23(4): p. 443-7.

117. Dobrucki, L.W., D.F. Meoli, J. Hu, M.M. Sadeghi, and A.J. Sinusas, Regional hypoxia correlates with the uptake of a radiolabeled targeted marker of angiogenesis in rat model of myocardial hypertrophy and ischemic injury. J Physiol Pharmacol, 2009. 60 Suppl 4: p. 117-23.

118. Parliament, M.B., J.D. Chapman, R.C. Urtasun, A.J. McEwan, L. Golberg, J.R. Mercer, R.H. Mannan, and L.I. Wiebe, Non-invasive assessment of human tumour hypoxia with 123I-iodoazomycin arabinoside: preliminary report of a clinical study. Br J Cancer, 1992. 65(1): p. 90-5.

119. Biskupiak, J.E., J.R. Grierson, J.S. Rasey, G.V. Martin, and K.A. Krohn, Synthesis of an (iodovinyl)misonidazole derivative for hypoxia imaging. J Med Chem, 1991. 34(7): p. 2165-8.

120. Martin, G.V., J.E. Biskupiak, J.H. Caldwell, J.S. Rasey, and K.A. Krohn, Characterization of iodovinylmisonidazole as a marker for myocardial hypoxia. J Nucl Med, 1993. 34(6): p. 918-24.

121. Strauss, H.W., A. Nunn, and K. Linder, Nitroimidazoles for imaging hypoxic myocardium. Journal of Nuclear Cardiology. 2(5): p. 437-445.

122. Whitmore, G.F. and A.J. Varghese, The biological properties of reduced nitroheterocyclics and possible underlying biochemical mechanisms. Biochemical Pharmacology, 1986. 35(1): p. 97-103.

123. Kedderis, G.L. and G.T. Miwa, The metabolic activation of nitroheterocyclic therapeutic agents. Drug Metabolism Reviews, 1988. 19(1): p. 33-62.

124. Jerabek, P.A., T.B. Patrick, M.R. Kilbourn, D.D. Dischino, and M.J. Welch, Synthesis and biodistribution of 18F-labeled fluoronitroimidazoles: potential in vivo markers of hypoxic tissue. Int J Rad Appl Instrum A, 1986. 37(7): p. 599-605.

125. Grunbaum, Z., S.J. Freauff, K.A. Krohn, D.S. Wilbur, S. Magee, and J.S. Rasey, Synthesis and characterization of congeners of misonidazole for imaging hypoxia. J Nucl Med, 1987. 28(1): p. 68-75.

126. Mathias, C.J., M.J. Welch, M.R. Kilbourn, P.A. Jerabek, T.B. Patrick, M.E. Raichle, K.A. Krohn, J.S. Rasey, and D.W. Shaw, Radiolabeled hypoxic cell sensitizers: tracers for assessment of ischemia. Life Sci, 1987. 41(2): p. 199-206.

127. Shelton, M.E., C.S. Dence, D.R. Hwang, M.J. Welch, and S.R. Bergmann, Myocardial kinetics of fluorine-18 misonidazole: a marker of hypoxic myocardium. J Nucl Med, 1989. 30(3): p. 351-8.

128. Martin, G.V., J.H. Caldwell, J.S. Rasey, Z. Grunbaum, M. Cerqueira, and K.A. Krohn, Enhanced binding of the hypoxic cell marker [3H]fluoromisonidazole in ischemic myocardium. J Nucl Med, 1989. 30(2): p. 194-201.

129. Shelton, M.E., C.S. Dence, D.R. Hwang, P. Herrero, M.J. Welch, and S.R. Bergmann, In vivo delineation of myocardial hypoxia during coronary occlusion using fluorine-18 fluoromisonidazole and positron emission tomography: a potential approach for identification of jeopardized myocardium. J Am Coll Cardiol, 1990. 16(2): p. 477-85.

130. Martin, G.V., J.H. Caldwell, M.M. Graham, J.R. Grierson, K. Kroll, M.J. Cowan, T.K. Lewellen, J.S. Rasey, J.J. Casciari, and K.A. Krohn, Noninvasive detection of hypoxic myocardium using fluorine-18-fluoromisonidazole and positron emission tomography. J Nucl Med, 1992. 33(12): p. 2202-8.

131. Linder, K.E., Y.W. Chan, J.E. Cyr, M.F. Malley, D.P. Nowotnik, and A.D. Nunn, TcO(PnA.O-1-(2-nitroimidazole)) [BMS-181321], a new technetium-containing

nitroimidazole complex for imaging hypoxia: synthesis, characterization, and xanthine oxidase-catalyzed reduction. J Med Chem, 1994. 37(1): p. 9-17.

132. Rumsey, W.L., J.E. Cyr, N. Raju, and R.K. Narra, A Novel [99m]Technetium-Labeled Nitroheterocycle Capable of Identification of Hypoxia in Heart. Biochemical and Biophysical Research Communications, 1993. 193(3): p. 1239-1246.

133. Rumsey, W.L., B. Patel, and K.E. Linder, Effect of graded hypoxia on retention of technetium-99m-nitroheterocycle in perfused rat heart. J Nucl Med, 1995. 36(4): p. 632-6.

134. Ng, C.K., A.J. Sinusas, B.L. Zaret, and R. Soufer, Kinetic analysis of technetium-99m-labeled nitroimidazole (BMS-181321) as a tracer of myocardial hypoxia. Circulation, 1995. 92(5): p. 1261-8.

135. Rumsey, W.L., B. Kuczynski, B. Patel, A. Bauer, R.K. Narra, S.M. Eaton, A.D. Nunn, and H.W. Strauss, SPECT imaging of ischemic myocardium using a technetium-99m-nitroimidazole ligand. J Nucl Med, 1995. 36(8): p. 1445-50.

136. Shi, C.Q., A.J. Sinusas, D.P. Dione, M.J. Singer, L.H. Young, E.N. Heller, B.D. Rinker, F.J. Wackers, and B.L. Zaret, Technetium-99m-nitroimidazole (BMS181321): a positive imaging agent for detecting myocardial ischemia. J Nucl Med, 1995. 36(6): p. 1078-86.

137. Biskupiak, J.E., J.R. Grierson, J.S. Rasey, G.V. Martin, and K.A. Krohn, Synthesis of an (iodovinyl)misonidazole derivative for hypoxia imaging. Journal of Medicinal Chemistry, 1991. 34(7): p. 2165-2168.

138. Ramalingam, K., N. Raju, P. Nanjappan, K.E. Linder, J. Pirro, W. Zeng, W. Rumsey, D.P. Nowotnik, and A.D. Nunn, The synthesis and in vitro evaluation of a 99mtechnetium-nitroimidazole complex based on a bis(amine-phenol) ligand: comparison to BMS-181321. J Med Chem, 1994. 37(24): p. 4155-63.

139. Melo, T., J. Duncan, J.R. Ballinger, and A.M. Rauth, BRU59-21, a second-generation 99mTc-labeled 2-nitroimidazole for imaging hypoxia in tumors. J Nucl Med, 2000. 41(1): p. 169-76.

140. Johnson, L.L., L. Schofield, P. Mastrofrancesco, T. Donahay, and L. Nott, Technetium-99m-nitroimadazole uptake in a swine model of demand ischemia. J Nucl Med, 1998. 39(8): p. 1468-75.

141. Johnson, L.L., L. Schofield, T. Donahay, and P. Mastrofrancesco, Myocardial uptake of a (99m)Tc-nitroheterocycle in a swine model of occlusion and reperfusion. J Nucl Med, 2000. 41(7): p. 1237-43.

142. Hoffend, J., G. Linke, A. Mohammed, C.P. Tiefenbacher, M. Eisenhut, and U. Haberkorn, 99mTcO(BAT-NI), a novel nitroimidazole tracer: in vivo uptake studies in ischaemic myocardium. Eur J Nucl Med Mol Imaging, 2003. 30(4): p. 494-501.

143. Sasai, K., Y. Shibamoto, M. Takahashi, M. Abe, J. Wang, L. Zhou, S. Nishimoto, and T. Kagiya, A new, potent 2-nitroimidazole nucleoside hypoxic cell radiosensitizer, RP170. Jpn J Cancer Res, 1989. 80(11): p. 1113-8.

144. Kaneta, T., Y. Takai, R. Iwata, T. Hakamatsuka, H. Yasuda, K. Nakayama, Y. Ishikawa, S. Watanuki, S. Furumoto, Y. Funaki, *et al.*, Initial evaluation of dynamic human imaging using 18F-FRP170 as a new PET tracer for imaging hypoxia. Ann Nucl Med, 2007. 21(2): p. 101-7.

145. Groshar, D., A.J. McEwan, M.B. Parliament, R.C. Urtasun, L.E. Golberg, M. Hoskinson, J.R. Mercer, R.H. Mannan, L.I. Wiebe, and J.D. Chapman, Imaging tumor hypoxia and tumor perfusion. J Nucl Med, 1993. 34(6): p. 885-8.

146. Piert, M., H.J. Machulla, M. Picchio, G. Reischl, S. Ziegler, P. Kumar, H.J. Wester, R. Beck, A.J. McEwan, L.I. Wiebe, *et al.*, Hypoxia-specific tumor imaging with 18F-fluoroazomycin arabinoside. J Nucl Med, 2005. 46(1): p. 106-13.

147. Koch, C.J., J.S. Scheuermann, C. Divgi, K.D. Judy, A.V. Kachur, R. Freifelder, J.S. Reddin, J. Karp, J.B. Stubbs, S.M. Hahn, *et al.*, Biodistribution and dosimetry of (18)F-EF5 in cancer patients with preliminary comparison of (18)F-EF5 uptake versus EF5 binding in human glioblastoma. Eur J Nucl Med Mol Imaging, 2010. 37(11): p. 2048-59.

148. Archer C, E., B, Kelly J, *Technetium labelled agents for imaging tissue hypoxia in vivo*. 1995: Padova, Italy: SGE Ditoriali.

149. Okada, R.D., G. Johnson, 3rd, K.N. Nguyen, B. Edwards, C.M. Archer, and J.D. Kelly, 99mTc-HL91. Effects of low flow and hypoxia on a new ischemia-avid myocardial imaging agent. Circulation, 1997. 95(7): p. 1892-9.

150. Okada, R.D., G. Johnson, K.N. Nguyen, L.R. Carlson, and D. Beju, HL-91-Technetium-99m: A new marker of viability in ischemic myocardium. Journal of Nuclear Cardiology. 6(3): p. 306-315.

151. Imahashi, K., K. Morishita, H. Kusuoka, Y. Yamamichi, S. Hasegawa, K. Hashimoto, Y. Shirakami, M. Kato-Azuma, and T. Nishimura, Kinetics of a putative hypoxic tracer, 99mTc-HL91, in normoxic, hypoxic, ischemic, and stunned myocardium. J Nucl Med, 2000. 41(6): p. 1102-7.

152. Okada, R.D., G. Johnson, 3rd, K.N. Nguyen, Z. Liu, B. Edwards, C.M. Archer, T.L. North, A.C. King, and J.D. Kelly, 99mTc-HL91: "hot spot" detection of ischemic myocardium in vivo by gamma camera imaging. Circulation, 1998. 97(25): p. 2557-66.

153. Fukuchi, K., H. Kusuoka, K. Yutani, S. Hasegawa, and T. Nishimura, Assessment of reperfused myocardium using a new ischaemia-avid imaging agent, technetium-99m HL91: comparison with myocardial glucose uptake. Eur J Nucl Med, 1998. 25(4): p. 361-6.

154. Wu, Y.W., C.M. Lee, Y.H. Huang, N.K. Chou, R.F. Yen, K.Y. Tzen, and P.J. Huang, 99mTc-HL91 is inferior to 201Tl in scintigraphic detection of chronic myocardial ischaemia. Nucl Med Commun, 2005. 26(12): p. 1119-23.

155. Yang, X.J., Y.M. He, Y.W. Wu, B. Zhang, J. Hui, T.B. Jiang, J.P. Song, Z.H. Liu, and W.P. Jiang, Hypoxia imaging of patients with acute myocardial infarction by using dual isotopes of 201Tl and 99mTc-HL91. Nucl Med Commun, 2008. 29(3): p. 230-8.

156. Liu, M., Z. Ma, X. Guo, J. Zhu, and J. Su, Technetium-99m-labelled HL91 and technetium-99m-labelled MIBI SPECT imaging for the detection of ischaemic viable myocardium: a preliminary study. Clin Physiol Funct Imaging, 2012. 32(1): p. 25-32.

157. French, F.A. and B.L. Freedlander, Carcinostatic action of polycarbonyl compounds and their derivatives. IV. Glyoxal bis (thiosemicarbazone) and derivatives. Cancer Res, 1958. 18(11): p. 1290-300.

158. French, F.A. and B.L. Freedlander, Carcinostatic action of polycarbonyl compounds and their derivatives. I. 3-Ethoxy-2-ketobutyraldehyde and related compounds. Cancer Res, 1958. 18(2): p. 172-5.

159. Sartorelli, A.C. and B.A. Booth, Inhibition of the growth of sarcoma 180 ascites cells by combinations of inhibitors of nucleic acid biosynthesis and the cupric chelate of kethoxal bis-(thiosemicarbazone). Cancer Res, 1967. 27(9): p. 1614-9.

160. Cappuccino, J.B., S. Brown, G. George, M. and Tarnowski, GS., The Effect of Copper and Other Metals Ions on the Antitumor Activty of Pyruvaldehyde Bis(thiosemicarbazone). Cancer Research, 1967. 27(1): p. 968- 973.

161. Petering, H.G., H.H. Buskirk, and J.A. Crim, The effect of dietary mineral supplements of the rat on the antitumor activity of 3-ethoxy-2-oxobutyraldehyde bis(thiosemicarbazone). Cancer Res, 1967. 27(6): p. 1115-21.

162. Dearling, J.L., J.S. Lewis, G.E. Mullen, M.T. Rae, J. Zweit, and P.J. Blower, Design of hypoxia-targeting radiopharmaceuticals: selective uptake of copper-64 complexes in hypoxic cells in vitro. Eur J Nucl Med, 1998. 25(7): p. 788-92.

163. Dearling, J.L.J., J.S. Lewis, D.W. McCarthy, M.J. Welch, and P.J. Blower, Redox-active metal complexes for imaging hypoxic tissues: structure-activity relationships in copper(II) bis(thiosemicarbazone) complexes. Chemical Communications, 1998(22): p. 2531-2532.

164. Fujibayashi, Y., K. Wada, H. Taniuchi, Y. Yonekura, J. Konishi, and A. Yokoyama, Mitochondria-selective reduction of 62Cu-pyruvaldehyde bis(N4-methylthiosemicarbazone) (62Cu-PTSM) in the murine brain; a novel radiopharmaceutical for brain positron emission tomography (PET) imaging. Biol Pharm Bull, 1993. 16(2): p. 146-9.

165. Taniuchi, H., Y. Fujibayashi, H. Okazawa, Y. Yonekura, J. Konishi, and A. Yokoyama, Cu-pyruvaldehyde-bis(N4-methylthiosemicarbazone) (Cu-PTSM), a metal complex with selective NADH-dependent reduction by complex I in brain mitochondria: a potential radiopharmaceutical for mitochondria-functional imaging with positron emission tomography (PET). Biol Pharm Bull, 1995. 18(8): p. 1126-9.

166. Cotton, F.A. and G. Wilkinson, *Advanced Inorganic Chemistry*. 5th ed. 1988, New York: John Wiley and Sons, INC.

167. Dearling, J.L., J.S. Lewis, G.E. Mullen, M.J. Welch, and P.J. Blower, Copper bis(thiosemicarbazone) complexes as hypoxia imaging agents: structure-activity relationships. J Biol Inorg Chem, 2002. 7(3): p. 249-59.

168. Petering, D.H., Physico-Chemical Properties of the Antitumor Agent, 3-Ethoxy-2-Oxobutyraldehyde bis(Thiosemicarbazonato) Copper(II). Bioinorganic Chemistry, 1972. 1: p. 225-271.

169. Fujibayashi, Y., H. Taniuchi, K. Wada, Y. Yonekura, J. Konishi, and A. Yokoyama, Differential mechanism of retention of Cu-pyruvaldehyde-bis(N4-methylthiosemicarbazone) (Cu-PTSM) by brain and tumor: a novel radiopharmaceutical for positron emission tomography imaging. Ann Nucl Med, 1995. 9(1): p. 1-5.

170. Green, M.A., D.L. Klippenstein, and J.R. Tennison, Copper(II) bis(thiosemicarbazone) complexes as potential tracers for evaluation of cerebral and myocardial blood flow with PET. J Nucl Med, 1988. 29(9): p. 1549-57.

171. John, E.K. and M.A. Green, Structure-activity relationships for metal-labeled blood flow tracers: comparison of keto aldehyde bis(thiosemicarbazonato)copper(II) derivatives. J Med Chem, 1990. 33(6): p. 1764-70.

172. Blower, P.J., J.S. Lewis, and J. Zweit, Copper radionuclides and radiopharmaceuticals in nuclear medicine. Nucl Med Biol, 1996. 23(8): p. 957-80.

173. Minkel, D.T., L.A. Saryan, and D.H. Petering, Structure-function correlations in the reaction of bis(thiosemicarbazonato) copper(II) complexes with Ehrlich ascites tumor cells. Cancer Res, 1978. 38(1): p. 124-9.

174. Fujibayashi, Y., H. Taniuchi, Y. Yonekura, H. Ohtani, J. Konishi, and A. Yokoyama, Copper-62-ATSM: a new hypoxia imaging agent with high membrane permeability and low redox potential. J Nucl Med, 1997. 38(7): p. 1155-60.

175. Dehdashti, F., P.W. Grigsby, J.S. Lewis, R. Laforest, B.A. Siegel, and M.J. Welch, Assessing tumor hypoxia in cervical cancer by PET with 60Cu-labeled diacetyl-bis(N4-methylthiosemicarbazone). J Nucl Med, 2008. 49(2): p. 201-5.

176. Dehdashti, F., P.W. Grigsby, M.A. Mintun, J.S. Lewis, B.A. Siegel, and M.J. Welch, Assessing tumor hypoxia in cervical cancer by positron emission tomography with 60Cu-ATSM: relationship to therapeutic response-a preliminary report. Int J Radiat Oncol Biol Phys, 2003. 55(5): p. 1233-8.

177. Dehdashti, F., M.A. Mintun, J.S. Lewis, J. Bradley, R. Govindan, R. Laforest, M.J. Welch, and B.A. Siegel, In vivo assessment of tumor hypoxia in lung cancer with 60Cu-ATSM. Eur J Nucl Med Mol Imaging, 2003. 30(6): p. 844-50.

178. Dietz, D.W., F. Dehdashti, P.W. Grigsby, R.S. Malyapa, R.J. Myerson, J. Picus, J. Ritter, J.S. Lewis, M.J. Welch, and B.A. Siegel, Tumor Hypoxia Detected by Positron Emission Tomography with (60)Cu-ATSM as a Predictor of Response and Survival in Patients Undergoing Neoadjuvant Chemoradiotherapy for Rectal Carcinoma: A Pilot Study. Dis Colon Rectum, 2008.

179. O'Donoghue, J.A., P. Zanzonico, A. Pugachev, B. Wen, P. Smith-Jones, S. Cai, E. Burnazi, R.D. Finn, P. Burgman, S. Ruan, *et al.*, Assessment of regional tumor hypoxia using 18F-fluoromisonidazole and 64Cu(II)-diacetyl-bis(N4-methylthiosemicarbazone) positron emission tomography: Comparative study featuring microPET imaging, Po2

probe measurement, autoradiography, and fluorescent microscopy in the R3327-AT and FaDu rat tumor models. Int J Radiat Oncol Biol Phys, 2005. 61(5): p. 1493-502.

180. Oh, M., T. Tanaka, M. Kobayashi, T. Furukawa, T. Mori, T. Kudo, S. Fujieda, and Y. Fujibayashi, Radio-copper-labeled Cu-ATSM: an indicator of quiescent but clonogenic cells under mild hypoxia in a Lewis lung carcinoma model. Nucl Med Biol, 2009. 36(4): p. 419-26.

181. Grigsby, P.W., R.S. Malyapa, R. Higashikubo, J.K. Schwarz, M.J. Welch, P.C. Huettner, and F. Dehdashti, Comparison of molecular markers of hypoxia and imaging with (60)Cu-ATSM in cancer of the uterine cervix. Mol Imaging Biol, 2007. 9(5): p. 278-83.

182. Takahashi, N., Y. Fujibayashi, Y. Yonekura, M.J. Welch, A. Waki, T. Tsuchida, N. Sadato, K. Sugimoto, and H. Itoh, Evaluation of 62Cu labeled diacetyl-bis(N4-methylthiosemicarbazone) as a hypoxic tissue tracer in patients with lung cancer. Ann Nucl Med, 2000. 14(5): p. 323-8.

183. Black, N.F., S. McJames, T.C. Rust, and D.J. Kadrmas, Evaluation of rapid dual-tracer (62)Cu-PTSM + (62)Cu-ATSM PET in dogs with spontaneously occurring tumors. Phys Med Biol, 2008. 53(1): p. 217-32.

184. Lewis, J.S., R. Laforest, F. Dehdashti, P.W. Grigsby, M.J. Welch, and B.A. Siegel, An imaging comparison of 64Cu-ATSM and 60Cu-ATSM in cancer of the uterine cervix. J Nucl Med, 2008. 49(7): p. 1177-82.

185. Obata, A., M. Yoshimoto, S. Kasamatsu, H. Naiki, S. Takamatsu, K. Kashikura, T. Furukawa, J.S. Lewis, M.J. Welch, H. Saji, *et al.*, Intra-tumoral distribution of (64)Cu-ATSM: a comparison study with FDG. Nucl Med Biol, 2003. 30(5): p. 529-34.

186. Tanaka, T., T. Furukawa, S. Fujieda, S. Kasamatsu, Y. Yonekura, and Y. Fujibayashi, Double-tracer autoradiography with Cu-ATSM/FDG and immunohistochemical interpretation in four different mouse implanted tumor models. Nucl Med Biol, 2006. 33(6): p. 743-50.

187. Yuan, H., T. Schroeder, J.E. Bowsher, L.W. Hedlund, T. Wong, and M.W. Dewhirst, Intertumoral differences in hypoxia selectivity of the PET imaging agent 64Cu(II)-diacetyl-bis(N4-methylthiosemicarbazone). J Nucl Med, 2006. 47(6): p. 989-98.

188. Matsumoto, K., L. Szajek, M.C. Krishna, J.A. Cook, J. Seidel, K. Grimes, J. Carson, A.L. Sowers, S. English, M.V. Green, *et al.*, The influence of tumor oxygenation on hypoxia imaging in murine squamous cell carcinoma using [64Cu]Cu-ATSM or [18F]Fluoromisonidazole positron emission tomography. Int J Oncol, 2007. 30(4): p. 873-81.

189. Kositwattanarerk, A., M. Oh, T. Kudo, Y. Kiyono, T. Mori, Y. Kimura, R. Maruyama, Y. Fujibayashi, S. Fujieda, and H. Okazawa, Different distribution of (2)Cu ATSM and (1)F-FDG in head and neck cancers. Clin Nucl Med, 2012. 37(3): p. 252-7.

190. Lohith, T.G., T. Kudo, Y. Demura, Y. Umeda, Y. Kiyono, Y. Fujibayashi, and H. Okazawa, Pathophysiologic correlation between 62Cu-ATSM and 18F-FDG in lung cancer. J Nucl Med, 2009. 50(12): p. 1948-53.

191. Minagawa, Y., K. Shizukuishi, I. Koike, C. Horiuchi, K. Watanuki, M. Hata, M. Omura, K. Odagiri, I. Tohnai, T. Inoue, *et al.*, Assessment of tumor hypoxia by 62Cu-ATSM PET/CT as a predictor of response in head and neck cancer: a pilot study. Ann Nucl Med, 2011. 25(5): p. 339-45.

192. Yoshii, Y., T. Furukawa, Y. Kiyono, R. Watanabe, A. Waki, T. Mori, H. Yoshii, M. Oh, T. Asai, H. Okazawa, *et al.*, Copper-64-diacetyl-bis (N4-methylthiosemicarbazone) accumulates in rich regions of CD133+ highly tumorigenic cells in mouse colon carcinoma. Nucl Med Biol, 2010. 37(4): p. 395-404.

193. Sheehan, J.P., B. Popp, S. Monteith, S. Toulmin, J. Tomlinson, J. Martin, C.P. Cifarelli, D.H. Lee, and D.M. Park, Trans sodium crocetinate: functional neuroimaging studies in a hypoxic brain tumor. J Neurosurg, 2011. 115(4): p. 749-53.

194. Lewis, J., R. Laforest, T. Buettner, S. Song, Y. Fujibayashi, J. Connett, and M. Welch, Copper-64-diacetyl-bis(N4-methylthiosemicarbazone): An agent for radiotherapy. Proc Natl Acad Sci U S A, 2001. 98(3): p. 1206-11.

195. Obata, A., S. Kasamatsu, J.S. Lewis, T. Furukawa, S. Takamatsu, J. Toyohara, T. Asai, M.J. Welch, S.G. Adams, H. Saji, *et al.*, Basic characterization of 64Cu-ATSM as a radiotherapy agent. Nucl Med Biol, 2005. 32(1): p. 21-8.

196. Aft, R.L., J.S. Lewis, F. Zhang, J. Kim, and M.J. Welch, Enhancing targeted radiotherapy by copper(II)diacetyl- bis(N4-methylthiosemicarbazone) using 2-deoxy-D-glucose. Cancer Res, 2003. 63(17): p. 5496-504.

197. Weeks, A.J., R.L. Paul, P.K. Marsden, P.J. Blower, and D.R. Lloyd, Radiobiological effects of hypoxia-dependent uptake of 64Cu-ATSM: enhanced DNA damage and cytotoxicity in hypoxic cells. Eur J Nucl Med Mol Imaging, 2010. 37(2): p. 330-8.

198. Yoshii, Y., T. Furukawa, Y. Kiyono, R. Watanabe, T. Mori, H. Yoshii, T. Asai, H. Okazawa, M.J. Welch, and Y. Fujibayashi, Internal radiotherapy with copper-64-diacetyl-bis (N4-methylthiosemicarbazone) reduces CD133+ highly tumorigenic cells and metastatic ability of mouse colon carcinoma. Nucl Med Biol, 2011. 38(2): p. 151-7.

199. Isozaki, M., Y. Kiyono, Y. Arai, T. Kudo, T. Mori, R. Maruyama, K. Kikuta, and H. Okazawa, Feasibility of 62Cu-ATSM PET for evaluation of brain ischaemia and misery perfusion in patients with cerebrovascular disease. Eur J Nucl Med Mol Imaging, 2011. 38(6): p. 1075-82.

200. Ikawa, M., H. Okazawa, T. Kudo, M. Kuriyama, Y. Fujibayashi, and M. Yoneda, Evaluation of striatal oxidative stress in patients with Parkinson's disease using [62Cu]ATSM PET. Nucl Med Biol, 2011. 38(7): p. 945-51.

201. Yoshii, Y., M. Yoneda, M. Ikawa, T. Furukawa, Y. Kiyono, T. Mori, H. Yoshii, N. Oyama, H. Okazawa, T. Saga, *et al.*, Radiolabeled Cu-ATSM as a novel indicator of overreduced intracellular state due to mitochondrial dysfunction: studies with mitochondrial DNA-less rho0 cells and cybrids carrying MELAS mitochondrial DNA mutation. Nucl Med Biol, 2012. 39(2): p. 177-85.

202. Fujibayashi, Y., C.S. Cutler, C.J. Anderson, D.W. McCarthy, L.A. Jones, T. Sharp, Y. Yonekura, and M.J. Welch, Comparative studies of Cu-64-ATSM and C-11-acetate in an acute myocardial infarction model: ex vivo imaging of hypoxia in rats. Nucl Med Biol, 1999. 26(1): p. 117-21.

203. Lewis, J.S., P. Herrero, T.L. Sharp, J.A. Engelbach, Y. Fujibayashi, R. Laforest, A. Kovacs, R.J. Gropler, and M.J. Welch, Delineation of hypoxia in canine myocardium using PET and copper(II)-diacetyl-bis(N(4)-methylthiosemicarbazone). J Nucl Med, 2002. 43(11): p. 1557-69.

204. Takahashi, N., Y. Fujibayashi, Y. Yonekura, M.J. Welch, A. Waki, T. Tsuchida, N. Sadato, K. Sugimoto, A. Nakano, J.D. Lee, *et al.*, Copper-62 ATSM as a hypoxic tissue tracer in myocardial ischemia. Ann Nucl Med, 2001. 15(3): p. 293-6.

205. Wada, K., Y. Fujibayashi, N. Tajima, and A. Yokoyama, Cu-ATSM, an intracellular-accessible superoxide dismutase (SOD)-like copper complex: evaluation in an ischemia-reperfusion injury model. Biol Pharm Bull, 1994. 17(5): p. 701-4.

206. Obata, A., E. Yoshimi, A. Waki, J.S. Lewis, N. Oyama, M.J. Welch, H. Saji, Y. Yonekura, and Y. Fujibayashi, Retention mechanism of hypoxia selective nuclear imaging/radiotherapeutic agent cu-diacetyl-bis(N4-methylthiosemicarbazone) (Cu-ATSM) in tumor cells. Ann Nucl Med, 2001. 15(6): p. 499-504.

207. Blower, P.J., M.J. Went, K.E. Martin, and G.E. Smith, Imaging hypoxia in vivo by controlling the electrochemistry of copper radionuclide complexes. 2007.

208. McQuade, P., K.E. Martin, T.C. Castle, M.J. Went, P.J. Blower, M.J. Welch, and J.S. Lewis, Investigation into 64Cu-labeled Bis(selenosemicarbazone) and Bis(thiosemicarbazone) complexes as hypoxia imaging agents. Nucl Med Biol, 2005. 32(2): p. 147-56.

209. Lewis, J.S., D.W. McCarthy, T.J. McCarthy, Y. Fujibayashi, and M.J. Welch, Evaluation of 64Cu-ATSM in vitro and in vivo in a hypoxic tumor model. J Nucl Med, 1999. 40(1): p. 177-83.

210. Berry, M.N., D.S. Friend, and J. Scheuer, Morphology and metabolism of intact muscle cells isolated from adult rat heart. Circ Res, 1970. 26(6): p. 679-87.

211. Powell, T. and V.W. Twist, A rapid technique for the isolation and purification of adult cardiac muscle cells having respiratory control and a tolerance to calcium. Biochem Biophys Res Commun, 1976. 72(1): p. 327-33.

212. Mitcheson, J.S., J.C. Hancox, and A.J. Levi, Cultured adult cardiac myocytes: future applications, culture methods, morphological and electrophysiological properties. Cardiovasc Res, 1998. 39(2): p. 280-300.

213. Decker, M.L., M. Behnke-Barclay, M.G. Cook, J.J. La Pres, W.A. Clark, and R.S. Decker, Cell shape and organization of the contractile apparatus in cultured adult cardiac myocytes. Journal of Molecular and Cellular Cardiology, 1991. 23(7): p. 817-832.

214. Powell, T., E.M. Steen, V.W. Twist, and N. Woolf, Surface characteristics of cells isolated from adult rat myocardium. J Mol Cell Cardiol, 1978. 10(3): p. 287-92.

215. Powell, T., D.A. Terrar, and V.W. Twist, Electrical properties of individual cells isolated from adult rat ventricular myocardium. J Physiol, 1980. 302: p. 131-53.

216. Chacon, E., D. Acosta, and J.J. Lemasters, *Primary Cultures of Cardiac Myocytes as In Vitro Models for Pharmacological and Toxicological Assessments*, in *In Vitro Methods in Pharmaceutical Research*, V.C. José and G.-L. María José, Editors. 1996, Academic Press: San Diego. p. 209-223.

217. Cavanaugh, M.W., Pulsation, migration and division in dissociated chick embryo heart cells in vitro. Journal of Experimental Zoology, 1955. 128(3): p. 573-589.

218. Kono, T., Roles of collagenases and other proteolytic enzymes in the dispersal of animal tissues. Biochim Biophys Acta, 1969. 178(2): p. 397-400.

219. Haddad, J., M.L. Decker, L.C. Hsieh, M. Lesch, A.M. Samarel, and R.S. Decker, Attachment and maintenance of adult rabbit cardiac myocytes in primary cell culture. Am J Physiol, 1988. 255(1 Pt 1): p. C19-27.

220. Poole, R.C., A.P. Halestrap, S.J. Price, and A.J. Levi, The kinetics of transport of lactate and pyruvate into isolated cardiac myocytes from guinea pig. Kinetic evidence for the presence of a carrier distinct from that in erythrocytes and hepatocytes. Biochem J, 1989. 264(2): p. 409-18.

221. Bouron, A., D. Potreau, C. Besse, and G. Raymond, An efficient isolation procedure of Ca-tolerant ventricular myocytes from ferret heart for applications in electrophysiological studies. Biol Cell, 1990. 70(3): p. 121-7.

222. Wolska, B.M. and R.J. Solaro, Method for isolation of adult mouse cardiac myocytes for studies of contraction and microfluorimetry. Am J Physiol, 1996. 271(3 Pt 2): p. H1250-5.

223. De Young, M.B., B. Giannattasio, and A. Scarpa, *Isolation of calcium-tolerant atrial and ventricular myocytes from adult rat heart*, in *Methods in Enzymology*, F. Sidney and F. Becca, Editors. 1989, Academic Press. p. 662-676.

224. Lundgren, E., T. Borg, and S. Mardh, Isolation, characterization and adhesion of calcium-tolerant myocytes from the adult rat heart. J Mol Cell Cardiol, 1984. 16(4): p. 355-62.

225. Frangakis, C.J., J.J. Bahl, H. McDaniel, and R. Bressler, Tolerance to physiological calcium by isolated myocytes from the adult rat heart; an improved cellular preparation. Life Sci, 1980. 27(10): p. 815-25.

226. Clark, M.G., B.J. Gannon, N. Bodkin, G.S. Patten, and M.N. Berry, An improved procedure for the high-yield preparation of intact beating heart cells from the adult rat biochemical and morphologic study. Journal of Molecular and Cellular Cardiology, 1978. 10(12): p. 1101-1121.

227. Claycomb, W.C., N.A. Lanson, Jr., B.S. Stallworth, D.B. Egeland, J.B. Delcarpio, A. Bahinski, and N.J. Izzo, Jr., HL-1 cells: a cardiac muscle cell line that contracts and retains phenotypic characteristics of the adult cardiomyocyte. Proc Natl Acad Sci U S A, 1998. 95(6): p. 2979-84.

228. Kehat, I., D. Kenyagin-Karsenti, M. Snir, H. Segev, M. Amit, A. Gepstein, E. Livne, O. Binah, J. Itskovitz-Eldor, and L. Gepstein, Human embryonic stem cells can differentiate into myocytes with structural and functional properties of cardiomyocytes. J Clin Invest, 2001. 108(3): p. 407-14.

229. Zhu, W.Z., B. Van Biber, and M.A. Laflamme, Methods for the derivation and use of cardiomyocytes from human pluripotent stem cells. Methods Mol Biol, 2011. 767: p. 419-31.

230. Cutilletta, A.F., M.-C. Aumont, A.C. Nag, and R. Zak, Separation of muscle and non-muscle cells from adult rat myocardium: An application to the study of RNA polymerase. Journal of Molecular and Cellular Cardiology, 1977. 9(5): p. 399-407.

231. Schwarzfeld, T.A. and S.L. Jacobson, Isolation and development in cell culture of myocardial cells of the adult rat. Journal of Molecular and Cellular Cardiology, 1981. 13(6): p. 563-575.

232. Nag, A.C. and R. Zak, Dissociation of adult mammalian heart into single cell suspension: an ultrastructural study. J Anat, 1979. 129(Pt 3): p. 541-59.

233. Snabaitis, A.K., A. Muntendorf, T. Wieland, and M. Avkiran, Regulation of the extracellular signal-regulated kinase pathway in adult myocardium: differential roles of Gq/11, Gi and G12/13 proteins in signalling by [alpha]1-adrenergic, endothelin-1 and thrombin-sensitive protease-activated receptors. Cellular Signalling, 2005. 17(5): p. 655-664.

234. Powell, T., The calcium paradox and isolated myocytes. Eur Heart J, 1983. 4 Suppl H: p. 105-11.

235. Slade, A.M., N.J. Severs, T. Powell, and V.W. Twist, Isolated calcium-tolerant myocytes and the calcium paradox: an ultrastructural comparison. Eur Heart J, 1983. 4 Suppl H: p. 113-22.

236. Zimmerman, A.N. and W.C. Hulsmann, Paradoxical influence of calcium ions on the permeability of the cell membranes of the isolated rat heart. Nature, 1966. 211(5049): p. 646-7.

237. Piper, H.M., I. Probst, P. Schwartz, F.J. Hutter, and P.G. Spieckermann, Culturing of calcium stable adult cardiac myocytes. J Mol Cell Cardiol, 1982. 14(7): p. 397-412.

238. Frisch, S.M. and R.A. Screaton, Anoikis mechanisms. Current Opinion in Cell Biology, 2001. 13(5): p. 555-562.

239. Michel, J.B., Anoikis in the cardiovascular system: known and unknown extracellular mediators. Arterioscler Thromb Vasc Biol, 2003. 23(12): p. 2146-54.

240. Randall, D., W. Burggren, and K. French, *Animal Physiology: Mechanisms and Adaptations*. 4th ed. 2000, New York: W. H. Freeman and Company.

241. Burgman, P., J.A. O'Donoghue, J.S. Lewis, M.J. Welch, J.L. Humm, and C.C. Ling, Cell line-dependent differences in uptake and retention of the hypoxia-selective nuclear imaging agent Cu-ATSM. Nucl Med Biol, 2005. 32(6): p. 623-30.

242. Vavere, A.L. and J.S. Lewis, Examining the relationship between Cu-ATSM hypoxia selectivity and fatty acid synthase expression in human prostate cancer cell lines. Nucl Med Biol, 2008. 35(3): p. 273-9.

243. Billups-Rothenburg, I. *Modular Incubation Chamber*. 2001; Available from: www.hypoxiachamber.com.

244. Pitts, K.R., J.M. Derry, K. Kerkof, W.A. Lawrence, and C.F. Toombs, Differentially regulated functional gene clusters identified during ischemia and reperfusion in isolated cardiac myocytes using coverslip hypoxia. J Pharmacol Toxicol Methods, 2008. 57(1): p. 42-51.

245. Pitts, K.R. and C.F. Toombs, Coverslip hypoxia: a novel method for studying cardiac myocyte hypoxia and ischemia in vitro. Am J Physiol Heart Circ Physiol, 2004. 287(4): p. H1801-12.

246. Pitts, K.R. and C.F. Toombs, Studying ischemia and reperfusion in isolated neonatal rat ventricular myocytes using coverslip hypoxia. Methods Mol Med, 2007. 139: p. 271-81.

247. Henry, P., A. Popescu, M. Puceat, M.E. Hinescu, and D. Escande, Acute simulated ischaemia produces both inhibition and activation of K+ currents in isolated ventricular myocytes. Cardiovasc Res, 1996. 32(5): p. 930-9.

248. Vanheel, B., L. Leybaert, A. De Hemptinne, and I. Leusen, Simulated ischemia and intracellular pH in isolated ventricular muscle. Am J Physiol, 1989. 257(2 Pt 1): p. C365-76.

249. Koch, C.J., A thin-film culturing technique allowing rapid gas-liquid equilibration (6 sec) with no toxicity to mammalian cells. Radiat Res, 1984. 97(2): p. 434-42.

250. Labglass, L., 2012.

251. Paul, R.D., J. Halstead, P. Balinger, J. Lewis, JS. Martin, K. McQuade, P. Marsden, PK. O'Doherty, MJ. Blower, PJ., P47 Son of CuATSM: Towards optimised second-generation copper complexes for hypoxia imaging. European Journal of Nuclear Medicine, 2005. 32(Supplement 1): p. S269.

252. Paul, R.H., P. Balinger, J. Marsden, PK. O'Doherty, MJ. Blower, PJ. Wood, K. Honess, DJ. Maxwell, RJ. Wilson, I. Saunders, MI., Production of 64Cu on the CTI RDS 112 11 MeV cyclotron and synthesis and biological evaluation of 64CuATSM second generation analogues. European Journal of Nuclear Medicine and Molecular Imaging, 2006. 33(Supplement 2): p. S269.

253. Mosmann, T., Rapid colorimetric assay for cellular growth and survival: application to proliferation and cytotoxicity assays. J Immunol Methods, 1983. 65(1-2): p. 55-63.

254. Slater, T.F., B. Sawyer, and U. Straeuli, STUDIES ON SUCCINATE-TETRAZOLIUM REDUCTASE SYSTEMS. III. POINTS OF COUPLING OF FOUR DIFFERENT TETRAZOLIUM SALTS. Biochim Biophys Acta, 1963. 77: p. 383-93.

255. Chen, M., Z. Zsengeller, C.Y. Xiao, and C. Szabo, Mitochondrial-to-nuclear translocation of apoptosis-inducing factor in cardiac myocytes during oxidant stress: potential role of poly(ADP-ribose) polymerase-1. Cardiovasc Res, 2004. 63(4): p. 682-8.

256. Gomez, L.A., A.E. Alekseev, L.A. Aleksandrova, P.A. Brady, and A. Terzic, Use of the MTT Assay in Adult Ventricular Cardiomyocytes to Assess Viability: Effects of Adenosine and Potassium on Cellular Survival. Journal of Molecular and Cellular Cardiology, 1997. 29(4): p. 1255-1266.

257. Seenarain, V., H.M. Viola, G. Ravenscroft, T.M. Casey, R.J. Lipscombe, E. Ingley, N.G. Laing, S.D. Bringans, and L.C. Hool, Evidence of altered guinea pig ventricular cardiomyocyte protein expression and growth in response to a 5 min in vitro exposure to H(2)O(2). J Proteome Res, 2010. 9(4): p. 1985-94.

258. Jacobson, S.L. and H.M. Piper, Cell cultures of adult cardiomyocytes as models of the myocardium. J Mol Cell Cardiol, 1986. 18(7): p. 661-78.

259. Severs, N.J., K.S. Shovel, A.M. Slade, T. Powell, V.W. Twist, and C.R. Green, Fate of gap junctions in isolated adult mammalian cardiomyocytes. Circ Res, 1989. 65(1): p. 22-42.

260. Mazet, F., B.A. Wittenberg, and D.C. Spray, Fate of intercellular junctions in isolated adult rat cardiac cells. Circ Res, 1985. 56(2): p. 195-204.

261. Piper, H.M., I. Probst, P. Schwartz, F.J. Hütter, and P.G. Spieckermann, Culturing of calcium stable adult cardiac myocytes. Journal of Molecular and Cellular Cardiology, 1982. 14(7): p. 397-412.

262. Spahr, R., S.L. Jacobson, B. Siegmund, P. Schwartz, and H.M. Piper, Substrate oxidation by adult cardiomyocytes in long-term primary culture. J Mol Cell Cardiol, 1989. 21(2): p. 175-85.

263. Claycomb, W.C., A.H. Burns, and R.E. Shepherd, Culture of the terminally differentiated ventricular cardiac muscle cell. Characterization of exogenous substrate oxidation and the adenylate cyclase system. FEBS Lett, 1984. 169(2): p. 261-6.

264. Gingras, B.A., T. Suprunchuk, and C.H. Bayley, The Preparation of some thiosemicarbazones and their copper complexes: Part III. Canadian Journal of Chemistry, 1962. 40(6): p. 1053-1059.

265. Borgers, M. and H.M. Piper, Calcium-shifts in anoxic cardiac myocytes. A cytochemical study. J Mol Cell Cardiol, 1986. 18(4): p. 439-48.

266. Piper, H.M., P. Schwartz, R. Spahr, J.F. Hutter, and P.G. Spieckermann, Absence of reoxygenation damage in isolated heart cells after anoxic injury. Pflugers Arch, 1984. 401(1): p. 71-6.

267. Schwartz, P., H.M. Piper, R. Spahr, and P.G. Spieckermann, Ultrastructure of cultured adult myocardial cells during anoxia and reoxygenation. Am J Pathol, 1984. 115(3): p. 349-61.

268. White, R.L. and B.A. Wittenberg, Effects of calcium on mitochondrial NAD(P)H in paced rat ventricular myocytes. Biophys J, 1995. 69(6): p. 2790-9.

269. Warburg, O., F. Wind, and E. Negelein, The Metabolism of Tumors in the Body. Journal of General Physiology, 1927. 8: p. 519- 530.

270. Gal, D., P.C. Macdonald, J.C. Porter, and E.R. Simpson, Cholesterol metabolism in cancer cells in monolayer culture. III. Low-density lipoprotein metabolism. International Journal of Cancer, 1981. 28(3): p. 315-319.

271. Langendorff, O., Untersuchungen am überlebenden Säugetierherzen Physiologie Bd, 1985. 61.

272. Radnoti, L.; Available from: http://www.radnoti.com/resources/applications/isolated_heart_perfusion/isolated_heart_perfusion_notes.

273. Sutherland, F.J. and D.J. Hearse, The isolated blood and perfusion fluid perfused heart. Pharmacol Res, 2000. 41(6): p. 613-27.

274. Southworth, R., S.C. Blackburn, K.A. Davey, G.K. Sharland, and P.B. Garlick, The low oxygen-carrying capacity of Krebs buffer causes a doubling in ventricular wall thickness in the isolated heart. Can J Physiol Pharmacol, 2005. 83(2): p. 174-82.

275. Garlick, P.B., G.K. Radda, P.J. Seeley, and B. Chance, Phosphorus NMR studies on perfused heart. Biochemical and Biophysical Research Communications, 1977. 74(3): p. 1256-1262.

276. Okada, R.D., G. Johnson, 3rd, K.N. Nguyen, L.R. Carlson, and D. Beju, HL-91-technetium-99m: a new marker of viability in ischemic myocardium. J Nucl Cardiol, 1999. 6(3): p. 306-15.

277. Raytest.Isotopenmessgeräte.GmbH. Available from: http://www.raytest.de/index2.html.

278. Garlick, P.B.R., G.K. Seeley, P.J., Studies on Acidosis in the Ischaemic Heart by Phosphorus Nuclear Magnetic Resonance. Biochem. J., 1979. 184: p. 547- 554.

279. Cave, A.C. and P.B. Garlick, Ischemic preconditioning and intracellular pH: a 31P NMR study in the isolated rat heart. Am J Physiol, 1997. 272(1 Pt 2): p. H544-52.

280. Skrzypiec-Spring, M., B. Grotthus, A. Szelag, and R. Schulz, Isolated heart perfusion according to Langendorff---still viable in the new millennium. J Pharmacol Toxicol Methods, 2007. 55(2): p. 113-26.

281. Winkelmann, D.A., Y. Bermke, and D.H. Petering, Comparative properties of the antineoplastic agent, 3-ethoxy-2-oxobutyraldehyde bis(thiosemicarbazonato) copper(II) and related chelates: linear free energy correlations. Bioinorg Chem, 1974. 3(3): p. 261-77.

282. Dearling. J.L.J, M.G.E.D., Lewis. J.S, Welch. M.J, Blower.P.J., Differential Brain Uptake of Two Hypoxia Tracers Dictated by Lipophilicity. J. Labelled Cpd. Radiopharm, 1999. 42(Suppl. 1): p. S276- S278.

283. Bessems, M., N.A. t Hart, R. Tolba, B.M. Doorschodt, H.G. Leuvenink, R.J. Ploeg, T. Minor, and T.M. van Gulik, The isolated perfused rat liver: standardization of a time-honoured model. Lab Anim, 2006. 40(3): p. 236-46.

284. Suner, S. and G. Jay, Carbon Monoxide Has Direct Toxicity on the Myocardium Distinct from Effects of Hypoxia in an Ex Vivo Rat Heart Model. Academic Emergency Medicine, 2008. 15(1): p. 59-65.

285. Kihara, Y., W. Grossman, and J.P. Morgan, Direct measurement of changes in intracellular calcium transients during hypoxia, ischemia, and reperfusion of the intact mammalian heart. Circ Res, 1989. 65(4): p. 1029-44.

286. Bailey, J.R. and W.R. Driedzic, Myoglobin supported oxygen consumption in isolated rat hearts under dysoxic conditions. J Mol Cell Cardiol, 1992. 24(8): p. 799-807.

287. Serizawa, T., W.M. Vogel, C.S. Apstein, and W. Grossman, Comparison of acute alterations in left ventricular relaxation and diastolic chamber stiffness induced by hypoxia and ischemia. Role of myocardial oxygen supply-demand imbalance. J Clin Invest, 1981. 68(1): p. 91-102.

288. Wardle, C.A. and R.A. Riemersma, Hypoxia-stimulated glycerol production from the isolated, perfused rat heart is mediated by non-adrenergic mechanisms. Basic Res Cardiol, 1994. 89(1): p. 29-38.

289. Backus, M., D. Piwnica-Worms, D. Hockett, J. Kronauge, M. Lieberman, P. Ingram, and A. LeFurgey, Microprobe analysis of Tc-MIBI in heart cells: calculation of mitochondrial membrane potential. Am J Physiol, 1993. 265(1 Pt 1): p. C178-87.

290. al-Haboubi, H.A. and B.J. Ward, Microvascular permeability of the isolated rat heart to various solutes in well-oxygenated and hypoxic conditions. Int J Microcirc Clin Exp, 1996. 16(6): p. 291-301.

291. Barnhart, A.J., W.D. Voorhees, and M.A. Green, Correlation of Cu(PTSM) localization with regional blood flow in the heart and kidney. Int J Rad Appl Instrum B, 1989. 16(7): p. 747-8.

292. Xiao, Z., P.S. Donnelly, M. Zimmermann, and A.G. Wedd, Transfer of copper between bis(thiosemicarbazone) ligands and intracellular copper-binding proteins. insights into mechanisms of copper uptake and hypoxia selectivity. Inorg Chem, 2008. 47(10): p. 4338-47.

293. Maurer, R.I., P.J. Blower, J.R. Dilworth, C.A. Reynolds, Y. Zheng, and G.E. Mullen, Studies on the mechanism of hypoxic selectivity in copper bis(thiosemicarbazone) radiopharmaceuticals. J Med Chem, 2002. 45(7): p. 1420-31.

294. Price, K.A., P.J. Crouch, I. Volitakis, B.M. Paterson, S. Lim, P.S. Donnelly, and A.R. White, Mechanisms Controlling the Cellular Accumulation of Copper Bis(thiosemicarbazonato) Complexes. Inorg Chem, 2011. 50(19): p. 9594-605.

Publications Arising from this Thesis

Handley MG, Medina RA, Nagel E, Blower PJ, Southworth R. (2011). PET Imaging of Cardiac Hypoxia: Opportunities and Challenges. Journal of Molecular and Cellular Cardiology. November 51 (5): 640-650.

Handley MG, Paul R, Blower PB, Southworth R. Abstract (2010). Isolated cardiomyocytes and isolated perfused rat heart as tools for screening and characterisation of ^{64}Cu-bis(thiosemicarbazone) complexes for delineating myocardial hypoxia. The Quarterly Journal of Nuclear Medicine and Molecular Imaging. 54 (2) Suppl. 1.